

**COMPUTATIONAL, STRUCTURAL  
AND ELECTROCHEMICAL  
PROPERTIES OF METAL(III)  
TRIS-BETADIKETONATO COMPLEXES**

*A dissertation submitted in accordance with the requirements for the degree*

**Magister Scientiae**

*in the*

**Department of Chemistry**

**Faculty of Natural and Agricultural Sciences**

*at the*

**University of the Free State**

*by*

**Roxanne Freitag**

*Supervisor*

**Prof. J. Conradie**

# Acknowledgements

---

I would like to thank all my friends, family and colleagues for their support, friendship and guidance throughout the, sometimes, very trying period of my studies. Special appreciation must be made to the following people:

My promoter (Prof. Jeanet Conradie) thank you for all your patience, leadership, diligence and perseverance throughout the course of this work.

My other half (Konrad Gostynski) thank you for the support, patience, motivation and love through the tough times that came with writing a dissertation. You withstood the hardships with me and we made it!

My parents (Gerda and Ulrich Freitag) and sister (Ullani Freitag), thank you for the support, patience, love and motivation throughout my studies. This dissertation would not have been possible without your kind and wise words.

My friend (Carla Pretorius), thank you for the support, motivation and patience for reading through this dissertation to help with language and grammar.

My friend (Elize van Heerden), thank you for the support, encouragement and for cheering me on throughout this study.

The Physical Chemistry group, thank you all for support, guidance and laughter throughout this study.

I wish to acknowledge Mr. T.J. Muller for the data collection and refinement of the crystal structure.

The Chemistry department and the University of the Free State, thank you for available facilities.

The National Research Foundation and the University of the Free State, thank you for the financial support.

# Table of contents.

---

<b>List of abbreviations.</b>	<b>v</b>
-------------------------------	----------

## **Chapter 1**

<b>Introduction.</b>	<b>1</b>
1.1 Tris( $\beta$ -diketonato)manganese(III), $\text{Mn}(\beta\text{-diketonato})_3$ .	1
1.2 Tris(acetylacetonato)metal(III), $\text{M}(\text{acac})_3$ ( $\text{M} = \text{V}, \text{Cr}, \text{Fe}$ and $\text{Co}$ ).	3
1.3 Aims of this study.	5

## **Chapter 2**

<b>Literature survey and fundamental aspects.</b>	<b>7</b>
2.1 Computational chemistry.	7
2.1.1 Introduction.	7
2.1.2 Quantum mechanics.	8
2.1.3 Basis sets.	9
2.1.4 Density functional theory (DFT).	10
2.1.5 Exchange-correlation functionals.	11
2.1.6 Amsterdam density functional (ADF).	12
2.2 Electrochemistry.	13
2.2.1 Introduction.	13
2.2.2 Cyclic voltammetry (CV).	13
2.2.3 Linear sweep voltammetry (LSV).	16
2.3 Basic concepts.	17
2.3.1 Point group theory.	17
2.3.2 Ligand field theory.	19
2.3.2.1 Crystal field theory.	20

2.3.2.2	Molecular orbital (MO) theory.	22
2.3.2.3	Low-spin and high-spin.	25
2.3.2.4	Jahn-Teller distortion.	26
2.4	Tris( $\beta$ -diketonato)manganese(III), $\text{Mn}(\beta\text{-diketonato})_3$ .	28
2.4.1	Introduction.	28
2.4.2	Synthesis.	29
2.4.3	Structure and properties.	31
2.4.4	Cyclic voltammetry.	33
2.5	Tris(acetylacetonato)metal(III), $\text{M}(\text{acac})_3$ (M = V, Cr, Fe and Co).	35
2.5.1	Introduction.	35
2.5.2	$\text{V}(\text{acac})_3$ .	35
2.5.2.1	Structural properties.	35
2.5.2.2	Cyclic voltammetry.	37
2.5.3	$\text{Cr}(\text{acac})_3$ .	38
2.5.3.1	Structural properties.	38
2.5.3.2	Cyclic voltammetry.	39
2.5.4	$\text{Fe}(\text{acac})_3$ .	41
2.5.4.1	Structural properties.	42
2.5.4.2	Cyclic voltammetry.	43
2.5.5	$\text{Co}(\text{acac})_3$ .	44
2.5.5.1	Structural properties.	44
2.5.5.2	Cyclic voltammetry.	46

## Chapter 3

### Results and discussion. 49

3.1	Tris( $\beta$ -diketonato)manganese(III) / $\text{Mn}(\beta\text{-diketonato})_3$ .	49
3.1.1	Synthesis.	49
3.1.2	Crystal Structure of $\text{Mn}(\text{dbm})_3$ .	52
3.1.3	Electrochemistry.	56
3.1.4	Computational study.	73
3.1.4.1	$\text{Mn}(\text{acetylacetonato})_3$ , $\text{Mn}(\text{acac})_3$ .	73
3.1.4.2	$\text{Mn}(\text{dbm})_3$ .	78
3.1.4.3	$\text{Mn}(\text{hfac})_3$	80



3.1.4.4	Mn( $\beta$ -diketonato) <sub>3</sub> .	82
3.2	Tris(acetylacetonato)metal(III), M(acac) <sub>3</sub> (M = V, Cr, Mn, Fe and Co).	85
3.2.1	Electrochemistry.	85
3.2.2	Computational study.	96
3.2.2.1	Spin state and symmetry of M(acac) <sub>3</sub> .	96
3.2.2.2	<i>d</i> -orbitals occupations of the M(acac) <sub>3</sub> complexes (M = V, Cr, Mn, Fe and Co).	99
3.2.2.3	Molecular orbital (MO) energy level diagram.	105
3.2.2.4	Reduction potential relationships.	106

## Chapter 4

<b>Experimental</b>	<b>109</b>
4.1	Materials. 109
4.2	Characterization techniques and instrumentation. 109
4.2.1	Spectroscopic measurements. 109
4.2.2	Melting point (m.p.) determination. 109
4.2.3	X-ray Diffraction (XRD). 109
4.2.4	Electrochemistry. 110
4.2.4.1	Acetonitrile (CH <sub>3</sub> CN) solvent system. 110
4.2.4.2	Dichloromethane (DCM) solvent system. 111
4.3	Synthesis. 111
4.3.1	Mn( $\beta$ -diketonato) <sub>3</sub> complexes [1], [4] – [7]. 111
4.3.1.1	Tris(acetylacetonato)manganese(III) {Mn(acac) <sub>3</sub> } [1]. 111
4.3.1.2	Tris(trifluoroacetylacetonato)manganese(III) {Mn(tfaa) <sub>3</sub> } [4]. 112
4.3.1.3	Tris(thenoyltrifluoroacetonato)manganese(III) {Mn(tfth) <sub>3</sub> } [5]. 112
4.3.1.4	Tris(trifluorofuroylacetonato)manganese(III) {Mn(tffu) <sub>3</sub> } [6]. 112
4.3.1.5	Tris(trifluorobenzoylacetonato)manganese(III) {Mn(tfba) <sub>3</sub> } [7]. 113
4.3.2	Mn( $\beta$ -diketonato) <sub>3</sub> complexes [2], [3]. 113
4.3.2.1	Tris(benzoylacetonato)manganese(III) {Mn(ba) <sub>3</sub> } [2]. 114
4.3.2.2	Tris(dibenzoylmethanato)manganese(III) {Mn(dbm) <sub>3</sub> } [3]. 114
4.3.3	Mn( $\beta$ -diketonato) <sub>3</sub> complex [8]. 115
4.3.3.1	Tris(hexafluoroacetylacetonato)manganese(III) {Mn(hfac) <sub>3</sub> } [8]. 115

4.4	Computational calculations.	115
4.4.1	Tris( $\beta$ -diketonato)manganese(III), $\text{Mn}(\beta\text{-diketonato})_3$ .	115
4.4.2	Tris(acetylacetonato)metal(III), $\text{M}(\text{acac})_3$ ( $\text{M} = \text{V}, \text{Cr}, \text{Fe}$ and $\text{Co}$ ).	116

## Chapter 5

### Concluding remarks and future perspectives. 117

5.1	Concluding remarks.	117
5.1.1	Tris( $\beta$ -diketonato)manganese(III) / $\text{Mn}(\beta\text{-diketonato})_3$ .	117
5.1.2	Tris(acetylacetonato)metal(III), $\text{M}(\text{acac})_3$ ( $\text{M} = \text{V}, \text{Cr}, \text{Fe}$ and $\text{Co}$ ).	119
5.2	Future perspectives.	119

### Appendix 121

A.	Crystal data.	121
B.	Mass spectrometry (MS).	128
C.	Cyclic Voltammetry data.	130
D.	Computational data.	137

### Abstract 153

### Opsomming 154

# List of abbreviations.

---

## $\beta$ -diketones

Hacac	2,4-pentanedione (acetylacetone)
Hba	1-phenyl-1,3-butanedione (benzoylacetone)
Hdbm	1,3-diphenyl-1,3-propanedione (dibenzoylmethane)
Hdpm	2,2,6,6-tetramethyl-3,5-heptanedione (dipivaloylmethane)
Htfaa	1,1,1-trifluoro-2,4-pentanedione (trifluoroacetylacetone)
Htfth	4,4,4-trifluoro-1-(2-thenoyl)-1,3-butanedione (trifluorothenoyletacetone)
Htffu	4,4,4-trifluoro-1-(2-furoyl)-1,3-butanedione (trifluorofuroyletacetone)
Htfba	4,4,4-trifluoro-1-(phenyl)-1,3-butanedione (trifluorobenzoylacetone)
Hhfaa	1,1,1,5,5,5-hexafluoro-2,4-pentanedione (hexafluoroacetylacetone)

\*The removal of H in the above abbreviations represents the anion (enolate) of the  $\beta$ -diketone.

## Solvents

THF	tetrahydrofuran
CH <sub>3</sub> CN	acetonitrile
DCM	dichloromethane
EtOH	ethanol

## Cyclic Voltammetry

CV	cyclic voltammetry
E <sup>0</sup>	formal reduction potential
E <sub>pa</sub>	anodic peak potential
E <sub>pc</sub>	cathodic peak potential
$\Delta E_p$	separation of anodic and cathodic peak potentials
i <sub>pa</sub>	anodic peak current
i <sub>pc</sub>	cathodic peak current
TBAPF <sub>6</sub>	tetrabutylammonium hexafluorophosphate [NBu <sub>4</sub> ][PF <sub>6</sub> ]
TEABF <sub>4</sub>	tetraethylammonium tetrafluoroborate
SCE	saturated calomel electrode

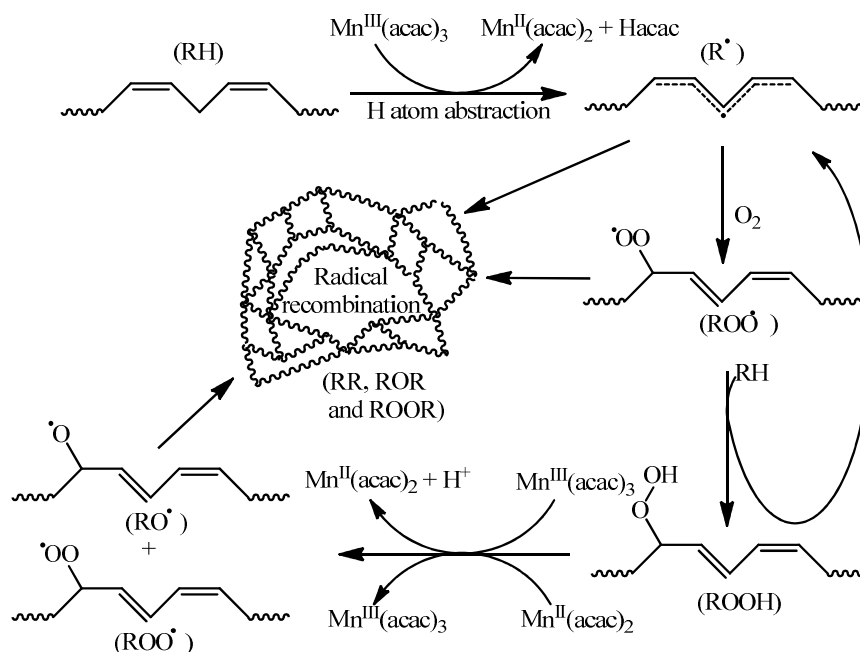
This study is concerned with the synthesis, electrochemistry and computational chemistry of tris( $\beta$ -diketonato)metal(III) complexes. A representative series was chosen, consisting of a series of eight  $\text{Mn}(\beta\text{-diketonato})_3$  complexes ( $\beta$ -diketonato = acetylacetonato (acac) [1], benzoylacetonato (ba) [2], dibenzoylmethanato (dbm) [3], trifluoroacetylacetonato (tfaa) [4], thenoyltrifluoroacetonato (tfth) [5], trifluorofuroylacetonato (tffu) [6], trifluorobenzoylacetonato (tfba) [7] and hexafluoroacetylacetonato (hfac) [8]) and a series of five  $\text{M}(\text{acetylacetonato})_3$  complexes ( $\text{M} = \text{V}, \text{Cr}, \text{Mn}, \text{Co}$  and  $\text{Fe}$ ).  $\text{M}(\beta\text{-diketonato})_3$  complexes are known for their application in homogeneous and heterogeneous catalysis, a few examples will be highlighted.

## 1.1 Tris( $\beta$ -diketonato)manganese(III), $\text{Mn}(\beta\text{-diketonato})_3$ .

The oxidation of unsaturated fatty acid ester side chains in the alkyd resin followed by the decay of the formed hydroperoxides is known as the chemical drying process of alkyd-based paints. Metal catalysts are used to increase the decay rate of the hydroperoxides ( $\text{ROOH}$ ) and improve the overall drying process rate of alkyd paints. The most widely used catalysts in the oxidative drying process are cobalt salts.<sup>1</sup> Since cobalt compounds are suspected to be carcinogenic a search for new catalysts in the drying process of alkyd paints is underway. Recently tris(acetylacetonato)manganese(III) [ $\text{Mn}(\text{acac})_3$ ] was found to have high catalytic activity in the autoxidation of ethyl linoleate (EL, alkyd resin model compound).<sup>1</sup> The catalytic process that takes place during the drying of alkyd paints is illustrated in **Scheme 1.1**.

<sup>1</sup> R. van Gorkum, E. Bouwman, J. Reedijk, *Inorg. Chem.* **2004** (43) 2456-2458.

## Introduction

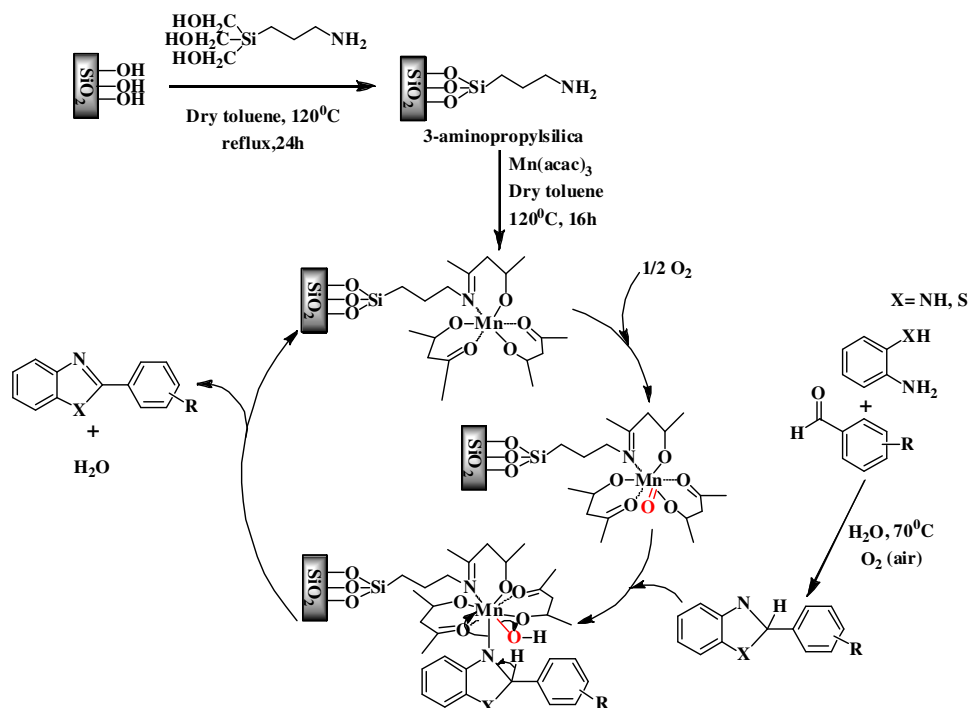


**Scheme 1.1:** The decay of ethyl linoleate (EL) catalyzed by the  $\text{Mn}(\text{acac})_3$  complex.

The radical initiation is proposed to occur by the hydrogen atom abstraction pathway. A free acetylacetone ligand and an ethyl linoleate radical was formed during a hydrogen atom transfer from the EL to the  $\text{Mn}^{\text{III}}(\text{acac})_3$ . The fast reaction between the ethyl linoleate radical and dioxygen forms a peroxy radical, which can abstract a hydrogen atom from another ethyl linoleate to produce a hydroperoxide. The hydroperoxides that were produced can be catalytically decayed by the use of both the  $\text{Mn}^{\text{III}}(\text{acac})_3$  and the  $\text{Mn}^{\text{II}}(\text{acac})_2$ . The  $\text{Mn}^{\text{III}}(\text{acac})_3$  catalyst is therefore regenerated by the catalyzed decay of hydroperoxides with the use of a  $\text{Mn}^{\text{II}}(\text{acac})_2$  catalyst. Manganese(III) is active in both the hydrogen abstraction and the hydroperoxide decay where the manganese(II) is only active in the decay of the hydroperoxides. These radicals form cross-linked networks which in turn create a hard coating of alkyd paint.

Due to the simplified recovery, recyclability and ease in handling of heterogeneous catalysts, the heterogeneous catalysts have taken over in popularity with regards to homogeneous catalysts. Heterogeneous catalysts are also seen as more environmentally disposable. Functionalized silica *via* covalent or non-covalent attachments have been studied more. The production of 2-benzimidazole and 2-benzothiazole are highly favoured due to their ability to lead to highly active pharmaceuticals. Silica functionalized  $\text{Mn}(\text{acac})_3$  can be used as a catalyst in the production of 2-benzimidazole and 2-benzothiazole, see **Scheme 1.2**.<sup>2</sup>

<sup>2</sup> R.K. Sodhi and S. Paul. *Catal. Lett.* **2011** (141) 608-615.



**Scheme 1.2:** The production of 2-benzimidazole and 2-benzothiazole by the use of silica functionalized with Mn(acac)<sub>3</sub>.

## 1.2 Tris(acetylacetonato)metal(III), M(acac)<sub>3</sub> ( M = V, Cr, Fe and Co).

Vanadium(III) complexes are known to mimic insulin and act as anti-inflammatories and anti-carcinogenic agents. In certain marine animals, known as ascidians, cellular vanadium was found at higher concentration than the sea water they live in. Vanadium(V) is absorbed from the surrounding seawater and incorporated into the vacuoles of the blood cells.<sup>3</sup> Taking advantage of the likeness of VO<sub>4</sub><sup>-3</sup> and PO<sub>4</sub><sup>-3</sup> the vanadium is absorbed through the phosphate channel. Vanadium is reduced to V<sup>IV</sup> and V<sup>III</sup> in the vacuoles. The role of the vanadium in the physiologic functions of these animals is still unknown.<sup>3</sup> The fact that vanadium is similar to molybdenum makes it possible for vanadium to function as metalloenzyme which is essential for xanthine oxidase, aldehyde oxidase and nitrogenase in biological systems.<sup>4</sup>

<sup>3</sup> F. Brito, M.L. Araujo, J.D. Martínez, Y. Hernández, A. Moh, V. Lubes, *Journal of Coordination Chemistry* **2009** (62) 52-62.

<sup>4</sup> M.A. Nawi, T.L. Riechel, *Inorg. Chem.* **1981** (20) 1974-1978.

Chromium(III) is a trace element that maintains the normal glucose metabolism in the human body, it is very important in the case of diabetes and at older age. The Cr(acac)<sub>3</sub> complex has been grafted onto mesoporous crystalline material (MCM-41) and used as a catalyst in the polymerization of ethylene. It was proven that Cr-MCM-41 is catalytically active in the gas- and slurry-phase polymerization at 100 °C. The catalytic activity is a function of the calcination temperature, support characteristics and the loading of the chromium.<sup>5</sup>

Iron acetylacetonate can be anchored on silica xerogel. The Fe<sup>III</sup> atoms that are anchored can be used as a heterogeneous catalyst in the epoxidation of alkenes. The same conditions as the homogeneous system are employed where molecular oxygen is used at atmospheric pressure as oxidant and the sacrificial reducing agent iso-butyraldehyde. The *cis*-cyclooctene was selectively epoxidized to *cis*-cyclooctene oxide when using the heterogeneous iron(III) acetylacetonate anchored on silica xerogel as a catalyst. It was found that *cis*-cyclooctene was 100 % selective and 39 % partially epoxidized to *cis*-cyclooctene oxide after 24 hours, which is not an improvement on the homogeneous system but it is clearly noted that the heterogeneous system has not been optimized yet. Therefore, the heterogeneous system can be studied further to optimize the epoxidation. The iron cation is not leached out under the conditions mentioned during the epoxidation.<sup>6</sup>

Co(acac)<sub>3</sub> (*d*<sup>6</sup>) is very different to the rest of the M(acac)<sub>3</sub> series discussed thus far. Co(acac)<sub>3</sub> is the only low spin diamagnetic complex meaning that there are no unpaired electrons in the *d*-orbitals of the cobalt metal. Co(acac)<sub>3</sub> has a relative low toxicity and is kinetically inert.<sup>7</sup>

---

<sup>5</sup> B.M. Weckhuysen, R.R. Rao, J. Pelgrims, R.A. Schoonheydt, P. Bodart, G. Denras, O. Collart, P. Van Der Voort, E.F. Vansant, *Chem. Eur. J.* **2000** (6) 2960-2970.

<sup>6</sup> M.C. Brasil, E.V. Benvenutti, J.R. Gregório, A.E. Gerbase, *Reactive & Functional Polymers* **2005** (63) 135-141.

<sup>7</sup> I. Diaz-Acosta, J. Baker, J.F. Hinton, P. Puley, *Spectrochimica Acta Part A* **2003** (59) 363-377.

### 1.3 Aims of this study.

The following goals were set for the  $\text{Mn}(\beta\text{-diketonato})_3$  study.

- i. The synthesis of novel and existing  $\text{Mn}(\beta\text{-diketonato})_3$  complexes.
- ii. The characterization of the synthesized  $\text{Mn}(\beta\text{-diketonato})_3$  complexes with a variety of methods, such as mass spectroscopy, elemental analysis, X-ray crystallography and melting points.
- iii. The investigation of the electrochemical behaviour of the  $\text{Mn}(\beta\text{-diketonato})_3$  complexes by utilizing cyclic voltammetry and linear sweep voltammetry.
- iv. To identify the three dimensional geometry and spin state of the  $\text{Mn}(\beta\text{-diketonato})_3$  complexes by use of DFT computational methods.
- v. The establishment of relationships between the experimental results [the reduction potential ( $E_{\text{pc}}$ ) of the  $\text{Mn}^{\text{III}}/\text{Mn}^{\text{II}}$  redox couple], DFT calculated properties [electron affinity (EA), highest occupied molecular orbital (HOMO) energy and lowest unoccupied molecular orbital (LUMO) energy] and electronic parameters [acid dissociation constant ( $\text{pK}_{\text{a}}$ ) of the uncoordinated  $\beta$ -diketonato ligands, total group electronegativities  $\{\Sigma(\chi_{\text{R}} + \chi_{\text{R}'})\}$  and Hammett sigma meta constants  $\{\Sigma(\sigma_{\text{R}} + \sigma_{\text{R}'})\}$  of the R and R' side groups ( $\text{RCOCHCOR}'$ )].

The following goals were set for the  $\text{M}(\text{acac})_3$  study where  $\text{M} = \text{V}, \text{Cr}, \text{Mn}, \text{Fe}$  and  $\text{Co}$ .

- i. The investigation of the electrochemical behaviour of the  $\text{M}(\text{acac})_3$  complexes by utilizing cyclic voltammetry.
- ii. The identification of the three dimensional geometry and the spin state of the neutral species of the  $\text{M}(\text{acac})_3$  complexes by the use of DFT computational methods.
- iii. The establishment of relationships between the experimental results the [reduction potential ( $E_{\text{pc}}$ ) of the  $\text{M}^{\text{III}}/\text{M}^{\text{II}}$  redox couple], DFT calculated properties [electron affinity (EA), highest molecular orbital (HOMO) energy and lowest unoccupied molecular orbital (LUMO) energy] and electronic parameters [acid dissociation constant ( $\text{pK}_{\text{a}}$ ) of the uncoordinated  $\beta$ -diketonato ligands, total group electronegativities  $\{\Sigma(\chi_{\text{R}} + \chi_{\text{R}'})\}$  and Hammett sigma meta constants  $\{\Sigma(\sigma_{\text{R}} + \sigma_{\text{R}'})\}$  of the R and R' side groups ( $\text{RCOCHCOR}'$ )].



# 2

## Literature survey and fundamental aspects.

---

### 2.1 Computational chemistry.

#### 2.1.1 Introduction.<sup>1,2</sup>

Chemistry is known as the science involved with the creation, transformation and properties of molecules. The combination of mathematical methods with fundamental physics to study chemical processes is known as theoretical chemistry. Instead of viewing molecules being made out of atoms it can be described as a collection of charged particles, positive nuclei and negative electrons. The Coulomb interaction is the most important physical force between the charge particles for chemical phenomena to take place.

Prior to 1950, before computers, theoretical chemistry was limited to the size of molecule that could be solved with high accuracy. Since then electronic computers were designed and the use thereof became incorporated into many branches of science. Using computers as an experimental tool gave birth to what we know as computational chemistry. Computational chemistry, a subfield of theoretical chemistry, is growing at an exponential rate and is focused on solving chemical problems, by means of calculations on computers utilizing high performance clusters. Computational chemistry is primarily used to calculate geometric arrangements and relative energies and vibration frequencies with high accuracy. Spectra and molecular properties such as IR, UV, NMR, transition state and spin state can also be determined. By calculating these properties before an experiment is done, it can be predicted whether the desired complex will be obtained. This is important as some experimental processes can be difficult, dangerous, time consuming or highly expensive. Computational chemistry can thus assist chemists in such experiments.

---

<sup>1</sup> F. Jensen, *Introduction to Computational Chemistry*, 2<sup>nd</sup> edition, John Wiley & Sons Ltd, England, **2007**, p1-2.

<sup>2</sup> D.C. Young, *Computational Chemistry: A Practical Guide for Applying Techniques to Real-World Problems*, Wiley-Interscience, New York, **2001**, p3-4.

Chemical phenomena can be described by rigorous mathematics but, there can be such great mathematical difficulty that it is just not possible to solve a problem accurately. Quantum mechanics (QM) gives a mathematical description of electron behaviour that has never been found wrong. However, the hydrogen atom remains the only system where the quantum mechanical equations have been exactly solved. Therefore approximations are an integral part of computational chemistry and the results that are obtained must be handled with caution.<sup>2</sup>

### 2.1.2 Quantum mechanics.<sup>3,4,5,6</sup>

Quantum mechanics can in theory predict any property of an individual atom or molecule exactly. In practise only the one electron system has been exactly solved by the use of QM. Methods for approximating the solution of multiple electron systems have been created. The end goal of quantum mechanics is to calculate (as accurately as possible) the time-independent, non-relativistic Schrödinger equation. The general time-independent Schrödinger equation is expressed as follows:

$$H\Psi = E\Psi \quad \text{Equation 2.1}$$

Where **H** is Hamiltonian operator, E is the energy and  $\Psi$  is the wave function.  $\Psi$  is a function of electron and nuclear positions in a multiple electron system. Therefore, electrons can be described as a wave and the probability of their position in a certain location can be described. The Hamiltonian operator contains kinetic (**T**) and potential (**V**) energy for all particles in a general *N*-particle system and can be seen in **Equation 2.2**.

$$H = T + V = -\sum_{i=1}^N \frac{\nabla_i^2}{2m_i} + \sum_{i>j}^N \frac{q_i q_j}{r_{ij}} \quad \text{Equation 2.2}$$

With

$$\nabla_i^2 = \frac{\partial^2}{\partial x_i^2} + \frac{\partial^2}{\partial y_i^2} + \frac{\partial^2}{\partial z_i^2} \quad \text{Equation 2.3}$$

---

<sup>3</sup> F. Jensen, *Introduction to Computational Chemistry*, 2<sup>nd</sup> edition, John Wiley & Sons Ltd, England, **2007**, p4-15.

<sup>4</sup> W. Koch, M.C. Holthausen, *A Chemist's Guide to Density Functional Theory*, 2<sup>nd</sup> edition, Wiley-VCH, Weinhiem, **2001**, p3-6.

<sup>5</sup> D.C. Young, *Computational Chemistry: A Practical Guide for Applying Techniques to Real-World Problems*, Wiley-Interscience, New York, **2001**, p10-11.

<sup>6</sup> W.J. Hehre, *A Guide to Molecular Mechanics and Quantum Chemical Calculations*, Wavefunction, Irvine, **2003**, p21-23.

where  $\nabla_i^2$  is the Laplacian operator acting on particle  $i$ . The particles consist of electrons and nuclei. The mass and charge of particle  $i$  is  $m_i$  and  $q_i$  respectively. The kinetic energy of the particle is within a wave function and the potential energy is due to the Coulomb interaction between the particles. As mentioned earlier, approximations are needed in the Schrödinger equation when dealing with more complex systems. To this end the Born-Oppenheimer and Hartree-Fock approximations were developed.

### 2.1.3 Basis sets.<sup>7,8</sup>

Information is derived by using *ab initio* methods which solves the Schrödinger equation without fitting parameters to experimental data. A lot of approximations exist to solve the Schrödinger equation. The performance of these approximations was compared to known experimental data. Therefore, experimental data is used in the selection process of the computational model and does not take part in the computational procedure. Basis sets are approximations that are essential in all *ab initio* methods and are a set of functions that describes the shape of the molecular orbitals. Unknown molecular orbitals can be seen as a function in the infinite coordinate system that is covered by a complete basis set. A complete basis set is impossible in calculations as an infinite amount of functions are needed. A finite basis set can only describe the molecular orbital components along the coordinate axes corresponding to the chosen basis. Smaller basis sets result in poorer descriptions. The accuracy is influenced by the type of basis functions that are used. The smallest possible basis set (without compromising the accuracy) is extremely important in the calculations, since the computational effort of *ab initio* methods scales formally as  $M_{\text{basis}}^4$ .

Slater type orbitals (STO) and Gaussian type orbitals (GTO) are the two general basis functions used in electronic structure calculations. Amsterdam density functional theory (ADF) unlike any other density functional theory programme uses STO instead of GTO. Two advantages of STO are the cusp behaviour at the nucleus and the appropriate long range decay. GTO need more functionals than STO to achieve the same level of basis set quality.

---

<sup>7</sup> F. Jensen, *Introduction to Computational Chemistry*, 2<sup>nd</sup> edition, John Wiley & Sons Ltd, England, **2007**, p192-198, 207-208.

<sup>8</sup> G. Te Velde, F.M. Bickelhaupt, E.J. Baerends, C.F. Guerra, S.J.A. Van Gisbergen, J.G. Snijders, T. Ziegler, *J. Comput. Chem.*, **2001** (22) 931-967.

The ADF has a large basis set database. The minimum basis set is single-zeta (SZ) with the smallest amount of functions. The term zeta derives from the fact that the exponent of the STO is frequently denoted as the Greek letter  $\zeta$  (zeta). Double-zeta (DZ) has twice the amount of the basis functions of the single-zeta basis. Different electron distribution in different directions can be better described by doubling the amount of basis functions. Chemical bonding occurs between valence orbitals and a better description of these orbitals' electrons will be obtained by doubling the valence's orbital-functions. The next basis set is triple-zeta (TZ) which has three times the amount of functions than the minimum basis (SZ). The frozen core approximation is where the deep-core atomic orbitals are frozen. This reduces the variational size of basis sets which decreases the computational time, without sacrificing good quality results.

Polarization functions are the combination of radial correlation and angular correlation. Radial correlation is where one electron is close to the nucleus and the other one far from it. Functions of the same type, but with different exponents are needed in a basis set to describe this phenomenon. Angular correlation refers to the phenomenon when two electrons are on opposite sides of the nucleus. These polarization functions can be combined with the different zeta basis sets for instance, triple-zeta plus polarization (TZP).

### 2.1.4 Density functional theory (DFT).<sup>9,10,11</sup>

DFT was born in 1964 when Hohenberg and Kohn created a theorem that states, the ground state electronic energy is only determined by the use of electron density ( $\rho$ ). Most problems encountered when using the direct density functionals could be attributed to the way the kinetic energy was determined. Kohn and Sham realized this and in their approach created a non-interacting reference system. This system consists of a set of orbitals, known as the Kohn-Sham orbitals, such that a major part of the kinetic energy can be obtained with good accuracy. The remainder is combined with the non-classical contributions to the electron-electron repulsion. Only a small part of the total energy is now left to be determined by the use of approximate functions. The DFT energy is expressed by the Kohn-Sham approach as:

$$E_{DFT} = T_s[\rho] + E_{ne}[\rho] + J[\rho] + E_{xc}[\rho] \quad \text{Equation 2.4}$$

<sup>9</sup> F. Jensen, *Introduction to Computational Chemistry*, 2<sup>nd</sup> edition, John Wiley & Sons Ltd, England, **2007**, p232-236.

<sup>10</sup> U. von Barth, *Physica Scripta*, **2004** (T109) 9-39.

<sup>11</sup> C.J. Cramer, *Essentials of Computational Chemistry – Theories and Models*, 2<sup>nd</sup> edition, John Wiley & Sons Ltd, Chichester, **2004**, p271, 252-256.

Here  $T_s$  symbolizes the non-interacting kinetic energy,  $E_{ne}$  is the attraction between nuclei and electrons,  $J$  is the Coulomb electron-electron repulsion,  $E_{xc}$  can be described by the energy after subtracting the non-interacting kinetic energy,  $E_{ne}$  and  $J$  potential energy terms, see **Equation 2.4**.  $E_{ee}[\rho]$  is the electron-electron repulsion that consists of the Coulomb and exchange part,  $J[\rho]$  and  $K[\rho]$ .

$$E_{xc}[\rho] = (T[\rho] - T_s[\rho]) + (E_{ee}[\rho] - J[\rho]) \quad \text{Equation 2.5}$$

The greatest advantage of DFT is that it is the most cost-effective method to achieve a given accuracy. No systematic way of improving DFT calculations exists as DFT results can only be improved by using better functionals.

### 2.1.5 Exchange-correlation functionals.<sup>12,13</sup>

The exchange-correlation functional is also known as the density functional. DFT methods differ in the choice of functional form for the exchange-correlation energy. There are four well known functionals:

- **Local density approximation (LDA):** Assumes density can locally be seen as a uniform electron gas. Therefore the energy ( $E_{xc}$ ) at a given position depends only on the density at that position.
- **Generalized gradient approximation (GGA):** The first derivative of density is included as a variable and it is required that the Fermi and Coulomb holes integrate to the values of -1 and 0.
- **Meta-GGA methods:** Is an extension of GGA. Meta-GGA depends on the orbital kinetic density.
- **Hybrid-GGA methods:** A connection can be made between the exchange-correlation energy and the corresponding hole potential connecting the non-interacting reference and the actual system, by looking at the Hamiltonian and the definition of the exchange-correlation energy.

<sup>12</sup> F. Jensen, *Introduction to Computational Chemistry*, 2<sup>nd</sup> edition, John Wiley & Sons Ltd, England, **2007**, p242-255.

<sup>13</sup> C.J. Cramer, *Essentials of Computational Chemistry – Theories and Models*, 2<sup>nd</sup> edition, John Wiley & Sons Ltd, Chichester, **2004**, p257-271.

In this study GGA functionals fall into three groups namely: exchange correction, correlation correction and the combined corrections (both exchange – and correlation corrections). Examples of these groups are listed below.

Exchange correction functionals:

- **Becke (B):** A.D. Becke proposed a correction in the LDA exchange energy in 1988.
- **PW91x:** Perdew and Wang proposed this correction in 1991.
- **OPTX:** Handy and Cohen proposed this correction in 2001.

Correlation correction functionals:

- **Perdew (P):** Perdew proposed this correlation correction in 1986.
- **PW91c:** Perdew and Wang proposed this correlation correction in 1991.
- **LYP:** Lee, Yang and Parr proposed this correlation correction in 1988.

Combined corrections:

- **BP86:** The combination of Becke (B) and Perdew (P).
- **PW91:** The combination of PW91x and PW91c.
- **B3LYP:** The combination of Becke 3 parameter functional (B3) and LYP.
- **OLYP:** The combination of OPTX and LYP.

### 2.1.6 Amsterdam density functional (ADF).<sup>14</sup>

ADF was created in the seventies and is still being improved. In the seventies ADF was known as Hartree-Fock-Slater (HFS). ADF was developed to exploit the computational advantages of DFT to a maximum. The Theoretical Chemistry groups of Amsterdam and Calgary made some additions and improvements to HFS to produce a first class package for quantum-chemistry, ADF. Calculations on atoms and molecules can be done in gas or solution. ADF can be used to study geometry optimization, transition states, spectroscopy characteristics, transition states and many more properties.

---

<sup>14</sup> G. Te Velde, F.M. Bickelhaupt, E.J. Baerends, C.F. Guerra, S.J.A. Van Gisbergen, J.G. Snijders, T. Ziegler, *J. Comput. Chem.*, **2001** (22) 931-967.

## 2.2 Electrochemistry.

### 2.2.1 Introduction.<sup>15</sup>

The branch of chemistry that investigates the relationship between the electrical and chemical effects of compounds is known as electrochemistry. Electrochemistry looks at the movement of charged particles between different interfaces for example electronic conductor (an electrode) and an ionic conductor (an electrolyte). The main focus is on how these particles move and the factors that affect the movement. Therefore, electrochemistry studies an analyte by measuring the potential and/or current in an electrochemical cell. An electrochemical cell consists of a working electrode, auxiliary electrode, reference electrode and a solvent system (electrolyte dissolved in a solvent). Electrochemical techniques are used for a variety of reasons. Some might be interested in the thermodynamics of a reaction, or they want to create radicals and study the decay or spectroscopy of it, or simply analyze an analyte for the presence of trace metal ions. There are many different electrochemical techniques available. This study will focus on two of these techniques namely cyclic voltammetry and linear sweep voltammetry.

### 2.2.2 Cyclic voltammetry (CV).<sup>16,17,18</sup>

Cyclic voltammetry is the electrochemical technique that is most widely used. Cyclic voltammetry is used in the study of oxidation and reduction reactions of the analyte (species being studied). During a cyclic voltammetry scan the potential of a working electrode changes linearly over time. The scan starts at a potential where no redox reaction takes place ( $E_i$ ) and moves to a potential just after the oxidation (or reduction) takes place ( $E_{\lambda 1}$ ). The direction of the linear change in potential is then reversed where the reduction (or oxidation) of the intermediates or products formed during the forward scan can be detected. The potential goes all the way back to the starting potential ( $E_{\lambda 2}$ ). The speed at which the potential changes (scan rate), can be

---

<sup>15</sup> A.J. Bard, L.R. Faulkner, *Electrochemical Methods: Fundamentals and Applications*, 2<sup>nd</sup> edition, John Wiley & Sons, Inc., New York, **2001**, p1-2.

<sup>16</sup> P.T. Kissinger, W.R. Heineman, *J. Chem. Educ.* **1983** (60) 702-706.

<sup>17</sup> D.H. Evans, K.M. O'Connell, R.A. Petersen, M.J. Kelly, *J. Chem. Educ.* **1983** (60) 290-293.

<sup>18</sup> D.A. Skoog, D.M. West, F.J. Holler, S.R. Crouch, *Fundamentals of Analytical Chemistry*, 8<sup>th</sup> edition, Brooks/Cole, Belmont, **2004**, p694-697.

determined by the gradient of the linear potential vs time line in **Figure 2.1**. The linear change in potential is in a triangular waveform and the cycle can be repeated as seen in **Figure 2.1**.

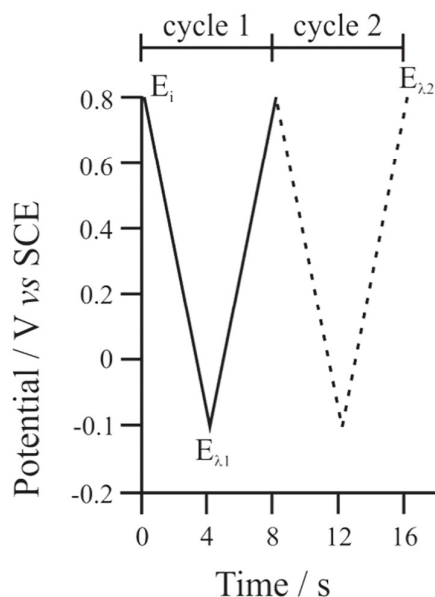


**Figure 2.1:** The linear change in potential over time.

The resulting voltammogram is given in **Figure 2.2**. The voltammogram is the current that was measured during the change of potential. The changes in the voltammogram after succession yield important information to help in the understanding of reaction mechanisms.

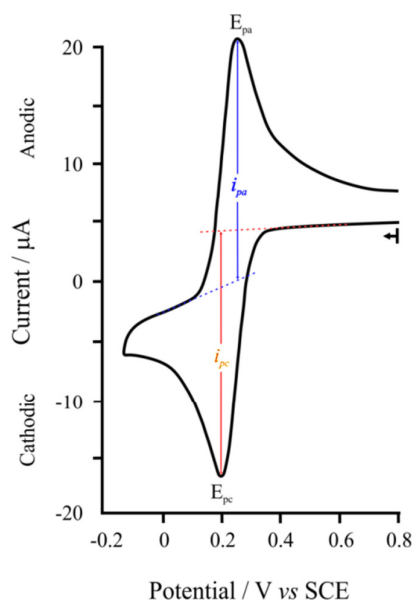


**Figure 2.2:** Cyclic voltammogram of 6 mM  $\text{K}_3\text{Fe}(\text{CN})_3$  in 1 M  $\text{KNO}_3$  at a scan rate of  $50 \text{ mV.s}^{-1}$ .<sup>19</sup>

<sup>19</sup> P.T. Kissinger, W.R. Heineman. *J. Chem. Educ.* **1983** (60) 702-706.



(i) *CV parameters of importance.*

The four most important parameters of cyclic voltammetry is the anodic peak potential ( $E_{pa}$ ), the cathodic peak potential ( $E_{pc}$ ) and the magnitudes of the anodic peak current ( $i_{pa}$ ) and the cathodic peak current ( $i_{pc}$ ), as illustrated in **Figure 2.2**. Obtaining the peak current is not as straight forward as the peak potential. The current is measured by drawing in a baseline and then calculating the current difference between the current at the peak maximum/minimum and the current at the baseline as shown in **Figure 2.2**. The accuracy of the baseline is essential in obtaining good current measurements. Baselines are sometimes difficult to draw when more complicated voltammograms are obtained. The formal reduction potential ( $E^{0'}$ ) for a reversible couple, where an anodic and cathodic reaction is observed, is between the  $E_{pa}$  and  $E_{pc}$ .

$$E^{0'} = \frac{E_{pa} + E_{pc}}{2} \quad \text{Equation 2.6}$$

The difference between the two peak potentials ( $\Delta E_p$ ) of a reversible redox couple is important in determining if the analyte is electrochemically reversible or irreversible. For a redox couple to be electrochemically reversible the theoretical value of  $\Delta E_p$  must be 59 mV at 25 °C for a one electron process. An experimental value of up to 90 mV is still seen as electrochemically reversible.<sup>20</sup> If the peak potential difference is higher than this it is most likely due to slow electron transfer at the electrode surface.

$$\Delta E_p = E_{pa} - E_{pc} \quad \text{Equation 2.7}$$

The Randle-Sevcik equation describes the peak current for a reversible system for the forward scan of the first cycle

$$i_p = (2.69 \times 10^5) n^{\frac{3}{2}} A D^{\frac{1}{2}} C v^{\frac{1}{2}} \quad \text{Equation 2.8}$$

where  $i_p$  is the peak current (Ampère, A),  $n$  is the stoichiometry of the electron,  $A$  is the electrode area (cm<sup>2</sup>),  $D$  is the diffusion coefficient (cm<sup>2</sup>.s<sup>-1</sup>),  $C$  is the concentration of the analyte (mol.cm<sup>-3</sup>) and  $v$  is the scan rate (V.s<sup>-1</sup>). The peak current is directly proportional to the concentration of the analyte. This means if the concentration of the analyte is increased the peak current will also increase. The current ratio is important in determining whether the redox couple is chemically reversible. The closer the current ratio is to 1 the more chemically reversible the redox couple. This means that the same amount of analyte reduced (or oxidized) is being oxidized (or reduced) back to the starting analyte.

$$\frac{i_{pa}}{i_{pc}} \quad \text{Equation 2.9}$$

---

<sup>20</sup> H.J. Gericke, N.I. Barnard, E. Erasmus, J.C. Swarts, M.J. Cook, M.A.S. Aquino, *Inorg. Chim. Acta* **2010** (363) 2222-2232.

(ii) *Solvent system.*

The solvent system is a very important part of an electrochemical cell. The solvent system consists of the supporting electrolyte and a solvent. This combination determines the solvent window (the potential range that can be studied). The electrolyte ensures that the charged particles can flow through the system without obstruction. A solvent system must therefore be electrochemically and chemically inert throughout the solvent window. This means that the solvent system must not undergo any electrochemical reactions nor any reaction with the intermediates and/or products formed during redox reactions of the analyte. To ensure the charged particles move as freely as possible through the system, the solvent must have low electrical resistance and the supporting electrolyte (e.g. tetrabutylammonium hexafluorophosphate) must lower electrical resistance.

### 2.2.3 Linear sweep voltammetry (LSV).<sup>21</sup>

Linear sweep voltammetry is where current is measured while potential is increased or decreased over time. The scan rate of LSV is normally in the range of 2 to 5 mV.s<sup>-1</sup>. The resulting voltammogram has the shape of a sigmoidal (J-shape) curve and is plotted as current against potential. LSV is used in conjunction with CV results in order to determine the amount of electrons taking part in the redox reactions of the analyte. This is only possible if an internal standard with a known electron redox process such as ferrocene (well-known one electron redox process) is used. The internal standard is added to the electrochemical cell with the same concentration as the analyte. The ratio between the two redox reaction heights will give the ratio of the electrons. For example, if the ratio of ferrocene:analyte is 1:3 it is clear that the analyte undergoes a 3 electron redox reaction. A typical LSV can be seen in **Figure 2.3**.

---

<sup>21</sup> D.A. Skoog, D.M. West, F.J. Holler, S.R. Crouch, *Fundamentals of Analytical Chemistry*, 8<sup>th</sup> edition, Brooks/Cole, Belmont, **2004**, 667-672.

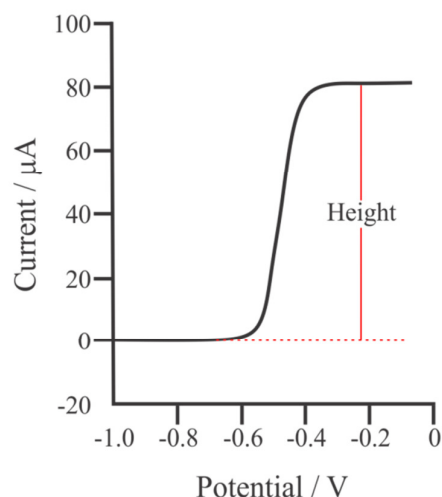


**Figure 2.3:** Typical linear sweep voltammogram of an analyte

## 2.3 Basic concepts.

### 2.3.1 Point group theory.<sup>22,23</sup>

A branch of mathematics called group theory is used in the systematic treatment of symmetry. Symmetry operations are actions where a part of the molecule can be interchanged with other parts of the molecule without changing the identity or the orientation of the molecule. The parts that interchange in this manner are equivalent to one another by symmetry. Every symmetry operation has a symmetry element (a point, line or plane) to which the symmetry operation is performed. At least one point of the molecule stays unchanged when performing these symmetry operations and that is why they are known as the operations of point group symmetry. The five important point group symmetry operations are:

(i) *Identity (E)*

The identity is the operation where no action is performed on the molecule. Therefore, each molecule at least has one symmetry operation by which they can be classified. This is needed if all molecules are to be classified by symmetry.

<sup>22</sup> F.A. Cotton, G. Wilkinson, P.L. Gaus, *Basic Inorganic Chemistry*, 3<sup>rd</sup> edition, John Wiley & Sons Ltd, New York, **1995**, p785-798.

<sup>23</sup> P.W. Atkins, T.L. Overton, J.P. Rourke, M.T. Weller, F.A. Armstrong, M. Hageman, *Shriver & Atkins' Inorganic Chemistry*, 5<sup>th</sup> edition, Oxford University Press, Great Britain, **2010**, p179-183.

(ii) *Proper rotation ( $C_n$ )*

Proper rotation is where rotation around an axis, that goes through a molecule, with an angle of  $360^\circ/n$  is possible and has a virtually unchanged molecule as a result. If this rotation is repeated  $n$  times the molecule will be in its original orientation. This operation is also known as an  $n$ -fold rotation axis abbreviated as  $C_n$ . A molecule can have more than one proper rotation operation. The operation with the highest order ( $n$ ) is called the principal axis. The principal axis is normally defined as the  $z$ -axis.

(iii) *Reflection ( $\sigma$ )*

Reflection operation is where all the atoms of a molecule can be reflected through a plane that passes through the molecule. This reflection operation ( $\sigma$ ) is also known as a mirror plane. There are three reflection operations possible. The first is a mirror plane parallel to the principal axis and is called vertical ( $\sigma_v$ ). The second is called horizontal ( $\sigma_h$ ) since the mirror plane is perpendicular to the principal axis. The third reflection operation is called dihedral which consists of a mirror plane that bisects the angle between two 2-fold rotational axes.

(iv) *Centre of inversion ( $i$ )*

The centre of inversion is where each atom of a molecule is projected through a single point to an equal distance on the other side.

(v) *Improper rotation ( $S_n$ )*

Improper rotation is defined as a rotation around an axis that goes through a molecule with an angle of  $360^\circ/n$  and then reflects all the atoms through a plane that is perpendicular to the axis. The same result will be obtained if the operation is carried out in reverse (first the reflection and then the rotations around the axis).

By using these five symmetry operations, molecules can be classified into different point groups. In this study it is important to know the difference between two of these point groups namely  $C_2$  and  $D_3$ . The  $C_2$  point group is defined as a molecule that has both an identity and a  $C_2$  proper rotation operation. This implies that the molecule has a rotation axis through the molecule where the molecule can rotate with an angle of  $180^\circ$  ( $360^\circ/2$ ). An example of a molecule that belongs to the  $C_2$  point group can be seen in **Figure 2.4**.

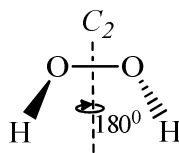


**Figure 2.4:** Hydrogen peroxide ( $\text{H}_2\text{O}_2$ ) is a simple example of a  $C_2$  molecule.

A molecule that belongs to the  $D_3$  point group can be seen in **Figure 2.5**. This molecule consists of the following symmetry operations; an identity, three  $C_2$  proper rotations and a  $C_3$  proper rotation.

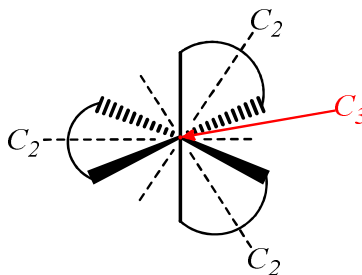


**Figure 2.5:** An octahedral example of  $D_3$  molecule.  $C_3$  proper rotation operation is perpendicular to the page.

### 2.3.2 Ligand field theory.<sup>24</sup>

Ligand field theory is the theoretical apparatus used in the understanding of the bonding and associated electronic properties of transition metal complexes. The valence theories that are applied to the compounds of main group elements can be applied to the transition metal compounds too, since the bonding of these compounds are fundamentally similar. Just as in other cases applying the molecular orbital (MO) theory to transition metal compounds gives useful results. However, two things that make the study of the electronic structures of transition metal compounds different from the remaining body of valance theory is; the presence of partly filled  $d$  and  $f$  orbitals as well as crystal field theory that provides a powerful yet simple method of understanding and comparing all of the properties that arise from these partly filled orbitals.

<sup>24</sup> F.A. Cotton, G. Wilkinson, P.L. Gaus, *Basic Inorganic Chemistry*, 3<sup>rd</sup> edition, John Wiley & Sons Ltd, New York, 1995, p503-504.

2.3.2.1 Crystal field theory.<sup>24,25</sup>

In crystal field theory the ligand pair is seen as a negative point charge that repels the electrons in the  $d$ -orbitals of the central metal ion. The electrons will therefore prefer to occupy the  $d$ -orbital(s) that are further away from these negative point charges. This results in the splitting of the  $d$ -orbitals into groups of different energies. The factors that influence the splitting of the five  $d$ -orbitals are the character and charge of the metal as well as the nature and manner in which the negative point group charges, ligands, are spread around the metal ion. The most common type of geometry in metal complexes is octahedral. The shape of the five  $d$ -orbitals of a metal can be seen in **Figure 2.6**.

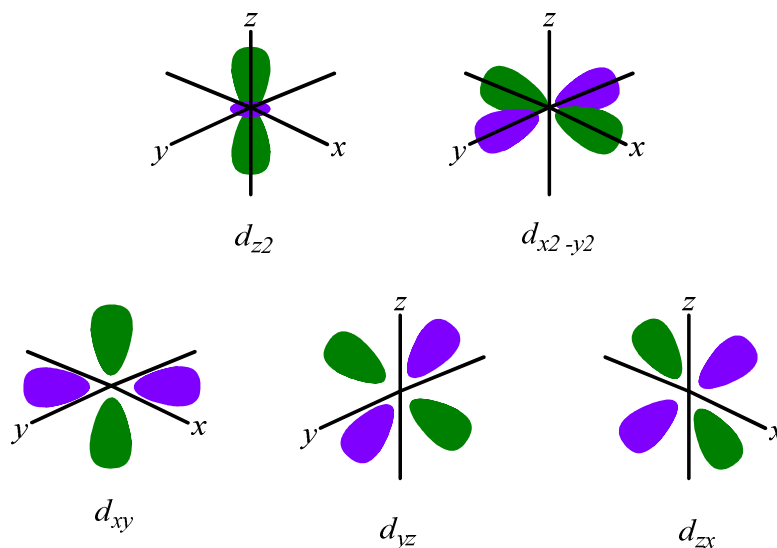


**Figure 2.6:** The electron density distribution of the five metal  $d$ -orbitals.

There are two orbitals where the lobes are directly on the axes namely the  $d_{z^2}$  (orbital on the  $z$ -axis) and the  $d_{x^2-y^2}$  (orbital on both the  $x$ - and the  $y$ -axis). The remaining three orbitals ( $d_{xy}$ ,  $d_{yz}$ ,  $d_{zx}$ ) are situated between the axes.

<sup>25</sup> P.W. Atkins, T.L. Overton, J.P. Rourke, M.T. Weller, F.A. Armstrong, M. Hageman, *Shriver & Atkins' Inorganic Chemistry*, 5<sup>th</sup> edition, Oxford University Press, Great Britain, **2010**, p473.

(i) *Octahedral complexes.*<sup>26,27</sup>

An octahedral complex is where six ligands surround a central metal octahedrally ( $ML_6$ ); a graphical representation of an octahedral complex can be seen in **Figure 2.7**.

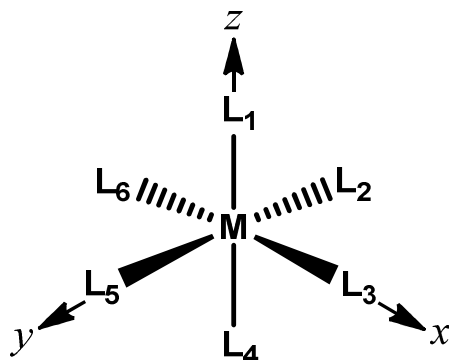


**Figure 2.7:** Octahedral complex.

These negative point charged ligands interact strongly with the metal ion. Since the  $d$ -orbitals are located in different positions they interact to different extents with the ligands. The orbitals that are located on the axes ( $d_{z^2}$ ,  $d_{x^2-y^2}$ ) and the ligands will have strong repulsion since they are in such close vicinity to each other. The other three orbitals ( $d_{xy}$ ,  $d_{yz}$ ,  $d_{xz}$ ) will have a small repulsion factor and therefore the electrons will prefer to be located in these three orbitals. The lower the repulsion factor the lower the energy of the orbital or the more stable the orbital. It is clear that the  $d$ -orbitals of the complex is divided into two groups, namely the lower in energy three degenerate  $t_{2g}$  orbital group ( $d_{xy}$ ,  $d_{yz}$ ,  $d_{xz}$ ) and the higher in energy doubly degenerate  $e_g$  orbital group ( $d_{z^2}$ ,  $d_{x^2-y^2}$ ). The splitting of the octahedral  $d$ -orbitals can be seen in **Figure 2.8**. The energy difference between the  $t_{2g}$  and the  $e_g$  orbital groups is known as  $\Delta_0$ . **Figure 2.8** shows that the  $t_{2g}$  orbital group is  $2/5 \Delta_0$  lower in energy than the  $d$ -orbitals in the spherical environment and  $e_g$  is  $3/5 \Delta_0$  higher in energy. This splitting pattern, where the algebraic sum of all the energy shifts of all orbitals is zero, is said to “maintain the center of gravity” of the set of levels. The  $\Delta_0$  value is dependent on the identity and oxidation state of the central metal ion and the character of the ligands.

<sup>26</sup> F.A. Cotton, G. Wilkinson, P.L. Gaus, *Basic Inorganic Chemistry*, 3<sup>rd</sup> edition, John Wiley & Sons Ltd, New York, **1995**, p505-506.

<sup>27</sup> P.W. Atkins, T.L. Overton, J.P. Rourke, M.T. Weller, F.A. Armstrong, M. Hageman, *Shriver & Atkins' Inorganic Chemistry*, 5<sup>th</sup> edition, Oxford University Press, Great Britain, **2010**, p473-475.

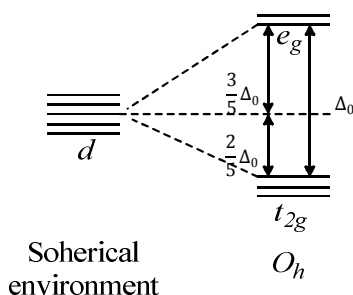


**Figure 2.8:** Octahedral  $d$ -orbital splitting.

### 2.3.2.2 Molecular orbital (MO) theory.<sup>28,29</sup>

Crystal field theory is a model that describes the  $d$ -orbital splitting into subsets in ligand environments. This theory has a drawback because it describes ligands as negative point charges and does not take into account that ligand and metal ion orbitals overlap each other. A more general, more comprehensive and potentially more accurate way to treat the electronic structures of complexes is by using MO theory. To explain the MO theory concept we will look at an octahedral complex ( $ML_6$ ), where the ligand first consists of  $\sigma$ -orbitals only after which the effect of  $\pi$ -orbital bonding will be explained.

#### (i) $\sigma$ -orbital bonding.

The six  $\sigma$ -orbitals are  $\sigma_x$  and  $\sigma_{-x}$  (from the ligands along the  $x$ -axis),  $\sigma_y$  and  $\sigma_{-y}$  (from the ligands along the  $y$ -axis), and  $\sigma_z$  and  $\sigma_{-z}$  (from the ligands along the  $z$ -axis). Ligand group orbitals can be formed by combining the  $\sigma$ -orbitals of the ligands. Every combination of the  $\sigma$ -orbitals has the proper symmetry to overlap with only one of the metal  $s$ ,  $p$  or  $d$  orbitals. These combinations and their matching metal orbitals can be seen in **Figure 2.9**.

<sup>28</sup> F.A. Cotton, G. Wilkinson, P.L. Gaus, *Basic Inorganic Chemistry*, 3<sup>rd</sup> edition, John Wiley & Sons Ltd, New York, **1995**, p509-512.

<sup>29</sup> P.W. Atkins, T.L. Overton, J.P. Rourke, M.T. Weller, F.A. Armstrong, M. Hageman, *Shriver & Atkins' Inorganic Chemistry*, 5<sup>th</sup> edition, Oxford University Press, Great Britain, **2010**, p483-487.



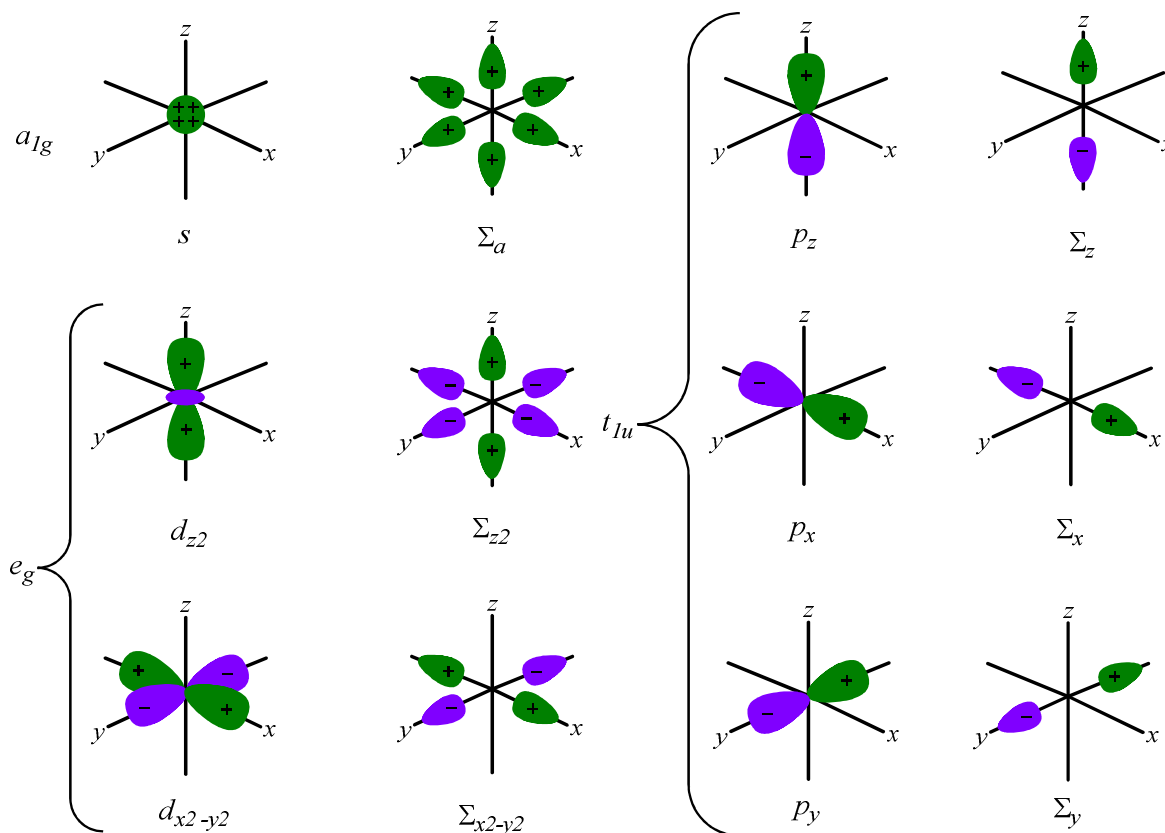


**Figure 2.9:** The six metal orbitals with  $\sigma$  symmetry and the ligand group orbitals ( $\Sigma$ ) that overlap these metal orbitals.

Every overlap forms a bonding MO and anti-bonding MO. The  $s$ -orbital of the metal and the ligand group orbital  $\Sigma_a$  overlap to give one bonding and one anti-bonding. The doubly degenerate  $e_g$  orbital group of the metal and the ligand group orbitals overlap to give two bonding and two anti-bonding molecular orbitals. The three  $t_{1u}$  metal orbitals and three  $t_{1u}$  ligand group orbitals give three bonding and three anti-bonding molecular orbitals. There are six bonding combinations and six anti-bonding combinations in total. The  $t_{2g}$  group orbitals of the metal are non-bonding and stay fully localized around the metal atom.

(ii)  $\pi$ -orbital bonding.

The MO approach can be generalized by assuming that the ligands also have  $\pi$ -orbitals. To understand the  $\pi$  bonding better it must be made clear that when atomic orbitals overlap strongly they mix strongly too. As a result, the bonding molecular orbitals are lower in energy and the anti-bonding molecular orbitals are higher in energy than the atomic energy. Atomic orbitals with different energies slightly mix even when the overlap is large. There are two different kinds of  $\pi$  ligands namely  $\pi$ -donor ligand and the  $\pi$ -acceptor ligands.

A  $\pi$ -donor ligand has filled  $\pi$ -orbitals, the energy of these orbitals are normally not higher than  $\sigma$ -donor orbitals and therefore will also be lower than the  $d$ -orbitals of the metal centre. Since the  $\pi$ -donor orbitals of the ligand are lower in energy than the partially filled metal  $d$ -orbitals the bonding molecular orbitals are lower in energy than the ligand orbitals and the anti-bonding molecular orbitals lie above the energy of the  $d$ -orbitals of the free metal atom. The ligand  $\pi$ -orbitals donate the electrons to the previously non-bonding orbitals in the octahedral  $t_{2g}$  orbital group of the central metal. The non-bonding orbitals are now newly formed anti-bonding  $t_{2g}$  orbitals and are closer in energy to the  $e_g$  group orbitals. An example of  $\pi$ -donor ligand orbital overlapping the  $d$ -orbital of the central metal can be seen in **Figure 2.10 (a)**.

The  $\pi$ -accepting ligand has empty  $\pi$ -orbitals that are ready to accept electrons. The energy of  $\pi$ -accepting orbitals is higher than the  $d$ -orbitals of the metal, therefore bonding  $t_{2g}$  molecular orbitals largely consist out of the metal  $d$ -orbitals. The bonding molecular orbital lies lower in energy than the  $d$ -orbitals of the metal. An example of  $\pi$ -accepting ligand orbital overlapping the  $d$ -orbital of the central metal can be seen in **Figure 2.10 (b)**.

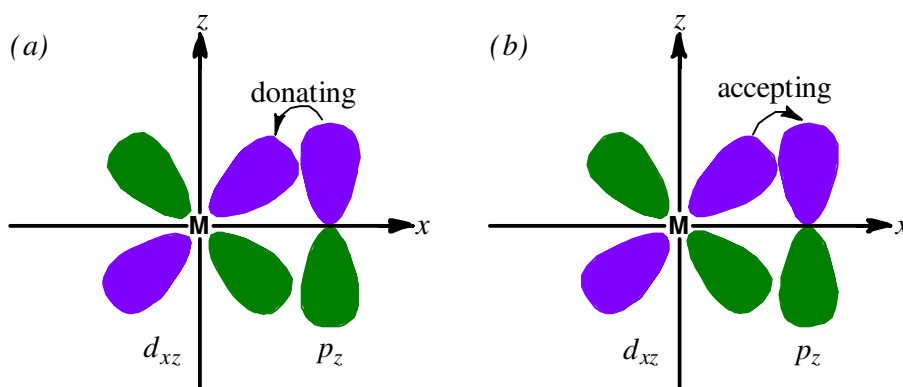


**Figure 2.10:** (a) The bond formation where  $d_{xz}$  orbital of the metal accept an electron(s) from the  $p_z$   $\pi$ -donor orbital of the ligand. (b) The bond formation where the empty anti-bonding  $p_z$  orbital of the ligand accepts electron(s) from the  $d_{xz}$  orbital of the metal.

### 2.3.2.3 Low-spin and high-spin.<sup>30</sup>

The electrons can occupy the  $d$ -orbitals of an octahedral complex in different manners; it all depends on the  $\Delta_0$  magnitude and the pairing energy of the electrons (P). The first three electrons can fill the orbitals without any hesitation as they follow Hund's first rule and fill the  $t_{2g}$  orbitals with their spins parallel regardless of the strength of the crystal field ( $\Delta_0$  magnitude). Similarly complexes that have a metal center with eight, nine or ten electrons in the  $d$ -orbitals ( $d^8$ ,  $d^9$  and  $d^{10}$  respectively) only have one possible orbital filling and this can be seen in **Figure 2.11**.

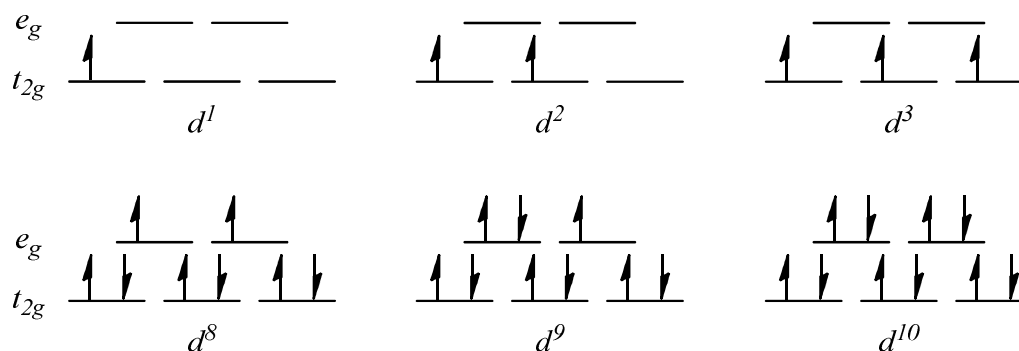


**Figure 2.11:** The  $d$ -orbital electron filling of  $d^1$ ,  $d^2$ ,  $d^3$ ,  $d^8$ ,  $d^9$  and  $d^{10}$  metal center.

When it comes to the complexes that have a metal ion with  $d^4$ ,  $d^5$ ,  $d^6$  and  $d^7$  configurations, two ways of orbital filling namely low-spin or high-spin are possible as illustrated in **Figure 2.12**. The configuration with the least amount of unpaired electrons is known as low-spin configuration and the one with the most unpaired electrons is known as high-spin configuration. The notation that is used to illustrate the amount of electrons in the  $t_{2g}$  orbital group is given by  $t_{2g}^3$  for three electrons. The two possibilities of a  $d^4$  metal ion are therefore written as  $t_{2g}^4 e_g^0$  and  $t_{2g}^3 e_g^1$ . Since the pairing energy is the same for all electrons it is safe to say that the determining factor on the spin state is the magnitude of  $\Delta_0$ . Therefore, if the magnitude of  $\Delta_0$  is higher in energy than the pairing energy the electrons will prefer to pair with the other electrons in  $t_{2g}$  first before going to the  $e_g$  orbital group since it takes up less energy (low-spin). When the magnitude of  $\Delta_0$  is lower than the pairing energy the electrons will prefer to be unpaired in the  $e_g$  orbital group before they will pair up with other electrons (high-spin).

<sup>30</sup> F.A. Cotton, G. Wilkinson, P.L. Gaus, *Basic Inorganic Chemistry*, 3<sup>rd</sup> edition, John Wiley & Sons Ltd, New York, 1995, p514-516.

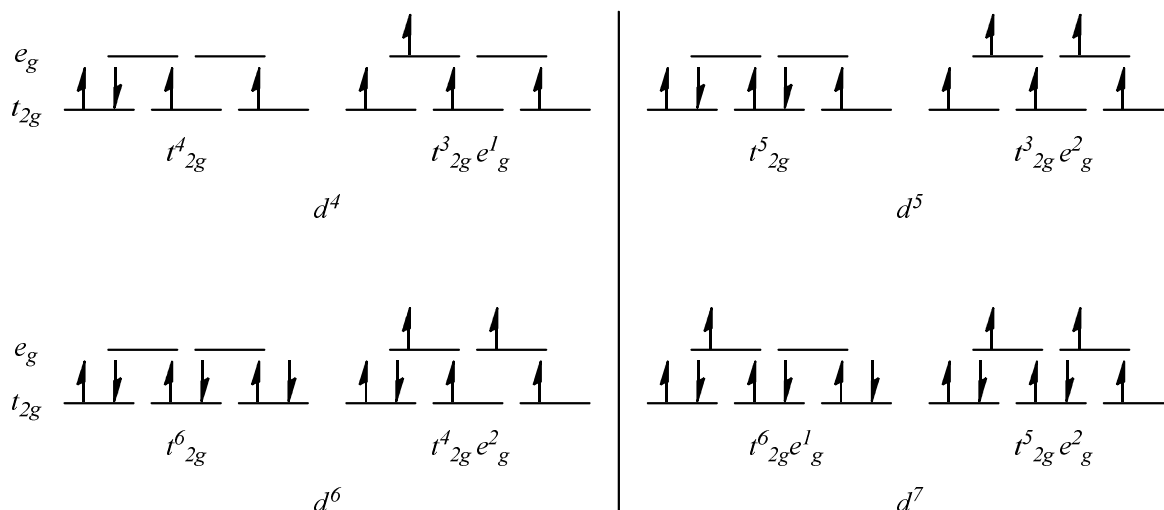


**Figure 2.12:** The  $d$ -orbital low-spin and high-spin electron filling possibilities of  $d^4$ ,  $d^5$ ,  $d^6$  and  $d^7$  metal center.

### 2.3.2.4 Jahn-Teller distortion.<sup>31,32</sup>

Jahn and Teller proved that no non-linear molecule can be stable in a degenerate electronic state. The molecule must be distorted to break the degeneracy. Octahedral complexes with  $d^9$  and high spin  $d^4$  ions are often distorted to do just this. There is one vacancy in the  $e_g$  orbital group, either in  $d_{x^2-y^2}$  or in  $d_{z^2}$  orbital. The two possible ways to fill these orbitals ( $d_{x^2-y^2}^2 d_{z^2}^1$  or  $d_{x^2-y^2}^1 d_{z^2}^2$  for  $d^9$ ,  $d_{x^2-y^2}^1 d_{z^2}^0$  or  $d_{x^2-y^2}^0 d_{z^2}^1$  for high spin  $d^4$ ) are of equal energy. According to Jahn and Teller this is not stable and the octahedron must distort in such a way that the two configurations as mentioned are not equal. When looking for example at the configuration of  $d_{x^2-y^2}^1 d_{z^2}^2$  ( $d^9$ ) and  $d_{x^2-y^2}^0 d_{z^2}^1$  ( $d^4$ ) the ligand in the  $z$ -axis is shielded more from the charge of the central metal ion than the other four ligands along the  $x$  and  $y$  axes. To remove this degeneracy the ligands on the  $z$ -axis will move further away from the central metal ion (negative Jahn-Teller distortion). This makes the  $d_{z^2}$  orbital more stable than the  $d_{x^2-y^2}$  orbital, as is shown in **Figure 2.13**. The opposite distortion is expected from the  $d_{x^2-y^2}^2 d_{z^2}^1$  ( $d^9$ ) and  $d_{x^2-y^2}^1 d_{z^2}^0$  ( $d^4$ ) configurations (positive Jahn-Teller distortion).

<sup>31</sup> F.A. Cotton, G. Wilkinson, P.L. Gaus, *Basic Inorganic Chemistry*, 3<sup>rd</sup> edition, John Wiley & Sons Ltd, New York, **1995**, p538-539.

<sup>32</sup> I. Diaz-Acosta, J. Baker, J.F. Hinton, P. Puley, *Spectrochimica Acta Part A* **2003** (59) 363-377.

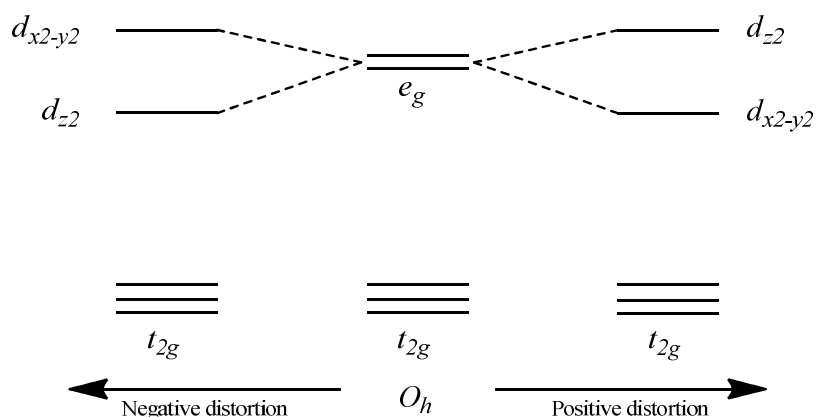


**Figure 2.13:** The Jahn-Teller distortion in the perspective of energy change of the  $e_g$  orbitals.

The Jahn-Teller distortion can also be explained by the use of point groups. When there is a change in the point group of the complex the  $d$ -orbitals of the metal changes in energy. These changes can be observed in **Figure 2.14**. The octahedral symmetry that is found in the middle has no distortion. The  $t_{2g}$  orbital split into an  $a$  and  $e$  component when going to the  $D_3$  symmetry. When a system is Jahn-Teller unstable, the highest occupied molecular orbital is degenerate and partially filled, it will spontaneously distort to the  $C_2$  symmetry.  $C_2$  symmetry is where the degeneracy of the  $e$  orbitals are split into an  $a + b$  components to stabilize the complex. High spin complexes such as  $d^2$  and  $d^4$  species would be Jahn-Teller unstable and therefore spontaneously distort to  $C_2$  symmetry.

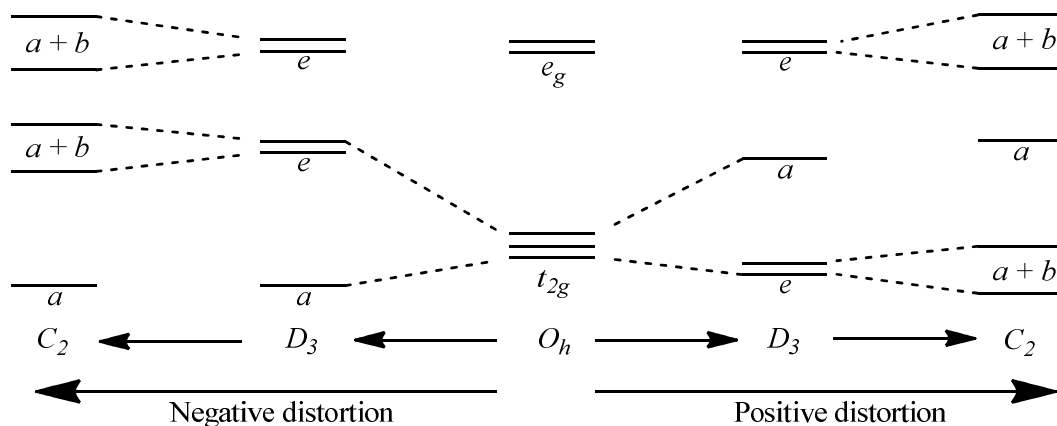


**Figure 2.14:** Octahedral orbital energy changes during Jahn-Teller distortion (Not done to scale).

A negative Jahn-Teller distortion is where there is an elongation of the M-L bond lengths on the  $z$ -axis or a shortening of the bond lengths on the  $x$  and  $y$  axes. The positive Jahn-Teller distortion is just the opposite, the shortening of M-L bond lengths on the  $z$ -axis or the elongation of the M-

L bond lengths on the  $x$ - and  $y$ -axes. The effect that the Jahn-Teller distortion has on the M-L bond lengths can be seen in **Figure 2.15**.

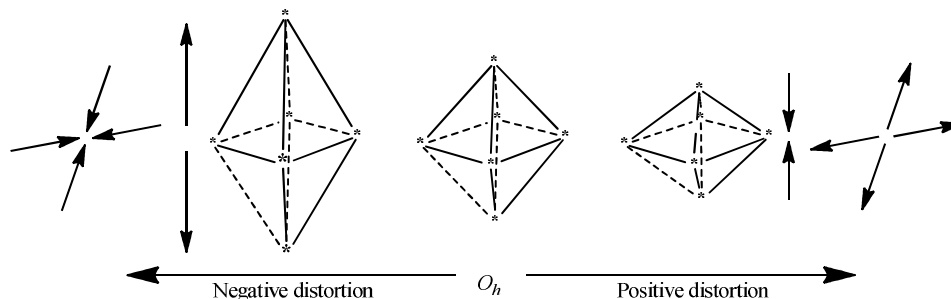


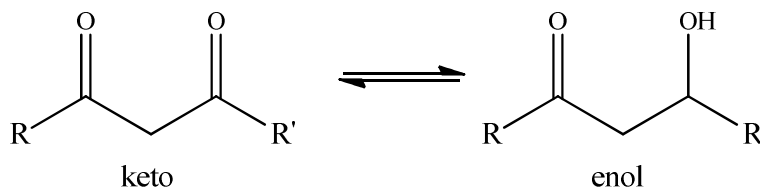
**Figure 2.15:** Negative and positive Jahn-Teller distortion effect on the M-L bond lengths.

## 2.4 Tris( $\beta$ -diketonato)manganese(III), $\text{Mn}(\beta\text{-diketonato})_3$ .

### 2.4.1 Introduction.<sup>33,34</sup>

Almost a third of all enzymes have a metal atom, especially transition metals, as an active catalytic centre. Mn, Fe, Co, Cu, Zn and Mo are involved in binding of substrates to ensure their orientation is correct for subsequent reaction, to facilitate oxidation/reduction and electron transport reactions through reversible changes in the metal oxidation state, and electrostatically stabilizing negative charges.

The general structure of a  $\beta$ -diketone is shown in **Scheme 2.1**. The free  $\beta$ -diketones are found in two forms namely the keto and enol form.



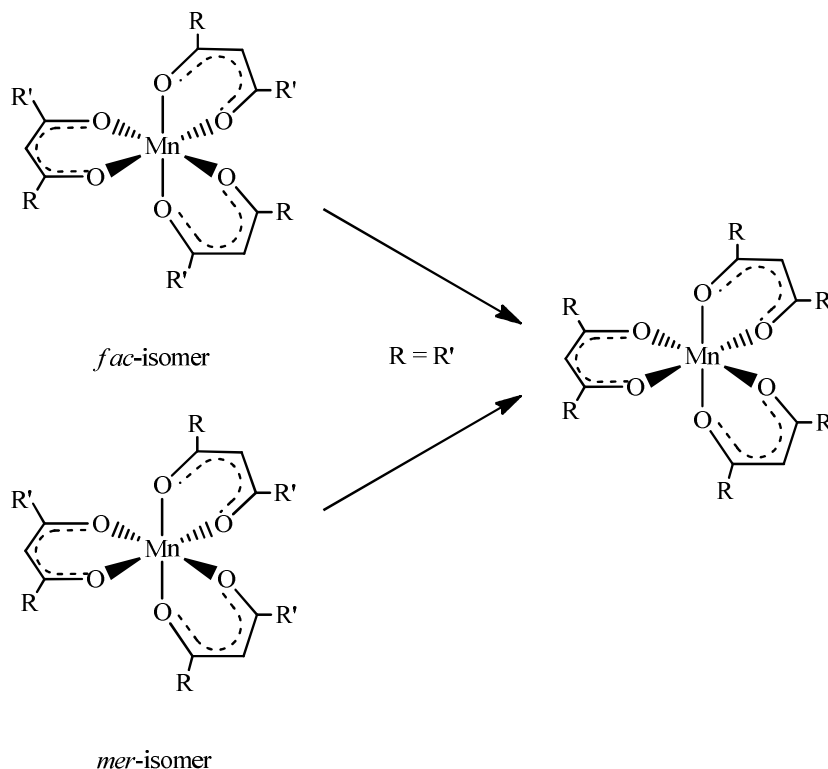
**Scheme 2.1:** General structure of a  $\beta$ -diketone (keto and enol form of a  $\beta$ -diketone).

$\beta$ -diketones can be symmetrical or non-symmetrical. A symmetrical  $\beta$ -diketonato ligand is where the R-groups are the same and a non-symmetrical  $\beta$ -diketonato ligand is where the R-groups differ. When non-symmetrical  $\beta$ -diketonato ligands bind to manganese to form  $\text{Mn}(\beta\text{-diketonato})_3$  two products are possible namely the *fac*-isomer and the *mer*-isomer. The

<sup>33</sup> I. Diaz-Acosta, J. Baker, J.F. Hinton, P. Puley, *Spectrochimica Acta Part A* **2003** (59) 363-377.

<sup>34</sup> R. van Gorkum, E. Bouwman, J. Reedijk, *Inorg. Chem.* **2004** (43) 2456-2458.

difference between the *fac*- and *mer*-isomers is that one of the  $\beta$ -diketonato ligand's R-groups are "switched around", as illustrated in **Scheme 2.2** (left). If  $\text{Mn}(\beta\text{-diketonato})_3$  complex has symmetrical  $\beta$ -diketonato ligands there is only one product possible, this can be seen in **Scheme 2.2** (right).



**Scheme 2.2:** Symmetrical  $\beta$ -diketonato ligands on manganese have only one product.

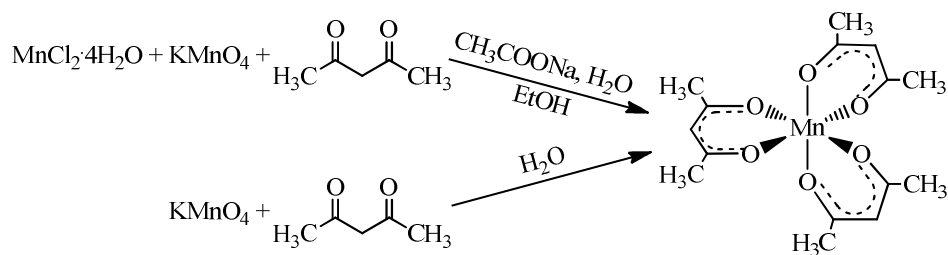
## 2.4.2 Synthesis.<sup>35,36</sup>

The well-known  $\text{Mn}(\text{acac})_3$  complex is generally synthesized by one of two methods shown in **Scheme 2.3**. In the first method acetylacetone is added to  $\text{MnCl}_2 \cdot 4\text{H}_2\text{O}$  dissolved in water:ethanol (1:1) and  $\text{KMnO}_4$  is then added slowly. Thereafter sodium acetate that has been dissolved in ethanol is added to the mixture in excess.<sup>35</sup>  $\text{KMnO}_4$  is used in the oxidation of  $\text{Mn}^{2+}$  with acetylacetone present. The precipitation of the product drives the reaction to completion. The excess sodium acetate can cause the product to be impure. The second method is known as a direct synthesis, where acetylacetone is added to an aqueous solution of  $\text{KMnO}_4$ .<sup>36</sup> The  $\text{Mn}(\text{acac})_3$  precipitates and drives the reaction to completion. Other  $\text{Mn}(\beta\text{-diketonato})_3$  complexes ( $\beta$ -diketonato = benzoylacetonato (ba), trifluoroacetylacetonato (tfaa),

<sup>35</sup> M.M. Ray, J.N. Adhya, N.G. Podder, S.N. Poddar, *Aust. J. Chem.* **1968** (21) 801-802.

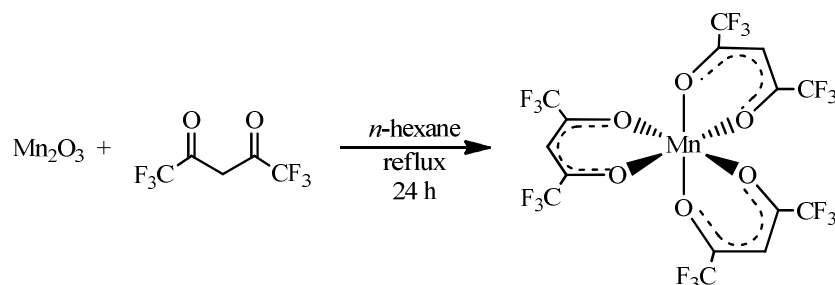
<sup>36</sup> M.N. Bhattacharjee, M.K. Chaudhuri, D.T Khathing, *Dalton Trans.* **1982** (3) 669-670.

thenoyltrifluoroacetato (tfth), trifluorobenzoylacetonato (tfba), dibenzoylmethanato (dbm), trifluorofuroylacetato (tffu)] were synthesized by the use of the same methods seen in **Scheme 2.3**.



**Scheme 2.3:** Methods used in synthesis of Mn(acac)<sub>3</sub>.

The Mn(hfac)<sub>3</sub> complex was synthesized by refluxing Mn<sub>2</sub>O<sub>3</sub> with hexafluoroacetylacetone (Hhfac) in dry *n*-hexane for 24 h under N<sub>2</sub> atmosphere. The excess solvent and Hhfac was then removed under vacuum. Recrystallization of the complex was done twice in an evacuated ampule at 55-60 °C<sup>37</sup> or by sublimation at 65 – 70 °C<sup>38</sup>. The reaction can be seen in **Scheme 2.4**.



**Scheme 2.4:** Method used to synthesize Mn(hfac)<sub>3</sub>.

<sup>37</sup> H. Zhang, B. Li, E.V. Dikarev, *J Clust Sci* **2008** (19) 311-321.

<sup>38</sup> J.R. Bryant, J.E. Taves, J.M. Mayer, *Inorg. Chem.* **2002** (41) 2769-2776.



### 2.4.3 Structure and properties.

Manganese(III) octahedral complexes are known to be high-spin complexes that undergo Jahn-Teller distortion<sup>39,40</sup> because of the partial filling of the doubly degenerate  $e_g$  orbital group. In 1964 Morosin and Brathovde<sup>41</sup> found that  $\text{Mn}(\text{acac})_3$  does not have the expected Jahn-Teller distortion. Later it was discovered that the crystal data Morosin and Barthovde had was that of  $\text{Co}(\text{acac})_3$  and not of  $\text{Mn}(\text{acac})_3$ . In 1973 new crystal data was obtained by Fackler and Avdeef<sup>42</sup> which showed that the  $\text{Mn}(\text{acac})_3$  complex does undergo Jahn-Teller distortion. Up to date only a few  $\text{Mn}(\beta\text{-diketonato})_3$  crystals have been solved. The data obtained from the solved  $\text{Mn}(\beta\text{-diketonato})_3$  crystals are summarized in **Table 2.1**. The summary includes the temperature at which the crystal data was collected. These  $\text{Mn}(\beta\text{-diketonato})_3$  crystals illustrated either a negative or positive Jahn-Teller distortion.

---

<sup>39</sup> I. Diaz-Acosta, J. Baker, J.F. Hinton, P. Puley, *Spectrochimica Acta Part A* **2003** (59) 363-377.

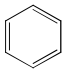
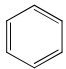

<sup>40</sup> S. Geremia, N. Demitri, *J. Chem. Educ.* **2005** (82) 460-465.

<sup>41</sup> B. Morosin, J.R. Brathovde, *Acta Crystallogr.* **1964** (17) 705.

<sup>42</sup> J.P. Fackler Junior, A. Avdeef, *Inorg. Chem.* **1974** (13) 1864.

# LITERATURE SURVEY AND FUNDAMENTAL ASPECTS

**Table 2.1:** Summary of the structural data of Mn( $\beta$ -diketonato)<sub>3</sub> crystals.

$\beta$ -diketone (RCOCHCOR')		Negative Jahn-Teller distortion		Positive Jahn-Teller distortion		Average O-Mn-O (°)	Temp. (K)	Ref
R	R'	Average Mn-O distance of the four shortest (Å)	Average Mn-O distance of the longest trans from each other (Å)	Average Mn-O distance of the four longest (Å)	Average Mn-O distance of the shortest trans from each other (Å)			
CH <sub>3</sub>	CH <sub>3</sub>	1.965	2.011	-	-	89.63	RT	<b>43</b>
		1.934	2.111	-	-	89.21	RT	<b>44</b>
		1.948	2.110	-	-	89.56	100	<b>45</b>
		1.952	2.086	-	-	89.41	100	
		-	-	2.019	1.916	89.07	RT	
		-	-	2.023	1.939	90.10	RT	
		-	-	2.008	1.967	88.63	RT	
		-	-	2.008	1.970	90.13	RT	
		-	-	2.026	1.924	89.43	223	<b>46</b>
		-	-	2.008	1.962	89.67	223	
		-	-	2.018	1.959	89.33	223	
		-	-	2.033	1.920	89.47	223	
		1.913	2.109	-	-	88.30	RT	<b>47</b>
		1.923	2.126	-	-	88.33	RT	<b>48</b>
CF <sub>3</sub>	CF <sub>3</sub>	-*	-*	-*	-*	-*	114.15	<b>49</b>
		-*	-*	-*	-*	-*	98.15	
		-	-	2.166	2.142	82.50	RT	<b>50</b>
		-	-	2.165	2.141	83.20	220	<b>51</b>
CF <sub>3</sub>		-*	-*	-*	-*	-*	-	<b>52</b>

\* No structural parameters available

**43** J.P. Fackler Junior, A. Avdeef, *Inorg. Chem.* **1974** (13) 1864-1875.

**44** B.R. Stults, R.S. Marianelli, V.W. Day, *Inorg. Chem.* **1979** (18) 1853-1858.

**45** S. Geremia, N. Demitri, *J. Chem. Educ.* **2005** (82) 460-465.

**46** R. Frohlich, R. Milan, S. Yadava, *Private communication* **2008**.

**47** E.G. Zaitseva, I.A. Baidina, P.A. Stabnikov, S.V. Borisov, I.K. Igumenov, *Zh. Strukt. Khim. (Russ.) (J. Struct. Chem.)* **1990** (31) 184.

**48** A.L. Barra, D. Gatteschi, R. Sessoli, G.L. Abbati, A. Cornia, A.C. Fabretti, M.G. Uytterhoeven, *Angew. Chem. Int. Ed.* **1997** (36) 2329.

**49** E. Bouwman, K.G. Caulton, G. Christou, K. Folting, C. Gasser, D.N. Hendrickson, J.C. Huffman, E.B. Lobkovsky, J.D. Martin, P. Michel, H. Tsai, Z. Xue, *Inorg. Chem.* **1993** (32) 3463.

**50** J.R. Bryant, J.E. Taves, J.M. Mayer, *Inorg. Chem.* **2002** (41) 2769.

**51** S. Parsons, R. Winpenney, P. Wood, *Private Communication* **2004** (2) 72.

**52** W.O. McSharry, M. Cefola, J.G. White, *Inorg. Chim. Acta* **1980** (38) 161.

It was found by Geremia and Demitri that the  $\text{Mn}(\text{acac})_3$  crystal can undergo a solid-solid phase transition (positive to a negative Jahn-Teller distortion) at a temperature of 180 K.<sup>45</sup> This new crystal stayed unchanged when temperatures were brought back to room temperature. An illustration of the two crystals can be seen in **Figure 2.16**.

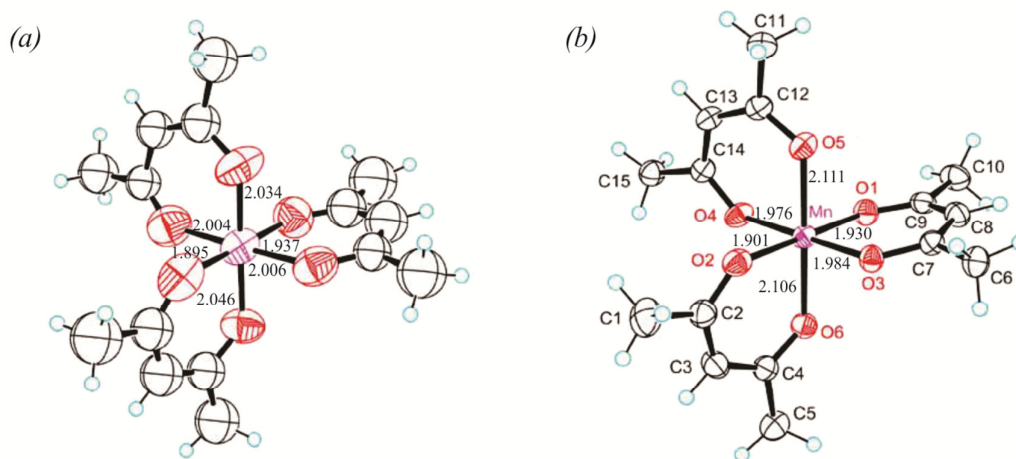


**Figure 2.16:** The solid-solid phase transition of  $\text{Mn}(\text{acac})_3$ . (a) The original crystal (positive Jahn-Teller distortion) at room temperature and (b) the transitioned crystal formed at 180 K (negative Jahn-Teller distortion).<sup>45</sup>

#### 2.4.4 Cyclic voltammetry.<sup>53,54,55</sup>

There were no extensive electrochemical studies done on  $\text{Mn}(\beta\text{-diketonato})_3$  complexes.  $\text{Mn}(\text{acac})_3$  is the only complex studied and an example is shown in **Figure 2.17**. Two redox reactions are observed during the cyclic voltammetry experiment. The metal centre is oxidized in a chemically and electrochemically reversible process at high potentials from  $\text{Mn}^{3+}$  to  $\text{Mn}^{4+}$  and reduced in an electrochemically irreversible process from  $\text{Mn}^{3+}$  to the  $\text{Mn}^{2+}$  species at lower potentials. Two studies, one from 1975 and the other from 2007, both suggested the same oxidation reaction where the  $[\text{Mn}^{\text{III}}(\text{acac})_3]^0$  oxidize to  $[\text{Mn}^{\text{IV}}(\text{acac})_3]^{+1}$  see **Scheme 2.5 (a)**. Bond proposed  $[\text{Mn}^{\text{II}}(\text{acac})_3]^{-1}$  forms during the reduction process, while Paczeński proposed that a  $\text{acac}^{-1}$  ligand is lost during the reduction process, see **Scheme 2.5 (b) and (c)**. The cyclic voltammogram information can be seen in **Table 2.2**.

<sup>53</sup> A.M. Bond, R.I. Martin, A.F. Masters, *Inorg. Chem.* **1975** (14) 1432–1435.

<sup>54</sup> T. Paczeński, P. Błoniarczyk, K. Rydel, A. Sobkowiak, *Electroanalysis* **2007** (19) 945–951.

<sup>55</sup> R. van Gorkum, E. Bouwman, J. Reedijk, *Inorg. Chem.* **2004** (43) 2456–2458.

## LITERATURE SURVEY AND FUNDAMENTAL ASPECTS

**Table 2.2:** Summary of cyclic voltammetry experiment data of  $\text{Mn}(\text{acac})_3$ .

$\beta$ -diketone ( $\text{RCOCHCOR}$ ) <sup>-</sup>		$\text{Mn}^{\text{III}} \rightarrow \text{Mn}^{\text{II}}$				$\text{Mn}^{\text{III}} \rightarrow \text{Mn}^{\text{IV}}$				Ref
R	R'	$E_{\text{pc}}$ (V)	$E_{\text{pa}}$ (V)	$\Delta E_{\text{p}}$ (mV)	$E^{0'}$ (V)	$E_{\text{pc}}$ (V)	$E_{\text{pa}}$ (V)	$\Delta E_{\text{p}}$ (mV)	$E^{0'}$ (V)	
$\text{CH}_3$	$\text{CH}_3$	-0.37	0.1	470	-0.135	0.86	0.99	130	0.925	<sup>56</sup> <sub>i</sub>
		-0.373	0.222	595	-0.0755	0.862	1.111	249	0.9865	<sup>57</sup> <sub>ii</sub>

*i* Solvent acetonitrile, supporting electrolyte tetraethylammonium perchlorate vs SCE at 100  $\text{mV.s}^{-1}$ .

*ii* Solvent acetonitrile, supporting electrolyte tetrabutylammonium hexafluorophosphate vs  $\text{Ag}/\text{AgCl}$  at 200  $\text{mV.s}^{-1}$ .

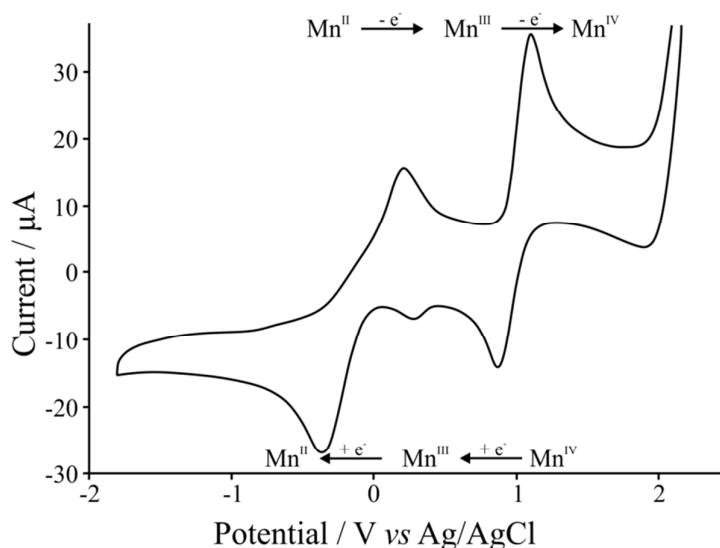
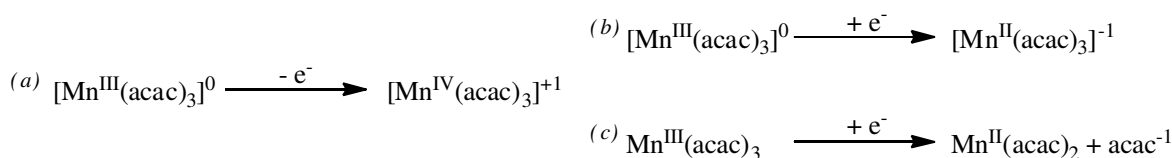


**Figure 2.17:** Cyclic voltammogram of  $\text{Mn}(\text{acac})_3$ .<sup>53</sup>



**Scheme 2.5:** (a) Proposed oxidation reaction of  $\text{Mn}^{\text{III}}$  to  $\text{Mn}^{\text{IV}}$ , (b) Proposed reduction of  $\text{Mn}^{\text{III}}$  to  $\text{Mn}^{\text{II}}$  from Bond, Martin and Masters in 1975,<sup>53</sup> (c) Proposed reduction of  $\text{Mn}^{\text{III}}$  to  $\text{Mn}^{\text{II}}$  from T. Paczeński, P. Błoniarczyk, K. Rydel and A. Sobkowiak in 2007.<sup>54</sup>

<sup>56</sup> T. Paczeński, P. Błoniarczyk, K. Rydel, A. Sobkowiak, *Electroanalysis* **2007** (19) 945-951.

<sup>57</sup> R. van Gorkum, E. Bouwman, J. Reedijk, *Inorg. Chem.* **2004** (43) 2456-2458.

## 2.5 Tris(acetylacetonato)metal(III), $M(\text{acac})_3$ ( $M = \text{V}, \text{Cr}, \text{Fe}$ and $\text{Co}$ ).

### 2.5.1 Introduction.<sup>58,59,60</sup>

Complexes that are easily obtained for the study of bonding, ligand coordination and Jahn-Teller distortion in organometallic systems are *tris*(acetylacetonato)metal(III) complexes  $[M(\text{acac})_3]$ . In the series  $M = \text{Ti}, \text{Cr}, \text{V}, \text{Mn}, \text{Fe}$  and  $\text{Co}$ , there are three potential complexes ( $M = \text{Ti}, \text{V}$  and  $\text{Mn}$ ) where Jahn-Teller distortion can occur due to the fractional  $d$ -shell occupancy. Unlike the other complexes  $\text{Co}(\text{acac})_3$  is low spin,<sup>58</sup> which makes it unusual. The two remaining complexes where  $M = \text{Cr}$  and  $\text{Fe}$  are high spin  $D_3$ <sup>58</sup> systems with no Jahn-Teller distortion.

### 2.5.2 $\text{V}(\text{acac})_3$ .<sup>61,62</sup>

Vanadium(III) complexes are known to be insulin mimetic agents and act as anti-inflammatories and anti-carcinogenic agents. The fact that vanadium is similar to molybdenum makes it possible for vanadium to function as metalloenzyme which is essential for xanthine oxidase, aldehyde oxidase and nitrogenase in biological systems.

#### 2.5.2.1 Structural properties.<sup>63,64</sup>

$\text{V}(\text{acac})_3$  ( $d^2$ ) like  $\text{Mn}(\text{acac})_3$  ( $d^4$ ) is a high spin  $C_2$  complex that undergoes Jahn-Teller distortion. The Jahn-Teller distortion in  $\text{V}(\text{acac})_3$  is smaller than the Jahn-Teller distortion of  $\text{Mn}(\text{acac})_3$ , in fact the geometric distortion is modest. This phenomenon is caused due to the fact that bonding  $d$ -orbitals originating from  $t_{2g}$  orbital group has less distortion than that of anti-bonding  $d$ -orbitals

<sup>58</sup> I. Diaz-Acosta, J. Baker, J.F. Hinton, P. Puley, *Spectrochimica Acta Part A* **2003** (59) 363-377.

<sup>59</sup> A.M. Bond, R.I. Martin, A.F. Masters, *Inorg. Chem.* **1975** (14) 1432-1435.

<sup>60</sup> T. Paczeński, P. Błoniarczyk, K. Rydel, A. Sobkowiak, *Electroanalysis* **2007** (19) 945-951.

<sup>61</sup> F. Brito, M.L. Araujo, J.D. Martínez, Y. Hernández, A. Moh, V. Lubes, *Journal of Coordination Chemistry* **2009** (62) 52-62.

<sup>62</sup> M.A. Nawi, T.L. Riechel, *Inorg. Chem.* **1981** (20) 1974-1978.

<sup>63</sup> I. Diaz-Acosta, J. Baker, J.F. Hinton, P. Puley, *Spectrochimica Acta Part A* **2003** (59) 363-377.

<sup>64</sup> C.A.L. Filgueiras, A. Horn Jr, R.A. Howie, J.M.S. Skakle, J.L. Wardell, *Acta Crystallographica Section E* **2001** (57) m157- m158.

originating from the  $e_g$  orbital group. The structure of a  $V(acac)_3$  crystal can be seen in **Figure 2.18** and the summarized data of all crystals is given in **Table 2.3**.

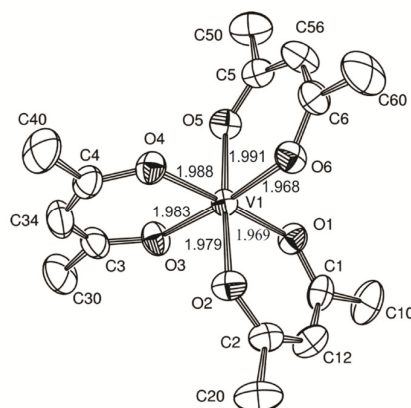


**Figure 2.18:** Crystal of  $V(acac)_3$  published by Filgueiras, Horn, Howie, Skakle and Wardell illustrating modest positive Jahn-Teller distortion.<sup>64</sup>

**Table 2.3:** Summary of the structural data of  $V(acac)_3$  crystals.

Positive Jahn-Teller distortion		Average O-M-O angle (°)	Ref.
Average M-O distance of the four longest (Å)	Average M-O distance of the shortest trans from each other (Å)		
1.919	1.886	85.83	65
1.983	1.972	87.98	66
1.990	1.981	87.38	
1.982	1.9755	87.83	67
1.974	1.968	87.46	68
1.987	1.978	87.79	69
1.987	1.975	87.88	70

<sup>65</sup> T.W. Hambley, C.J. Hawkins, T.A. Kabanos, *Inorg. Chem.* **1987** (26) 3740.

<sup>66</sup> B. Morosin, H. Montgomery, *Acta Crystallogr. Section B* **1969** (25) 1354.

<sup>67</sup> C.A.L. Filgueiras, A. Horn Junior, R.A. Howie, J.M.S. Skakle, J.L. Wardell, *Acta Crystallogr. Section E* **2001** (57) m157.

<sup>68</sup> F. Sanz-Ruiz, S. Martinez-Carrera, S. Garcia-Blanco, *An. R. Soc. Esp. Fis. Quim. Part A*, **1970** (66) 309.

<sup>69</sup> S.J. Kavitha, K. Panchanatheswaran, J.N. Low, C. Glidewell, *Acta Crystallogr. Section E* **2005** (61) m1326.

<sup>70</sup> A. Behrens, D. Rehder, *Private Communication* **2009** (2) 72 (CSD reference code: VAACAC14).

### 2.5.2.2 Cyclic voltammetry.<sup>71</sup>

The electrochemistry studies done on  $V(\beta\text{-diketonato})_3$  are few and are mostly concentrated on  $VO(\text{acac})_3$ . A typical cyclic voltammogram of  $V(\text{acac})_3$  is illustrated in **Figure 2.19**. The proposed redox equations that take place during a cyclic voltammetry experiment is given in **Scheme 2.6** and can be correlated with the cyclic voltammogram.

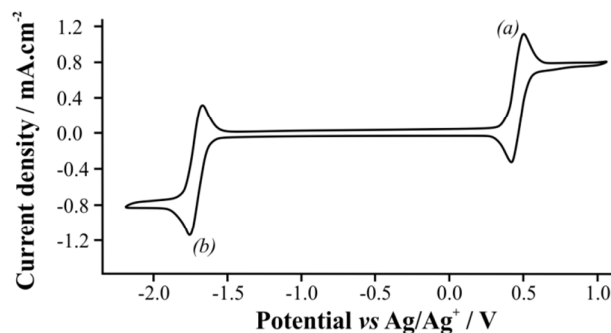
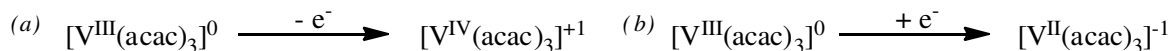


**Figure 2.19:** Cyclic voltammogram of 0.1 M  $V(\text{acac})_3$  in acetonitrile with 0.1 M tetraethylammonium tetrafluoroborate ( $\text{TEABF}_4$ ) as supporting electrolyte at a scan rate of  $10 \text{ mV.s}^{-1}$ .<sup>71</sup>



**Scheme 2.6:** Proposed redox reactions taking place during cyclic voltammetry experiment.<sup>71</sup>

During the cyclic voltammogram  $V(\text{acac})_3$  undergoes a single electron oxidation or reduction with the mean separation of the anodic and cathodic peaks ( $E^0$ ) in acetonitrile being for reaction (a) 0.46 V and -1.72 V for reaction (b).<sup>i71</sup> Both redox reactions are chemically and electrochemically reversible.

*i* Solvent acetonitrile, supporting electrolyte tetraethylammonium tetrafluoroborate vs  $\text{Ag/Ag}^+$  at  $10 \text{ mV.s}^{-1}$ .

<sup>71</sup> A.A. Shinkle, A.E.S. Sleightholme, L.D. Griffith, L.T. Thompson, C.W. Monroe, *Journal of Power Sources* **2012** (206) 490-496.

### 2.5.3 Cr(acac)<sub>3</sub>.<sup>72,73,74</sup>

Chromium(III) is a trace element that maintains the normal glucose metabolism in the human body, which is very important in the case of diabetes and at older age. This complex has been grafted onto mesoporous crystalline material (MCM-41) and used as a catalyst in the polymerization of ethylene. It was proven that Cr-MCM-41 is catalytically active in gas- and slurry-phase polymerization at 100 °C. The catalytic activity is a function of the calcination temperature, support characteristics and the loading of the chromium.<sup>72</sup>

#### 2.5.3.1 Structural properties.<sup>75</sup>

Cr(acac)<sub>3</sub> ( $d^3$ ) is a known high spin  $D_3$  complex that undergoes no Jahn-Teller distortion. There are many Cr(acac)<sub>3</sub> crystals published and an example of a crystal structure can be seen in **Figure 2.20**. The summary of the crystal data is tabulated in **Table 2.4**.

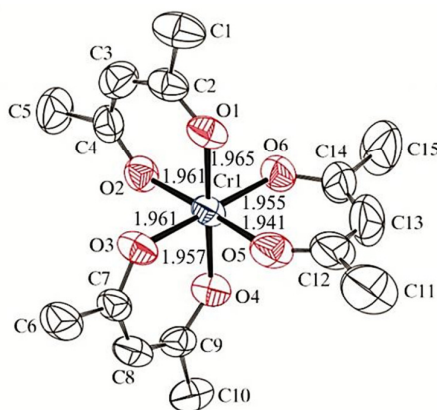


**Figure 2.20:** Crystal structure of Cr(acac)<sub>3</sub> obtained by von Chrzanowski, Lutz and Spek illustrating the  $D_3$  symmetry of the complex.<sup>76</sup>

<sup>72</sup> B.M. Weckhuysen, R.R. Rao, J. Pelgrims, R.A. Schoonheydt, P. Bodart, G. Denras, O. Collart, P. Van Der Voort, E.F. Vansant, *Chem. Eur. J.* **2000** (6) 2960-2970.

<sup>73</sup> Q. Liu, A.A. Shinkle, Y. Li, C.W. Monroe, L.T. Thompson, A.E.S. Sleightholme, *Electrochemistry Communications* **2010** (12) 1634-1637.

<sup>74</sup> L.S. von Chrzanowski, M. Lutz, A.L. Spek, *Acta Crystallogr. Section C* **2007** (63) m377-m382.

<sup>75</sup> I. Diaz-Acosta, J. Baker, J.F. Hinton, P. Puley, *Spectrochimica Acta Part A* **2003** (59) 363-377.

<sup>76</sup> L.S. von Chrzanowski, M. Lutz, A.L. Spek, *Acta Crystallogr. Section C* **2007** (63) m377-m382.



**Table 2.4:** Structural data of Cr(acac)<sub>3</sub> crystals.

Average of all six M-O distances (Å)	Average O-M-O angle (°)	Ref
1.956	91.10	<b>77</b>
_*	_*	<b>78</b>
1.954	91.11	<b>79</b>
1.953	91.00	<b>80</b>
_*	_*	<b>81</b>
1.957	91.15	<b>82</b>
1.961	91.17	
1.964	91.26	
1.962	91.08	
1.964	91.13	
1.962	91.08	
1.963	91.15	
1.955	91.23	<b>83</b>
1.961	91.08	<b>84</b>
1.962	90.46	
1.947	90.83	<b>85</b>
1.938	91.03	
1.947	91.30	<b>86</b>

\* No structural parameters available

### 2.5.3.2 Cyclic voltammetry.<sup>87</sup>

Cr(acac)<sub>3</sub> (supporting electrolyte tetraethylammonium tetrafluoroborate (TEABF<sub>4</sub>) in acetonitrile) was used as the active species in redox flow battery (RFB). It was found that the solubility of the active species, Cr(acac)<sub>3</sub>, in acetonitrile is low and is therefore the limiting factor.<sup>87</sup> The cyclic voltammogram of Cr(acac)<sub>3</sub> showed four redox reactions (see **Figure 2.21**)

<sup>77</sup> B. Morosin, *Acta Crystallogr.* **1965** (19) 131-137.

<sup>78</sup> B.L. Trus, R.E. Marsh, *ACA Abstr. Papers (Winter)* **1969** 30.

<sup>79</sup> S.Z. Haider, K.M.A. Malik, A. Hashem, M.B. Hursthouse, *Dhaka Univ. Stud. Part B* **1982** (30) 145.

<sup>80</sup> I. Diaz-Acosta, J. Baker, W. Cordes, P. Pulay, *J. Phys. Chem. Part A* **2001** (105) 238-244.

<sup>81</sup> E.A. Shugam, L.M. Shkol'nikova, *Kristallografiya(Russ.)(Crystallogr.Rep.)* **1956** (1) 478.

<sup>82</sup> L.S. von Chrzanowski, M. Lutz, A.L. Spek, *Acta Crystallogr Section C* **2007** (63) m377-m382.

<sup>83</sup> A. Gairola, G.V. Kunte, D. Chopra, T.N.G. Row, A.M. Umarji, S.A. Shivashankar, *Polyhedron* **2010** (29) 2680.

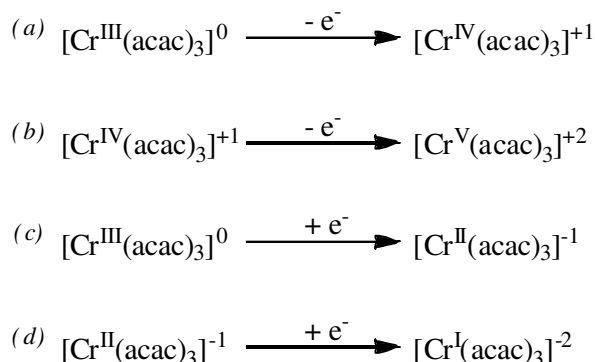
<sup>84</sup> R. Kuroda, S.F. Mason, *J. Chem. Soc. Dalton Trans.* **1979** 273.

<sup>85</sup> S.G. Bott, B.D. Fahlman, M.L. Pierson, A.R. Barron, *J. Chem. Soc. Dalton Trans.* **2001** 2148.

<sup>86</sup> S.Z. Haider, K.M.A. Malik, A. Hashem, M.B. Hursthouse, *Dhaka Univ. Stud. Part B* **1982** (30) 145.

<sup>87</sup> Q. Liu, A.A. Shinkle, Y. Li, C.W. Monroe, L.T. Thompson, A.E.S. Sleightholme, *Electrochemistry Communications* **2010** (12) 1634-1637.

which is proposed to be the reduction of  $\text{Cr}^{\text{II}}$  to  $\text{Cr}^{\text{I}}$  and the oxidation of  $\text{Cr}^{\text{IV}}$  to  $\text{Cr}^{\text{V}}$  as given in **Scheme 2.7**.



**Scheme 2.7:** The redox reactions that takes place during a cyclic voltammetry study of  $\text{Cr}(\text{acac})_3$  proposed by Liu, Shinkle, Li, Monroe, Thompson and Sleightholme.<sup>87</sup>

Anderson, Lung and Nile reported only the two-step reduction processes that corresponds to reaction (c) and (d) with reduction potentials -1.89 V and -2.11 V respectively.<sup>i 88</sup> Tsiamis, Hadjikostas, Karageorgiou and Manoussakis reported on the mean separation of the anodic and cathodic peaks ( $E^0$ ) for reaction (c) and (d) as -1.94 V and -2.4 V respectively.<sup>ii 89</sup>

*i* Solvent acetonitrile, supporting electrolyte tetrabutylammonium perchlorate vs  $\text{Ag}/\text{AgCl}$  at  $100 \text{ mV}\cdot\text{s}^{-1}$ .

*ii* solvent acetonitrile, supporting electrolyte tetraethylammonium perchlorate vs SCE.

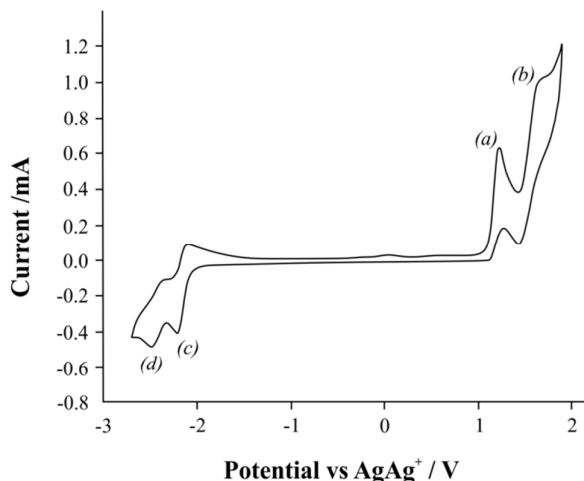


**Figure 2.21:** Typical  $\text{Cr}(\text{acac})_3$  cyclic voltammogram with a concentration of 0.05 M  $\text{Cr}(\text{acac})_3$  in acetonitrile with 0.5 M  $\text{TEABF}_4$  as supporting electrolyte.<sup>87</sup> Reactions (a) – (d) are proposed in **Scheme 2.7**.

<sup>88</sup> C.W. Anderson, K.R. Lung, T.A. Nile, *Inorg. Chim. Acta* **1984** (85) 33-36.

<sup>89</sup> C. Tsiamis, C.C. Hadjikostas, S. Karageorgiou, G. Manoussakis, *Inorg. Chim. Acta* **1988** (143) 17-23.

### 2.5.4 Fe(acac)<sub>3</sub>.<sup>90,91</sup>

Relative high concentrations of iron are found in the human body, 5.4 g per 70 kg, and most of it is involved in enzyme functions. Metal chelates with O,O donor atoms in ligands of complexes produce free radicals during thermal decomposition. The rate of polymerization by the use of Fe(acac)<sub>3</sub> as an initiator was found to be directly proportional to the concentration of the Fe(acac)<sub>3</sub> complex. The reaction mechanism of vinyl polymerization can be divided into four steps: formation of the active complex, initiation, propagation and termination.

Iron(III) acetylacetonate can be anchored on silica xerogel. The Fe<sup>III</sup> atoms that are anchored can be used as a heterogeneous catalyst in the epoxidation of alkenes. The same conditions as the homogeneous system, where molecular oxygen is used at atmospheric pressure as oxidant and the sacrificial reducing agent iso-butyraldehyde, were used. The *cis*-cyclooctene was selectively epoxidized to *cis*-cyclooctene oxide when using the heterogeneous iron(III) acetylacetonate anchored on silica xerogel as a catalyst. It was found that *cis*-cyclooctene was 100 % selective and 39 % partially epoxidized to *cis*-cyclooctene oxide after 24 hours, which is not an improvement to the homogeneous system but it is clearly noted that the heterogeneous system has not been optimized yet. Therefore, the heterogeneous system can be studied further to optimize the epoxidation. The iron cation is not leached out under the conditions during the epoxidation.

---

<sup>90</sup> S. Lenka, P.L. Nayak, *Journal of Macromolecular Science Part A* **1982** (18) 695-707.

<sup>91</sup> M.C. Brasil, E.V. Benvenutti, J.R. Gregório, A.E. Gerbase, *Reactive & Functional Polymers* **2005** (63) 135-141.

#### 2.5.4.1 Structural properties.<sup>92</sup>

Fe(acac)<sub>3</sub> (*d*<sup>5</sup>) like Cr(acac)<sub>3</sub> is a high spin complex with *D*<sub>3</sub> symmetry and no Jahn-Teller distortion has been reported. The oxygen atoms are arranged in an octahedral geometry around the iron centre. The crystal data of published Fe(acac)<sub>3</sub> crystals that are summarized in **Table 2.5** confirm the *D*<sub>3</sub> symmetry.

**Table 2.5:** Summary of Fe(acac)<sub>3</sub> crystal data.

Average of all six M-O distances (Å)	Average O-M-O angle (°)	Ref
1.994	87.47	<b>93</b>
2.000	86.80	<b>94</b>
1.978	87.71	<b>95</b>
1.992	87.06	<b>96</b>
1.990	88.67	<b>97</b>
1.991	87.43	<b>98</b>
1.948	89.37	<b>99</b>
1.992	87.43	<b>100</b>
—*	—*	<b>101</b>
1.991	87.37	<b>102</b>
1.996	87.80	
1.996	87.37	<b>103</b>
1.999	88.03	<b>104</b>

\* No structural parameters available

- 
- <sup>92</sup> I. Diaz-Acossta, J. Baker, W. Cordes, P. Pulay, *J. Phys. Chem. Part A* **2001** (105) 238-244.
- <sup>93</sup> L. Pang, R.C. Hynes, M.A. Whitehead, *Acta Crystallogr. Section C* **1992** (48) 1594.
- <sup>94</sup> L. Pang, E.A.C. Lucken, G. Bernardinelli, *J. Am. Chem. Soc.* **1990** (112) 8754.
- <sup>95</sup> A. Lennartson, *Inorg. Chim. Acta* **2011** (365) 451.
- <sup>96</sup> J. Iball, C.H. Morgan, *Acta Crystallogr.* **1967** (23) 239.
- <sup>97</sup> M. Kabak, A. Elmali, S. Ozbey, O. Atakol, A. Kenar, *Z. Kristallogr.* **1996** (211) 831.
- <sup>98</sup> M.L. Hu, Z.M. Jin, Q. Miao, L.P. Fang, *Z. Kristallogr.* **2001** (216) 597.
- <sup>99</sup> R.B. Roof Jr, *Acta Crystallogr.* **1956** (9) 781.
- <sup>100</sup> I. Diaz-Acosta, J. Baker, W. Cordes, P. Pulay, *J. Phys. Chem. Part A* **2001** (105) 238.
- <sup>101</sup> L.M. Shkol'nikova, *Kristallografiya (Russ.) (Crystallogr. Rep.)* **1959** (4) 419.
- <sup>102</sup> P.A. Stabnikov, N.V. Pervukhina, I.A. Baidina, L.A. Sheludyakova, S.V. Borisov, *Zh. Strukt. Khim. (Russ.) (J.Struct.Chem.)* **2007** (48) 183.
- <sup>103</sup> S. Weng, C. Ke, F. Chen, Y. Lyu, G. Lin, *Tetrahedron* **2011** (67) 1640.
- <sup>104</sup> L.R. Nassimbeni, M.M. Thackeray, *Acta Crystallogr. Section B* **1974** (30) 1072.

### 2.5.4.2 Cyclic voltammetry.<sup>105,106,107,108</sup>

Cyclic voltammetry gives valuable information about the catalytic activity of the analyte that is being studied.  $\text{Fe}(\text{acac})_3$  has a simple cyclic voltammogram since only two peaks are visible. The peaks are associated with the reduction of the  $\text{Fe}^{\text{III}}$  metal centre to the  $\text{Fe}^{\text{II}}$  species and the reverse process where  $\text{Fe}^{\text{II}}$  is oxidized back to the  $\text{Fe}^{\text{III}}$  complex species. The cyclic voltammogram of  $\text{Fe}(\text{acac})_3$  is illustrated in **Figure 2.22**. The two proposed redox reactions can be seen in **Scheme 2.8**. The summary of published cyclic voltammetry data obtained for  $\text{Fe}(\text{acac})_3$  is tabulated in **Table 2.6**.

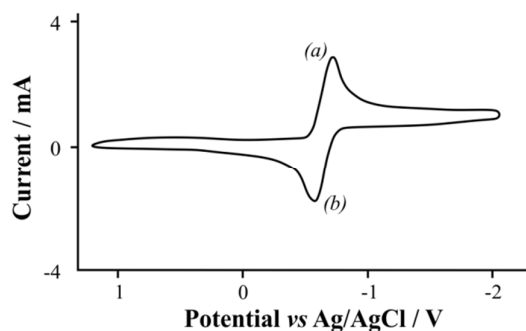
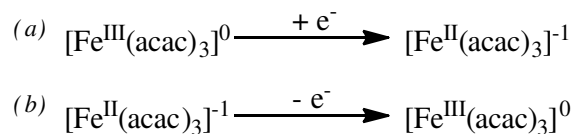


**Figure 2.22:** Cyclic voltammogram of 3.5 mM  $\text{Fe}(\text{acac})_3$  in acetonitrile with 0.1 M tetrabutylammonium perchlorate as supporting electrolyte at a scan rate of  $100 \text{ mV.s}^{-1}$ .<sup>106</sup> (Note: notation of the x-axis is from positive to negative, the other cyclic voltammogram in this dissertation will range from negative to positive)



**Scheme 2.8:** The redox reactions proposed to take place during a cyclic voltammetry experiment of  $\text{Fe}(\text{acac})_3$ .

<sup>105</sup> T. Paczeński, P. Błoniarz, K. Rydel, A. Sobkowiak, *Electroanalysis* **2007** (19) 945-951.

<sup>106</sup> C.W. Anderson, K.R. Lung, *Inorganica Chimica Acta* **1984** (85) 33-36.

<sup>107</sup> C. Tsiamis, C. Micheal, A.D. Jannakoudakis, P.D. Jannakoudakis, *Inorganica Chimica Acta* **1986** (120) 1-9.

<sup>108</sup> B.D. Beaver, L.C. Hall, C.M. Lukehart, L.D. Preston, *Inorganica Chimica Acta* **1981** (47) 25-30.

**Table 2.6:** Summary of cyclic voltammetry experiment data of Fe(acac)<sub>3</sub>.

E <sub>pc</sub> (V)	E <sub>pa</sub> (V)	ΔE <sub>p</sub> (mV)	E <sup>0</sup> (V)	Refereene
-0.65	-0.59	60	-0.62	<b>109<sub>i</sub></b>
-0.68	-0.55	130	-0.62	<b>110<sub>ii</sub></b>
-0.68	-0.55	130	-0.62	<b>111<sub>iii</sub></b>
-0.74	-0.63	110	-0.69	<b>112<sub>iv</sub></b>

*i* Solvent dimethylformamide, supporting electrolyte tetraethylammonium perchlorate vs SCE at 100 mV.s<sup>-1</sup>.

*ii* Solvent dimethylformamide, supporting electrolyte tetraethylammonium perchlorate vs Ag/AgCl at 100 mV.s<sup>-1</sup>.

*iii* Solvent acetonitrile, supporting electrolyte tetrabutylammonium perchlorate vs Ag/AgCl at 100 mV.s<sup>-1</sup>.

*iv* Solvent acetonitrile, supporting electrolyte tetraethylammonium perchlorate vs SCE at 100 mV.s<sup>-1</sup>.

## 2.5.5 Co(acac)<sub>3</sub>.<sup>113</sup>

Co(acac)<sub>3</sub> (*d*<sup>6</sup>) is very different than the rest of the M(acac)<sub>3</sub> series discussed. Co(acac)<sub>3</sub> is the only low spin complex, this means that the electrons in the *d*-orbitals of the cobalt centre prefer to pair with each other rather than to be unpaired. This complex is also the only one that can be characterized by the use of nuclear magnetic resonance (NMR) since it is the only diamagnetic complex in the series investigated in this study. Co(acac)<sub>3</sub> has a relative low toxicity and is kinetically inert.

### 2.5.5.1 Structural properties.<sup>114,115</sup>

Co(acac)<sub>3</sub> is known to have *D*<sub>3</sub> symmetry and there are quite a number of Co(acac)<sub>3</sub> crystals published throughout the years. The typical structure of a Co(acac)<sub>3</sub> crystal is illustrated in **Figure 2.23**. A summary of the crystal data is tabulated in **Table 2.7**.

<sup>109</sup> S. Misumi, M. Aihara, Y. Nonaka, *Bull. Chem. Soc. Jpn.* **1970** (43) 774-778.

<sup>110</sup> K. Endo, M. Furukawa, H. Yamatera, H. Sano, *Bull. Chem. Soc. Jpn.* **1980** (53) 407-410.

<sup>111</sup> C.W. Anderson, K.R. Lung, T.A. Nile, *Inorg. Chim. Acta* **1984** (85) 33-36.

<sup>112</sup> T. Paczeński, P. Błoniarz, K. Rydel, A. Sobkowiak, *Electroanalysis* **2007** (19) 945-951.

<sup>113</sup> I. Diaz-Acosta, J. Baker, J.F. Hinton, P. Puley, *Spectrochimica Acta Part A* **2003** (59) 363-377.

<sup>114</sup> T. Paczeński, P. Błoniarz, K. Rydel, A. Sobkowiak, *Electroanalysis* **2007** (19) 945-951.

<sup>115</sup> L.S. von Chrzanowski, M. Lutz, A.L. Spek, *Acta Crystallogr. Section C* **2007** (63) m283- m288.

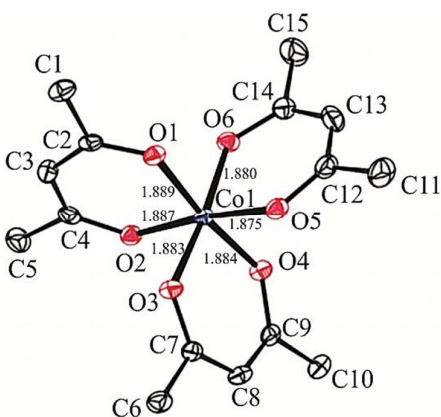


**Figure 2.23:** Crystal of  $\text{Co}(\text{acac})_3$  solved by von Chrzanowski, Lutz and Spek at the temperature of 110 K.<sup>116</sup>

**Table 2.7:** Summary of  $\text{Co}(\text{acac})_3$  crystal data

Average of all six M-O distances (Å)	Average O-M-O angle (°)	Ref	Average of all six M-O distances (Å)	Average O-M-O angle (°)	Ref
1.887	96.51	117	1.883	96.60	118
1.888	96.03	119	1.883	96.65	
1.957	78.10	120	1.884	96.63	
1.897	97.32	121	1.885	96.70	
1.885	96.55	122	1.886	96.72	
—*	—*	123	2.059	88.00	124
—*	—*	125	—*	—*	126

\* No structural parameters available

<sup>116</sup> L.S. von Chrzanowski, M. Lutz, A.L. Spek, *Acta Crystallogr. Section C* **2007** (63) m283- m288.

<sup>117</sup> V.P. Nikolaev, L.A. Butman, M.A. Porai-Koshits, V.I. Sokol, V.A. Avilov, I.I. Moiseev, *Koord. Khim. (Russ.) (Coord.Chem.)* **1979** (5) 882.

<sup>118</sup> L.S. von Chrzanowski, M. Lutz, A.L. Spek, *Acta Crystallogr. Section C* **2007** (63) m283.

<sup>119</sup> W.B. Wright, E.A. Meyers, *Cryst. Struct. Commun.* **1980** (9) 1173.

<sup>120</sup> V.M. Padmanabhan, *Proc. Ind. Acad. Sci. Part A* **1958** (47) 329.

<sup>121</sup> P.K. Hon, C.E. Pfluger, *J. Coord. Chem.* **1973** (3) 67.

<sup>122</sup> G.J. Kruger, E.C. Reynhardt, *Acta Crystallogr. Section B* **1974** (30) 822.

<sup>123</sup> R.B. van Dreele, R.C. Fay, *J. Am. Chem. Soc.* **1971** (93) 4936.

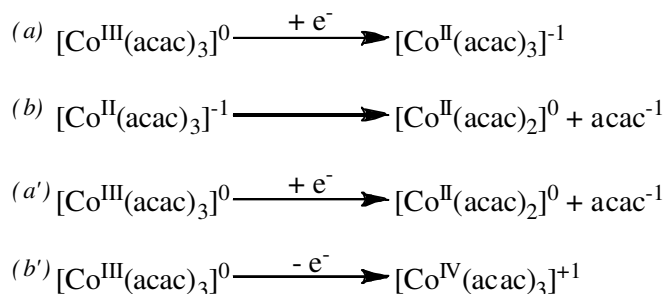
<sup>124</sup> X. Li, G. Musie, D.R. Powell, *Acta Crystallogr. Section E* **2003** (59) m717.

<sup>125</sup> L.M. Shkol'nikova, *Kristallografiya (Russ.) (Crystallogr. Rep.)* **1959** (4) 419.

<sup>126</sup> B.D. Santarsiero, A. Esmaili, V. Schomaker, E.C. Lingafelter, *Acta Crystallogr. Section A* **1981** (37) C234.

### 2.5.5.2 Cyclic voltammetry.<sup>127,128</sup>

Little research has been done on the cyclic voltammetry of  $\text{Co}(\text{acac})_3$ . The redox reactions taking place during a cyclic voltammogram experiment of  $\text{Co}(\text{acac})_3$  are illustrated in **Scheme 2.9**. An example of a typical cyclic voltammogram of this complex can be seen in **Figure 2.24** and a summary of all the data collected during these studies is tabulated in **Table 2.8**.



**Scheme 2.9:** The reactions Anderson and Lung suggested that take place during a cyclic voltammetry experiment of  $\text{Co}(\text{acac})_3$  is illustrated by (a) and (b).<sup>128</sup> The reduction and oxidation reactions, (a') and (b') is proposed by Paczeński, Błoniarz, Rydel and Sobkowiak.<sup>127</sup>

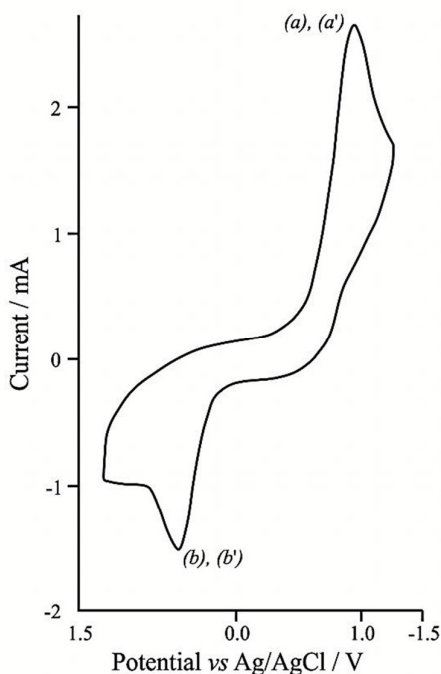


**Figure 2.24:** Cyclic voltammogram of 3.8 mM  $\text{Co}(\text{acac})_3$  in acetonitrile with 0.1 M tetrabutylammonium perchlorate as supporting electrolyte at a scan rate of  $100 \text{ mV} \cdot \text{s}^{-1}$ .<sup>128</sup> (Note: notation of the x-axis is from positive to negative, the other cyclic voltammogram in this dissertation will range from negative to positive)

<sup>127</sup> T. Paczeński, P. Błoniarz, K. Rydel, A. Sobkowiak, *Electroanalysis* **2007** (19) 945-951.

<sup>128</sup> C.W. Anderson, K.R. Lung, *Inorganica Chimica Acta* **1984** (85) 33-36.



**Table 2.8:** Summary of cyclic voltammetry experiment data of  $\text{Co}(\text{acac})_3$ .

$\text{Co}^{\text{III}} \longrightarrow \text{Co}^{\text{II}}$	$\text{Co}^{\text{II}} \longrightarrow \text{Co}^{\text{III}}$	$\text{Co}^{\text{III}} \longrightarrow \text{Co}^{\text{IV}}$	Ref
$E_{\text{pa}}$ (V)	$E_{\text{pc}}$ (V)	$E_{\text{pc}}$ (V)	
-1.04	0.47	-	<b>129</b> <sub>i</sub>
-0.86	0.31	-	<b>130</b> <sub>ii</sub>
-	0.95	1.65	<b>131</b> <sub>iii</sub>

- i* Solvent dimethylformamide, supporting electrolyte tetraethylammonium perchlorate vs Ag/AgCl at 100  $\text{mV.s}^{-1}$ .  
*ii* Solvent acetonitrile, supporting electrolyte tetrabutylammonium perchlorate vs Ag/AgCl at 100  $\text{mV.s}^{-1}$ .  
*iii* Solvent acetonitrile, supporting electrolyte tetraethylammonium perchlorate vs SCE at 100  $\text{mV.s}^{-1}$ .

**129** K. Endo, M. Furukawa, H. Yamatera, H. Sano, *Bull. Chem. Soc. Jpn.* **1980** (53) 407-410.

**130** C.W. Anderson, K.R. Lung, T.A. Nile, *Inorg. Chim. Acta* **1984** (85) 33-36.

**131** T. Paczeński, P. Błoniarz, K. Rydel, A. Sobkowiak, *Electroanalysis* **2007** (19) 945-951.

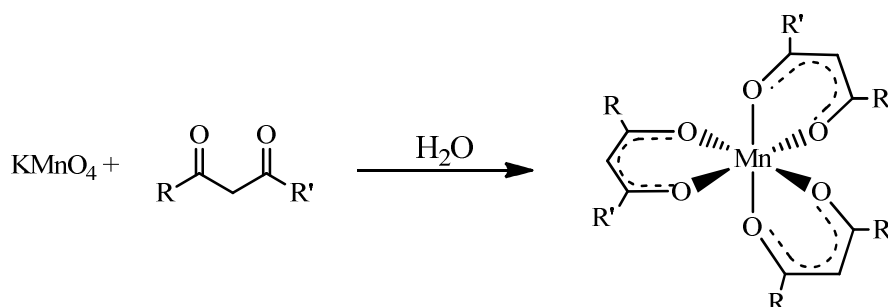
# 3

## Results and discussion.

### 3.1 Tris( $\beta$ -diketonato)manganese(III) / $\text{Mn}(\beta\text{-diketonato})_3$ .

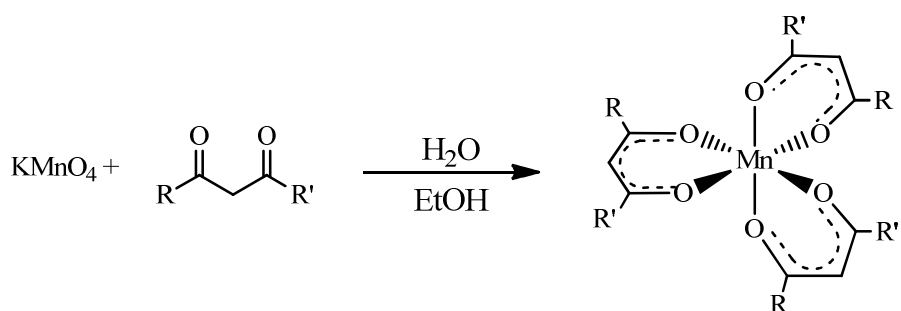
#### 3.1.1 Synthesis.

By the use of adapted methods four new ( $\beta$ -diketonato = benzoylacetato (ba) [2], trifluoroacetylacetato (tfaa) [4], thenoyltrifluoroacetato (tfth) [5], trifluorobenzoylacetato (tfba) [7]) and four known ( $\beta$ -diketonato = acetylacetato (acac) [1], dibenzoylmethanato (dbm) [3], trifluorofuroylacetato (tffu) [6], hexafluoroacetylacetato (hfac) [8])  $\text{Mn}(\beta\text{-diketonato})_3$  complexes were synthesized.<sup>1</sup> Three methods were used in the preparation of  $\text{Mn}(\beta\text{-diketonato})_3$  complexes. The group 1 complexes ([1], [4], [5], [6], [7]), group 2 complexes ([2], [3]) and the third group ([8]) were prepared according to **Scheme 3.1**, **Scheme 3.2** and **Scheme 3.3** respectively.



**Scheme 3.1:** General method for preparing  $\text{Mn}(\beta\text{-diketonato})_3$  [1], [4], [5], [6], [7] complexes.

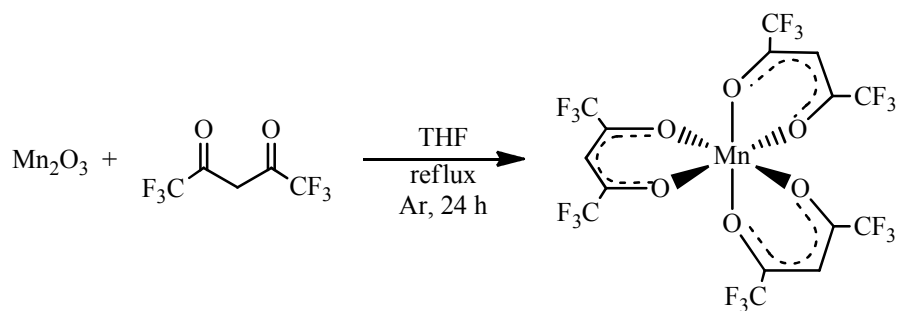
<sup>1</sup> M.N. Bhattacharjee, M.K. Chaudhuri, D.T. Khathing, *Dalton Trans.* **1982** (3) 669-670.



**Scheme 3.2:** General method for preparing  $\text{Mn}(\beta\text{-diketonato})_3$  [2] and [3] complexes.

The synthesis was carried out using the  $\beta$ -diketone as a reducing agent to reduce the  $[\text{MnO}_4]^-$  to form the tris chelate complex. This reduction is observed by the change of the reaction mixture colour (purple  $\text{Mn}^{7+}$  to brown-black  $\text{Mn}^{3+}$ ). The excess  $\beta$ -diketone serves as the driving force for the reaction. This kind of reaction normally needs a buffer to maintain the perfect pH for the formation of the complex. The formation of the complex in the direct method however acts as a buffer and no sodium acetate as buffer is needed. In group 1 the complexes'  $\beta$ -diketones are liquid or were soluble in water therefore,  $\text{H}_2\text{O}$  was used as a solvent. Group 2 complexes were synthesized by dissolving the  $\beta$ -diketones first in EtOH before adding it to the  $\text{KMnO}_4$  solution with a 1:1 solvent ratio of  $\text{H}_2\text{O}:\text{EtOH}$ . The reaction mixture was stirred vigorously and heated over a steam bath for five minutes to dissolve the  $\beta$ -diketone thoroughly.

Due to the hygroscopic nature of hexafluoroacetylacetone (Hhfac) the  $\text{Mn}(\text{hfac})_3$  [8] complex was prepared under argon (Ar) atmosphere according to **Scheme 3.3**.



**Scheme 3.3:** Preparation of  $\text{Mn}(\text{hfac})_3$ .

### CHAPTER 3

Mn(hfac)<sub>3</sub> was synthesized by refluxing Mn<sub>2</sub>O<sub>3</sub> and an excess of Hhfac for 24h under Ar. The Mn<sub>2</sub>O<sub>3</sub> is a black powder that is insoluble in THF. With the formation of the Mn(hfac)<sub>3</sub> complex a greenish colour was observed. The excess THF and Hhfac were removed by the use of vacuum. The product was sublimed under vacuum at 60 °C, a yellow powder was collected from the cold finger. In the presence of H<sub>2</sub>O, Mn(hfac)<sub>3</sub> turns to Mn(hfac)<sub>3</sub>.2H<sub>2</sub>O therefore, a yield could not be determined.

The complexes were characterized by the use of elemental analysis and mass spectroscopy (section 4.3.1, chapter 4). <sup>1</sup>H NMR could not be used as a characterization technique due to the paramagnetic properties of Mn<sup>III</sup> complexes. The different characteristics of the Mn(β-diketonato)<sub>3</sub> complexes are summarized in **Table 3.1**.

**Table 3.1:** Characteristics data and results of the synthesis of Mn(β-diketonato)<sub>3</sub> complexes.

Complex	R	R'	Yield	Colour	Melting point
Mn(acac) <sub>3</sub>	CH <sub>3</sub>	CH <sub>3</sub>	20%	black	155.7 °C
Mn(ba) <sub>3</sub>	CH <sub>3</sub>	Ph	70%	green	184.3 °C
Mn(dbm) <sub>3</sub>	Ph	Ph	80%	black	235.7 °C
Mn(tfaa) <sub>3</sub>	CF <sub>3</sub>	CH <sub>3</sub>	69%	dark brown-black	116.7 °C
Mn(tfth) <sub>3</sub>	CF <sub>3</sub>	C <sub>4</sub> H <sub>3</sub> S	97%	brown	157.5 °C
Mn(tffu) <sub>3</sub>	CF <sub>3</sub>	C <sub>4</sub> H <sub>3</sub> O	73%	black	170.6 °C
Mn(tfba) <sub>3</sub>	CF <sub>3</sub>	Ph	98%	black	89.7 °C
Mn(hfac) <sub>3</sub>	CF <sub>3</sub>	CF <sub>3</sub>	- <sup>i</sup>	yellow	- <sup>i</sup>

<sup>i</sup> Mn(hfac)<sub>3</sub> is hygroscopic, thus can not be determined

Yields of 69-98 % were obtained, except for complex [1] which had a yield of 20 %. The poor yield of complex [1] could be attributed to the volatility of the β-diketone at room temperature. The complexes varied from green, dark brown-black or black in colour.

### 3.1.2 Crystal Structure of Mn(dbm)<sub>3</sub>.

As additional characterization X-ray diffraction (XRD) studies were done on Mn(dbm)<sub>3</sub>. The crystal was obtained by slow evaporation at room temperature after dissolving the product in acetone. X-ray studies on Mn(acac)<sub>3</sub> showed a positive Jahn-Teller distortion at room temperature and a negative Jahn-Teller distortion at 180 K.<sup>2</sup> Published crystal structures of Mn(dbm)<sub>3</sub> showed a negative Jahn-Teller distortion at 295 K (room temperature).<sup>3,4</sup> Since the Mn(acac)<sub>3</sub> crystal showed different Jahn-Teller distortions at different temperatures, the Jahn-Teller distortion of Mn(dbm)<sub>3</sub> at 100 K was studied.

The crystal data and structure refinement of Mn(dbm)<sub>3</sub> of this study at 100 K are summarized in **Table 3.3**. A molecular diagram showing atom labelling and a schematic diagram showing bond lengths and the coordination environment around the manganese centre of Mn(dbm)<sub>3</sub> is illustrated in **Figure 3.1**. Mn(dbm)<sub>3</sub> crystalized in the *P2<sub>1</sub>/c* space group with four molecules in the unit cell. The Mn(dbm)<sub>3</sub> crystal's average O-Mn-O angles deviates 1.34 ° from the 90 ° expected for an octahedral complex. The crystal data that was obtained showed that the phenyl groups of the β-diketonato ligands are not co-planar with the β-diketonato backbone, but distort to form angles of 12-34 °, see **Table 3.2**.

**Table 3.2:** The angle between phenyl (Ph) rings and their respective β-diketonato backbone found in the crystal of the Mn(dbm)<sub>3</sub> complex.

Ligand	Angle between ligand back bone and Ph (°)	Angle between ligand back bone and Ph' (°)
Ligand 1	12.03	14.12
Ligand 2	26.37	33.46
Ligand 3	15.49	25.40

<sup>2</sup> S. Geremia, N. Demitri, *J. Chem. Educ.* **2005** (82) 460-465.

<sup>3</sup> E.G. Zaitseva, I.A. Baidina, P.A. Stabnikov, S.V. Borisov, I.K. Igumenov, *Zh. Strukt. Khim. (Russ.) (J. Struct. Chem.)* **1990** (31) 184.

<sup>4</sup> A.L. Barra, D. Gatteschi, R. Sessoli, G.L. Abbati, A. Cornia, A.C. Fabretti, M.G. Uytterhoeven, *Angew. Chem. Int. Ed.* **1997** (36) 2329.

## CHAPTER 3

**Table 3.3:** Crystal data and structure refinement of Mn(dbm)<sub>3</sub>.

<b>Empirical formula</b>	C <sub>45</sub> H <sub>33</sub> O <sub>6</sub> Mn
<b>Formula weight</b>	724.65
<b>Temperature</b>	100(2) K
<b>Wavelength</b>	0.71073 Å
<b>Crystal system</b>	Monoclinic
<b>Space group</b>	<i>P</i> 2 <sub>1</sub> / <i>c</i>
<b>Unit cell dimensions</b>	a = 16.6293(4) Å b = 9.8443(2) Å c = 21.4271(3) Å a = 90° b = 92.7560(10)° g = 90°
<b>Volume</b>	3503.64(12) Å <sup>3</sup>
<b>Z</b>	4
<b>Density (calculated)</b>	1.374 Mg/m <sup>3</sup>
<b>Absorption coefficient</b>	0.428 mm <sup>-1</sup>
<b>F(000)</b>	1504
<b>Crystal size</b>	0.19 x 0.16 x 0.10 mm <sup>3</sup>
<b>Theta range for data collection</b>	1.90 to 28.33°.
<b>Index ranges</b>	-22 ≤ h ≤ 21, -13 ≤ k ≤ 13, -28 ≤ l ≤ 28
<b>Reflections collected</b>	46135
<b>Independent reflections</b>	8720 [R(int) = 0.0551]
<b>Completeness to theta = 28.33°</b>	99.7 %
<b>Absorption correction</b>	Semi-empirical from equivalents
<b>Max. and min. transmission</b>	0.9584 and 0.9230
<b>Refinement method</b>	Full-matrix least-squares on F <sup>2</sup>
<b>Data / restraints / parameters</b>	8720 / 0 / 469
<b>Goodness-of-fit on F<sup>2</sup></b>	1.028
<b>Final R indices [I &gt; 2σ(I)]</b>	R1 = 0.0412, wR2 = 0.0873
<b>R indices (all data)</b>	R1 = 0.0654, wR2 = 0.0992
<b>Largest diff. peak and hole</b>	0.333 and -0.488 e.Å <sup>-3</sup>

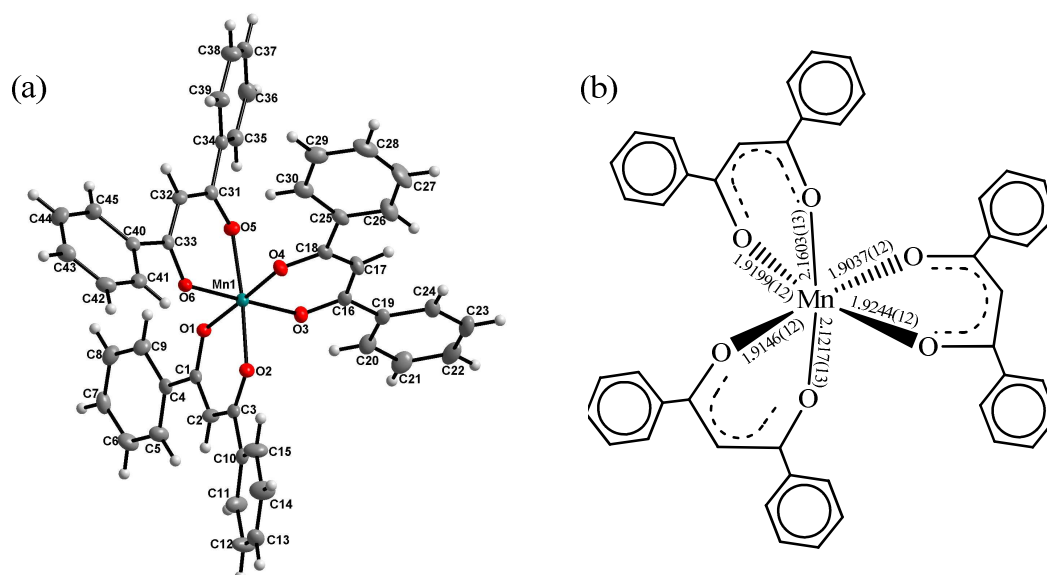


**Figure 3.1:** (a) The molecular structure of  $\text{Mn}(\text{dbm})_3$ , with 50% probability displacement ellipsoids. (b) Diagram with selected bond lengths (Å).

Since two opposite Mn-O bond lengths were more than 0.2 Å longer than the other four Mn-O bond lengths, the  $\text{Mn}(\text{dbm})_3$  crystal of this study exhibits a negative Jahn-Teller distortion. The crystal structure at room temperature (previously published)<sup>5,6</sup> also showed a difference of *ca.* 0.2 Å see **Table 3.4**. DFT calculations were done on  $\text{Mn}(\text{dbm})_3$  to gain more insight in the structure of the  $\text{Mn}(\text{dbm})_3$  crystal. The lowest energy optimized geometry of  $\text{Mn}(\text{dbm})_3$  also showed a negative Jahn-Teller distortion (see **Figure 3.2**) with a difference of 0.25 Å. DFT gas phase studies usually overestimate M-L bond lengths. However, all studies exhibit the same trend. See paragraph 3.1.4.2 for additional results obtained from the DFT study.

**Table 3.4:** The Mn-O bond lengths of  $\text{Mn}(\text{dbm})_3$  from different studies.

Study	Mn-O bond lengths (Å)								Temp (°C)
	1	2	3	4	Average bond length of 1-4	5	6	Average bond length of 5-6	
This study	1.904	1.915	1.92	1.924	1.916	2.106	2.122	2.114	-173.15
pub 1 <sup>5</sup>	1.89	1.912	1.919	1.932	1.913	2.091	2.126	2.109	RT
pub 2 <sup>6</sup>	1.908	1.917	1.931	1.935	1.923	2.109	2.142	2.126	RT
DFT calc.	1.964	1.969	1.975	1.979	1.972	2.217	2.233	2.225	RT

<sup>5</sup> E.G. Zaitseva, I.A. Baidina, P.A. Stabnikov, S.V. Borisov, I.K. Igumenov, *Zh. Strukt. Khim. (Russ.) (J. Struct. Chem.)* **1990** (31) 184.

<sup>6</sup> A.L. Barra, D. Gatteschi, R. Sessoli, G.L. Abbati, A. Cornia, A.C. Fabretti, M.G. Uytterhoeven, *Angew. Chem. Int. Ed.* **1997** (36) 2329.

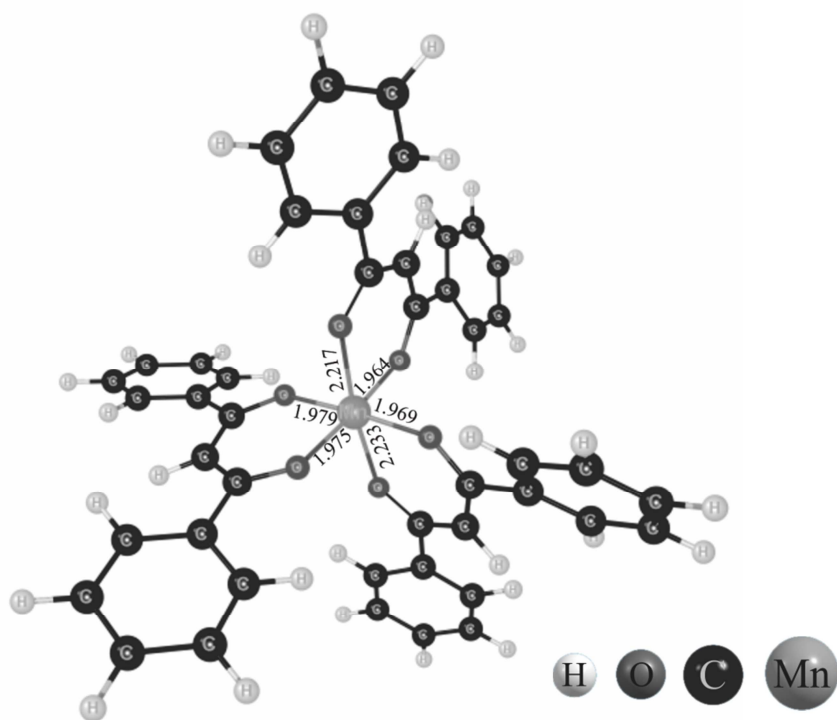


**Figure 3.2:** Optimized geometry of  $\text{Mn}(\text{dbm})_3$  with M-O bond lengths shown in Å.

$\pi$ - $\pi$  interactions are important non-covalent intermolecular forces that are similar to H-bonding. The  $\pi$ - $\pi$  stacking of aromatic rings can generally be divided into four different manners namely edge-to-face (T-shape), face-to-face parallel, slipped parallel and slipped non-parallel (**Figure 3.3**).  $\pi$ - $\pi$  stacked aromatic groups are normally separated by inter-planar distances ranging from 3.3-3.8 Å.<sup>7,8</sup>

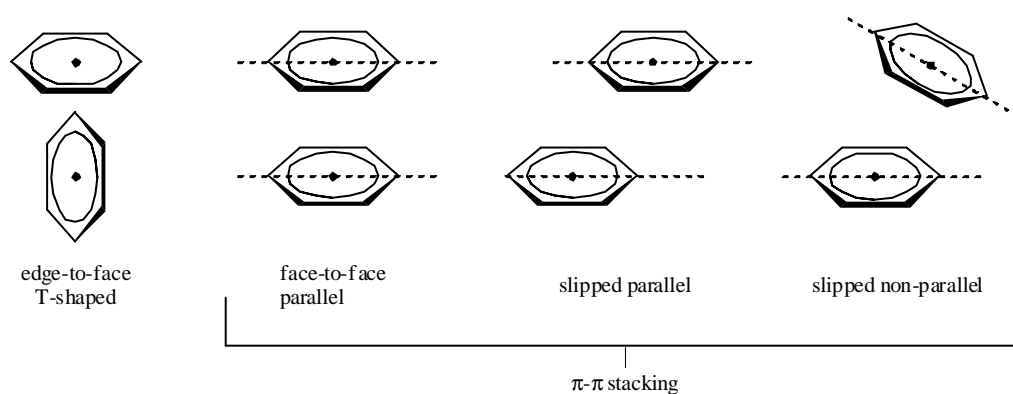


**Figure 3.3:** Different  $\pi$ - $\pi$  stacking of aromatic rings.

A slipped parallel  $\pi$ - $\pi$  stacking of the benzene rings attached to the  $\beta$ -diketonato ligands in the  $\text{Mn}(\text{dbm})_3$  crystal was observed and illustrated in **Figure 3.4**. The  $\pi$ - $\pi$  interaction parameters are

<sup>7</sup> C. Janiak, *J. Chem. Soc., Dalton Trans.* **2000** 3885-3896.

<sup>8</sup> G.B. McGuaghey, M. Gagné, A.K. Rappé, *J. Bio. Chem.* **1998** (273) 15458-15463.



tabulated in **Table 3.5**. The inter-planar distance ( $d_2$ ) of 3.32 Å falls well in the range for  $\pi$ - $\pi$  stacking.

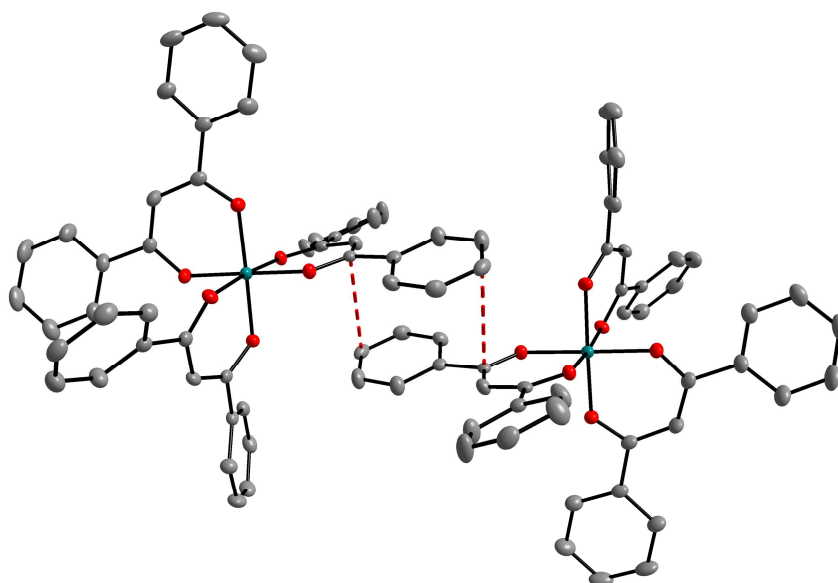
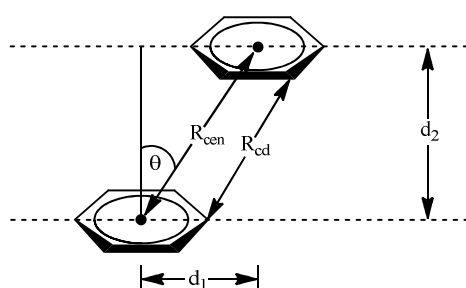


Figure 3.4:  $\pi$ - $\pi$  stacking in  $\text{Mn}(\text{dbm})_3$ .

**Table 3.5:**  $\pi$ - $\pi$  interaction parameters for the stacking in  $\text{Mn}(\text{dbm})_3$ .



$\theta$ / °	70.25
$R_{\text{cen}}$ / Å	3.59
$R_{\text{cd}}$ / Å [C8-C5]	3.37
$d_1$ / Å	1.37
$d_2$ / Å	3.32

$\theta$  = displacement angle of centroids  
 $R_{\text{cen}}$  = centroid-centroid displacement  
 $R_{\text{cd}}$  = closest contact distance between the rings  
 $d_1$  = horizontal displacement of centroids  
 $d_2$  = interplanar distance

### 3.1.3 Electrochemistry.

The redox active species in the  $\text{Mn}(\beta\text{-diketonato})_3$  complexes that is being investigated, is the manganese centre. To study the redox reactions that take place during a cyclic voltammogram of the  $\text{Mn}(\text{acac})_3$  complex an internal standard (ferrocene,  $C_{\text{ferrocene}} = 0.5 \text{ mM}$ , known one electron redox reaction) was added to a 0.5 mM  $\text{Mn}(\text{acac})_3$  solution. The resulting cyclic voltammogram can be seen in **Figure 3.5**.  $\text{Mn}(\text{acac})_3$  showed two redox couples, a chemically and electrochemically irreversible couple with  $E_{\text{pc}} = -882 \text{ mV}$  and an electrochemically irreversible ( $\Delta E_p = 240 \text{ mV}$ ) but chemically reversible ( $i_{\text{pa}}/i_{\text{pc}} \approx 1$ ) redox couple with  $E_{\text{pa}} = 659 \text{ mV}$ . Linear

sweep voltammograms were taken to investigate the  $\text{electron}_{\text{ferrocene}}:\text{electron}_{\text{Mn(acac)}_3}$  ratio of the reactions that take place. A 1:1 ratio was obtained in both the forward and backward redox reaction of the  $\text{Mn(acac)}_3$  complex relative to the redox reaction of the ferrocene. This implies that both the redox reactions of the  $\text{Mn(acac)}_3$  complex are one electron processes. The two redox couples were assigned to the  $\text{Mn}^{\text{III}}/\text{Mn}^{\text{IV}}$  redox couple and the  $\text{Mn}^{\text{III}}/\text{Mn}^{\text{II}}$  redox couple. This result is in good agreement with previously published results.<sup>9,10</sup>

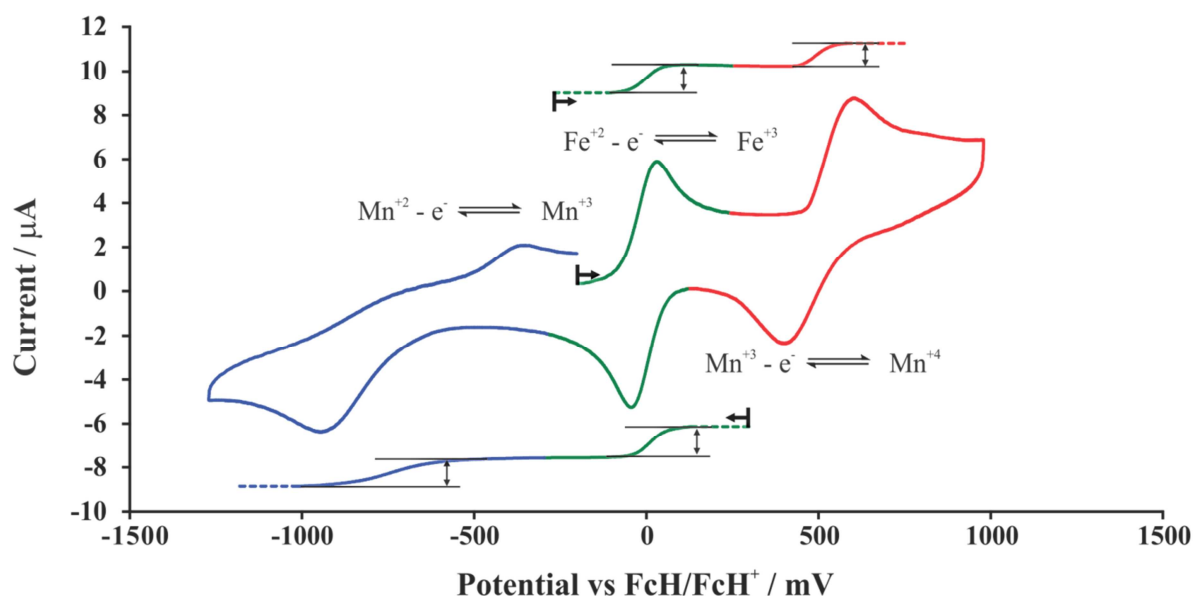


**Figure 3.5:** Redox reactions that take place during a cyclic voltammetry experiment of  $\text{Mn(acac)}_3$  with ferrocene as internal standard, solvent dichloromethane, supporting electrolyte tetrabutylammonium hexafluorophosphate, working electrode glassy carbon, concentration of 0.5 mM  $\text{Mn(acac)}_3$  with potential vs  $\text{FcH/FcH}^+$  at scan rate of 100  $\text{mV.s}^{-1}$ . Scan initiated in the positive direction as indicated by the arrow.

An electrochemical solvent study was done on  $\text{Mn(acac)}_3$  to find the conditions that will give the best cyclic voltammetry results. This involved keeping the supporting electrolyte (TBAHFP, see list of abbreviations) and complex concentration ( $C_{\text{Mn(acac)}_3} = 0.5 \text{ mM}$ ) the same, while changing the solvent (acetonitrile and dichloromethane). The results of this study are summarized in **Table 3.6**. The smaller  $\Delta E_p$  values observed at the  $\text{Mn}^{\text{III}}/\text{Mn}^{\text{II}}$  and  $\text{Mn}^{\text{III}}/\text{Mn}^{\text{IV}}$  redox couples in dichloromethane (DCM) proved that it was the best solvent. Ultimately due to the solubility problems of some  $\text{Mn}(\beta\text{-diketonato})_3$  complexes in DCM, acetonitrile was chosen as the solvent of this study. The solvents' effect on the electrochemical study of  $\text{Mn(acac)}_3$  can be seen in **Figure 3.6**.

<sup>9</sup> T. Paczeński, P. Błoniarczyk, K. Rydel, A. Sobkowiak, *Electroanalysis* **2007** (19) 945-951.

<sup>10</sup> R. van Gorkum, E. Bouwman, J. Reedijk, *Inorg. Chem.* **2004** (43) 2456-2458.

## Results and discussion

**Table 3.6:** Electrochemistry solvent study on  $\text{Mn}(\text{acac})_3$  for  $\text{Mn}^{\text{III}}/\text{Mn}^{\text{II}}$  and  $\text{Mn}^{\text{III}}/\text{Mn}^{\text{IV}}$  couples.

Solvent	$\text{Mn}^{\text{III}}/\text{Mn}^{\text{II}}$ redox couple							$\text{Mn}^{\text{III}}/\text{Mn}^{\text{IV}}$ redox couple						
	$E_{\text{pa}}$ (mV)	$E_{\text{pc}}$ (mV)	$\Delta E_p$ (mV)	$\frac{E_{\text{pc}} - E_{\text{pa}}}{2}$ (mV)	$i_{\text{pa}}$ ( $\mu\text{A}$ )	$i_{\text{pc}}$ ( $\mu\text{A}$ )	$i_{\text{pa}}/i_{\text{pc}}$	$E_{\text{pa}}$ (mV)	$E_{\text{pc}}$ (mV)	$\Delta E_p$ (mV)	$\frac{E_{\text{pc}} - E_{\text{pa}}}{2}$ (mV)	$i_{\text{pa}}$ ( $\mu\text{A}$ )	$i_{\text{pc}}$ ( $\mu\text{A}$ )	$i_{\text{pc}}/i_{\text{pa}}$
DCM <sup>i</sup>	-344	-995	652	-669	2.35	3.94	0.60	608	388	221	498	5.05	3.52	0.69
$\text{CH}_3\text{CN}^{\text{ii}}$	-117	-924	807	-520	1.88	4.71	0.40	659	418	240	538	3.09	2.94	0.95

*i* Solvent dichloromethane, supporting electrolyte tetrabutylammonium hexafluorophosphate, working electrode glassy carbon, concentration of 0.5 mM  $\text{Mn}(\text{acac})_3$  with potential vs  $\text{FcH}/\text{FcH}^+$

*ii* Solvent acetonitrile, supporting electrolyte tetrabutylammonium hexafluorophosphate, working electrode glassy carbon, concentration of 0.5 mM  $\text{Mn}(\text{acac})_3$  with potential vs  $\text{FcH}/\text{FcH}^+$

\*  $\frac{E_{\text{pc}} - E_{\text{pa}}}{2}$  was used since the redox couple is electrochemically irreversible ( $\Delta E_p > 90$  mV) and  $E^\circ$  is not the correct notation (this is applicable throughout this study).

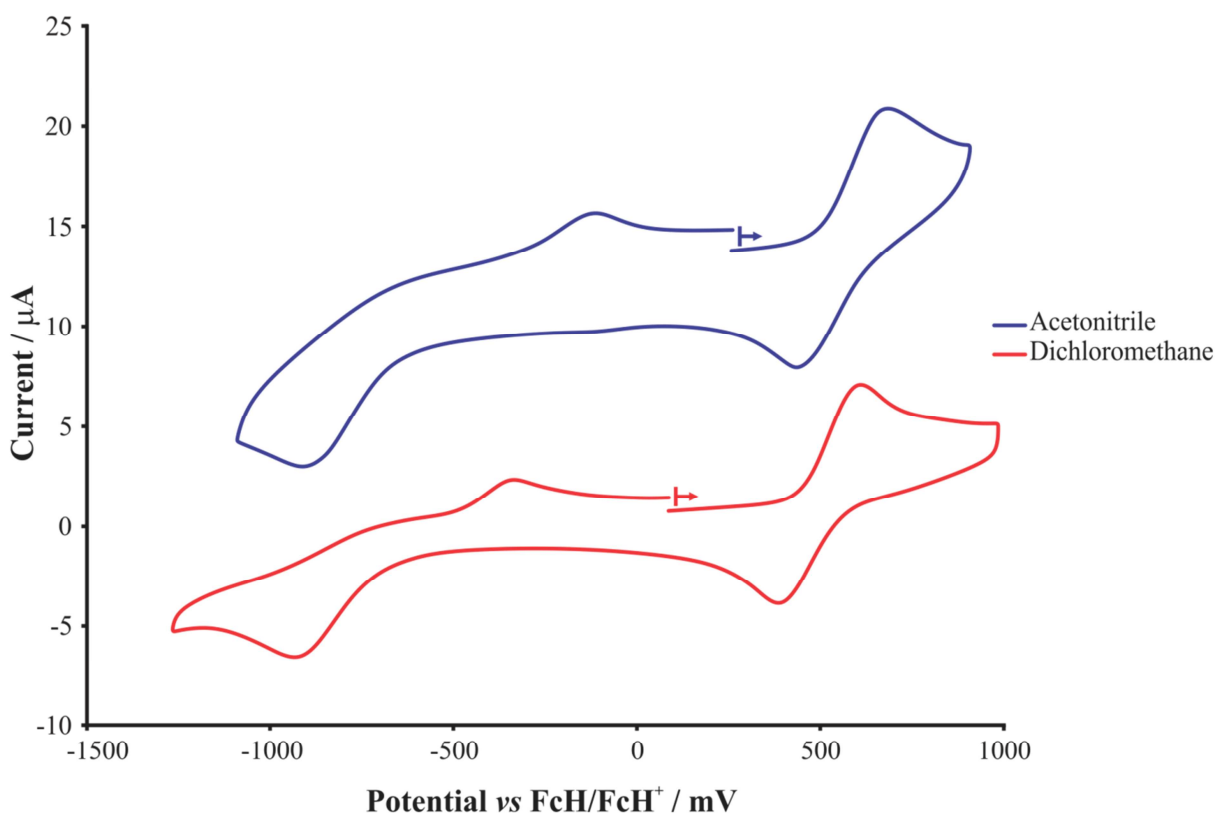


**Figure 3.6:** Cyclic voltammogram of  $\text{Mn}(\text{acac})_3$  ( $C_{\text{Mn}(\text{acac})_3} = 0.5$  mM) in acetonitrile and dichloromethane with supporting electrolyte tetrabutylammonium hexafluorophosphate and glassy carbon working electrode at a scan rate of  $100 \text{ mV} \cdot \text{s}^{-1}$  with potential vs  $\text{FcH}/\text{FcH}^+$ .

A concentration and supporting electrolyte study was done to determine the effect of the  $\text{Mn}(\text{acac})_3$  concentration and the type of supporting electrolyte on  $\text{Mn}(\text{acac})_3$ 's cyclic voltammograms. The concentration study was carried out by changing the concentration of the  $\text{Mn}(\text{acac})_3$  ( $C_{\text{Mn}(\text{acac})_3} = 0.5$  mM, 0.25 mM) while keeping the solvent and supporting electrolyte the same. The cyclic voltammogram and data comparing the two concentrations can be seen in

**Table 3.7** and **Figure 3.7**. The higher current value that was observed at higher concentrations was expected as the current is directly proportional to concentration. This is described by the Randle-Sevcik equation, see **Equation 3.1**.

$$i_p = (2.69 \times 10^5) n^{\frac{3}{2}} A D^{\frac{1}{2}} C v^{\frac{1}{2}} \quad \text{Equation 3.1}$$

Thus if the concentration of a complex is doubled one can expect current values that is double that of the original concentration's current values. The  $\Delta E_p$  values of both the  $\text{Mn}^{\text{III}}/\text{Mn}^{\text{II}}$  and  $\text{Mn}^{\text{III}}/\text{Mn}^{\text{IV}}$  couples are smaller with the  $\text{Mn}(\text{acac})_3$  concentration being 0.25 mM. The current ratio for the  $\text{Mn}^{\text{III}}/\text{Mn}^{\text{II}}$  couple are similar for both the concentrations and the current ratio of the  $\text{Mn}^{\text{III}}/\text{Mn}^{\text{IV}}$  couple is closer to one when the concentration is 0.25 mM. Therefore, the 0.25 mM concentration gives better results. In this study the concentration 0.5 mM was used since the peaks of the  $\text{Mn}^{\text{III}}/\text{Mn}^{\text{II}}$  couple were more observable.

**Table 3.7:** Electrochemical concentration study on  $\text{Mn}(\text{acac})_3$  for  $\text{Mn}^{\text{III}}/\text{Mn}^{\text{II}}$  and  $\text{Mn}^{\text{III}}/\text{Mn}^{\text{IV}}$  couples in dichloromethane with supporting electrolyte tetrabutylammonium hexafluorophosphate and glassy carbon working electrode at a scan rate of  $100 \text{ mV.s}^{-1}$  with potential vs  $\text{FcH}/\text{FcH}^+$ .

$C_{\text{Mn}(\text{acac})_3}$ (mM)	$\text{Mn}^{\text{III}} / \text{Mn}^{\text{II}}$				$\text{Mn}^{\text{III}} / \text{Mn}^{\text{IV}}$			
	$\Delta E_p$ (mV)	$i_{pa}$ ( $\mu\text{A}$ )	$i_{pc}$ ( $\mu\text{A}$ )	$i_{pa}/i_{pc}$	$\Delta E_p$ (mV)	$i_{pa}$ ( $\mu\text{A}$ )	$i_{pc}$ ( $\mu\text{A}$ )	$i_{pc}/i_{pa}$
0.5	652	2.35	3.94	0.60	221	5.05	3.52	0.85
0.25	504	1.14	2.06	0.55	167	2.55	2.48	0.97

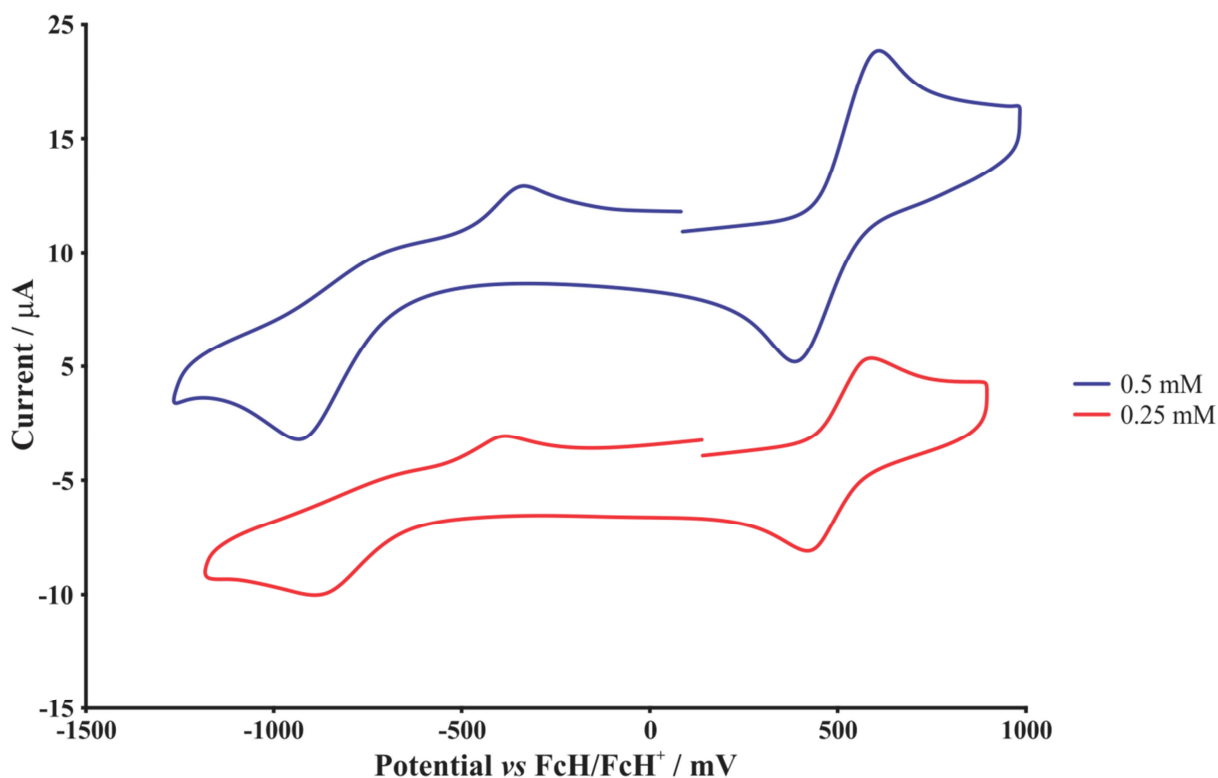


**Figure 3.7:** Cyclic voltammogram of  $\text{Mn}(\text{acac})_3$  ( $C_{\text{Mn}(\text{acac})_3} = 0.5 \text{ mM}$  and  $0.25 \text{ mM}$ ) in dichloromethane with supporting electrolyte tetrabutylammonium hexafluorophosphate and glassy carbon working electrode at a scan rate of  $100 \text{ mV.s}^{-1}$  with potential vs  $\text{FcH}/\text{FcH}^+$ .

The supporting electrolyte study involved keeping the complex concentration ( $C_{\text{Mn}(\text{acac})_3} = 0.5 \text{ mM}$ ) and solvent (acetonitrile) the same, while changing the supporting electrolyte. Two supporting electrolytes were used in this study namely tetrabutylammonium hexafluorophosphate (TBAHFP) and tetraethylammonium tetrafluoroborate ( $\text{TEABF}_4$ ). The results of the study are summarized in **Table 3.8** and illustrated in **Figure 3.8**. A shift within experimental error of  $6 \text{ mV}$  to the right was observed in the  $E_{\text{pc}}$  value of the  $\text{Mn}^{\text{III}}/\text{Mn}^{\text{II}}$  couple when  $\text{TEABF}_4$  was used as the supporting electrolyte.

**Table 3.8:** Electrochemical study of the supporting electrolyte effect on  $\text{Mn}(\text{acac})_3$  for  $\text{Mn}^{\text{III}}/\text{Mn}^{\text{II}}$  and  $\text{Mn}^{\text{III}}/\text{Mn}^{\text{IV}}$  couples.

Supporting electrolyte	$\text{Mn}^{\text{III}} / \text{Mn}^{\text{II}}$				$\text{Mn}^{\text{III}} / \text{Mn}^{\text{IV}}$				$\text{FcH}/\text{FcH}^+$	
	$\Delta E_{\text{p}}$ (mV)	$i_{\text{pa}}$ ( $\mu\text{A}$ )	$i_{\text{pc}}$ ( $\mu\text{A}$ )	$i_{\text{pa}}/i_{\text{pc}}$	$\Delta E_{\text{p}}$ (mV)	$i_{\text{pa}}$ ( $\mu\text{A}$ )	$i_{\text{pc}}$ ( $\mu\text{A}$ )	$i_{\text{pc}}/i_{\text{pa}}$	$E^0$ (mV)	Shift
TBAHFP	807	1.88	4.71	0.40	253	3.09	2.94	0.95	90	0
$\text{TEABF}_4$	722	1.23	3.51	0.35	228	3.82	2.49	0.65	84	6

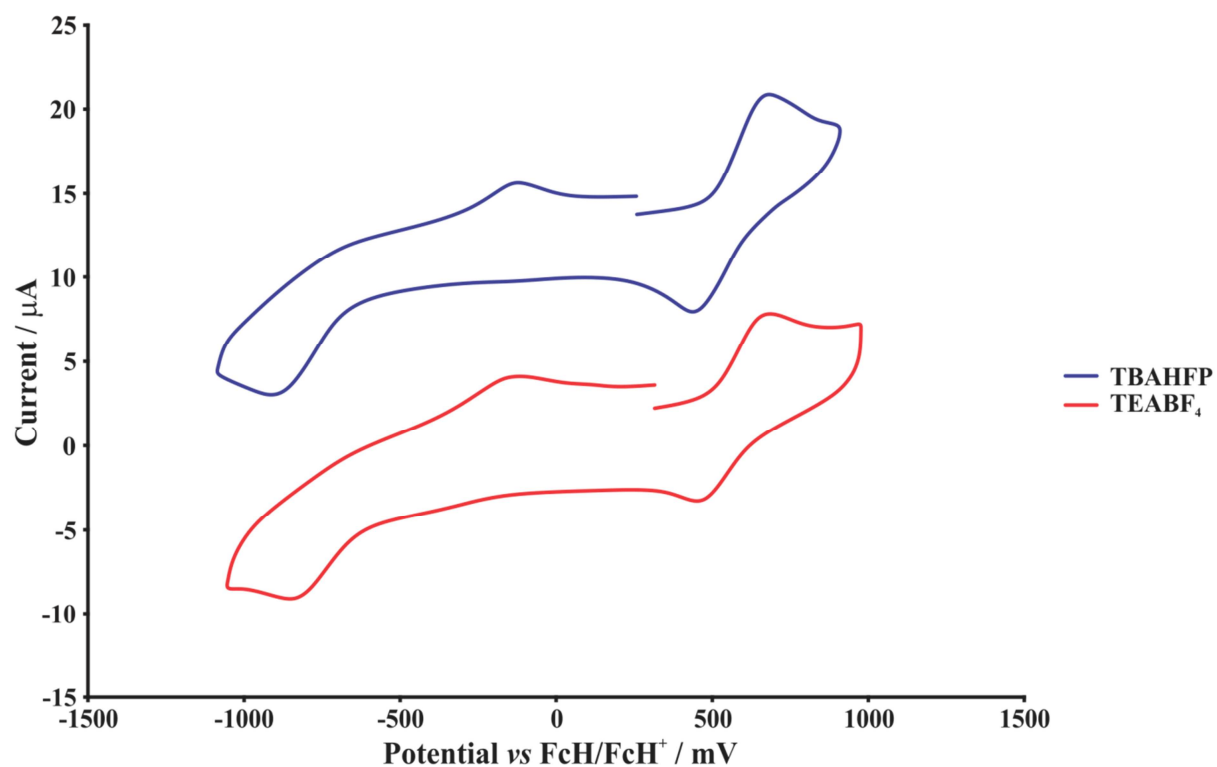


**Figure 3.8:** Cyclic voltammogram of  $\text{Mn}(\text{acac})_3$  ( $C_{\text{Mn}(\text{acac})_3} = 0.5 \text{ mM}$ ) in acetonitrile with supporting electrolyte (TBAHFP and  $\text{TEABF}_4$ ) and glassy carbon working electrode at a scan rate of  $100 \text{ mV}\cdot\text{s}^{-1}$  with potential vs  $\text{FcH}/\text{FcH}^+$ .

The cyclic voltammetry data of  $\text{Mn}(\text{acac})_3$  ( $C_{\text{Mn}(\text{acac})_3} = 0.5 \text{ mM}$ ) at various scan rates with acetonitrile as the solvent and TBAHFP as the supporting electrolyte are summarized in **Table 3.9** and illustrated in **Figure 3.9** and **Figure 3.10**.

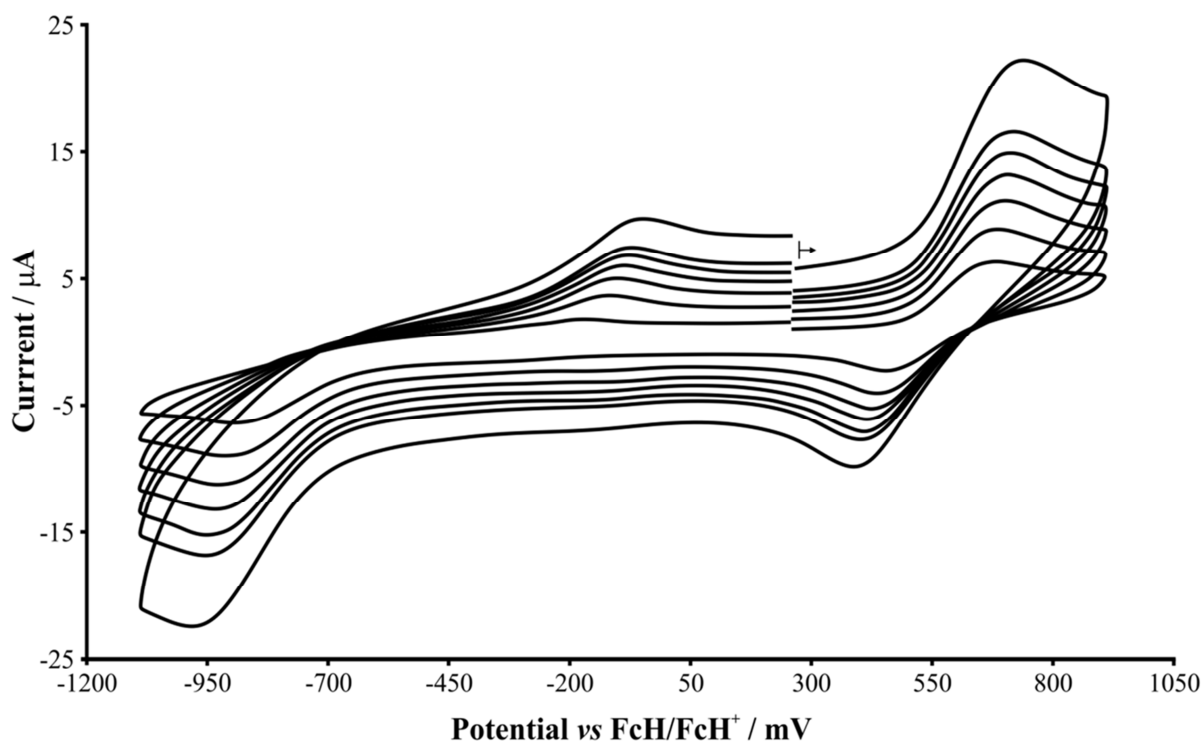


**Figure 3.9:** Cyclic voltammogram of  $\text{Mn}(\text{acac})_3$  at different scan rates (50, 100, 150, 200, 250, 300, 500  $\text{mV.s}^{-1}$ ), solvent acetonitrile, supporting electrolyte tetrabutylammonium hexafluorophosphate, working electrode glassy carbon, concentration of 0.5 mM  $\text{Mn}(\text{acac})_3$  with potential vs  $\text{FcH}/\text{FcH}^+$ .

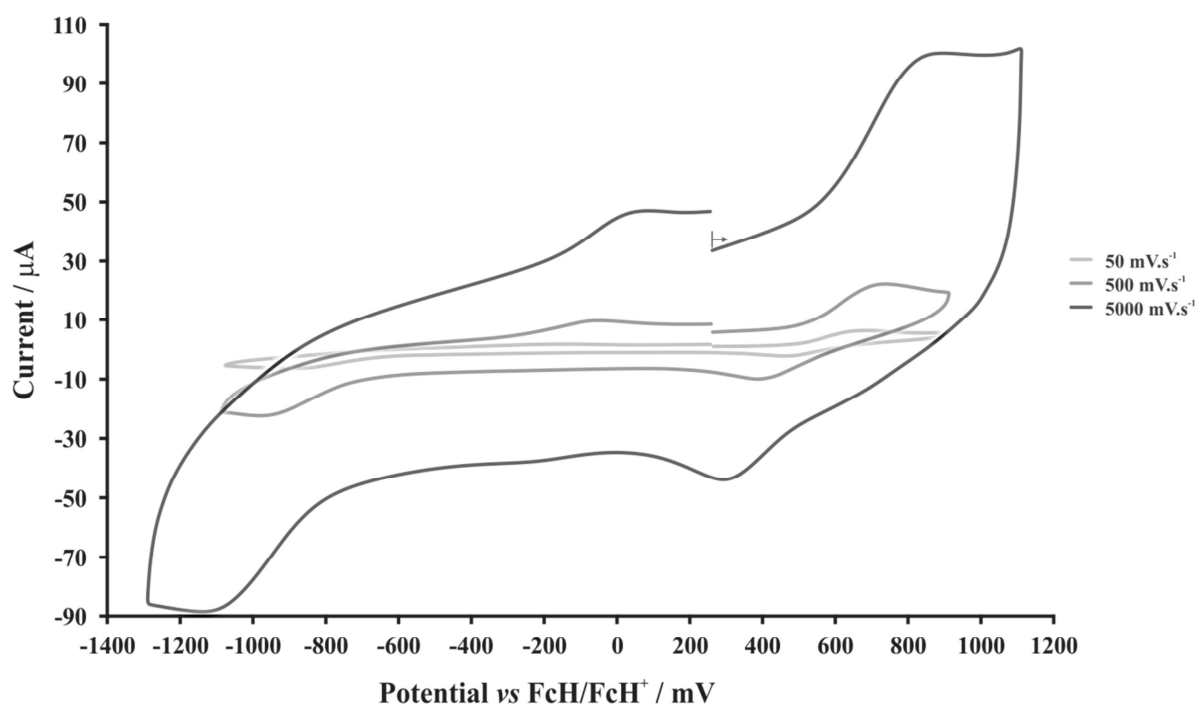


**Figure 3.10:** Cyclic voltammetry of  $\text{Mn}(\text{acac})_3$  at scan rates of 50, 500 and 5000  $\text{mV.s}^{-1}$ , solvent acetonitrile, supporting electrolyte tetrabutylammonium hexafluorophosphate, working electrode glassy carbon, concentration of 0.5 mM  $\text{Mn}(\text{acac})_3$  with potential vs  $\text{FcH}/\text{FcH}^+$ .

## CHAPTER 3

The scan rates were done up to two orders of magnitude of the slowest scan rate (50 mV.s<sup>-1</sup> - 5000 mV.s<sup>-1</sup>), to make sure that the same redox couples were seen at very fast scan rates (see **Figure 3.10**).

**Table 3.9:** Electrochemical data<sup>i</sup> of Mn(acac)<sub>3</sub> obtained from different scan rates.

Scan Rate (mV.s <sup>-1</sup> )	Mn <sup>III</sup> / Mn <sup>II</sup>							Mn <sup>III</sup> / Mn <sup>IV</sup>						
	E <sub>pa</sub> (mV)	E <sub>pc</sub> (mV)	ΔE <sub>p</sub> (mV)	$\frac{E_{pc} - E_{pa}}{2}$ (mV)	i <sub>pa</sub> (μA)	i <sub>pc</sub> (μA)	i <sub>pa</sub> /i <sub>pc</sub>	E <sub>pa</sub> (mV)	E <sub>pc</sub> (mV)	ΔE <sub>p</sub> (mV)	$\frac{E_{pc} - E_{pa}}{2}$ (mV)	i <sub>pa</sub> (μA)	i <sub>pc</sub> (μA)	i <sub>pc</sub> /i <sub>pa</sub>
50	-170	-896	727	-533	0.71	2.96	0.24	684	459	225	572	3.79	3.74	0.99
100	-117	-924	807	-520	1.88	4.71	0.40	698	445	253	572	5.08	4.94	0.97
150	-107	-937	830	-522	2.41	5.56	0.43	715	432	283	574	5.43	5.28	0.97
200	-90	-943	853	-516	2.93	6.85	0.43	715	418	297	567	5.70	5.54	0.97
250	-77	-955	879	-516	3.33	7.41	0.45	730	418	313	574	6.85	6.52	0.95
300	-71	-959	888	-515	4.00	10.66	0.38	734	404	330	569	8.23	7.14	0.87
500	-46	-1012	966	-529	4.80	11.40	0.42	747	395	352	571	10.51	9.14	0.87
5000	69	-1130	1199	-531	15.63	24.38	0.64	841	190	651	515	36.25	15.00	0.41

<sup>i</sup> Solvent acetonitrile, supporting electrolyte tetrabutylammonium hexafluorophosphate, working electrode glassy carbon, concentration of 0.5 mM Mn(acac)<sub>3</sub> with potential vs FcH/FcH<sup>+</sup>

Mn(acac)<sub>3</sub> was electrochemically irreversible as indicated by the large ΔE<sub>p</sub> values of both the Mn<sup>III</sup>/Mn<sup>IV</sup> and Mn<sup>III</sup>/Mn<sup>II</sup> redox reaction peaks. The low i<sub>pa</sub>/i<sub>pc</sub> ratio for the Mn<sup>III</sup>/Mn<sup>II</sup> couple was attributed to the fact that the E<sub>pa</sub> of the reduced Mn<sup>II</sup> diffused into the bulk solution away from the electrodes before reoxidation back to Mn<sup>III</sup> could take place. The low i<sub>pa</sub>/i<sub>pc</sub> ratio at 50 mV.s<sup>-1</sup> and the higher i<sub>pa</sub>/i<sub>pc</sub> ratio observed at a higher scan rate of 5000 mV.s<sup>-1</sup> were consistent with this fact. The Mn<sup>III</sup>/Mn<sup>IV</sup> redox couple had an i<sub>pc</sub>/i<sub>pa</sub> ratio ≈ 1 at the scan rates of 50 - 500 mV.s<sup>-1</sup> which made the couple chemically reversible.

Three of the Mn(β-diketonato)<sub>3</sub> complexes of this study (β-diketonato = acac [1], ba [2] and dbm [3]) showed both the Mn<sup>III</sup>/Mn<sup>II</sup> and the Mn<sup>III</sup>/Mn<sup>IV</sup> redox couples in the solvent window. These complexes' cyclic voltammograms at a scan rate of 100 mV.s<sup>-1</sup> are illustrated in **Figure 3.11** and the data is given in **Table 3.10**.



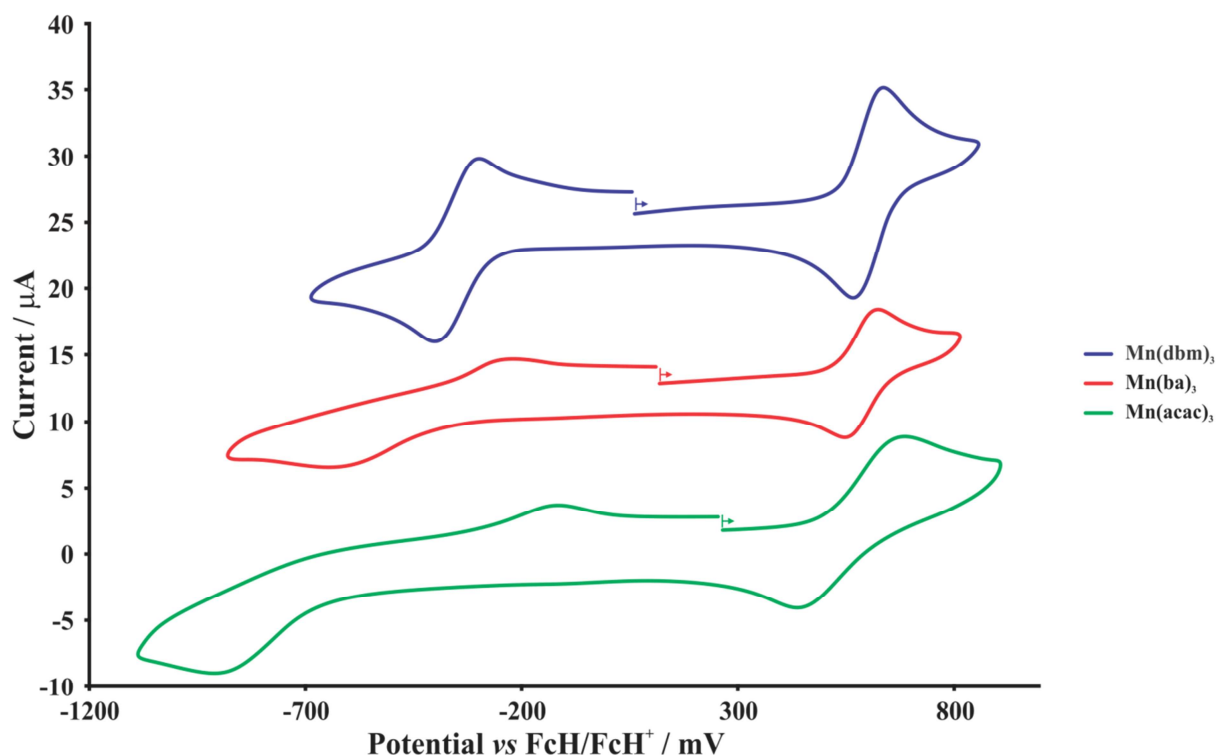


**Figure 3.11:** Cyclic voltammogram of  $\text{Mn}(\beta\text{-diketonato})_3$  ( $\beta\text{-diketonato}$  = acac, ba and dbm) with the concentrations of 0.5 mM in acetonitrile with supporting electrolyte tetrabutylammonium hexafluorophosphate and glassy carbon working electrode at a scan rate of  $100 \text{ mV.s}^{-1}$  with potential vs  $\text{FcH/FcH}^+$ .

**Table 3.10:** Electrochemical data of  $\text{Mn}(\beta\text{-diketonato})_3$  complexes ( $\beta\text{-diketonato}$  = acac, ba and dbm) with the concentrations of 0.5 mM in acetonitrile with supporting electrolyte tetrabutylammonium hexafluorophosphate and glassy carbon working electrode at a scan rate of  $100 \text{ mV.s}^{-1}$  with potential vs  $\text{FcH/FcH}^+$ .

Complex	$\text{Mn}^{\text{III}}/\text{Mn}^{\text{II}}$							$\text{Mn}^{\text{III}}/\text{Mn}^{\text{IV}}$						
	$E_{\text{pa}}$ (mV)	$E_{\text{pc}}$ (mV)	$\Delta E_{\text{p}}$ (mV)	$\frac{E_{\text{pc}} - E_{\text{pa}}}{2}$ (mV)	$i_{\text{pa}}$ ( $\mu\text{A}$ )	$i_{\text{pc}}$ ( $\mu\text{A}$ )	$i_{\text{pa}}/i_{\text{pc}}$	$E_{\text{pa}}$ (mV)	$E_{\text{pc}}$ (mV)	$\Delta E_{\text{p}}$ (mV)	$\frac{E_{\text{pc}} - E_{\text{pa}}}{2}$ (mV)	$i_{\text{pa}}$ ( $\mu\text{A}$ )	$i_{\text{pc}}$ ( $\mu\text{A}$ )	$i_{\text{pc}}/i_{\text{pa}}$
$\text{Mn}(\text{acac})_3$	-117	-924	807	-520	1.88	4.71	0.40	698	445	253	572	5.08	4.94	0.97
$\text{Mn}(\text{ba})_3$	-226	-635	409	-431	1.38	2.38	0.58	633	553	80	593	4.15	4.10	0.99
$\text{Mn}(\text{dbm})_3$	-302	-400	99	-351	5.94	6.18	0.96	647	580	67	613	4.13	4.00	0.97

In evaluating the  $\text{Mn}^{\text{III}}/\text{Mn}^{\text{II}}$  couple of the  $\text{Mn}(\beta\text{-diketonato})_3$  complexes ( $\beta\text{-diketonato}$  = acac [1], ba [2] and dbm [3]), it was observed that as more phenyl (Ph) groups were added to the  $\beta\text{-diketonato}$  backbone going from  $\text{Mn}(\text{acac})_3$  (no Ph) to  $\text{Mn}(\text{ba})_3$  (one Ph group) to  $\text{Mn}(\text{dbm})_3$  (two Ph groups) that the  $\Delta E_{\text{p}}$  values decreased and the  $i_{\text{pa}}/i_{\text{pc}}$  ratio increased. The  $i_{\text{pa}}/i_{\text{pc}}$  ratio implies that the reduced species became more stable in going from complex 1 to 3.

Reduction involves the adding of an electron to the lowest unoccupied molecular orbital (LUMO) of  $\text{Mn}^{\text{III}}(\beta\text{-diketonato})_3$ . A relationship between the LUMO energy of the  $\text{Mn}^{\text{III}}(\beta\text{-diketonato})_3$  complexes where  $\beta\text{-diketonato} = \text{acac}$ ,  $\text{ba}$  and  $\text{dbm}$  and the reduction potential  $E_{\text{pc}}$  was expected and can be seen in **Figure 3.12** and described with the following linear equation  $E_{\text{LUMO}} = -0.024 E_{\text{pc}} - 353.95$ .

**Table 3.11:** The LUMO energies of the three  $\text{Mn}^{\text{III}}(\beta\text{-diketonato})_3$  complexes where  $\beta\text{-diketonato} = \text{acac}$  [1],  $\text{ba}$  [2] and  $\text{dbm}$  [3] and their respective reduction potential of the  $\text{Mn}^{\text{III}}/\text{Mn}^{\text{II}}$  couple.

Complex	$E_{\text{LUMO}}$ ( $\text{kJ}\cdot\text{mol}^{-1}$ )	$E_{\text{pc}}$
$\text{Mn}(\text{acac})_3$ [1]	-332.5	-924
$\text{Mn}(\text{ba})_3$ [2]	-339.3	-635
$\text{Mn}(\text{dbm})_3$ [3]	-344.0	-400

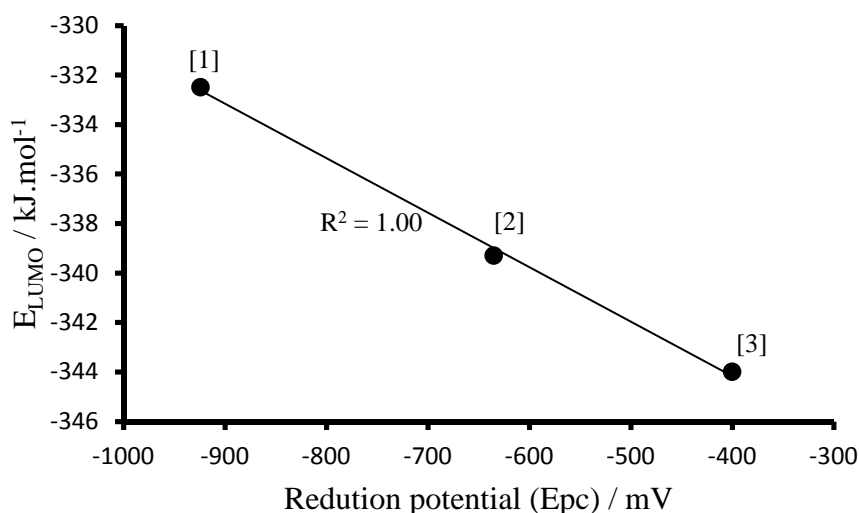


**Figure 3.12:** The correlation of the reduction potential ( $E_{\text{pc}}$ ) of  $\text{Mn}(\beta\text{-diketonato})_3$  complexes ( $\beta\text{-diketonato} = \text{acac}$  [1],  $\text{ba}$  [2] and  $\text{dbm}$  [3]) with their respective LUMO energies ( $E_{\text{LUMO}}$ ) of  $\text{Mn}^{\text{III}}(\beta\text{-diketonato})_3$ .

In evaluating the  $\text{Mn}^{\text{III}}/\text{Mn}^{\text{IV}}$  couple it was observed that the introduction of phenyl groups on the  $\beta\text{-diketonato}$  backbone of the  $\text{Mn}(\beta\text{-diketonato})_3$  complexes, leads to an electrochemically ( $\Delta E_{\text{p}} < 90 \text{ mV}$ ) reversible redox couple (see **Table 3.10**). Both the  $\text{Mn}(\text{ba})_3$  and  $\text{Mn}(\text{dbm})_3$  complexes are thus electrochemically and chemically reversible. DFT results of the complexes 1-3 will be presented in section 3.1.4, but some relevant results are given here. Since the oxidation of the  $\text{Mn}^{\text{III}}$  involves the removal of an electron from the HOMO of  $\text{Mn}^{\text{III}}$ , it was expected that a relationship between  $\frac{E_{\text{pc}} - E_{\text{pa}}}{2}$  and  $E_{\text{HOMO}}$  would exist (see **Figure 3.13**).

## Results and discussion

The linear equation obtained from **Figure 3.13** that describes the relationship between  $\frac{E_{pc} - E_{pa}}{2}$  and  $E_{HOMO}$  is as follows:

$$E_{HOMO} = -0.1812 \frac{E_{pc} - E_{pa}}{2} - 288.84$$

**Table 3.12:** The HOMO energies of the three  $Mn(\beta\text{-diketonato})_3$  complexes where  $\beta\text{-diketonato}$  = acac [1], ba [2] and dbm [3] and their respective  $\frac{E_{pc} - E_{pa}}{2}$  values of the  $Mn^{III}/Mn^{IV}$  couple.

Complex	$E_{HOMO}$ ( $\text{kJ}\cdot\text{mol}^{-1}$ )	$\frac{E_{pc} - E_{pa}}{2}$ (mV)
$Mn(acac)_3$ [1]	-386.8	572
$Mn(ba)_3$ [2]	-394.5	593
$Mn(dbm)_3$ [3]	-401.2	613

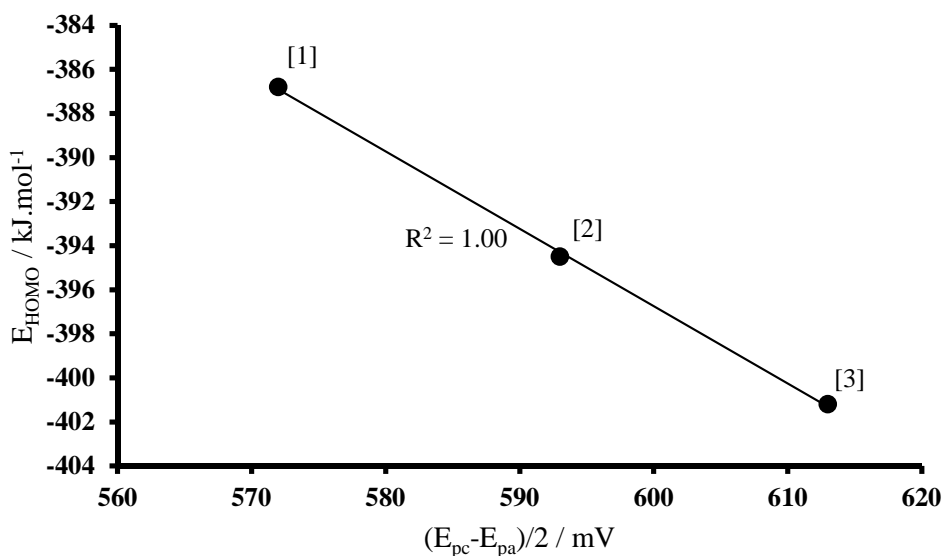


**Figure 3.13:** The correlation of the  $\frac{E_{pc} - E_{pa}}{2}$  of  $Mn^{III}(\beta\text{-diketonato})_3$  complexes ( $\beta\text{-diketonato}$  = acac [1], ba [2] and dbm [3]) with their respective highest occupied molecular orbital energies ( $E_{HOMO}$ ) for  $Mn^{III}(\beta\text{-diketonato})_3$ .

The rest of this study will focus on the reduction potential of the  $Mn^{III}/Mn^{II}$  redox couple since, the  $Mn^{III}/Mn^{IV}$  couple could not be observed for  $Mn^{III}(\beta\text{-diketonato})_3$  complexes ( $\beta\text{-diketonato}$  = tfaa [4], tfth[5], tffu [6], tfba [7] and hfac [8]) due to the solvent window that ranges from -2000 mV to 1500 mV which can be seen in **Figure 3.14**.

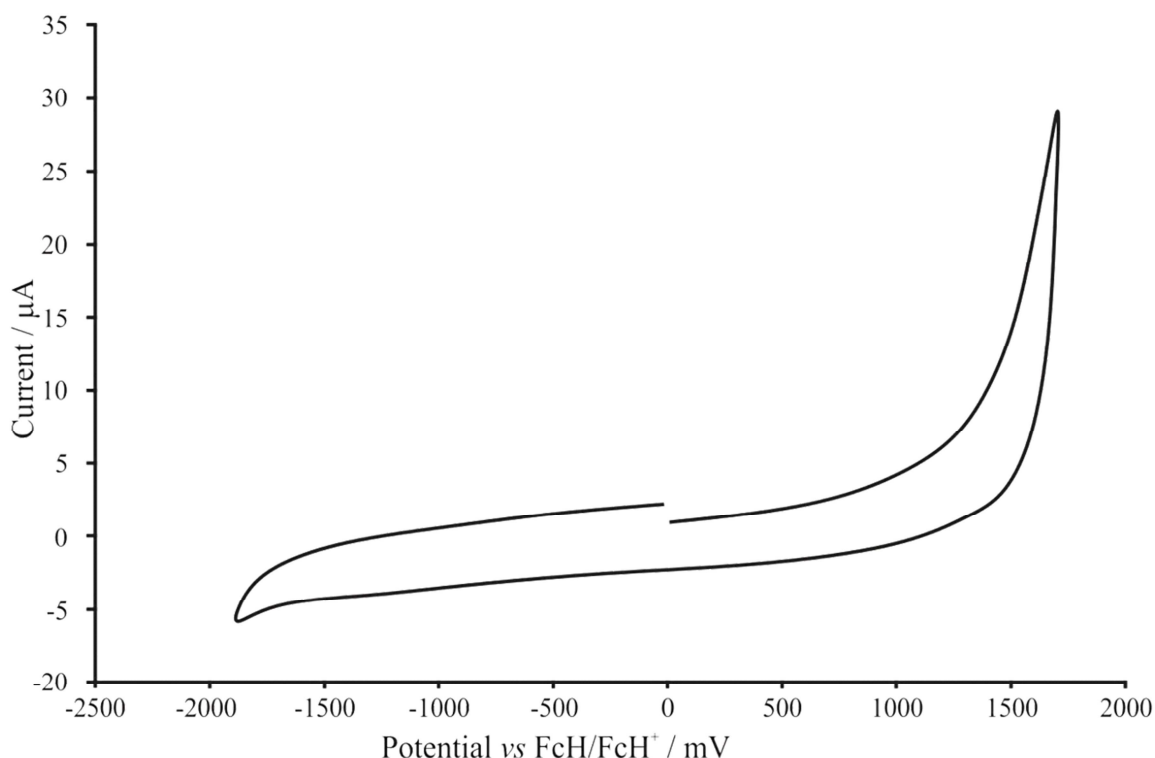


**Figure 3.14:** The solvent window observed at a scan rate of  $100 \text{ mV.s}^{-1}$ , solvent acetonitrile, supporting electrolyte tetrabutylammonium hexafluorophosphate, working electrode glassy carbon with potential vs  $\text{FcH/FcH}^+$ .

$\text{Mn}(\text{acac})_3$  is the only complex that was studied by cyclic voltammetry (CV) that had been published.<sup>11,12,13</sup> The results of  $\text{Mn}(\beta\text{-diketonato})_3$  complexes ( $\beta\text{-diketonato} = \text{ba}$  [2],  $\text{dbm}$  [3],  $\text{tfaa}$  [4],  $\text{tfth}$  [5],  $\text{tfu}$  [6],  $\text{tfba}$  [7] and  $\text{hfac}$  [8]) are reported here for the first time. The influence on the reduction potential ( $\text{Mn}^{\text{III}}/\text{Mn}^{\text{II}}$  couple) of the  $\text{Mn}(\beta\text{-diketonato})_3$  complexes, when more electronegative groups are introduced on the  $\beta\text{-diketonato}$  backbone is studied. **Figure 3.15** and **Figure 3.16** shows the  $\text{Mn}^{\text{III}}/\text{Mn}^{\text{II}}$  redox couple of the different  $\text{Mn}(\beta\text{-diketonato})_3$  complexes at a scan rate of  $100 \text{ mV.s}^{-1}$ . In **Figure 3.15** the cyclic voltammograms of the complex group with no  $\text{CF}_3$  groups starts with a  $\text{Mn}^{\text{III}}(\beta\text{-diketonato})_3$  specie and the rest of the complexes starts with a  $\text{Mn}^{\text{II}}(\beta\text{-diketonato})_3$  specie. At the start of all the cyclic voltammograms in **Figure 3.16** the manganese centre is in the  $\text{Mn}^{\text{III}}(\beta\text{-diketonato})_3$  specie. The electrochemical data that was obtained from **Figure 3.15** and **Figure 3.16** is summarized in **Table 3.13** and **Table 3.14** respectively. The electronic parameters [data acid dissociation constant ( $pK_a$ ) of the uncoordinated  $\beta\text{-diketone}$ , total group electronegativity [ $\Sigma(\chi_R + \chi_{R'})$ ] and total Hammett sigma meta constant [ $\Sigma(\sigma_R + \sigma_{R'})$ ] of the R and R' side groups of the  $\beta\text{-diketonato}$  ligands in  $\text{Mn}(\beta\text{-diketonato})_3$  are given in **Table 3.14**.

<sup>11</sup> A.M. Bond, R.I. Martin, A.F. Masters, *Inorg. Chem.* **1975** (14) 1432–1435.

<sup>12</sup> T. Paczeński, P. Błoniarz, K. Rydel, A. Sobkowiak, *Electroanalysis* **2007** (19) 945–951.

<sup>13</sup> R. van Gorkum, E. Bouwman, J. Reedijk, *Inorg. Chem.* **2004** (43) 2456–2458.

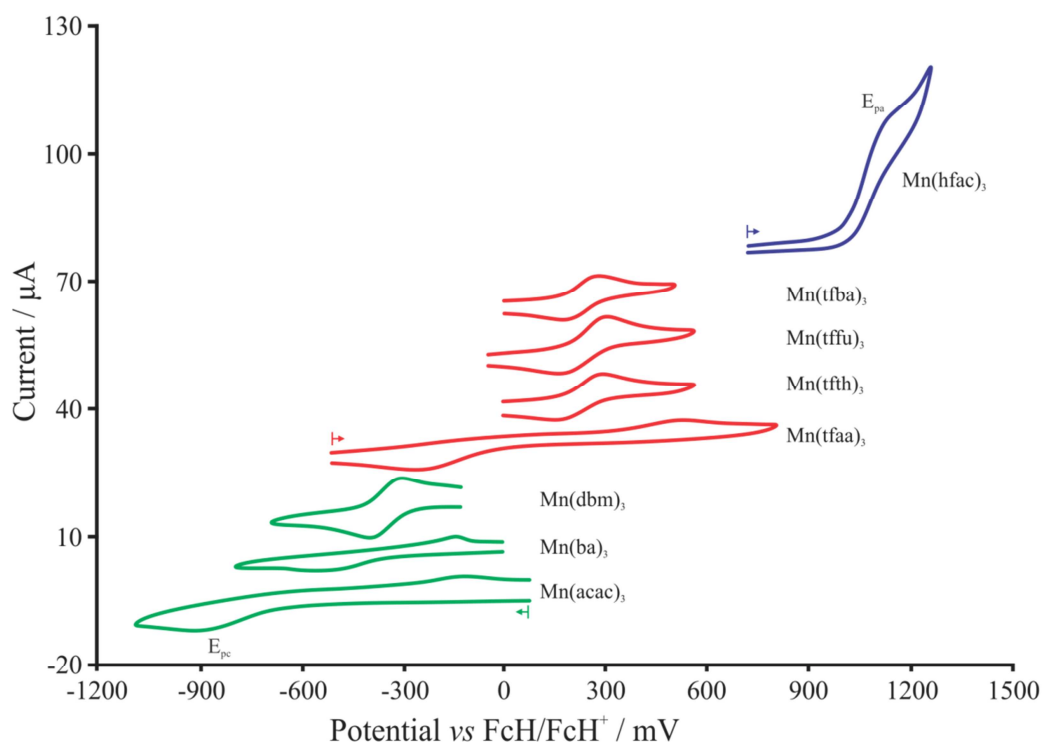


**Figure 3.15:** The shift observed of the  $\text{Mn}^{\text{III}}/\text{Mn}^{\text{II}}$  reduction couples of the different  $\text{Mn}(\beta\text{-diketonato})_3$  complexes with a scan rate of  $100 \text{ mV.s}^{-1}$ , solvent acetonitrile, supporting electrolyte tetrabutylammonium hexafluorophosphate, working electrode glassy carbon, concentration of  $0.5 \text{ mM Mn(acac)}_3$  vs  $\text{FcH}/\text{FcH}^+$ . Scans are initiated in the direction indicated by the arrows.

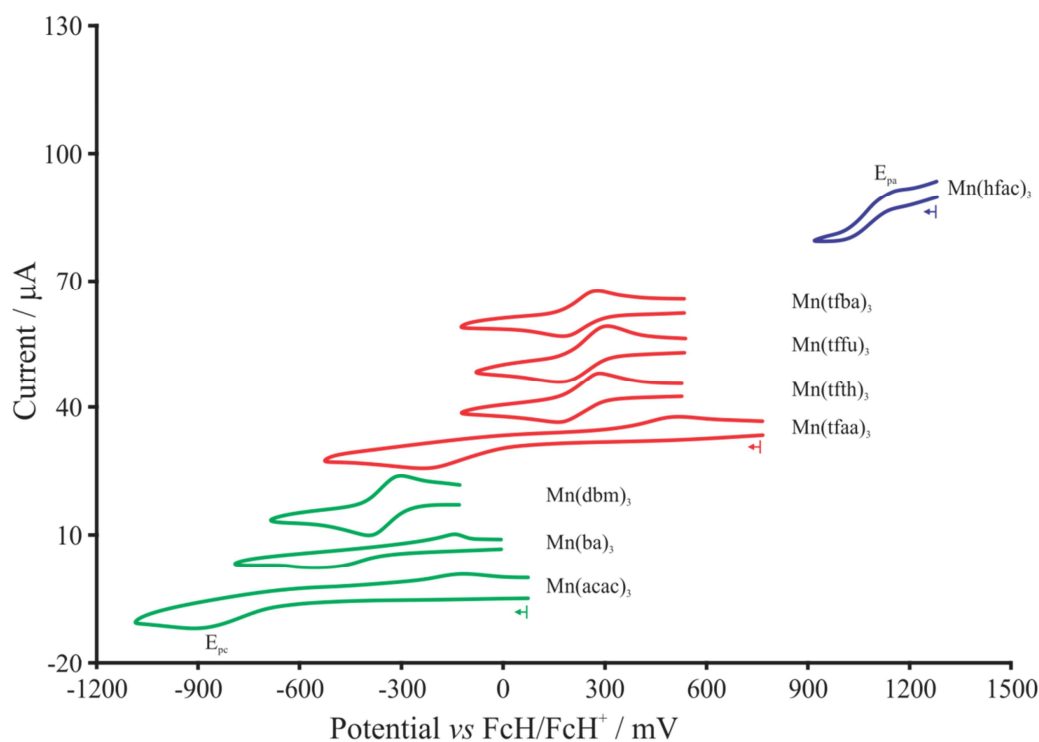


**Figure 3.16:** The shift observed of the  $\text{Mn}^{\text{III}}/\text{Mn}^{\text{II}}$  reduction couples of the different  $\text{Mn}(\beta\text{-diketonato})_3$  complexes with a scan rate of  $100 \text{ mV.s}^{-1}$ , solvent acetonitrile, supporting electrolyte tetrabutylammonium hexafluorophosphate, working electrode glassy carbon, concentration of  $0.5 \text{ mM Mn(acac)}_3$  vs  $\text{FcH}/\text{FcH}^+$ . Scans are initiated in the direction indicated by the arrows.

## CHAPTER 3

The reduction of  $\text{Mn}^{\text{III}}(\beta\text{-diketonato})_3$  to  $[\text{Mn}^{\text{II}}(\beta\text{-diketonato})_3]^{-1}$  involves the addition of an  $e^-$  to the complex. Thus, the more positive the  $\text{Mn}^{\text{III}}$  centre, the easier it would be to add an  $e^-$ . Therefore, it was expected that  $\text{Mn}^{\text{III}}(\beta\text{-diketonato})_3$  complexes with electron withdrawing R and R' groups on the  $\beta$ -diketonato ligands  $(\text{RCOCHCOR}')^-$  would be easier to reduce. A relationship between any electronic parameter that describes the electron density or withdrawing properties of the R and R' groups and the reduction potential  $E_{\text{pc}}$  ( $\text{Mn}^{\text{III}}/\text{Mn}^{\text{II}}$ ) was expected.

**Table 3.13:** Electrochemical data of all the  $\text{Mn}(\beta\text{-diketonato})_3$  complexes from **Figure 3.15**.

Complex	R	R'	Electrochemical data <sup>i</sup>						
			$E_{\text{pa}}$ (mV)	$E_{\text{pc}}$ (mV)	$\Delta E_{\text{p}}$ (mV)	$\frac{E_{\text{pc}} - E_{\text{pa}}}{2}$ (mV)	$i_{\text{pa}}$ ( $\mu\text{A}$ )	$i_{\text{pc}}$ ( $\mu\text{A}$ )	$i_{\text{pa}}/i_{\text{pc}}$
$\text{Mn}(\text{acac})_3$	$\text{CH}_3$	$\text{CH}_3$	-117	-924	807	-520	1.88	4.71	0.40
$\text{Mn}(\text{ba})_3$	$\text{CH}_3$	Ph	-226	-635	409	-431	1.38	2.38	0.58
$\text{Mn}(\text{dbm})_3$	Ph	Ph	-302	-400	99	-351	5.94	6.18	0.96
$\text{Mn}(\text{tfaa})_3$	$\text{CF}_3$	$\text{CH}_3$	520	-256	775	132	2.35	4.59	0.50
$\text{Mn}(\text{tfth})_3$	$\text{CF}_3$	$\text{C}_4\text{H}_3\text{S}$	296	149	147	223	3.51	3.62	0.97
$\text{Mn}(\text{tffu})_3$	$\text{CF}_3$	$\text{C}_4\text{H}_3\text{O}$	309	162	147	236	4.73	4.82	0.98
$\text{Mn}(\text{tfba})_3$	$\text{CF}_3$	Ph	279	171	109	225	4.15	4.33	0.96
$\text{Mn}(\text{hfac})_3$	$\text{CF}_3$	$\text{CF}_3$	1149	1041	108	1095	4.42	9.06	0.49

i Solvent acetonitrile, supporting electrolyte tetrabutylammonium hexafluorophosphate, concentration of  $\text{Mn}(\beta\text{-diketonato})_3 = 0.5 \text{ mM}$  with potential vs  $\text{FcH}/\text{FcH}^+$ , scan rate  $100 \text{ mV.s}^{-1}$ .

ii  $\Sigma$  is the sum of all three the  $\beta$ -diketonato ligands' group electronegativity and Hammett sigma meta constants.

**Table 3.14:** Electronic parameters and the electrochemical data of all the  $\text{Mn}(\beta\text{-diketonato})_3$  complexes from **Figure 3.16**.

Complex	R	R'	Electronic parameters			Electrochemical data <sup>i</sup>						
			$\text{pK}_a$	$\Sigma(\chi_{\text{R}} + \chi_{\text{R'}})^{ii}$	$\Sigma(\sigma_{\text{R}} + \sigma_{\text{R'}})^{ii}$	$E_{\text{pa}}$ (mV)	$E_{\text{pc}}$ (mV)	$\Delta E_{\text{p}}$ (mV)	$\frac{E_{\text{pc}} - E_{\text{pa}}}{2}$ (mV)	$i_{\text{pa}}$ ( $\mu\text{A}$ )	$i_{\text{pc}}$ ( $\mu\text{A}$ )	$i_{\text{pa}}/i_{\text{pc}}$
$\text{Mn}(\text{acac})_3$	$\text{CH}_3$	$\text{CH}_3$	8.95	14.04	-0.41	-117	-924	807	-520	1.88	4.71	0.40
$\text{Mn}(\text{ba})_3$	$\text{CH}_3$	Ph	8.70	13.65	-0.03	-226	-635	409	-431	1.38	2.38	0.58
$\text{Mn}(\text{dbm})_3$	Ph	Ph	8.89	12.60	0.36	-302	-400	99	-351	5.94	6.18	0.96
$\text{Mn}(\text{tfaa})_3$	$\text{CF}_3$	$\text{CH}_3$	6.30	16.05	1.08	517	-230	747	143	2.13	4.26	0.50
$\text{Mn}(\text{tfth})_3$	$\text{CF}_3$	$\text{C}_4\text{H}_3\text{S}$	6.48	15.33	1.56	289	165	124	227	4.79	4.79	1.00
$\text{Mn}(\text{tffu})_3$	$\text{CF}_3$	$\text{C}_4\text{H}_3\text{O}$	6.50	15.39	1.47	309	168	141	238	5.28	5.28	1.00
$\text{Mn}(\text{tfba})_3$	$\text{CF}_3$	Ph	6.30	15.66	1.47	280	178	102	229	4.15	4.17	1.00
$\text{Mn}(\text{hfac})_3$	$\text{CF}_3$	$\text{CF}_3$	4.35	18.06	2.58	1159	1009	150	1084	4.23	7.56	0.56

i Solvent acetonitrile, supporting electrolyte tetrabutylammonium hexafluorophosphate, concentration of  $\text{Mn}(\beta\text{-diketonato})_3 = 0.5 \text{ mM}$  with potential vs  $\text{FcH}/\text{FcH}^+$ , scan rate  $100 \text{ mV.s}^{-1}$ .

ii  $\Sigma$  is the sum of all three the  $\beta$ -diketonato ligands' group electronegativity and Hammett sigma meta constants.

Evaluation of the cyclic voltammograms displayed in **Figure 3.15** and **Figure 3.16** showed that the complexes could be divided into three groups namely the green group with no CF<sub>3</sub> side group, the red group with one CF<sub>3</sub> side group and the blue group with two CF<sub>3</sub> side groups. Electronic parameters that are often used to describe the electron donating power of the R groups are known as the Gordy scale group electronegativities<sup>14,15</sup> or Hammett constants<sup>16,17,18</sup>. The R group is in a meta position in the six-membered ring relative to the metal thus the Hammett meta values were used.<sup>19</sup> All the Mn(β-diketonato)<sub>3</sub> complexes have three R and three R' groups, thus the total group electronegativity and the Hammett sigma meta constants were 3(χ<sub>R</sub> + χ<sub>R'</sub>) and 3(σ<sub>R</sub> + σ<sub>R'</sub>) respectively. The total group electronegativities, total Hammett sigma meta constants of the R and R' groups and the acid dissociation constants of the un-coordinated β-diketones are tabulated in **Table 3.14**. From **Table 3.13** and **Table 3.14** it is clear that the ΔE<sub>p</sub> of the complexes with one CF<sub>3</sub> group improved and the current ratios of the complexes with one and two CF<sub>3</sub> groups are closer to one in **Table 3.14**. Since better results were obtained from **Figure 3.16**, only these results will be used in the correlations between cyclic voltammetry data and electronic parameters. It can be seen from **Table 3.14** that with the increase of the total group electronegativity [Σ(χ<sub>R</sub> + χ<sub>R'</sub>), Gordy scale] an increase of the reduction potential (E<sub>pc</sub>) followed. The relationships between the reduction potential (E<sub>pc</sub>), acid dissociation constants (pK<sub>a</sub>) of the un-coordinated β-diketones (RCOCH<sub>2</sub>COR'), total group electronegativities [Σ(χ<sub>R</sub> + χ<sub>R'</sub>)] and total Hammett sigma meta constants [Σ(σ<sub>R</sub> + σ<sub>R'</sub>)] of the R and R' groups are shown in **Figure 3.17**.

<sup>14</sup> W.C. du Plessis, T.G. Vosloo, J.C. Swarts, *J. Chem. Soc. Dalton Trans.* **1998** 2507.

<sup>15</sup> R.E. Kagarise, *J. Am. Chem. Soc.* **995** (77) 1377.

<sup>16</sup> L.P. Hammett, *Chem. Rev.* **1935** (17) 125.

<sup>17</sup> L.P. Hammett, *J. Am. Chem. Soc.* **1937** (59) 96.

<sup>18</sup> C. Hansch, A. Leo, R.W. Taft, *Chem. Rev.* **1991** (91) 165.

<sup>19</sup> R.L. Lintvedt, H.D. Russell, H.F. Holtzclaw, *Inorg. Chem.* **1966** (5) 1603.

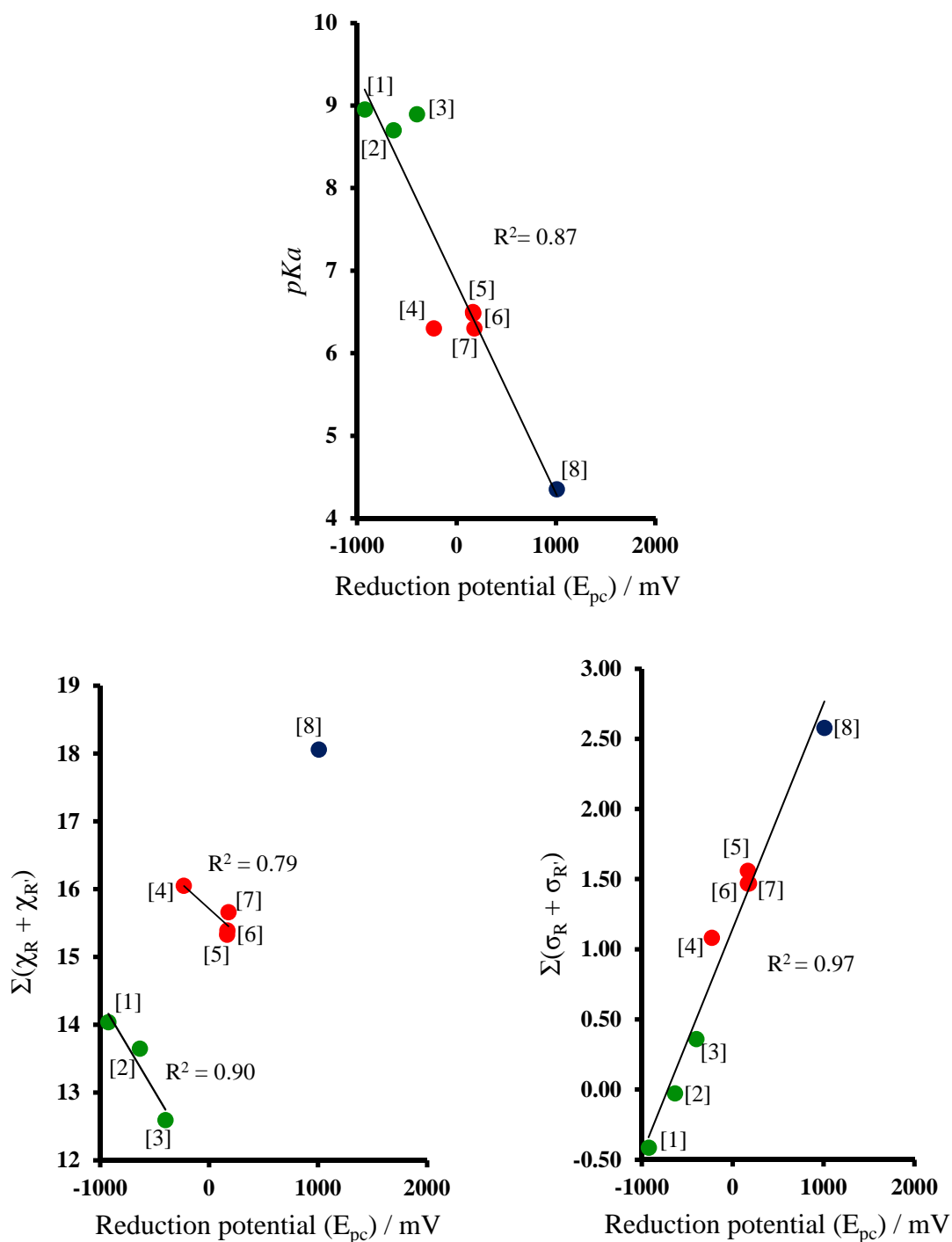


**Figure 3.17:** The correlation of the reduction potential ( $E_{pc}$ ) of Mn( $\beta$ -diketonato)<sub>3</sub> complexes ( $\beta$ -diketonato = acac [1], ba [2], dbm [3], tfaa [4], tfth[5], tffu [6], tfba [7] and hfac [8]) with the acid dissociation constants ( $pK_a$ ) of the un-coordinated  $\beta$ -diketones ( $RCOCH_2COR'$ ), the total group electronegativity [ $\Sigma(\chi_R + \chi_{R'})$ ] and the total Hammett sigma meta constant [ $\Sigma(\sigma_R + \sigma_{R'})$ ] of the R and R' groups. The  $\beta$ -diketonato ligands in green, red and blue groups contain none, one and two  $CF_3$  R-groups respectively.



The correlation of the reduction potential ( $E_{pc}$ ) of the  $Mn^{III}/Mn^{II}$  couple in **Figure 3.17** showed the following trends:

**$E_{pc}$  versus  $pK_a$ :** Showed that  $E_{pc}$  increased with decreasing  $pK_a$ . The manganese metal centre is relatively more electron-rich with a higher, more basic  $pK_a$  of the un-coordinated  $\beta$ -diketone. The more negative the  $E_{pc}$  the harder it was to reduce the  $Mn^{III}(\beta\text{-diketonato})_3$  complexes.

**$E_{pc}$  versus  $\Sigma(\chi_R + \chi_{R'})$ :** A general trend was observed that showed three separate trends for the green, red and blue groups, where the  $\beta$ -diketonato ligands contained none, one and two  $CF_3$  R-groups respectively. As the total group electronegativity of the R-groups increased the reduction potential generally became more positive. The trend within the three groups showed an opposite behaviour (the  $E_{pc}$  slightly decreased with the increase of the total group electronegativities).

**$E_{pc}$  versus  $\Sigma(\sigma_R + \sigma_{R'})$ :** Showed that with increasing the total Hammett sigma meta constant there was an increase in  $E_{pc}$ . The larger the Hammett sigma constant, the relatively more electron-deficient the manganese metal centre and consequently the  $Mn^{III}(\beta\text{-diketonato})_3$  complexes reduced more easily.

The linear equations in **Figure 3.17** defining the relationships between  $E_{pc}$  and the parameters above are:

$$\begin{aligned}
 pK_a &= (-0.0025)E_{pc} + 6.85 & R^2 &= 0.86 \\
 \chi_R + \chi_{R'} &= (-0.0027)E_{pc} + 11.66 & R^2 &= 0.93 & (\text{green group, R and R}' \neq CF_3) \\
 \chi_R + \chi_{R'} &= (-0.0015)E_{pc} + 15.70 & R^2 &= 0.77 & (\text{red group, R or R}' = CF_3) \\
 \chi_R + \chi_{R'} &= 18.06 & & & (\text{blue group, R and R}' = CF_3) \\
 \sigma_R + \sigma_{R'} &= (0.0016)E_{pc} + 1.14 & R^2 &= 0.96
 \end{aligned}$$

The above equations allows one to predict the reduction potential of the  $Mn^{III}/Mn^{II}$  couple if the acid dissociation constant of the un-coordinated  $\beta$ -diketone, the electronegativities or Hammett sigma meta constants of  $Mn(\beta\text{-diketonato})_3$  complexes are known. The  $Mn^{III}/Mn^{II}$  redox couple of the  $Mn(\beta\text{-diketonato})_3$  complexes with phenyl or aromatic rings are more electrochemically (smaller  $\Delta E_p$  values) and chemically ( $i_{pc}/i_{pa}$  closer to 1) reversible. The  $Mn(\beta\text{-diketonato})_3$  complexes with one  $CF_3$  R group began in the reduced  $Mn^{II}(\beta\text{-diketonato})_3$  species and follows with the oxidation to the  $Mn^{III}(\beta\text{-diketonato})_3$  at 0 mV vs  $FcH/FcH^+$ . The addition of an aromatic R group leads to smaller  $\Delta E_p$  values for the  $Mn(\beta\text{-diketonato})_3$  complexes 5-7.

### 3.1.4 Computational study.

#### 3.1.4.1 Mn(acetylacetonato)<sub>3</sub>, Mn(acac)<sub>3</sub>.

The Mn<sup>III</sup>(β-diketonato)<sub>3</sub> series are d<sup>4</sup> complexes, which can have a spin state of S = 0, 2/2 or 4/2. The spin state of Mn<sup>III</sup>(acac)<sub>3</sub> was determined by computationally calculating the lowest energy optimized structure (ADF, OLYP) of the possible spin states. The comparison of the spin state data is summarized in **Table 3.15**.

**Table 3.15:** Calculated relative energies of the optimized geometries (ADF, OLYP) of Mn(acac)<sub>3</sub> for different spin states.

Complex	Spin state	Symmetry	Relative energies (kJ.mol <sup>-1</sup> )
Mn <sup>III</sup> (acac) <sub>3</sub>	0/2	C <sub>2</sub>	97.0
	2/2	C <sub>2</sub>	31.5
	4/2	C <sub>2</sub>	0.0

From the spin state study the Mn(acac)<sub>3</sub> ground state was clearly identified as 4/2 spin state, which was in agreement with experimental data.<sup>20</sup> By comparing the calculated optimized structure of Mn(acac)<sub>3</sub> (S = 4/2) with crystal structures from previous studies, the computational method was validated. The functionals that were used to validate the method is OLYP, B3LYP, BP86 and PW91. The comparison between the optimized structures and crystal data are given in **Table 3.16**.

**Table 3.16:** Experimental and calculated Mn-O bond lengths.

Functional / Crystal	Bond length (Mn-O) (Å)					
	1	2	3	4	5	6
OLYP	1.974	1.974	1.993	1.993	2.245	2.245
B3LYP	1.939	1.939	1.957	1.957	2.173	2.173
BP86	1.946	1.946	1.960	1.960	2.187	2.187
PW91	1.944	1.944	1.958	1.958	2.184	2.184
Crystal average <sup>21,22,23</sup>	1.920	1.936	1.969	1.975	2.084	2.075

<sup>20</sup> I. Diaz-Acosta, J. Baker, J.F. Hinton, P. Puley, *Spectrochimica Acta Part A* **2003** (59) 363-377.

<sup>21</sup> B.R. Stults, R.S. Marianelli, V.W. Day, *J. Inorg. Chem.* **1979** (18) 1853-1858.

<sup>22</sup> J.P. Fackler, A. Avdeef, *Inorg. Chem.* **1974** (13) 1864-1875.

<sup>23</sup> S. Geremia, N. Demitri, *J. Chem. Educ.* **2005** (82) 460-465.

## Results and discussion

All functionals gave the Mn-O bonds within 0.1 Å of the average experimental values. B3LYP is the functional that had Mn-O bond lengths closest to the crystal data. It is known that GGA functionals overestimate bond lengths<sup>24</sup> which accounted for the slightly longer calculated bond lengths seen in **Table 3.16**. Since this study concentrated on relative energies and the OLYP functional is known to calculate good energies, the OLYP functional was used in the rest of the study. The symmetry of Mn(acac)<sub>3</sub> was determined by optimizing all the possible spin states ( $S = 0/2, 2/2$  and  $4/2$ ) with  $D_3$  and  $C_2$  symmetries with the use of the OLYP functional. The relative energies are summarized in **Table 3.17**.

**Table 3.17:** Relative energies of the different spin states and symmetries possible for Mn(acac)<sub>3</sub>.

Spin state	Symmetry	Relative energy (kJ.mol <sup>-1</sup> )
0/2	$D_3$	-
2/2	$D_3$	31.5
4/2	$D_3$	13.0
0/2	$C_2$	97.0
2/2	$C_2$	31.5
4/2	$C_2$	0.0

From **Table 3.17** it was concluded that Mn(acac)<sub>3</sub> prefers the spin state of 4/2 and the  $C_2$  symmetry, this is in agreement with both experimental and computational studies.<sup>25,26</sup> The  $C_2$  symmetry was in agreement with the Jahn-Teller distortion of the Mn(acac)<sub>3</sub> complex observed experimentally.<sup>25</sup> From the discussion in section 2.3.2.4 and **Figure 2.13** it follows that many  $d^4$  species are generally Jahn-Teller unstable and exhibit  $C_2$  symmetry. The electron filling of the  $d$ -orbitals of Mn(acac)<sub>3</sub> was thus expected to be either  $t_{2g}^3 d_{z^2}^1$  or  $t_{2g}^3 d_{x^2-y^2}^1$ , see **Figure 3.19**. The highest occupied molecular orbital (HOMO) of Mn(acac)<sub>3</sub> is therefore either  $d_{z^2}$  or  $d_{x^2-y^2}$ . The HOMO of the optimized Mn(acac)<sub>3</sub> complex, see **Figure 3.18**, is mainly of  $d_{z^2}$  character, pointing in the directions of the ligands on the  $z$ -axis. A negative Jahn-Teller could thus be expected due to the large electrostatic repulsion between the  $d_{z^2}$ -orbital of the manganese centre and the ligands on the  $z$ -axis.

<sup>24</sup> A.C. Schiener, J. Baker, J.W. Andzelm, *J. Comput. Chem.* **1997** (18) 775-795.

<sup>25</sup> I. Diaz-Acosta, J. Baker, J.F. Hinton, P. Puley, *Spectrochimica Acta Part A* **2003** (59) 363-377.

<sup>26</sup> S. Geremia, N. Demitri, *J. Chem. Educ.* **2005** (82) 460-465.

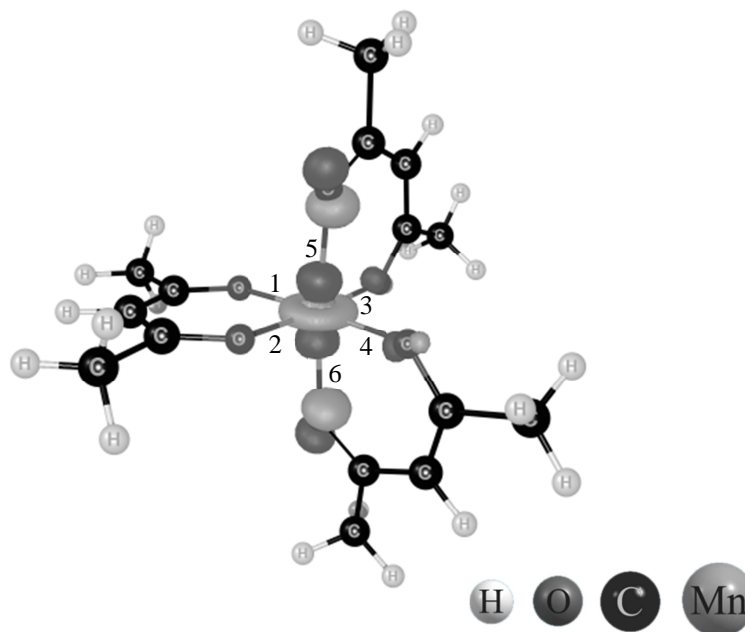


**Figure 3.18:** ADF/OLYP HOMO orbital of the optimized  $\text{Mn}(\text{acac})_3$  complex.

The large electrostatic repulsion causes an elongation of the Mn-O bond lengths along the  $z$ -axis, which can be seen as bond lengths 5 and 6 in **Table 3.18**.

**Table 3.18:** Mn-O bond lengths of optimized  $\text{Mn}(\text{acac})_3$  complex. (refer to **Figure 3.18** for Mn-O numbering)

Complex	Bond length (Mn-O) (Å)					
	1	2	3	4	5	6
$\text{Mn}(\text{acac})_3$	1.974	1.974	1.993	1.993	2.245	2.245

It is known from previous studies that  $\text{Mn}(\text{acac})_3$  crystals can undergo a negative or a positive Jahn-Teller distortion.<sup>27</sup> The electron  $d$ -orbital fillings of these two distortions are illustrated in **Figure 3.19**.

<sup>27</sup> S. Geremia, N. Demitri, *J. Chem. Educ.* **2005** (82) 460-465.

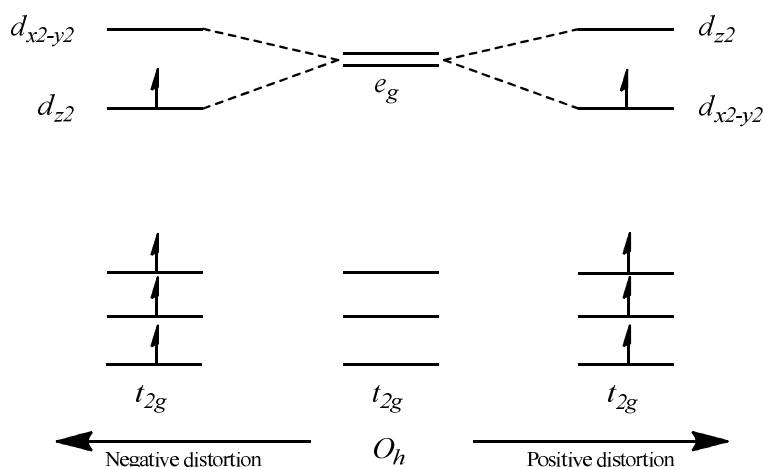


**Figure 3.19:** Splitting of the  $e_g$  orbital group during Jahn-Teller distortion with the possible electron fillings of a  $d^4$  complex.

The alternative electron filling of the  $d$ -orbitals,  $t_{2g}^3 d_{x^2-y^2}^1$ , was calculated by specifying the occupation of the HOMO orbital to be  $d_{x^2-y^2}$  during the computational calculations. The energy of the electronic state with alternative electron filling is  $3.6 \text{ kJ.mol}^{-1}$  relative to the lowest energy state. The  $\text{Mn}(\text{acac})_3$  complex with the  $d_{z^2}$  HOMO had the lowest energy. The ADF/OLYP results of this study thus showed that  $\text{Mn}(\text{acac})_3$  exists mainly with a negative Jahn-Teller distortion. The Boltzmann equation (**Equation 3.2**) was used to calculate the population of  $\text{Mn}(\text{acac})_3$  that will occur with a negative Jahn-Teller distortion as 79 % : 21 %.

$$\ln \frac{n_j}{n_i} = - \frac{(E_j - E_i)}{kT} \quad \text{Equation 3.2}$$

The HOMO of the alternative electron filling ( $t_{2g}^3 d_{x^2-y^2}^1$ ) is illustrated in **Figure 3.20**. It is clear that the alternative electron filling HOMO shows mainly  $d_{x^2-y^2}$  character.

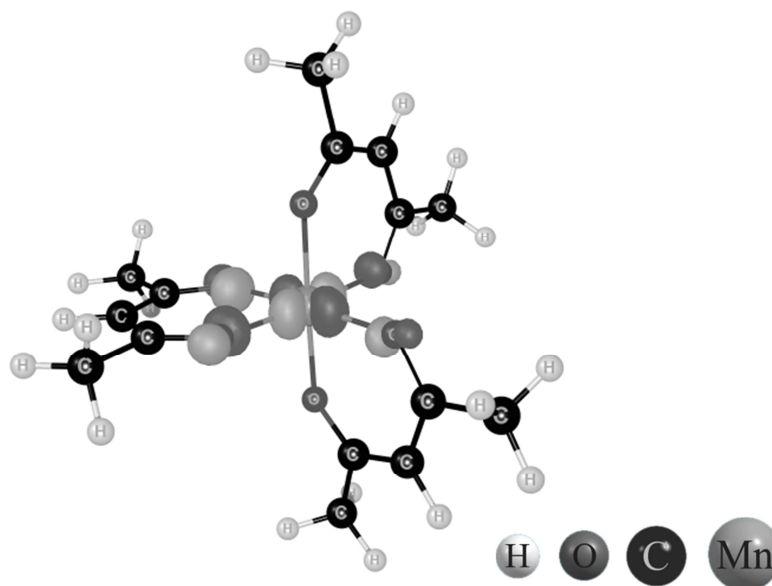


**Figure 3.20:** ADF/OLYP HOMO orbital of the optimized alternative electron filling  $\text{Mn}(\text{acac})_3$  complex.

The Mn-O bond lengths of the calculated and crystal structures are summarized in **Table 3.19**.

**Table 3.19:** Mn-O bond lengths of computational calculations (ADF/OLYP/TZP) and crystal results.

Computational / experimental	Negative Jahn-Teller distortion		Positive Jahn-Teller distortion		Ref
	Average Mn-O distance of the four shortest (Å) bonds	Average Mn-O distance of the four shortest (Å) bonds	Average Mn-O distance of the four longest (Å) bonds	Average Mn-O distance of the shortest trans bonds from each other (Å)	
HOMO $d_{z^2}$	1.984	2.245	-	-	
Crystal average 1	1.950	2.079	-	-	28
					29
					30
HOMO $d_{x^2-y^2}$	-	-	2.120	1.944	
Crystal average 2	-	-	2.009	1.945	31
					32

From **Table 3.19** it can be seen that with a specified occupation of the HOMO orbital ( $d_{z^2}$ ) there was a negative Jahn-Teller distortion. With the HOMO orbital specified to be  $d_{x^2-y^2}$  a positive Jahn-Teller distortion was observed.

<sup>28</sup> B.R. Stults, R.S. Marianelli, V.W. Day, *J. Inorg. Chem.* **1979** (18) 1853-1858.

<sup>29</sup> J.P. Fackler, A. Avdeef, *Inorg. Chem.* **1974** (13) 1864-1875.

<sup>30</sup> S. Geremia, N. Demitri, *J. Chem. Educ.* **2005** (82) 460-465.

<sup>31</sup> J.P. Fackler, A. Adeef, *J. Inorg. Chem.*, **1974** (13) 1864-1875.

<sup>32</sup> R. Frohlich, R. Milan, S. Yadava, *Private communication* **2008**.

### 3.1.4.2 Mn(dbm)<sub>3</sub>.

As the spin state of Mn(dbm)<sub>3</sub> is  $S = 4/2$  it was expected to have a  $d$ -orbital filling of  $t^3_{2g}d^1_{z^2}$  or  $t^3_{2g}d^1_{x^2-y^2}$ . The calculated HOMO of the optimized Mn(dbm)<sub>3</sub> complex is illustrated in **Figure 3.21** and shows  $d_{z^2}$  character. A negative Jahn-Teller distortion is associated with the HOMO having  $d_{z^2}$  character.

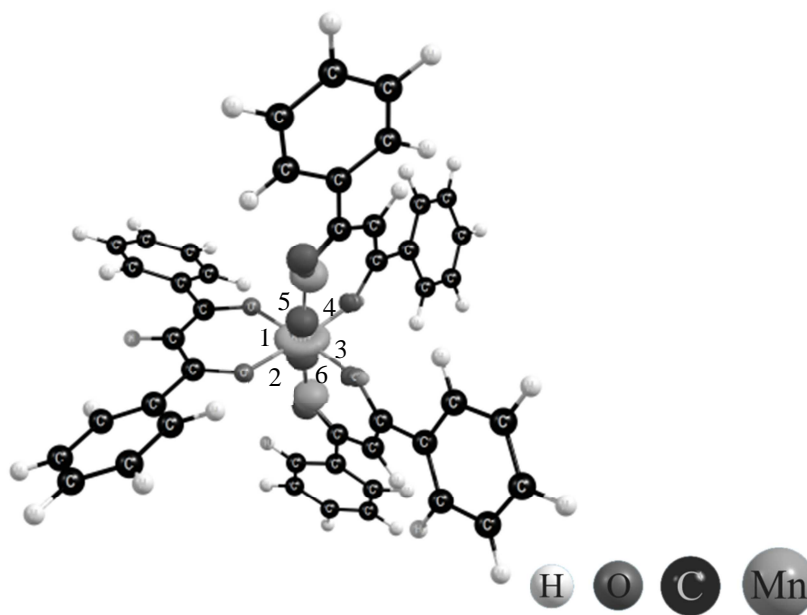


**Figure 3.21:** ADF/OLYP HOMO orbital of the optimized Mn(dbm)<sub>3</sub> complex.

The large electrostatic repulsion causes an elongation of the Mn-O bond lengths along the  $z$ -axis, which can be seen as bond lengths 5 and 6 in **Table 3.20**.

**Table 3.20:** Mn-O bond lengths of optimized Mn(dbm)<sub>3</sub> complex (refer to **Figure 3.21** for Mn-O numbering).

Complex	Bond length (Mn-O) (Å)					
	1	2	3	4	5	6
Mn(dbm) <sub>3</sub>	1.965	1.965	1.974	1.974	2.217	2.217

The alternative electron filling of the  $d$ -orbitals,  $t^3_{2g}d^1_{x^2-y^2}$ , was calculated by specifying the occupation of the HOMO orbital to be  $d_{x^2-y^2}$  during the computational calculations. The HOMO of Mn(dbm)<sub>3</sub> with the specified occupation is illustrated in **Figure 3.22** with the Mn-O bond lengths summarized in **Table 3.21**.

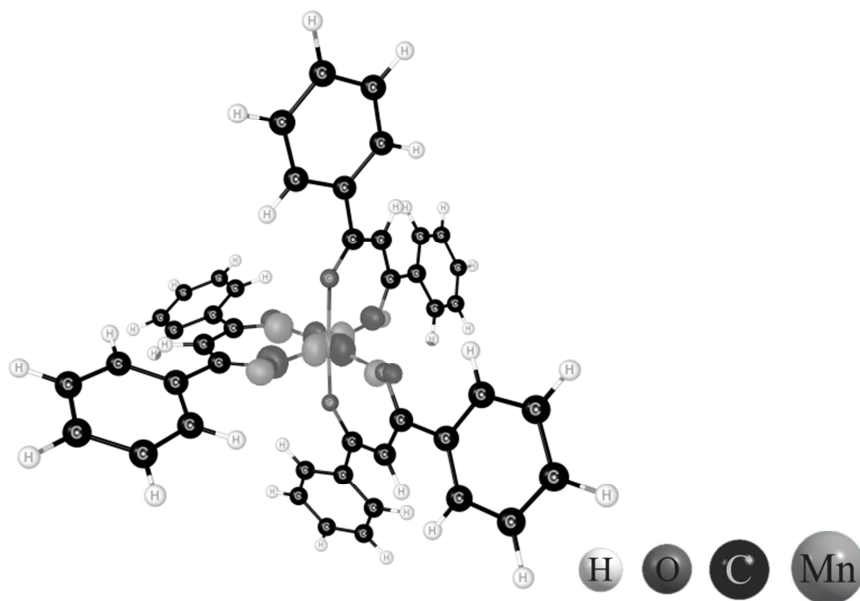


**Figure 3.22:** ADF/OLYP HOMO orbital of the optimized alternative electron filling  $\text{Mn}(\text{dbm})_3$  complex.

**Table 3.21:** Mn-O bond lengths of the alternative optimized  $\text{Mn}(\text{dbm})_3$  complex.

Complex	Bond length (Mn-O) (Å)					
	1	2	3	4	5	6
$\text{Mn}(\text{dbm})_3$	2.100	2.100	2.112	2.112	1.934	1.934

From the Mn-O bond lengths of the alternative optimized  $\text{Mn}(\text{dbm})_3$  complex it was clear that a positive Jahn-Teller distortion was calculated, since the Mn-O bond lengths 5 and 6 were shorter than the four others. The relative energy of the electronic state with alternative electron filling is  $5.6 \text{ kJ.mol}^{-1}$ . The  $\text{Mn}(\text{dbm})_3$  complex with the  $d_{z^2}$  HOMO had the lowest energy. The ADF/OLYP results of this study thus showed that  $\text{Mn}(\text{dbm})_3$  exists mainly with a negative Jahn-Teller distortion. The Boltzmann equation (**Equation 3.2**) was used to calculate the population of  $\text{Mn}(\text{dbm})_3$  that will occur with a negative Jahn-Teller distortion as 91 % : 9 %. Thus the crystals of this and previous studies that only showed negative Jahn-Teller distortion could be explained by the calculated population percentage.<sup>33,34</sup>

<sup>33</sup> E.G. Zaitseva, I.A. Baidina, P.A. Stabnikov, S.V. Borisov, I.K. Igumenov, *Zh. Strukt. Khim. (Russ.) (J. Struct. Chem.)* **1990** (31) 184.

<sup>34</sup> A.L. Barra, D. Gatteschi, R. Sessoli, G.L. Abbati, A. Cornia, A.C. Fabretti, M.G. Uytterhoeven, *Angew. Chem. Int. Ed.* **1997** (36) 2329.



### 3.1.4.3 Mn(hfac)<sub>3</sub>.

Like Mn(dbm)<sub>3</sub>, Mn(hfac)<sub>3</sub> has a spin of  $S = 4/2$  and was therefore also expected to have a  $d$ -orbital filling of  $t^3_{2g}d^1_{z^2}$  or  $t^3_{2g}d^1_{x^2-y^2}$ . The calculated HOMO of the optimized Mn(hfac)<sub>3</sub> complex is illustrated in **Figure 3.23** and shows  $d_{z^2}$  character. A negative Jahn-Teller distortion is associated with the HOMO having  $d_{z^2}$  character.

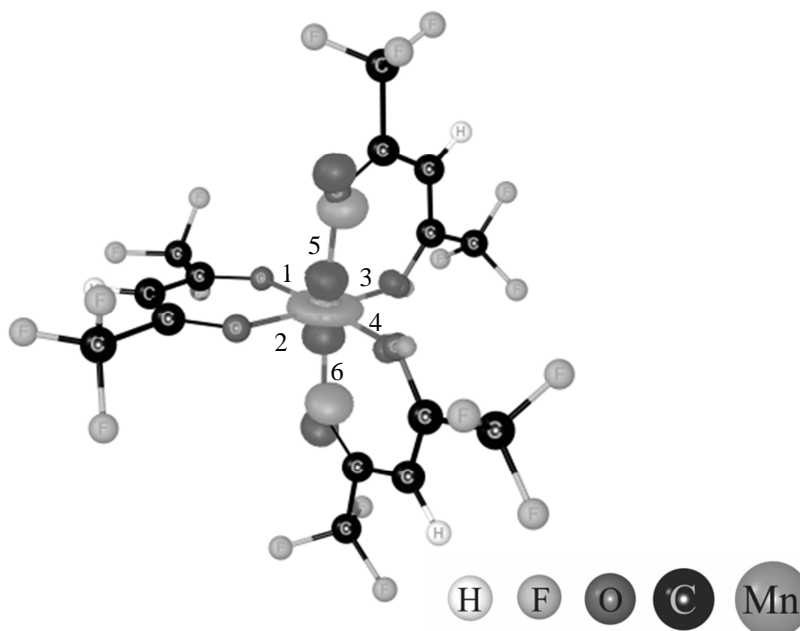


**Figure 3.23:** ADF/OLYP HOMO orbital of the optimized Mn(hfac)<sub>3</sub> complex.

The large electrostatic repulsion causes an elongation of the Mn-O bond lengths along the  $z$ -axis, which can be seen as bond lengths 5 and 6 in Table 3.21.

**Table 3. 22:** Mn-O bond lengths of optimized Mn(hfac)<sub>3</sub> complex (refer to **Figure 3.23** for Mn-O numbering).

Complex	Bond length (Mn-O) (Å)					
	1	2	3	4	5	6
Mn(hfac) <sub>3</sub>	1.998	1.998	1.970	1.970	2.240	2.240

The alternative electron filling of the  $d$ -orbitals,  $t^3_{2g}d^1_{x^2-y^2}$ , was calculated by specifying the occupation of the HOMO orbital to be  $d_{x^2-y^2}$  during the computational calculations. The HOMO of Mn(hfac)<sub>3</sub> with the specified occupation is illustrated in **Figure 3.24** with the Mn-O bond lengths summarized in **Table 3.23**.

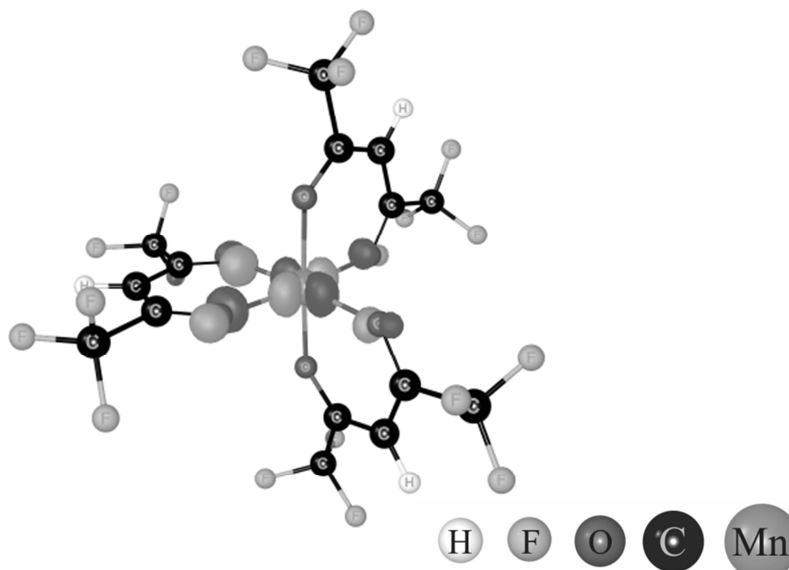


**Figure 3.24:** ADF/OLYP HOMO orbital of the optimized alternative electron filling  $\text{Mn}(\text{hfac})_3$  complex.

**Table 3.23:** Mn-O bond lengths of the alternative optimized  $\text{Mn}(\text{hfac})_3$  complex.

Complex	Bond length (Mn-O) (Å)					
	1	2	3	4	5	6
$\text{Mn}(\text{hfac})_3$	2.117	2.117	2.129	2.129	1.949	1.949

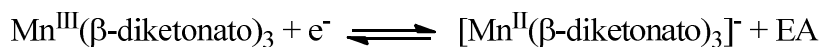
From the Mn-O bond lengths of the alternative optimized  $\text{Mn}(\text{hfac})_3$  complex it was clear that a positive Jahn-Teller distortion was calculated, since the Mn-O bond lengths 5 and 6 were shorter than the four others. The relative energy of the electronic state with alternative electron filling is  $3.5 \text{ kJ.mol}^{-1}$ . The  $\text{Mn}(\text{hfac})_3$  complex with the  $d_{z^2}$  HOMO had the lowest energy. The ADF/OLYP results of this study thus showed that  $\text{Mn}(\text{hfac})_3$  exists mainly with a negative Jahn-Teller distortion. The Boltzmann equation (**Equation 3.2**) was used to calculate the population of  $\text{Mn}(\text{hfac})_3$  that will occur with a negative Jahn-Teller distortion as 81 % : 19 %. Thus there is a possibility to obtain  $\text{Mn}(\text{hfac})_3$  crystals that shows positive Jahn-Teller distortion, which was seen in previous studies.<sup>35,36</sup>

<sup>35</sup> J.R. Bryant, J.E. Taves, J.M. Mayer, *Inorg. Chem.* **2002** (41) 2769.

<sup>36</sup> S. Parsons, R. Winpenny, P. Wood, *Private Communication* **2004** (2) 72.

### 3.1.4.4 Mn( $\beta$ -diketonato)<sub>3</sub>.

Electron affinity (EA) is known as the amount of energy released when an electron is added to a complex giving it a negative charge.



The EA can thus be calculated as the difference between the neutral and the reduced complex (see **Equation 3.3**).

$$\text{EA} = E_{\text{Mn}^{\text{III}}(\beta\text{-diketonato})_3} - E_{[\text{Mn}^{\text{II}}(\beta\text{-diketonato})_3]^-} \quad \text{Equation 3.3}$$

The energies of the ground state  $\text{Mn}^{\text{III}}(\beta\text{-diketonato})_3$  and the reduced species  $[\text{Mn}^{\text{II}}(\beta\text{-diketonato})_3]^-$  is tabulated in **Table 3.24**. For complexes containing unsymmetrical  $\beta$ -diketonato ligands two isomers are possible (*fac*- and *mer*-isomer, see **Figure 3.25**). In calculating the effective energy of  $\text{Mn}(\beta\text{-diketonato})_3$  complexes containing unsymmetrical  $\beta$ -diketonato ligands the Boltzmann equation was used.

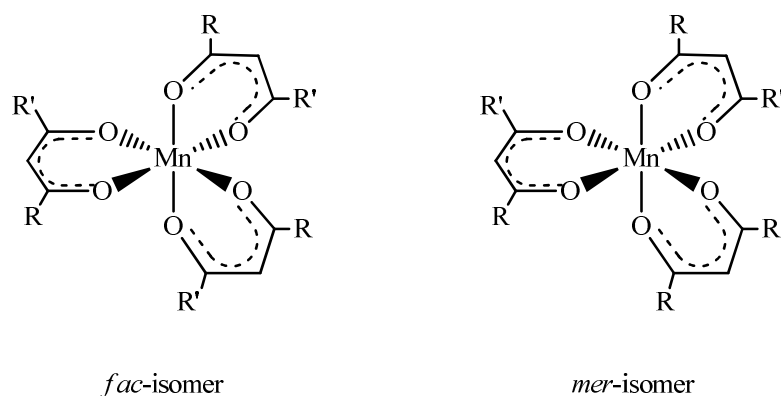


**Figure 3.25:** The *fac*- and *mer*-isomer of  $\text{Mn}(\beta\text{-diketonato})_3$  complexes containing unsymmetrical  $\beta$ -diketonato ligands.

**Table 3.24:** The calculated ground state and anionic energies of  $\text{Mn}(\beta\text{-diketonato})_3$ . The electron affinity is also given.

Complex	$E_{\text{ground state}} \text{ (kJ.mol}^{-1}\text{)}$	$E_{\text{reduced specie}} \text{ (kJ.mol}^{-1}\text{)}$	$\text{EA (kJ.mol}^{-1}\text{)}$	$E_{\text{LUMO}} \text{ (kJ.mol}^{-1}\text{)}$	$E_{\text{pc}} \text{ (mV)}$
$\text{Mn}(\text{acac})_3$ [1]	-24524.4	-24721.3	196.9	-332.5	-924
$\text{Mn}(\text{ba})_3$ [2]	-38922.5	-39140.7	218.2	-338.8	-635
$\text{Mn}(\text{dbm})_3$ [3]	-53322.0	-53554.0	232.0	-344.0	-400
$\text{Mn}(\text{tfaa})_3$ [4]	-24740.5	-25031.1	290.6	-433.5	-230
$\text{Mn}(\text{tfth})_3$ [5]	-33040.8	-33342.0	301.2	-428.4	165
$\text{Mn}(\text{tffu})_3$ [6]	-33782.2	-34074.5	292.2	-413.2	168
$\text{Mn}(\text{tfba})_3$ [7]	-39141.2	-39440.3	299.1	-423.6	178
$\text{Mn}(\text{hfac})_3$ [8]	-24909.8	-25300.4	390.6	-531.6	1009

The reduction potential ( $E_{pc}$ ) is included in **Table 3.24**. The relationship between the calculated electron affinity (EA) and  $E_{pc}$  is graphically shown in **Figure 3.26**.

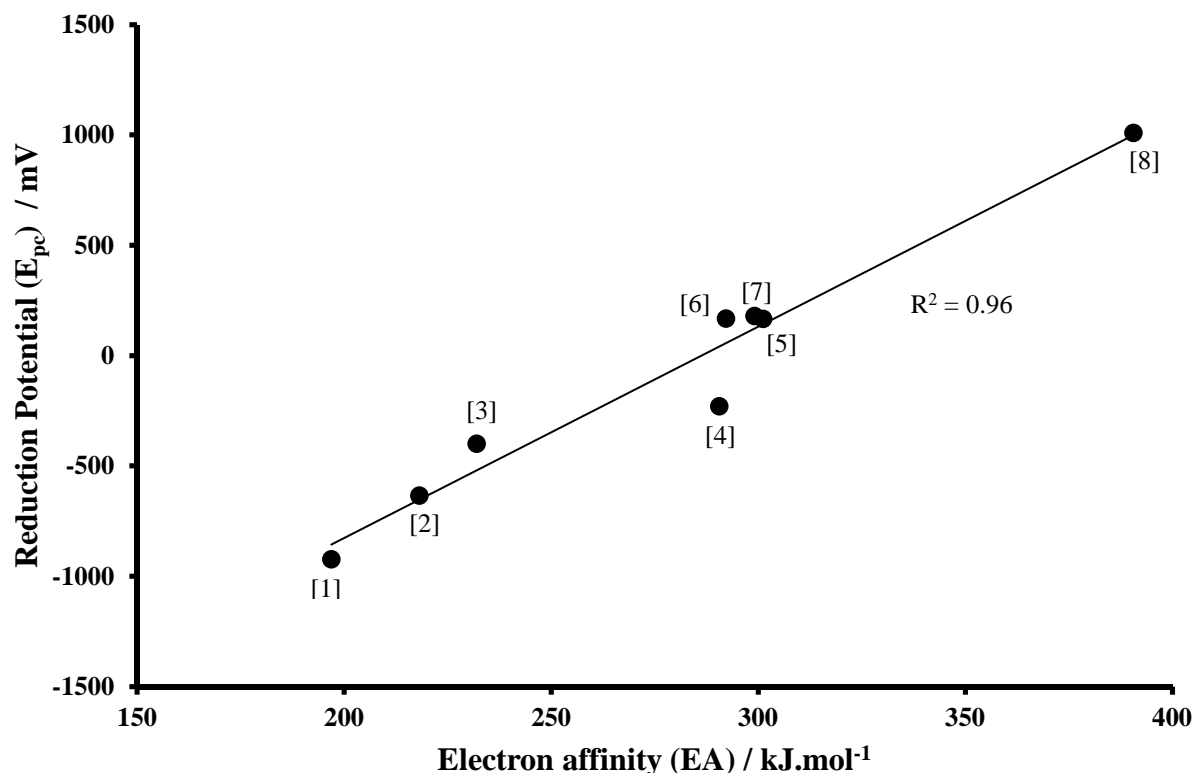


**Figure 3.26:** Electron affinity (EA) plotted against the reduction potential ( $E_{pc}$ ) of the  $Mn^{III}/Mn^{II}$  redox couple. Complex numbering is according to **Table 3.24**.

The correlation between the reduction potential and the calculated electron affinity showed that, EA increased as the  $E_{pc}$  increased. This implies that complex [8] with a larger EA (greater affinity to accept an electron) would be easier to reduce to  $[Mn^{II}(\beta\text{-diketonato})_3]^-$  than complex [1]. The linear equation describing the relationship is given as:  $E_{pc} = (9.5366)EA - 2719.8$ . This equation can be used to determine the reduction potential ( $E_{pc}$ ) of  $Mn^{III}(\beta\text{-diketonato})_3$  complexes when the calculated electron affinity is known.

## Results and discussion

The relationship between the LUMO energy of the different  $\text{Mn}(\beta\text{-diketonato})_3$  complexes, tabulated in **Table 3.24**, and  $E_{\text{pc}}$  is graphically shown in **Figure 3.27**. Due to the large  $\Delta E_{\text{p}}$  values of the  $\text{Mn}(\beta\text{-diketonato})_3$  complexes no correlation was found between the LUMO energy ( $E_{\text{LUMO}}$ ) and the reduction potential ( $E_{\text{pc}}$ ).

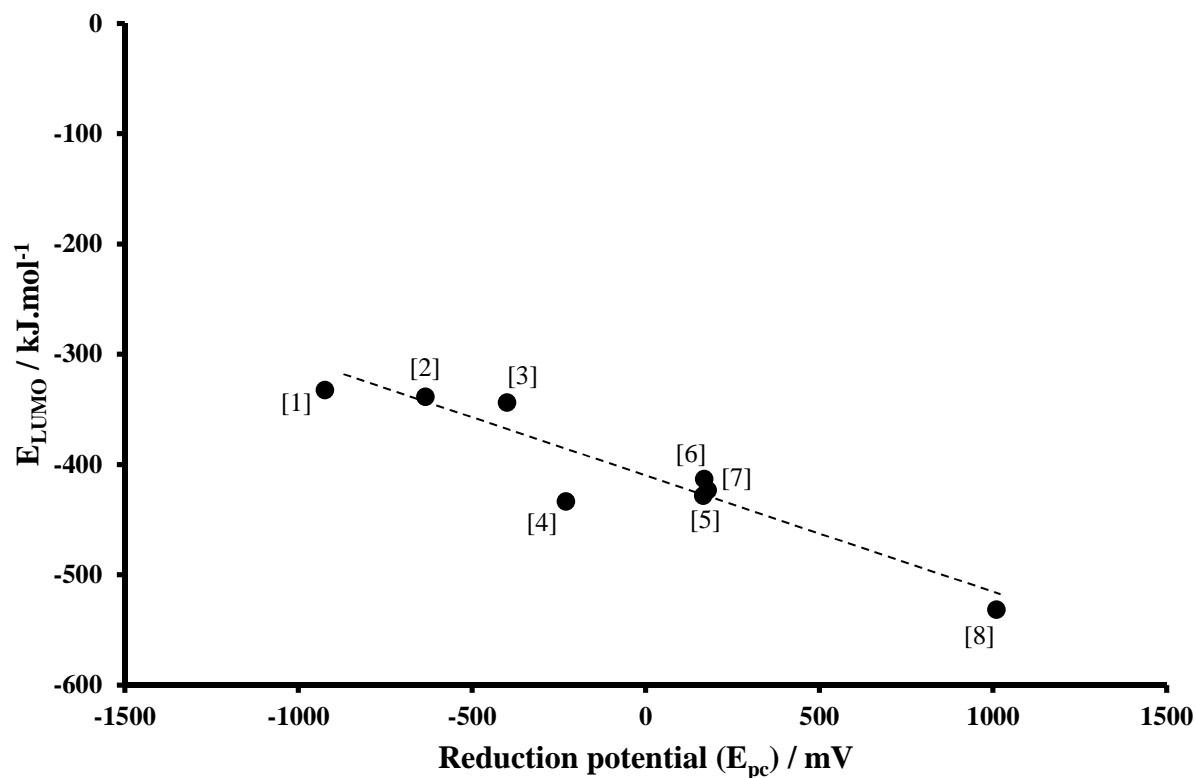


**Figure 3.27:** LUMO energy ( $E_{\text{LUMO}}$ ) plotted against the reduction potential ( $E_{\text{pc}}$ ) of the  $\text{Mn}^{\text{III}}/\text{Mn}^{\text{II}}$  redox couple. Complex numbering is according to **Table 3.24**.

## 3.2 Tris(acetylacetonato)metal(III), $M(\text{acac})_3$ ( $M = \text{V}, \text{Cr}, \text{Mn}, \text{Fe}$ and $\text{Co}$ ).

### 3.2.1 Electrochemistry.

In this section the cyclic voltammograms of the different  $M(\text{acac})_3$  will be discussed first, which will be followed by the investigation of the effect of different metal centres on the reduction potential of the  $M^{\text{III}}/M^{\text{II}}$  redox couple. Two redox reactions ( $\text{V}^{\text{III}}/\text{V}^{\text{IV}}$  and  $\text{V}^{\text{III}}/\text{V}^{\text{II}}$ ) of the  $\text{V}(\text{acac})_3$  complex were observed in the solvent window of the cyclic voltammograms. The cyclic voltammetry data of  $\text{V}(\text{acac})_3$  at various scan rates in acetonitrile as the solvent are summarized in **Table 3.25** and illustrated in **Figure 3.28** and **Figure 3.29**.

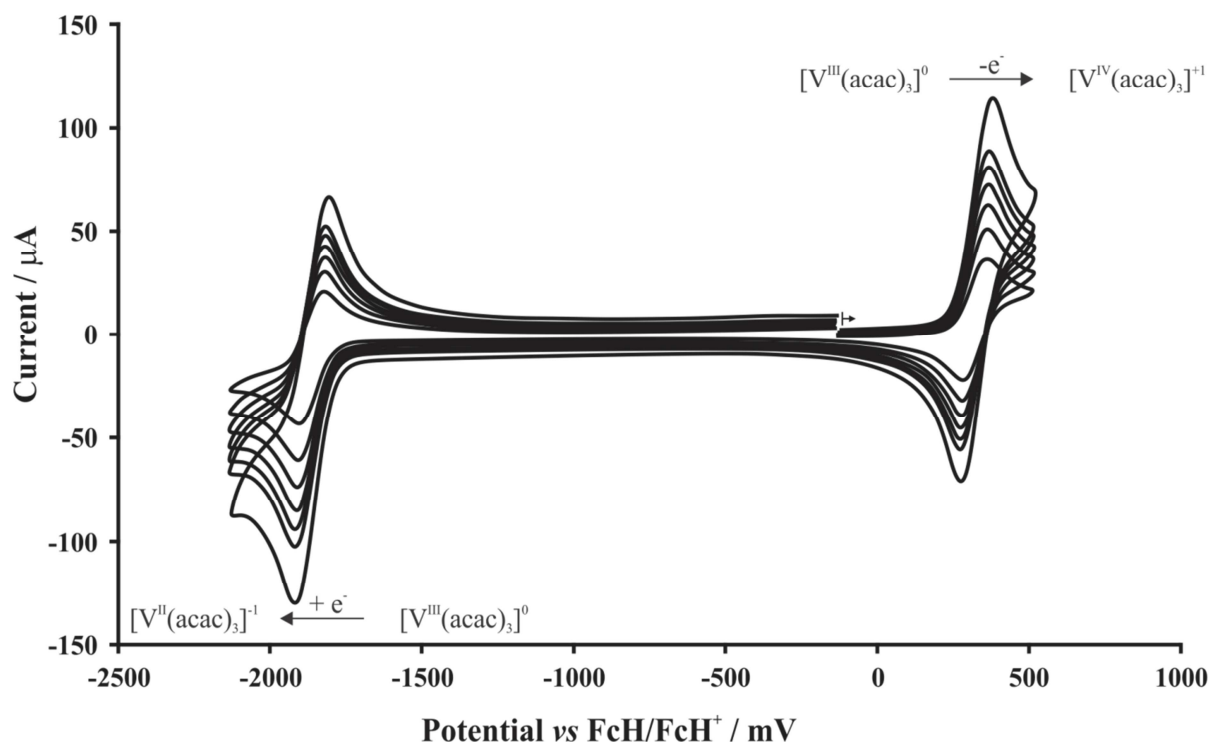


**Figure 3.28:** Cyclic voltammogram of  $\text{V}(\text{acac})_3$  at different scan rates (50, 100, 150, 200, 250, 300, 500  $\text{mV}\cdot\text{s}^{-1}$ ), solvent acetonitrile, supporting electrolyte tetraethylammonium tetrafluoroborate, working electrode glassy carbon with potential vs  $\text{FcH}/\text{FcH}^+$ .

## Results and discussion

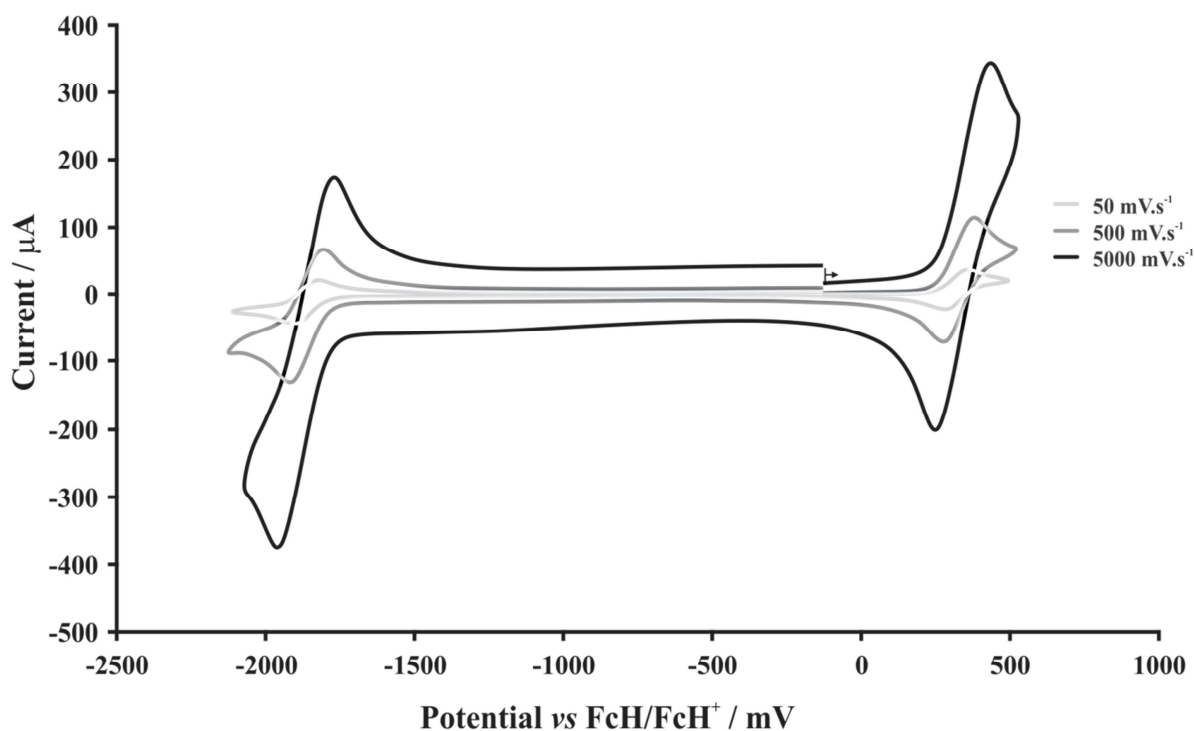


**Figure 3.29:** Cyclic voltammogram of  $V(acac)_3$  at scan rates of 50, 500 and 5000  $mV.s^{-1}$ , solvent acetonitrile, supporting electrolyte tetraethylammonium tetrafluoroborate, working electrode glassy carbon with potential vs  $FcH/FcH^+$ .

The scan rates were done up to two orders of magnitude of the slowest scan rate (50  $mV.s^{-1}$  – 5000  $mV.s^{-1}$ ), to ensure that the same redox couples were observed at very fast scan rates (see **Figure 3.29**)

**Table 3.25:** Electrochemical data<sup>i</sup> of  $V(acac)_3$  obtained from different scan rates.

Scan Rate ( $mV.s^{-1}$ )	$V^{III} / V^{II}$							$V^{III} / V^{IV}$						
	$E_{pa}$ (mV)	$E_{pc}$ (mV)	$\Delta E_p$ (mV)	$E^{0'}$ (mV)	$i_{pa}$ ( $\mu A$ )	$i_{pc}$ ( $\mu A$ )	$i_{pa}/i_{pc}$	$E_{pa}$ (mV)	$E_{pc}$ (mV)	$\Delta E_p$ (mV)	$E^{0'}$ (mV)	$i_{pa}$ ( $\mu A$ )	$i_{pc}$ ( $\mu A$ )	$i_{pa}/i_{pc}$
50	-1322	-1403	81	-1363	32.98	36.13	0.91	858	774	84	816	32.57	30.47	0.94
100	-1322	-1403	81	-1363	45.86	50.37	0.91	861	774	87	817	47.33	44.29	0.94
150	-1322	-1410	88	-1366	57.59	62.83	0.92	861	774	87	817	57.80	56.02	0.97
200	-1318	-1417	99	-1368	65.60	70.74	0.93	861	766	95	813	62.94	60.28	0.96
250	-1318	-1417	99	-1368	71.81	78.37	0.92	861	766	95	813	71.81	67.73	0.94
300	-1318	-1417	99	-1368	79.43	90.25	0.88	861	766	95	813	82.09	75.89	0.92
500	-1311	-1420	109	-1366	99.29	113.48	0.88	872	763	109	817	104.61	95.74	0.92
5000	-1285	-1477	192	-1381	231.58	294.74	0.79	918	733	185	826	268.42	227.37	0.85

<sup>i</sup> Solvent acetonitrile, supporting electrolyte tetraethylammonium tetrafluoroborate, working electrode glassy carbon with potential vs  $FcH/FcH^+$ .

Both the redox couples ( $V^{III}/V^{IV}$  and  $V^{III}/V^{II}$ ) of  $V(acac)_3$  are electrochemically reversible from scan rate  $50 - 300 \text{ mV.s}^{-1}$  indicate by the  $83 - 99 \text{ mV}$  range of the  $\Delta E_p$  values. The  $i_{pa}/i_{pc}$  ratios for both the redox couples were greater than 0.9 at scan rates  $50 - 250 \text{ mV.s}^{-1}$  and are therefore chemically reversible at these scan rates.

There were four redox reactions ( $Cr^{III}/Cr^{IV}$ ,  $Cr^{IV}/Cr^V$ ,  $Cr^{III}/Cr^{II}$  and  $Cr^{II}/Cr^I$ ) observed in the solvent window of the cyclic voltammograms of  $Cr(acac)_3$ . The cyclic voltammetry data of  $Cr(acac)_3$  at various scan rates with acetonitrile as the solvent are summarized (see **Table 3.26** and **Table 3.27**) and illustrated in **Figure 3.30** and **Figure 3.31**.

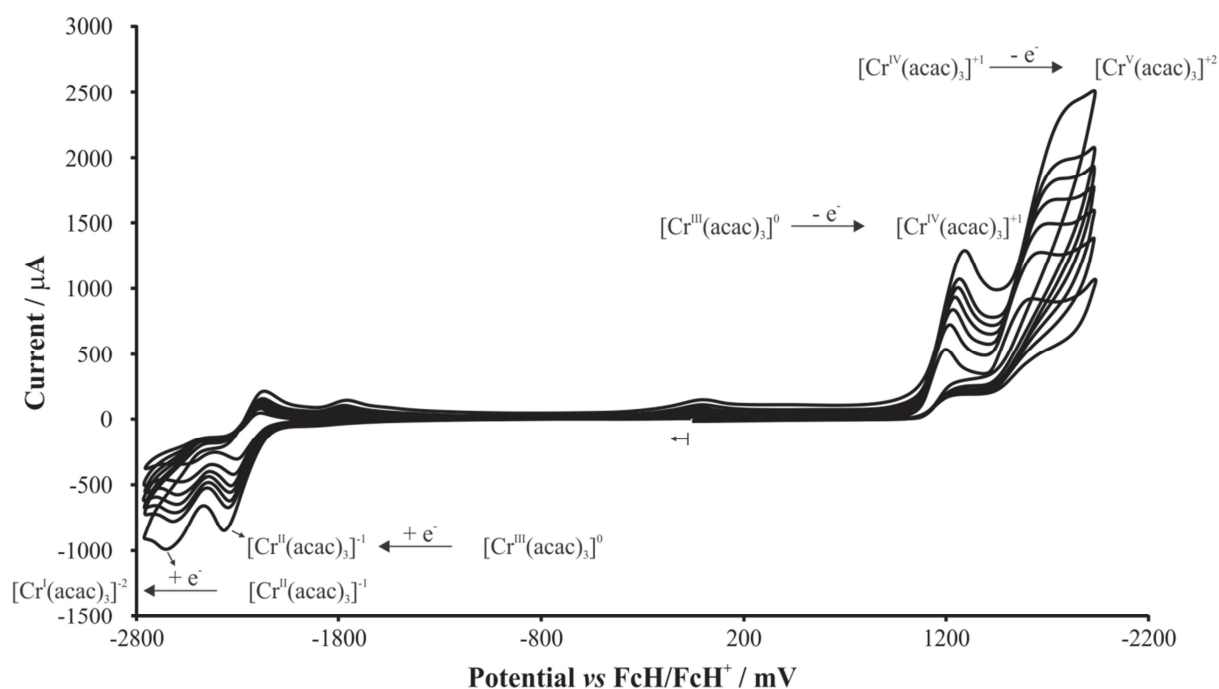


**Figure 3.30:** Cyclic voltammogram of  $Cr(acac)_3$  at different scan rates ( $50, 100, 150, 200, 250, 300, 500 \text{ mV.s}^{-1}$ ), solvent acetonitrile, supporting electrolyte tetraethylammonium tetrafluoroborate, working electrode glassy carbon, concentration of  $25 \text{ mM } Cr(acac)_3$  with potential vs  $FcH/FcH^+$ .



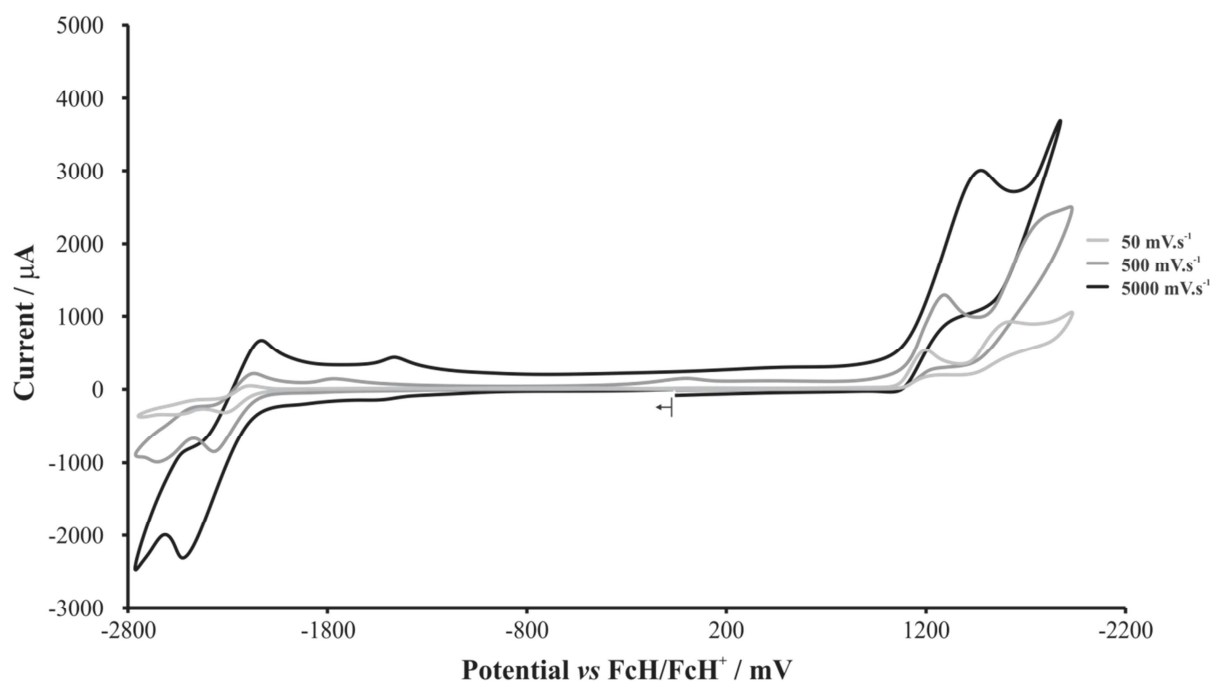


**Figure 3.31:** Cyclic voltammogram of  $\text{Cr}(\text{acac})_3$  at scan rates of 50, 500 and 5000  $\text{mV.s}^{-1}$ , solvent acetonitrile, supporting electrolyte tetraethylammonium tetrafluoroborate, working electrode glassy carbon, concentration of 25 mM  $\text{Cr}(\text{acac})_3$  with potential vs  $\text{FcH}/\text{FcH}^+$ .

**Table 3.26:** Electrochemical data<sup>i</sup> of  $\text{Cr}(\text{acac})_3$  obtained for redox couples  $\text{Cr}^{\text{III}}/\text{Cr}^{\text{IV}}$  and  $\text{Cr}^{\text{IV}}/\text{Cr}^{\text{V}}$  at different scan rates

Scan Rate ( $\text{mV.s}^{-1}$ )	$\text{Cr}^{\text{III}} / \text{Cr}^{\text{IV}}$		$\text{Cr}^{\text{IV}} / \text{Cr}^{\text{V}}$	
	$E_{\text{pa}}$ (mV)	$i_{\text{pa}}$ ( $\mu\text{A}$ )	$E_{\text{pa}}$ (mV)	$i_{\text{pa}}$ ( $\mu\text{A}$ )
50	1190	511.70	1612	516.08
100	1218	713.45	1668	717.84
150	1232	748.26	1690	850.69
200	1248	815.97	1728	868.06
250	1252	863.87	1732	971.20
300	1252	921.47	1766	1034.03
500	1290	1049.74	1806	1261.78
5000	1326	1089.62	-	-

<sup>i</sup> Solvent acetonitrile, supporting electrolyte tetraethylammonium tetrafluoroborate, working electrode glassy carbon, concentration of 25 mM  $\text{Cr}(\text{acac})_3$  with potential vs  $\text{FcH}/\text{FcH}^+$ .

The cyclic voltammograms of  $\text{Cr}(\text{acac})_3$  showed that  $\text{Cr}^{\text{III}}(\text{acac})_3$  was oxidized to  $\text{Cr}^{\text{IV}}(\text{acac})_3$  and then further oxidized from  $\text{Cr}^{\text{IV}}(\text{acac})_3$  to  $\text{Cr}^{\text{V}}(\text{acac})_3$ . No reduction of the  $\text{Cr}^{\text{V}}(\text{acac})_3$  species was

### CHAPTER 3

observed. Thus, there were no  $\text{Cr}^{\text{IV}}(\text{acac})_3$  specie available to reduce to  $\text{Cr}^{\text{III}}(\text{acac})_3$ . This implies that the  $\text{Cr}^{\text{III}}/\text{Cr}^{\text{IV}}$  and  $\text{Cr}^{\text{IV}}/\text{Cr}^{\text{V}}$  couples are chemically and electrochemically irreversible. The data of the  $\text{Cr}^{\text{IV}}/\text{Cr}^{\text{V}}$  couple at the scan rate of  $5000 \text{ mV.s}^{-1}$  shifted out of the scanning potential and therefore the data of this couple could not be obtained. The peaks that were observed at 0 mV and 1700 mV are due to reoxidation or decomposition of unknown reduced specie.

**Table 3.27:** Electrochemical data<sup>i</sup> of  $\text{Cr}(\text{acac})_3$  obtained for redox couples  $\text{Cr}^{\text{III}}/\text{Cr}^{\text{II}}$  and  $\text{Cr}^{\text{II}}/\text{Cr}^{\text{I}}$  at different scan rates

Scan Rate ( $\text{mV.s}^{-1}$ )	$\text{Cr}^{\text{III}} / \text{Cr}^{\text{II}}$					$\text{Cr}^{\text{II}} / \text{Cr}^{\text{I}}$	
	$E_{\text{pa}}$ (mV)	$E_{\text{pc}}$ (mV)	$\Delta E_{\text{p}}$ (mV)	$\frac{E_{\text{pc}} - E_{\text{pa}}}{2}$ (mV)	$i_{\text{pa}}/i_{\text{pc}}$	$E_{\text{pc}}$ (mV)	$i_{\text{pc}}$ ( $\mu\text{A}$ )
50	-2228	-2328	100	-50	0.53	-2588	70.18
100	-2228	-2338	110	-55	0.38	-2594	102.34
150	-2228	-2350	122	-61	0.41	-2610	104.17
200	-2228	-2352	124	-62	0.38	-2618	121.53
250	-2208	-2370	162	-81	0.31	-2618	159.69
300	-2208	-2370	162	-81	0.32	-2634	170.16
500	-2176	-2388	212	-106	0.38	-2670	212.04
5000	-2151	-2539	388	-194	0.45	-	-

<sup>i</sup> Solvent acetonitrile, supporting electrolyte tetraethylammonium tetrafluoroborate, working electrode glassy carbon, concentration of 25 mM  $\text{Cr}(\text{acac})_3$  with potential vs  $\text{FcH}/\text{FcH}^+$ .

The  $\text{Cr}^{\text{III}}/\text{Cr}^{\text{II}}$  redox couple was electrochemically ( $\Delta E_{\text{p}} > 100 \text{ mV}$ ) and chemically ( $i_{\text{pa}}/i_{\text{pc}}$  ratios  $< 1$ ) irreversible. The  $\text{Cr}^{\text{II}}/\text{Cr}^{\text{I}}$  showed a reduction reaction,  $\text{Cr}^{\text{II}}(\text{acac})_3 + e^- \longrightarrow \text{Cr}^{\text{I}}(\text{acac})_3$ , with no oxidation and is therefore electrochemically and chemically irreversible.

Only one redox couple ( $\text{Fe}^{\text{III}}/\text{Fe}^{\text{II}}$ ) was found in the cyclic voltammetry experiment of the  $\text{Fe}(\text{acac})_3$  complex. The cyclic voltammetry data of  $\text{Fe}(\text{acac})_3$  at various scan rates with acetonitrile as the solvent are summarized in **Table 3.28** and illustrated in **Figure 3.32** and **Figure 3.33**.

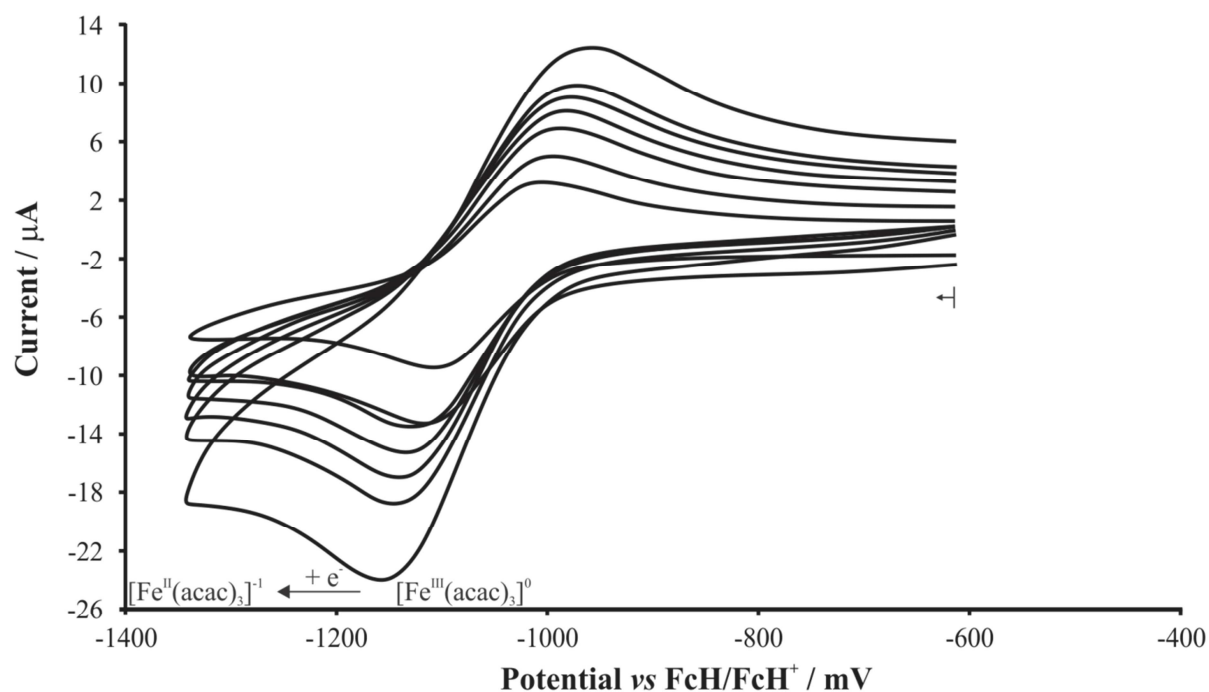


**Figure 3.32:** Cyclic voltammogram of  $\text{Fe}(\text{acac})_3$  at different scan rates (50, 100, 150, 200, 250, 300, 500  $\text{mV.s}^{-1}$ ), solvent acetonitrile, supporting electrolyte tetrabutylammonium hexafluorophosphate, working electrode glassy carbon, concentration of 0.5 mM  $\text{Fe}(\text{acac})_3$  with potential vs  $\text{FcH}/\text{FcH}^+$ .

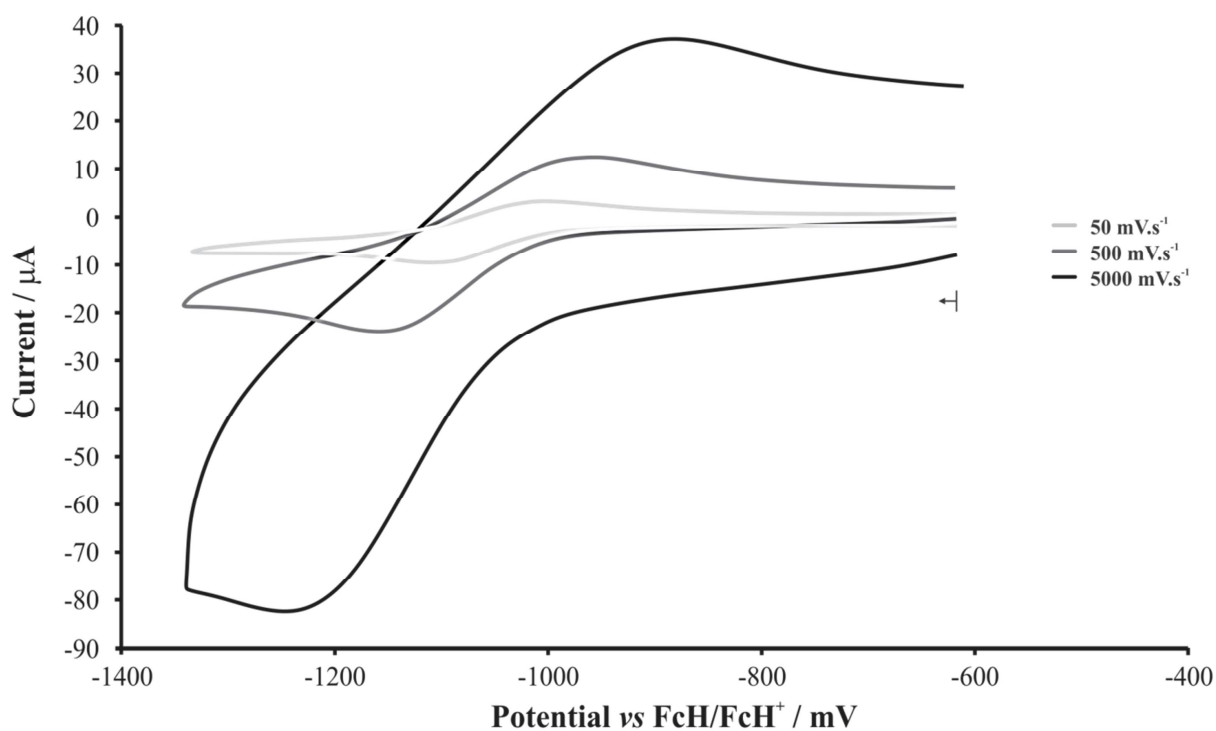


**Figure 3.33:** Cyclic voltammogram of  $\text{Fe}(\text{acac})_3$  at scan rates of 50, 500 and 5000  $\text{mV.s}^{-1}$ , solvent acetonitrile, supporting electrolyte tetrabutylammonium hexafluorophosphate, working electrode glassy carbon, concentration of 0.5 mM  $\text{Fe}(\text{acac})_3$  with potential vs  $\text{FcH}/\text{FcH}^+$ .

## CHAPTER 3

**Table 3.28:** Electrochemical data<sup>i</sup> of Fe(acac)<sub>3</sub> obtained at different scan rates.

Scan Rate (mV.s <sup>-1</sup> )	Fe <sup>III</sup> /Fe <sup>II</sup>				
	E <sub>pa</sub> (mV)	E <sub>pc</sub> (mV)	ΔE <sub>p</sub> (mV)	$\frac{E_{pc} - E_{pa}}{2}$ (mV)	<i>i</i> <sub>pa</sub> / <i>i</i> <sub>pc</sub>
50	-1006	-1110	104	-1058	0.74
100	-995	-1117	122	-1056	0.65
150	-990	-1126	135	-1058	0.59
200	-979	-1135	156	-1057	0.62
250	-975	-1139	164	-1057	0.63
300	-968	-1143	175	-1056	0.64
500	-959	-1155	195	-1057	0.57
5000	-891	-1247	356	-1069	0.49

<sup>i</sup> Solvent acetonitrile, supporting electrolyte tetrabutylammonium hexafluorophosphate, working electrode glassy carbon, concentration of 0.5 mM Fe(acac)<sub>3</sub> with potential vs FcH/FcH<sup>+</sup>.

The Fe<sup>III</sup>/Fe<sup>II</sup> couple with low *i*<sub>pa</sub>/*i*<sub>pc</sub> ratios (*i*<sub>pa</sub>/*i*<sub>pc</sub> < 1) and high ΔE<sub>p</sub> (ΔE<sub>p</sub> > 90 mV) values indicated that the couple was neither chemically nor electrochemically reversible.

Two redox couples (Co<sup>III</sup>/Co<sup>II</sup> and Co<sup>III</sup>/Co<sup>IV</sup>) were observed in the cyclic voltammograms of the Co(acac)<sub>3</sub> complex. The cyclic voltammetry data of Co(acac)<sub>3</sub> at various scan rates with acetonitrile as the solvent are summarized in **Table 3.29** and illustrated in **Figure 3.34** and **Figure 3.35**.

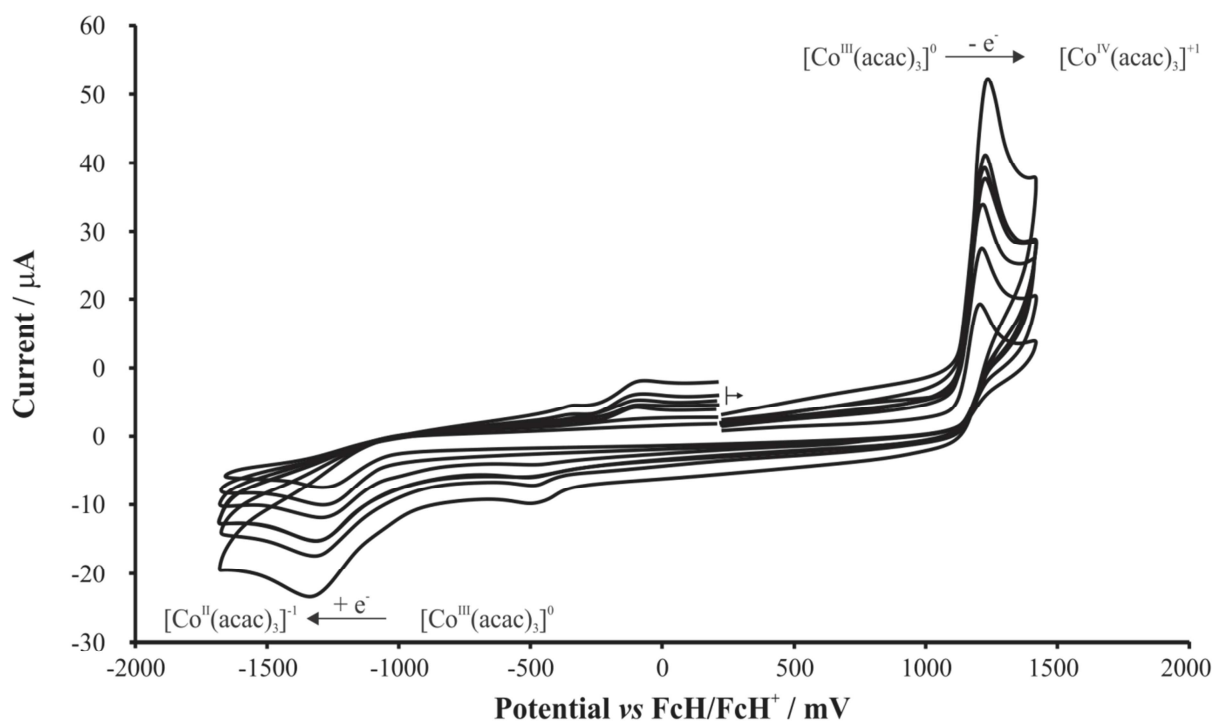


**Figure 3.34:** Cyclic voltammogram of  $\text{Co}(\text{acac})_3$  at different scan rates (50, 100, 150, 200, 250, 300, 500  $\text{mV.s}^{-1}$ ), solvent acetonitrile, supporting electrolyte tetrabutylammonium hexafluorophosphate, working electrode glassy carbon, concentration of 0.5 mM  $\text{Co}(\text{acac})_3$  with potential vs  $\text{FcH}/\text{FcH}^+$ .

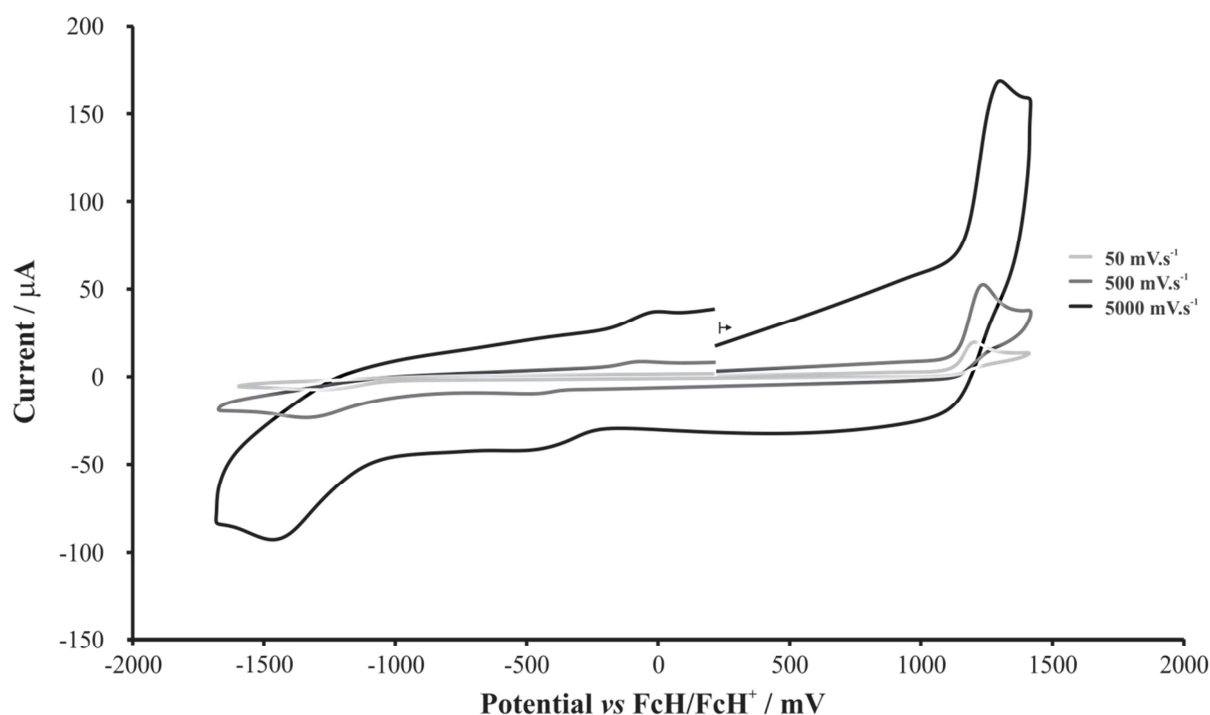


**Figure 3.35:** Cyclic voltammogram of  $\text{Co}(\text{acac})_3$  at scan rates of 50, 500 and 5000  $\text{mV.s}^{-1}$ , solvent acetonitrile, supporting electrolyte tetrabutylammonium hexafluorophosphate, working electrode glassy carbon, concentration of 0.5 mM  $\text{Co}(\text{acac})_3$  with potential vs  $\text{FcH}/\text{FcH}^+$ .

**Table 3.29:** Electrochemical data<sup>i</sup> of Co(acac)<sub>3</sub> obtained at different scan rates.

Scan Rate (mV.s <sup>-1</sup> )	Co <sup>III</sup> /Co <sup>II</sup>		Co <sup>III</sup> /Co <sup>IV</sup>	
	E <sub>pc</sub> (mV)	i <sub>pc</sub> (μA)	E <sub>pa</sub> (mV)	i <sub>pa</sub> (μA)
50	-1278	4.58	1220	15.39
100	-1297	5.52	1236	21.15
150	-1293	6.58	1236	28.19
200	-1303	6.95	1241	30.37
250	-1314	8.38	1241	32.98
300	-1314	8.53	1255	34.50
500	-1349	8.90	1220	41.83
5000	-1454	38.31	1305	92.74

<sup>i</sup> Solvent acetonitrile, supporting electrolyte tetrabutylammonium hexafluorophosphate, working electrode glassy carbon, concentration of 0.5 mM Co(acac)<sub>3</sub> with potential vs FcH/FcH<sup>+</sup>.

Both the redox couples observed for the Co(acac)<sub>3</sub> complex were chemically and electrochemically irreversible due to the fact that there were no back oxidation and reduction of the Co<sup>III</sup>/Co<sup>II</sup> and Co<sup>III</sup>/Co<sup>IV</sup> redox couples respectively. Thus, the formed Co<sup>IV</sup>(acac)<sub>3</sub> and Co<sup>II</sup>(acac)<sub>3</sub> were so unstable that they could not be reduced and oxidized back to Co<sup>III</sup>(acac)<sub>3</sub>.

In this section the cyclic voltammograms of the M<sup>III</sup>/M<sup>II</sup> couple of M(acac)<sub>3</sub> with M = V, Cr, Mn, Fe and Co is presented to evaluate the influence of the metal centre on the reduction potential (E<sub>pc</sub>). The supporting electrolyte that was generally used in the electrochemistry study of M(acac)<sub>3</sub> is TBAHFP for M(acac)<sub>3</sub> with M = Mn, Fe and Co and TEABF<sub>4</sub> for M = V and Cr. Only the metal centres' redox activities in the M(acac)<sub>3</sub> complexes (M = V, Cr, Mn, Fe and Co) were studied in this section. The common redox reaction that took place during a cyclic voltammetry study of the M(acac)<sub>3</sub> series is the M<sup>III</sup>/M<sup>II</sup> reaction. The analysis of the M<sup>III</sup>/M<sup>II</sup> redox couple was performed in an attempt to illustrate the effect of the metal centre on reduction potential of the M<sup>III</sup>/M<sup>II</sup> couple. The electrochemical data that was obtained from **Figure 3.36** is summarized in **Table 3.30** with the metal electronegativity (χ, Pauling and Mullikan scale).

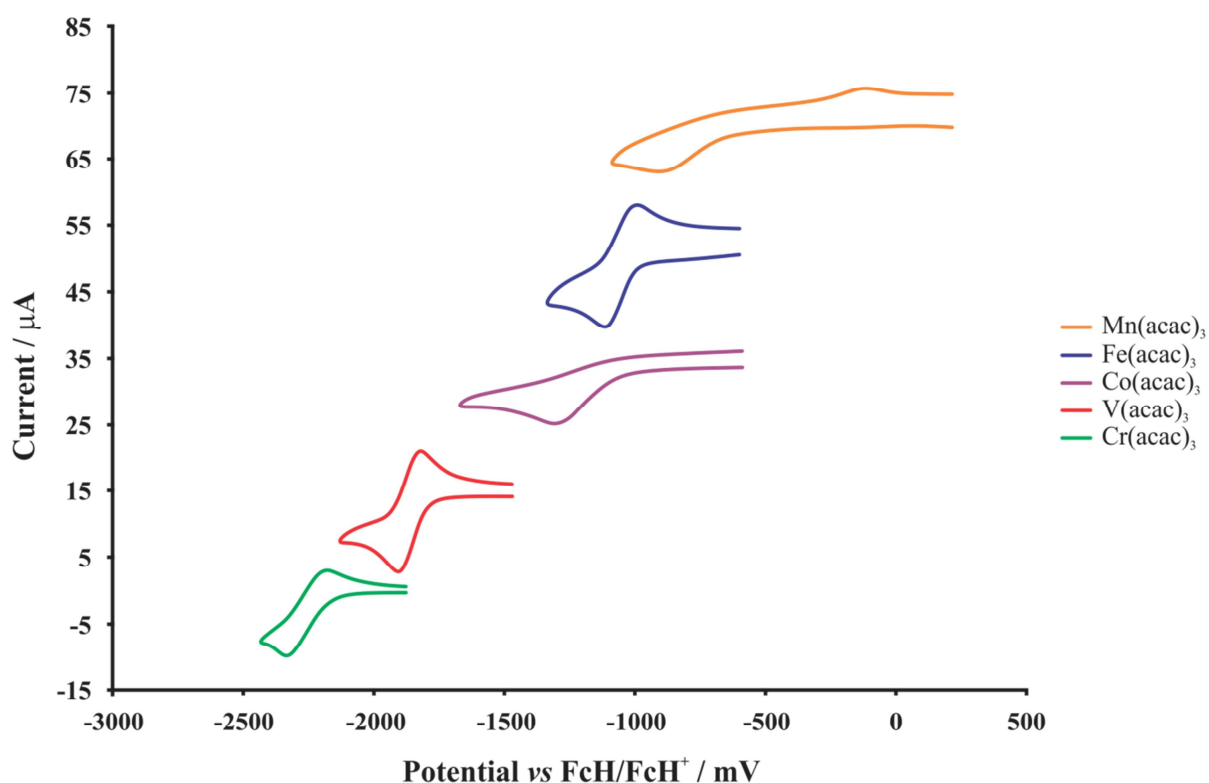


**Figure 3.36:** The shift observed of the  $M^{III}/M^{II}$  reduction couples of the different  $M(acac)_3$  complexes with a scan rate of  $100 \text{ mV}\cdot\text{s}^{-1}$ .

The cyclic voltammetry experiments of the  $M(acac)_3$  complexes showed that  $Co(acac)_3$  had no oxidation peak [ $Co^{II}(acac)_3 + e^- \rightarrow Co^{III}(acac)_3$ ]. The reduction potential ( $E_{pc}$ ) showed the following trend  $Cr(acac)_3 < V(acac)_3 < Co(acac)_3 < Fe(acac)_3 < Mn(acac)_3$ . A relationship between any electronic parameter that described the electron withdrawing properties of the metal centre and the reduction potential  $E_{pc}$  ( $M^{III}/M^{II}$ ) was expected. The  $i_{pa}/i_{pc}$  ratio of the  $M(acac)_3$  complexes where  $M = V$  and  $Fe$  were closer to 1 but were still chemically irreversible.  $M(acac)_3$  with  $M = V$ ,  $Cr$  and  $Fe$  had smaller  $\Delta E_p$  which made these complexes more electrochemically reversible.

**Table 3.30:** Electronic parameters and the electrochemical data of all the  $M(\text{acac})_3$  complexes.

Complex	$E_{pa}$ (mV)	$E_{pc}$ (mV)	$\Delta E_p$	$\frac{E_{pc} - E_{pa}}{2}$ (mV)	$i_{pa}$ ( $\mu\text{A}$ )	$i_{pc}$ ( $\mu\text{A}$ )	$i_{pa}/i_{pc}$	$\chi_{\text{Pauling}}$	$\chi_{\text{Mulliken}}$
$\text{V}(\text{acac})_3$	-1322	-1403	81	-1363 <sup>i</sup>	45.86	50.37	0.91	1.63	3.6
$\text{Cr}(\text{acac})_3$	-2228	-2338	110	-2283 <sup>ii</sup>	0.38	-2228	-2338	1.66	3.72
$\text{Mn}(\text{acac})_3$	-117	-924	807	-520 <sup>ii</sup>	1.88	4.71	0.40	1.55	3.72
$\text{Fe}(\text{acac})_3$	-995	-1117	122	-1056 <sup>ii</sup>	0.65	-995	-1117	1.83	4.06
$\text{Co}(\text{acac})_3$	-	-1297	-	- <sup>i</sup>	-	5.52	-	1.88	4.3

<sup>i</sup> Solvent dichloromethane, supporting electrolyte tetraethylammonium tetrafluoroborate, working electrode glassy carbon, concentration of 0.5 mM  $M(\text{acac})_3$  vs  $\text{FcH}/\text{FcH}^+$ , scan rate  $100 \text{ mV.s}^{-1}$ .

<sup>ii</sup> Solvent acetonitrile, supporting electrolyte tetrabutylammonium hexafluorophosphate, working electrode glassy carbon, concentration of 0.5 mM  $M(\text{acac})_3$  vs  $\text{FcH}/\text{FcH}^+$ , scan rate  $100 \text{ mV.s}^{-1}$ .

From **Table 3.30** it can be seen that there was no real correlation between the position of the metal in the periodic table and the reduction potential of the  $M(\text{acac})_3$   $M^{\text{III}}/M^{\text{II}}$  redox couple. The graphs of the reduction potential ( $E_{pc}$ ) versus the electronegativity ( $\chi_{\text{Pauling}}$  and  $\chi_{\text{Mulliken}}$ ) of the free metal are shown in **Figure 3.37**.

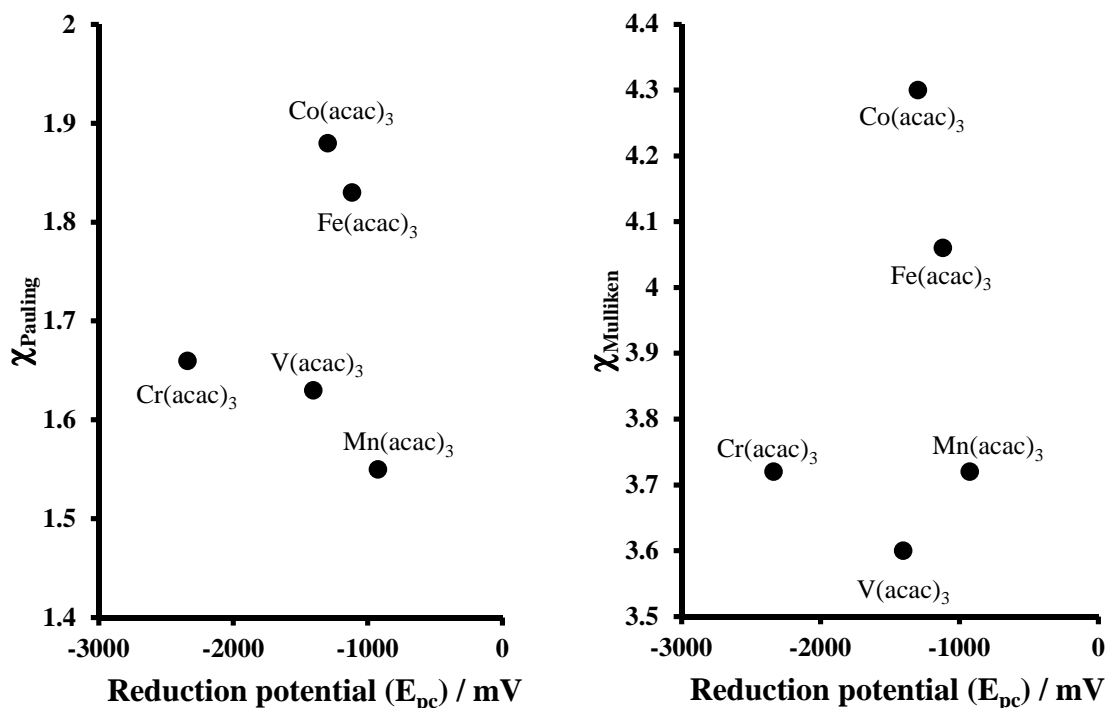


**Figure 3.37:** The graphs of the reduction potential ( $E_{pc}$ ) of  $M(\text{acac})_3$  complexes ( $M = \text{V}, \text{Cr}, \text{Mn}, \text{Fe}$  and  $\text{Co}$ ) versus the electronegativities ( $\chi_{\text{Pauling}}$  and  $\chi_{\text{Mulliken}}$ ) of the free metals.



There was no correlation found between the reduction potentials ( $E_{pc}$ ) and the electronegativity ( $\chi_{Pauling}$  and  $\chi_{Mulliken}$ ) of the free metal.

### 3.2.2 Computational study.

From section 2.3.2.4 it was seen that the high spin  $d^4$  species  $[Mn^{III}(acac)_3]$  is Jahn-Teller unstable but it is also known that the high spin  $d^2$   $[V^{III}(acac)_3]$  species is Jahn-Teller unstable.<sup>37</sup> The electron filling of the  $d$ -orbitals of the  $V(acac)_3$  complex were expected to be in the  $t_{2g}$  orbital group where, the HOMO could be one of the following three orbitals  $d_{xy}$ ,  $d_{yz}$  or  $d_{xz}$ . Since the  $t_{2g}$  orbitals are lower in energy than the  $e_g$  orbitals, the Jahn-Teller distortion of  $V(acac)_3$  was expected to be less noticeable than the Jahn-Teller distortion of  $Mn(acac)_3$ . Due to the partially filled degenerate  $e$ -orbital of  $Mn(acac)_3$  and  $t_{2g}$ -orbital of  $V(acac)_3$  in the  $D_3$  symmetry, the complex would spontaneously distort to the  $C_2$  symmetry (see section 2.3.2.4). Thus, there are only two metals in the series of  $M(acac)_3$  ( $M = V, Cr, Mn, Fe$  and  $Co$ ) that are Jahn-Teller unstable, namely vanadium and manganese. The Jahn-Teller distortion of  $Mn(acac)_3$  is fully discussed in section 3.1.4.1.

#### 3.2.2.1 Spin state and symmetry of $M(acac)_3$ .

The spin state and symmetry of  $M^{III}(acac)_3$  was determined by computationally calculating the optimized structure (ADF, OLYP) of all the possible spin states and symmetries of the ground states. The comparison of the spin state and symmetry data is summarized in **Table 3.31**.

---

<sup>37</sup> I. Diaz-Acosta, J. Baker, J.F. Hinton, P. Puley, *Spectrochimica Acta Part A* **2003** (59) 363-377.

## CHAPTER 3

**Table 3.31:** Calculated relative energies of spin state and symmetry study (ADF, OLYP) of  $M(\text{acac})_3$ .

Complex	Spin state	Symmetry	Relative energy ( $\text{kJ.mol}^{-1}$ )
$\text{V}(\text{acac})_3$	0/2	$C_2$	43.7
	2/2	$C_2$	0.0
	0/2	$D_3$	71.6
	2/2	$D_3$	7.0
$\text{Cr}(\text{acac})_3$	1/2	$C_2$	112.6
	3/2	$C_2$	0.0
	1/2	$D_3$	112.6
	3/2	$D_3$	0.0
$\text{Mn}(\text{acac})_3$	0/2	$C_2$	97.0
	2/2	$C_2$	31.5
	4/2	$C_2$	0.0
	0/2	$D_3$	-
	2/2	$D_3$	31.5
	4/2	$D_3$	13.0
$\text{Fe}(\text{acac})_3$	1/2	$C_2$	-
	3/2	$C_2$	-
	5/2	$C_2$	0.0
	1/2	$D_3$	61.8
	3/2	$D_3$	76.7
	5/2	$D_3$	0.0
$\text{Co}(\text{acac})_3$	0/2	$C_2$	0.3
	2/2	$C_2$	74.6
	4/2	$C_2$	63.4
	0/2	$D_3$	0.0
	2/2	$D_3$	99.0
	4/2	$D_3$	63.4

From the spin state and symmetry study of the  $\text{V}(\text{acac})_3$  ground state it was found that the complex prefers a 2/2 spin state and a symmetry of  $C_2$ . The spin and the symmetry of the  $\text{V}(\text{acac})_3$  complex obtained from **Table 3.31** implies that this complex showed a Jahn-Teller distortion., which is in agreement with the experimental data.<sup>38,39,40,41,42,43</sup> The comparison of the

<sup>38</sup> T.W. Hambley, C.J. Hawkins, T.A. Kabanos, *Inorg. Chem.* **1987** (26) 3740.

<sup>39</sup> B. Morosin, H. Montgomery, *Acta Crystallogr. Section B* **1969** (25) 1354.

## Results and discussion

calculated optimized structure of  $V(acac)_3$  ( $S = 2/2$ ) with an average of the crystal structures from previous studies can be seen in **Table 3.32**.

**Table 3.32:** Calculated (ADF, OLYP) and experimental V-O bond lengths.

Computational / experimental	Average M-O distance of the four longest (Å)	Average M-O distance of the shortest trans from each other (Å)
Computational study	2.026	2.020
Crystal average	1.969	1.967

Both the calculated and the experimental data showed that  $V(acac)_3$  had a small (nearly insignificant) positive Jahn-Teller distortion. The smaller Jahn-Teller distortion of the  $V(acac)_3$  complex in comparison to the  $Mn(acac)_3$  complex is fully discussed in section 2.5.2.1. The Jahn-Teller distortion of the  $V(acac)_3$  complex was within experimental error. The HOMO of the  $V(acac)_3$  complex is illustrated in **Figure 3.38** and shows that it mainly has  $d_{xz}$  character.

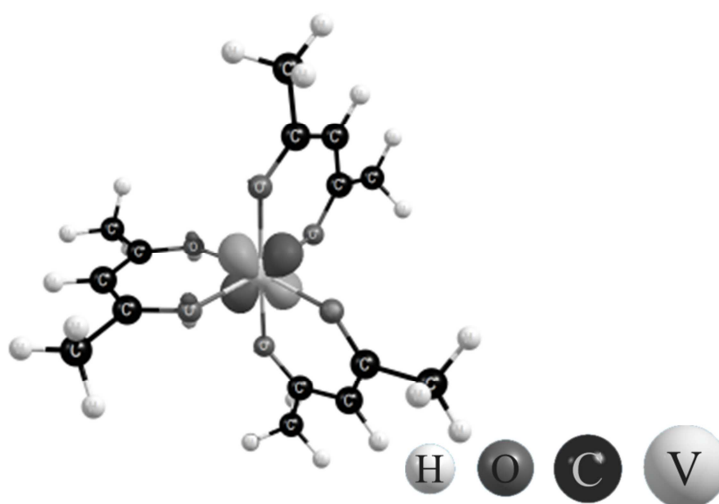


**Figure 3.38:** ADF/OLYP HOMO orbital of the optimized  $V(acac)_3$  complex.

From the spin state study of  $Cr(acac)_3$ ,  $Fe(acac)_3$  and  $Co(acac)_3$  the complexes were calculated to have  $3/2$ ,  $5/2$  and  $0/2$  spin states respectively. From **Table 3.31** it is seen that the  $D_3$  and  $C_2$  symmetries' relative energies of  $Cr(acac)_3$ ,  $Fe(acac)_3$  and  $Co(acac)_3$  are the same. The M-O bond lengths were investigated to help explain this phenomenon (see **Table 3.33**).

<sup>40</sup> C.A.L. Filgueiras, A. Horn Junior, R.A. Howie, J.M.S. Skakle, J.L. Wardell, *Acta Crystallogr. Section E* **2001** (57) m157.

<sup>41</sup> F. Sanz-Ruiz, S. Martinez-Carrera, S. Garcia-Blanco, *An. R. Soc. Esp. Fis. Quim. Part A*, **1970** (66) 309.

<sup>42</sup> S.J. Kavitha, K. Panchanatheswaran, J.N. Low, C. Glidewell, *Acta Crystallogr. Section E* **2005** (61) m1326.

<sup>43</sup> A. Behrens, D. Rehder, *Private Communication* **2009** (2) 72.

**Table 3.33:** The relative energies and M-O bond lengths of M(acac)<sub>3</sub> (Cr, Fe and Co) with their preferred spin state.

Complex	Spin state	Symmetry	Relative energy (kJ.mol <sup>-1</sup> )	Bond length (Mn-O) (Å)					
				1	2	3	4	5	6
Cr(acac) <sub>3</sub>	3/2	C <sub>2</sub>	0.0	2.008	2.008	2.008	2.008	2.008	2.008
	3/2	D <sub>3</sub>	0.0	2.008	2.008	2.008	2.008	2.008	2.008
Fe(acac) <sub>3</sub>	5/2	C <sub>2</sub>	0.0	2.072	2.072	2.072	2.072	2.072	2.072
	5/2	D <sub>3</sub>	0.0	2.072	2.072	2.072	2.072	2.072	2.072
Co(acac) <sub>3</sub>	0/2	C <sub>2</sub>	0.3	1.928	1.928	1.928	1.928	1.928	1.928
	0/2	D <sub>3</sub>	0.0	1.928	1.928	1.928	1.928	1.928	1.928

**Table 3.33** showed that the M-O bond lengths of C<sub>2</sub> symmetry of the different M(acac)<sub>3</sub> (Cr, Fe and Co) were all the same. Thus it can be concluded that the M(acac)<sub>3</sub> (Cr, Fe and Co) complexes prefer S = 3/2, 5/2 and 0/2 respectively with D<sub>3</sub> symmetry, which is in agreement with previous studies.<sup>44</sup>

### 3.2.2.2 *d*-orbitals occupations of the M(acac)<sub>3</sub> complexes (M = V, Cr, Mn, Fe and Co).

The filling of M(acac)<sub>3</sub> complexes' *d*-orbitals will be studied in this section. The following orbitals are expected for the M(acac)<sub>3</sub> complexes:

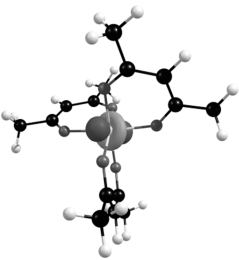
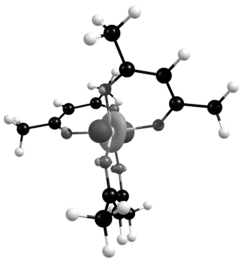
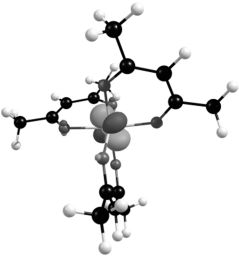
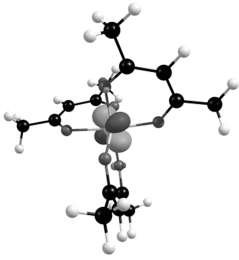
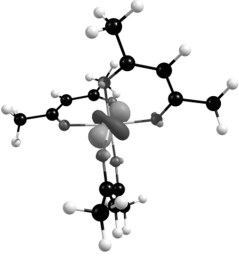
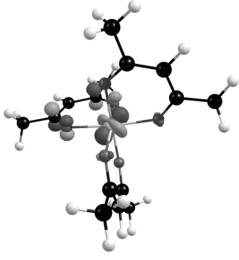
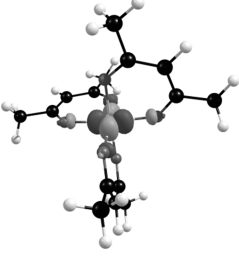
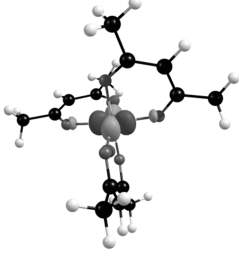
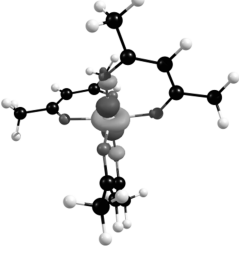
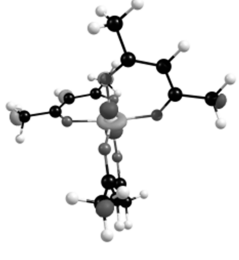
- V(acac)<sub>3</sub> complex (S = 2/2), two filled alpha (α) *d*-HOMO orbitals, three α *d*-LUMO and five beta (β) *d*-LUMO orbitals.
- Cr(acac)<sub>3</sub> complex (S = 3/2), three filled α *d*-HOMO orbitals, two α *d*-LUMO and five β *d*-LUMO orbitals.
- Mn(acac)<sub>3</sub> complex (S = 4/2), four filled α *d*-HOMO orbitals, one α *d*-LUMO and five β *d*-LUMO orbitals.
- Fe(acac)<sub>3</sub> complex (S = 5/2), five filled α *d*-HOMO orbitals and five β *d*-LUMO orbitals.
- Co(acac)<sub>3</sub> complex (S = 0/2), three filled α *d*-HOMO orbitals, two α *d*-LUMO orbitals and five β *d*-LUMO orbitals which were the same as the α orbitals because of the 0/2 spin.

The calculated α *d*-orbitals and their corresponding β *d*-orbitals occupations of the different M(acac)<sub>3</sub> complexes are shown in **Table 3.34** through to **Table 3.38**

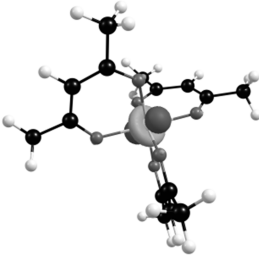
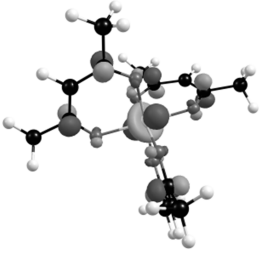
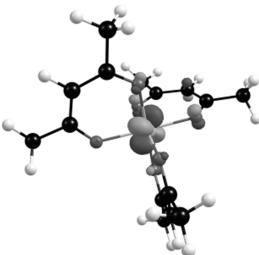
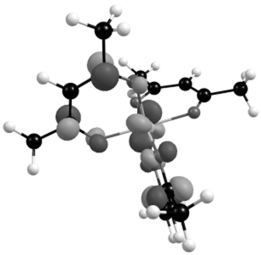
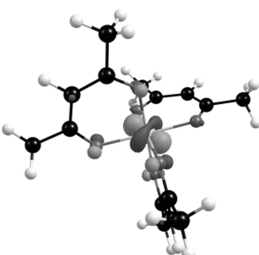
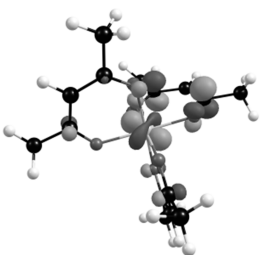
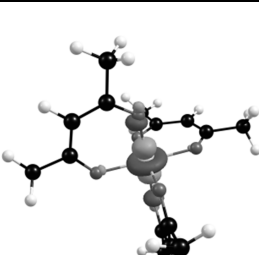
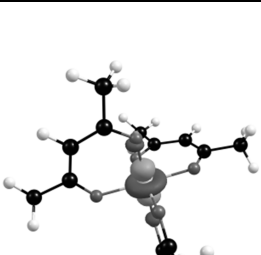
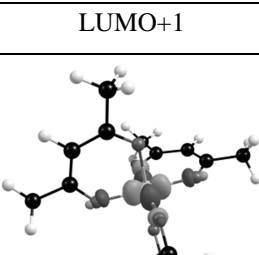
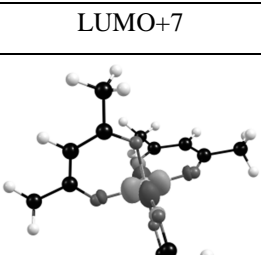
<sup>44</sup> I. Diaz-Acosta, J. Baker, J.F. Hinton, P. Puley, *Spectrochimica Acta Part A* **2003** (59) 363-377.

## Results and discussion

**Table 3.34:** The illustration of the calculated (ADF, OLYP) five  $d$ -orbitals of  $V(acac)_3$ .

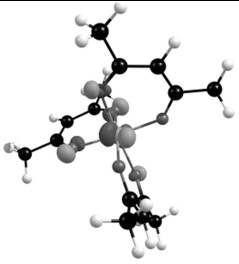
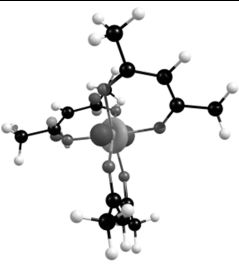
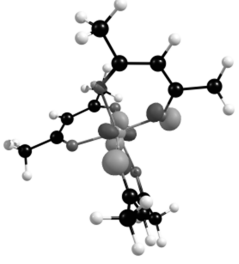
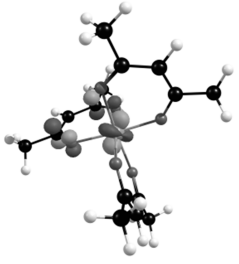
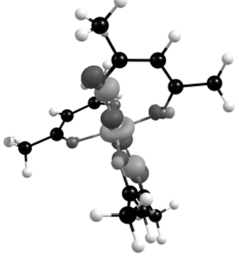
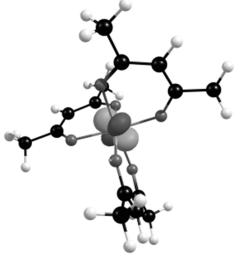
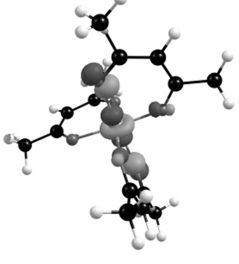
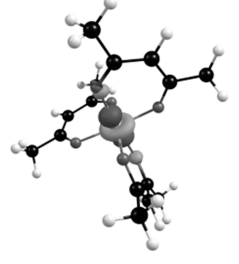
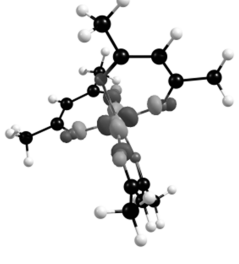
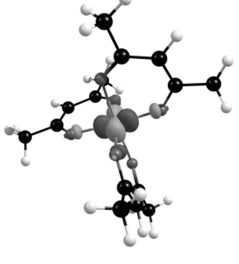
$V(acac)_3$		
$\alpha$	$d$ -orbital character	$\beta$
	$d_{yz}$	
HOMO-1		LUMO+11
	$d_{xz}$	
HOMO		LUMO+10
	$d_{xy}$	
LUMO		LUMO+7
	$d_{x^2-y^2}$	
LUMO+8		LUMO+14
	$d_{z^2}$	
LUMO+9		LUMO+18

**Table 3.35:** The illustration of the calculated (ADF, OLYP) five *d*-orbitals of Cr(acac)<sub>3</sub>.

Cr(acac) <sub>3</sub>		
$\alpha$	<i>d</i> -orbital character	$\beta$
	$d_{xz}$	
HOMO-2		LUMO
	$d_{yz}$	
HOMO-1		LUMO+3
	$d_{xy}$	
HOMO		LUMO+2
	$d_{z^2}$	
LUMO+1		LUMO+7
	$d_{x^2-y^2}$	
LUMO+2		LUMO+8

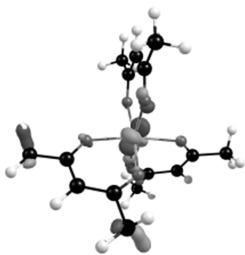
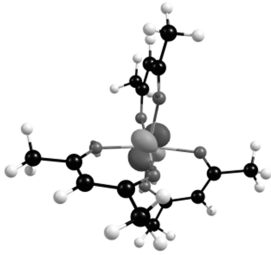
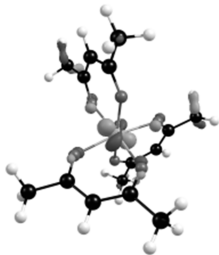
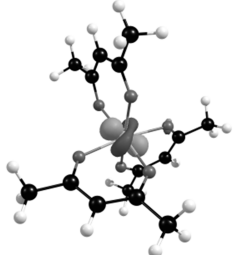
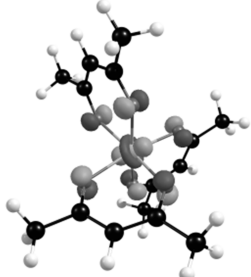
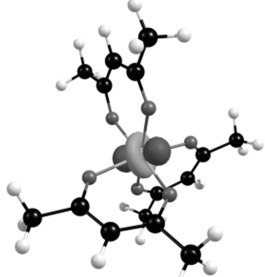
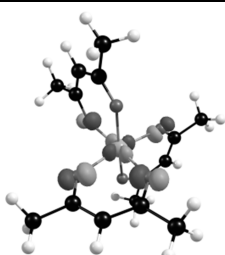
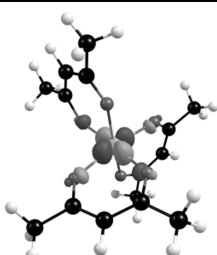
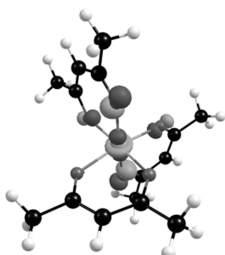
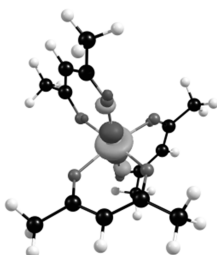
## Results and discussion

**Table 3.36:** The illustration of the calculated (ADF, OLYP) five *d*-orbitals of Mn(acac)<sub>3</sub>.

Mn(acac) <sub>3</sub>		
$\alpha$	<i>d</i> -orbital character	$\beta$
	$d_{xy}$	
HOMO-12		LUMO+1
	$d_{yz}$	
HOMO-10		LUMO+5
	$d_{xz}$	
HOMO-5		LUMO+3
	$d_{z^2}$	
HOMO		LUMO+11
	$d_{x^2-y^2}$	
LUMO		LUMO+10

# CHAPTER 3

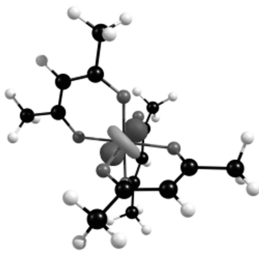
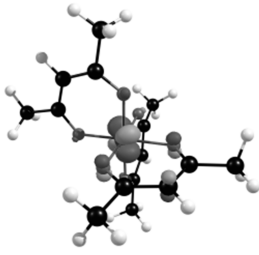
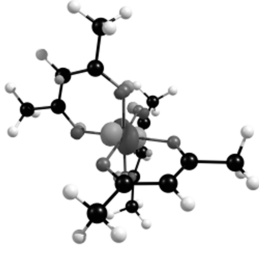
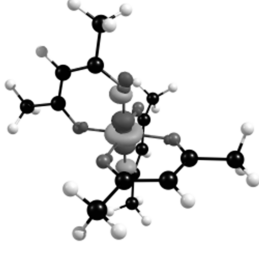
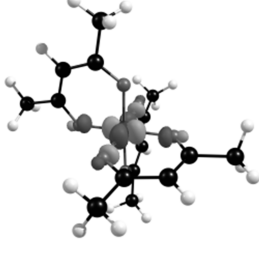
**Table 3.37:** The illustration of the calculated (ADF, OLYP) five *d*-orbitals of Fe(acac)<sub>3</sub>.

Fe(acac) <sub>3</sub>		
$\alpha$	<i>d</i> -orbital character	$\beta$
	$d_{xz}$	
HOMO-24		LUMO+2
	$d_{xy}$	
HOMO-23		LUMO+1
	$d_{yz}$	
HOMO-13		LUMO
	$d_{x^2-y^2}$	
HOMO-1		LUMO+3
	$d_{z^2}$	
HOMO		LUMO+4



## Results and discussion

**Table 3.38:** The illustration of the calculated (ADF, OLYP) five *d*-orbitals of Co(acac)<sub>3</sub>.

Co(acac) <sub>3</sub>	
$\alpha$	<i>d</i> -orbital character
	$d_{yz}$
HOMO-3	
	$d_{xz}$
HOMO-2	
	$d_{xy}$
HOMO-1	
	$d_{z^2}$
LUMO+1	
	$d_{x^2-y^2}$
LUMO+2	

### 3.2.2.3 Molecular orbital (MO) energy level diagram.

The MO energies of the  $M(\text{acac})_3$  complexes ( $M = \text{V}, \text{Cr}, \text{Mn}, \text{Fe}$  and  $\text{Co}$ ) were calculated and are illustrated in **Figure 3.39**. The  $d$ -orbitals of the  $M(\text{acac})_3$  complexes are highlighted in this MO energy figure.

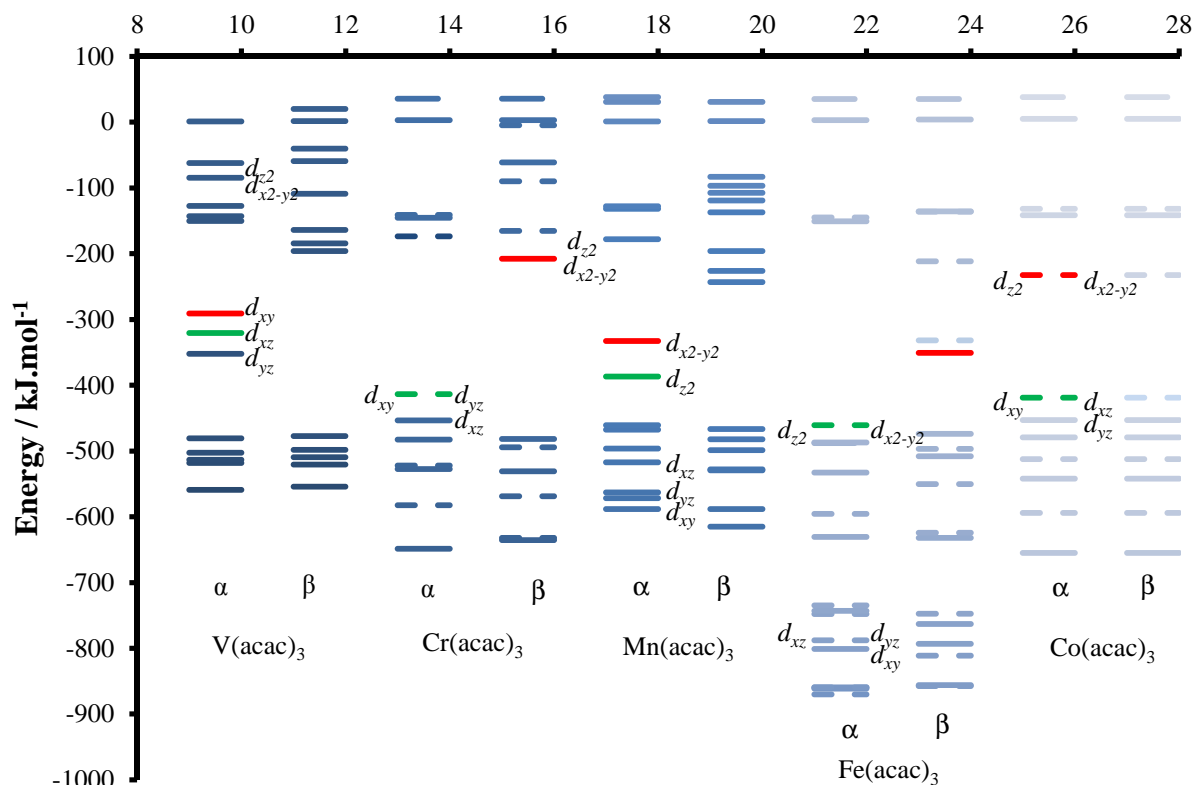


**Figure 3.39:** Molecular orbital energy level graph of  $M(\text{acac})_3$  with  $M = \text{V}, \text{Cr}, \text{Mn}, \text{Fe}$  and  $\text{Co}$ .

Only the  $\alpha$   $d$ -orbitals were labelled in **Figure 3.39**. From **Figure 3.39** the LUMO (lowest unoccupied molecular orbital) orbitals on the  $M(\text{acac})_3$  is shown in the red and the HOMO (highest molecular orbital) orbitals are shown in green. Both the  $\alpha$  and  $\beta$  orbitals are shown in the MO energy level graph.

In the MO energy level diagram **Figure 3.39** the splitting of the  $e_g$  and  $t_{2g}$  orbital groups were clearly visible. The large HOMO-LUMO gap of  $\text{Cr}(\text{aca})_3$  and  $\text{Co}(\text{acac})_3$  could be attributed to the fact that the  $t_{2g}$   $\alpha$  orbital group has electrons in it and the  $e_g$   $\alpha$  orbital group is empty. The small difference between the  $\alpha$  HOMO and  $\alpha$  HOMO-1 for  $\text{V}(\text{acac})_3$  and  $\text{Mn}(\text{acac})_3$  was also observed. This small  $\alpha$  HOMO and  $\alpha$  HOMO-1 difference could explain why the alternative occupation is possible for these two complexes.

### 3.2.2.4 Reduction potential relationships.

The LUMO energy was expected to have a relationship with the  $E_{pc}$  value since the electron that the complex would receive would go into the LUMO, which would become the new HOMO.  $Co(acac)_3$  was the only complex in the series that had a low spin with a totally chemically irreversible  $M^{III}/M^{II}$  couple and seemed to react differently from the rest of the  $M(acac)_3$  complexes. Thus,  $Co(acac)_3$  was not used in the correlation study between the  $E_{pc}$  and the LUMO energy. The reduction potentials ( $E_{pc}$ ) of the  $M(acac)_3$  complexes ( $M = V, Cr, Mn, Fe$  and  $Co$ ) with their respective LUMO energies and electron affinities are summarized in **Table 3.39**.

**Table 3.39:** The reduction potentials (*versus*  $FcH/FcH^+$ ) of  $M(acac)_3$  complexes ( $M = V, Cr, Mn, Fe$  and  $Co$ ) with their respective calculated electron affinities and LUMO energies.

Complex	$E_{pc}$ (mV)	LUMO energy ( $kJ.mol^{-1}$ )	EA ( $kJ.mol^{-1}$ )
$V(acac)_3$	-1403	-290.8	60.8
$Cr(acac)_3$	-2338	-207.5	61.0
$Mn(acac)_3$	-924	-332.5	196.9
$Fe(acac)_3$	-1117	-350.6	158.4
$Co(acac)_3$	-1297	-232.7	87.9

The relationship between the reduction potentials ( $E_{pc}$ ) of the  $M(acac)_3$  complexes and the LUMO energies is graphically shown in **Figure 3.40**.

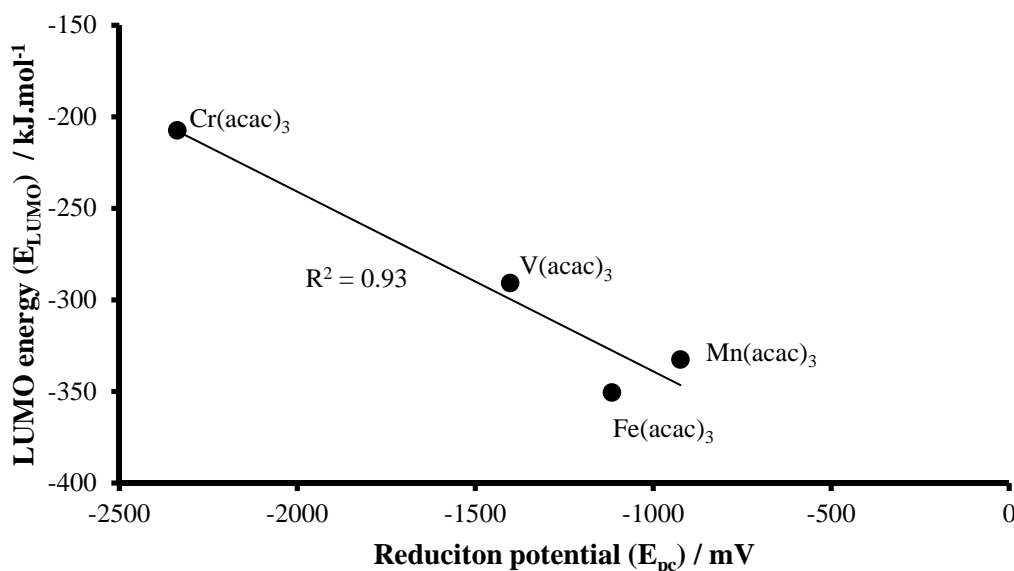


**Figure 3.40:** LUMO energies plotted against the reduction potentials of the  $M(acac)_3$  complexes ( $M = V, Cr, Mn$  and  $Fe$ ).

The correlation between the reduction potential and the calculated LUMO energies showed that, the LUMO energy decreased as the reduction potential increased. The linear equation describing the relationship is given as:  $E_{pc} = -0.098(E_{LUMO}) - 437.3$ . The relationship between the electron affinities (EA) and the reduction potentials ( $E_{pc}$ ) of the  $M(acac)_3$  complexes can be seen in **Figure 3.41**.

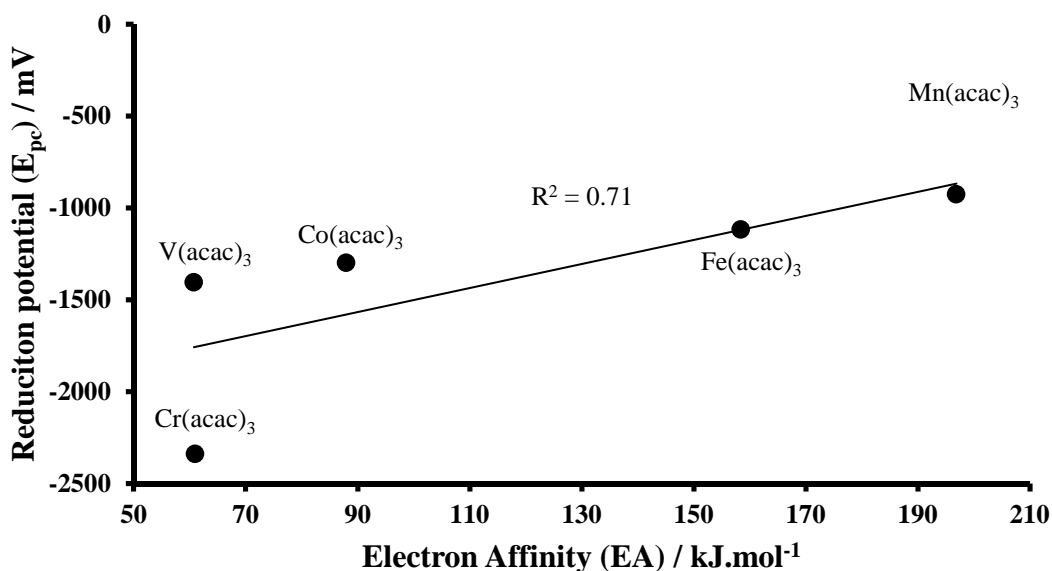


**Figure 3.41:** Electron affinities (EA) plotted against the reduction potentials ( $E_{pc}$ ) of the  $M(acac)_3$  complexes (  $M = V, Cr, Mn, Fe$  and  $Co$ ).

**Figure 3.41** showed that as the reduction potential increased the electron affinity increased. The linear equation describing the relationship is given as:  $E_{pc} = 8.84(EA) - 2307.3$ . This equation can be used to determine the reduction potential ( $E_{pc}$ ) of  $M(acac)_3$  complexes when the calculated electron affinity is known.

# 4

# Experimental.

---

## 4.1 Materials.

Solid and liquid reagents (Merk, Sigma Aldrich) were used in the synthesis without further purification. Solvents were used in the preparation and characterization of products as is unless otherwise specified.

## 4.2 Characterization techniques and instrumentation.

### 4.2.1 Spectroscopic measurements.

$^1\text{H}$  NMR could not be used as a characterization technique due to paramagnetic (complexes with at least one unpaired electron in the *d*-orbitals) properties of synthesized manganese(III) complexes.

### 4.2.2 Melting point (m.p.) determination.

The melting points were determined on an Olympus BX51 microscope that is fitted with a Linkam THMS600 hot stage that is connected to a Linkam TMS94 temperature programmer. The melting points given were the onset temperature of melting.

### 4.2.3 X-ray Diffraction (XRD).

The reflection datasets were collected on a Bruker X8 Apex II 4K Kappa CCD diffractometer using the Apex2 software package<sup>1</sup>. The optimum measurement method to collect more than a hemisphere of reciprocal space was predicted by COSMO<sup>2</sup>. Frame integration and data reduction were performed using the SAINT-Plus and XPREP<sup>3</sup> software packages, and a multi-scan

---

<sup>1</sup> Bruker **2011**, Apex2 (Version 2011. 4-1), Bruker AXS Inc., Madison, Wisconsin, USA.

<sup>2</sup> Bruker **2008**, COSMO (Version 1.58), Bruker AXS Inc., Madison, Wisconsin, USA.

<sup>3</sup> Bruker **2008**, SAINT-Plus (Version 7.68) (including XPREP), Bruker AXS Inc., Madison, Wisconsin, USA.

absorption correction was performed on the data using SADABS<sup>4</sup>. The structures were solved by the direct methods package SIR97<sup>5</sup>, and refinement using the WinGX<sup>6</sup> software package incorporating SHELXL<sup>7</sup>, all non H-atoms were refined anisotropically. All H-atoms were positioned geometrically and refined using the riding model with fixed C-H distances for aromatic C-H of 0.93 Å (CH) [ $U_{\text{iso}}(\text{H}) = 1.2 U_{\text{eq}}$ ] and for methyl C-H of 0.96 Å (CH) [ $U_{\text{iso}}(\text{H}) = 1.5 U_{\text{eq}}$ ]. Molecular diagrams were drawn using the DIAMOND<sup>8</sup> package with a 50 % thermal ellipsoid probability for non-hydrogen atoms. General crystal data and refinement parameters are presented in Section 3.1.2. A complete list of atomic coordinates, equivalent isotropic parameters, bond distances and angles, anisotropic displacement parameters and hydrogen coordinates for each individual dataset is given in Appendix A.

#### 4.2.4 Electrochemistry.

Cyclic voltammetry (CV), linear sweep voltammetry (LSV) was done by the use of a Princeton Applied Research PARSTAT 2273 voltammograph where the data was recorded using PowerSuite (Version 2.58) and a BAS100B Electrochemical Analyzer where data was recorded using BAS100W (Version 2.3). The three electrodes used during measurements are a Pt auxiliary electrode, Ag/Ag<sup>+</sup> (0.01 mM AgNO<sub>3</sub> in CH<sub>3</sub>CN) reference electrode mounted on a Luggin capillary and a glassy carbon (surface area 0.1257 cm<sup>2</sup>) working electrode. The working electrode was polished on a Bühler polishing mat first with 1 micron and then with ¼ micron diamond paste.

##### 4.2.4.1 Acetonitrile (CH<sub>3</sub>CN) solvent system.

The electrochemistry measurements were performed in CH<sub>3</sub>CN containing 0.1 M tetrabutylammonium hexafluorophosphate (TBAHFP, [NBu<sub>4</sub>][PF<sub>6</sub>]) as supporting electrolyte. The voltammogram was obtained at room temperature under a blanket of argon. The concentration of the analyte was 0.5 mM. Ferrocene was used as an internal standard. The

---

<sup>4</sup> Bruker **2008**, SADABS (Version 2008/1), Bruker AXS Inc., Madison, Wisconsin, USA.

<sup>5</sup> A. Altomare, M.C. Burla, M Camalli, G.L. Cascarano, C Giacovazzo, A Guagliardi, A.G.G. Moliterni, G Polidori, R Spagna, *J. Appl Cryst.* **1999** (32) 115.

<sup>6</sup> L.J. Farrugia, WinGX, *J. Appl. Cryst.* **1999** (32) 837.

<sup>7</sup> G.M. Sheldrick, SHELXL97 **1997**( *Program for crystal structure refinement*), University of Göttingen, Germany.

<sup>8</sup> K. Brandenburg, H Putz, DIAMOND **2005**, Release 3.0c, Crystal Impact GbR, Bonn, Germany.

supporting electrolyte used in the measurements of  $\text{Cr}(\text{acac})_3$  and  $\text{V}(\text{acac})_3$  voltammograms was tetraethylammonium tetrafluoroborate ( $\text{TEABF}_4$ ).

#### 4.2.4.2 Dichloromethane (DCM) solvent system.

Voltammograms were performed in spectrochemical grade DCM (Sigma-Aldrich) containing 0.1 M tetrabutylammonium hexafluorophosphate ( $\text{TBAHFP}$ ,  $[\text{NBu}_4][\text{PF}_6]$ ) as supporting electrolyte. The measurements were obtained at room temperature under a blanket of argon. Analyte concentration used was 0.5 mM. Ferrocene was used as an internal standard.

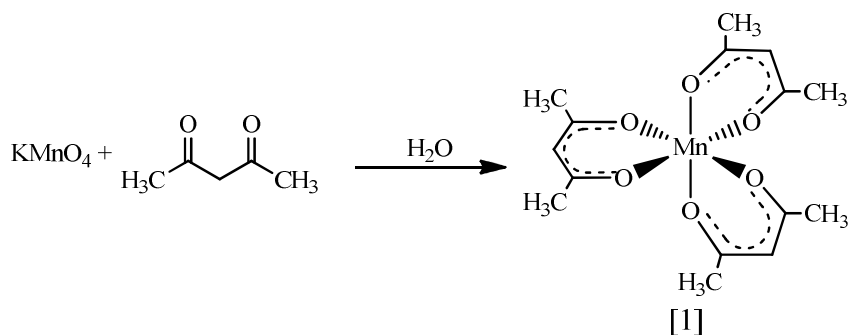
### 4.3 Synthesis.

#### 4.3.1 $\text{Mn}(\beta\text{-diketonato})_3$ complexes [1], [4] – [7].

The  $\text{Mn}(\beta\text{-diketonato})_3$  complexes [1], [4], [5], [6] and [7] were synthesized by the following adapted procedure.<sup>9</sup>

Potassium permanganate (0.25 g, 1.59 mmol) dissolved in a minimum amount of water was filtered.  $\beta$ -diketone (11 mmol) was added to the filtrate with vigorous stirring over a steam bath for five minutes. After the mixture was left to cool for ten minutes the precipitate was filtered and washed with water to obtain the desired  $\text{Mn}(\beta\text{-diketonato})_3$  complex.

##### 4.3.1.1 Tris(acetylacetonato)manganese(III) $\{\text{Mn}(\text{acac})_3\}$ [1].

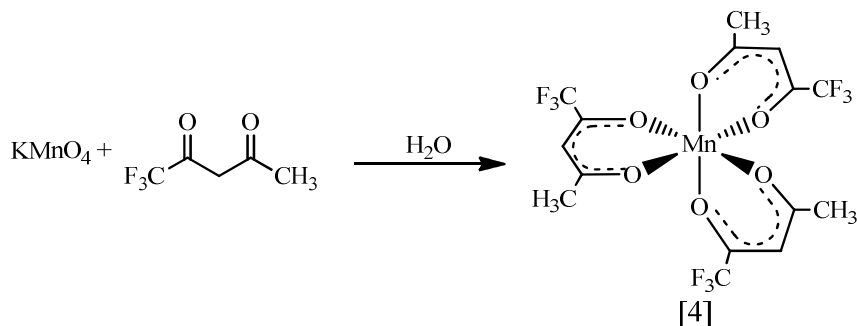


Yield 20 %. Colour: Black. Melting point 155.7 °C.

<sup>9</sup> M.N. Bhattacharjee, M.K. Chaudhuri, D.T Khathing, *Dalton Trans.* **1982** (3) 669-670.

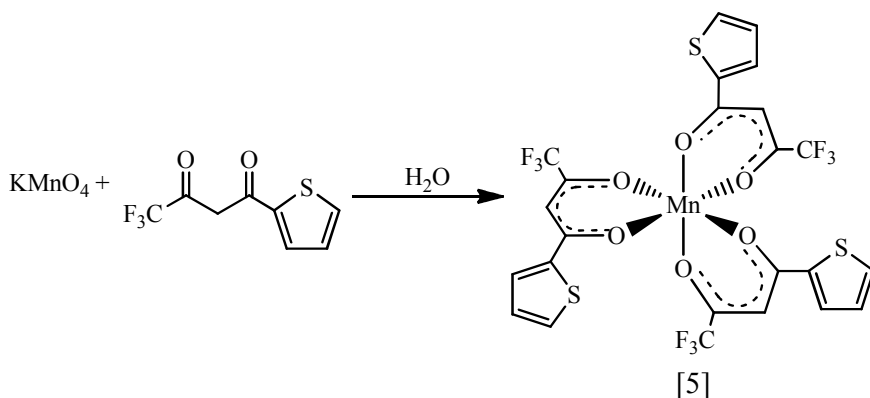
## Experimental

### 4.3.1.2 Tris(trifluoroacetylacetonato)manganese(III) {Mn(tfaa)<sub>3</sub>} [4].



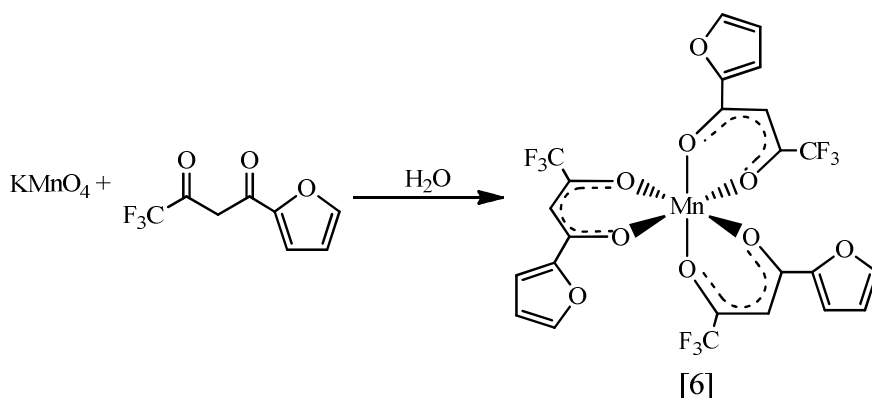
Yield 69 %. Colour: Dark brown-black. Melting point 116.7 °C. MS Calculated: Mr = 514.18 g/mol, Found: 515.1 g/mol. Elemental analysis; Calculated for MnC<sub>15</sub>H<sub>12</sub>O<sub>6</sub>F<sub>9</sub>: C, 35.0; H, 2.4 Found: C, 33.6; H, 2.3.

### 4.3.1.3 Tris(thenoyltrifluoroacetonato)manganese(III) {Mn(tfth)<sub>3</sub>} [5].



Yield 97 %. Colour: Brown. Melting point 157.5 °C. MS Calculated: Mr = 718.45 g/mol, Found: 722.1 g/mol. Elemental analysis; Calculated for MnC<sub>24</sub>H<sub>12</sub>O<sub>6</sub>F<sub>6</sub>S<sub>3</sub>: C, 40.1; H, 1.7 Found: C, 40.7; H, 1.99.

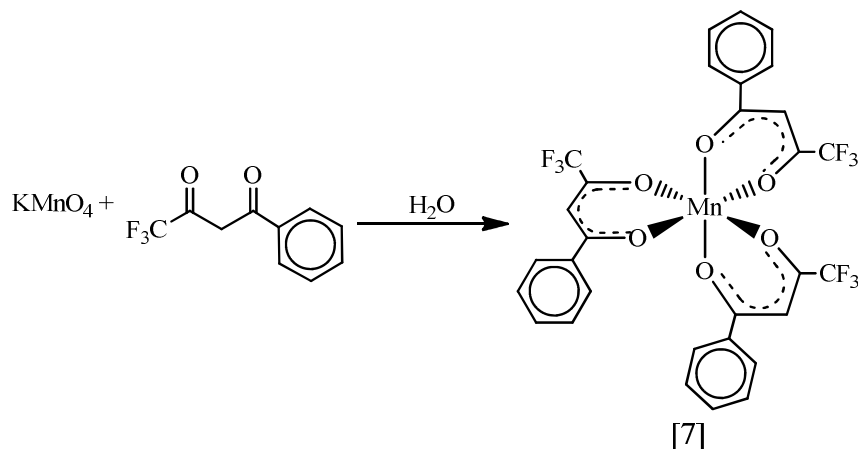
### 4.3.1.4 Tris(trifluorofuroylacetonato)manganese(III) {Mn(tffu)<sub>3</sub>} [6].





Yield 73 %. Colour: Black. Melting point 170.6 °C. MS Calculated: Mr = 670.27 g/mol, Found: 681.2 g/mol. Elemental analysis; Calculated for  $\text{MnC}_{24}\text{H}_{12}\text{O}_9\text{F}_9$ : C, 43.0; H, 1.8 Found: C, 42.25; H, 1.78.

#### 4.3.1.5 Tris(trifluorobenzoylacetonato)manganese(III) $\{\text{Mn}(\text{tfba})_3\}$ [7].



Yield 98 %. Colour: Black. Melting point 89.7 °C. MS Calculated: Mr = 700.39 g/mol, Found: 703.25 g/mol. Elemental analysis; Calculated for  $\text{MnC}_{30}\text{H}_{18}\text{O}_6\text{F}_9$ : C, 51.4; H, 2.6 Found: C, 54.6; H, 3.0.

### 4.3.2 $\text{Mn}(\beta\text{-diketonato})_3$ complexes [2], [3].

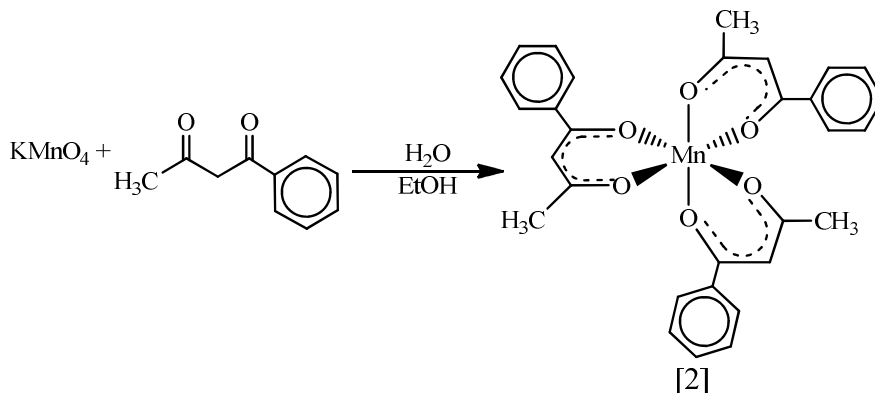
The  $\text{Mn}(\beta\text{-diketonato})_3$  complexes [2] and [3] were synthesized by the following adapted procedure.<sup>10</sup>

Potassium permanganate (0.25 g, 1.59 mmol) dissolved in a minimum amount of water was filtered.  $\beta$ -diketone (11 mmol) dissolved in ethanol was added to the filtrate with vigorous stirring over a steam bath for five minutes. The precipitate was filtered and washed with water after the mixture was left to cool for ten minutes to obtain the desired  $\text{Mn}(\beta\text{-diketonato})_3$  complex.

<sup>10</sup> M.N. Bhattacharjee, M.K. Chaudhuri, D.T Khathing, *Dalton Trans.* **1982** (3) 669-670.

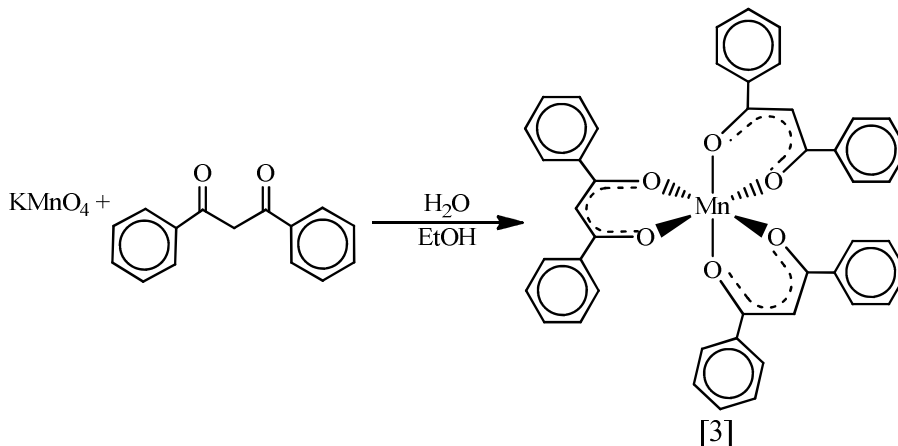
## Experimental

### 4.3.2.1 Tris(benzoylacetonato)manganese(III) {Mn(ba)<sub>3</sub>} [2].



Yield 70 %. Colour: Green. Melting point 184.3 °C. MS Calculated: Mr = 538.48 g/mol, Found: 540.3 g/mol. Elemental analysis; Calculated for MnC<sub>30</sub>H<sub>27</sub>O<sub>6</sub>: C, 66.9; H, 5.1 Found: C, 72.3; H, 5.8.

### 4.3.2.2 Tris(dibenzoylmethanato)manganese(III) {Mn(dbm)<sub>3</sub>} [3].



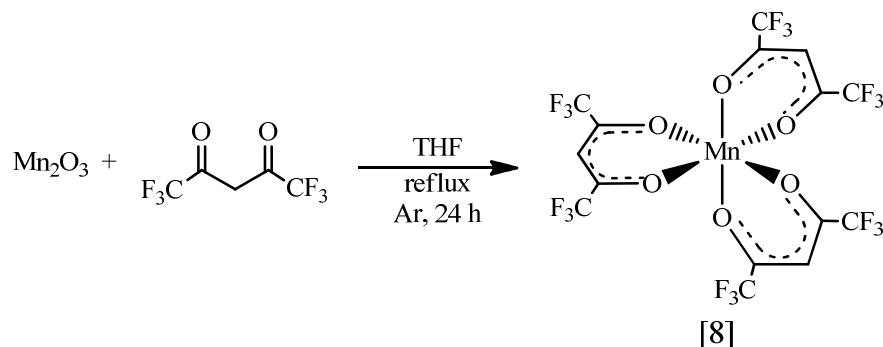
Yield 80 %. Colour: Black. Melting point 235.7 °C. Elemental analysis; Calculated for MnC<sub>45</sub>H<sub>33</sub>O<sub>6</sub>: C, 74.6; H, 4.6 Found: C, 76.5; H, 4.72.

### 4.3.3 Mn( $\beta$ -diketonato)<sub>3</sub> complex [8].

The Mn( $\beta$ -diketonato)<sub>3</sub> complex [8] was synthesized by the following adapted procedure.<sup>11,12</sup>

A reaction mixture of Mn<sub>2</sub>O<sub>3</sub> (0.418 g, 2.65 mmol), Hhfac (3 mL, 21.19 mmol) and dry THF (20 mL) was refluxed under Ar for 24 h. Excess solvent and Hhfac were removed under vacuum. The dark green residue was then sublimed under vacuum at 60 °C. The yellow Mn(hfac)<sub>3</sub> was collected from the cold finger. The yield and melting point could not be determined due to the hygroscopic nature of Mn(hfac)<sub>3</sub>.

#### 4.3.3.1 Tris(hexafluoroacetylacetonato)manganese(III) {Mn(hfac)<sub>3</sub>} [8].



## 4.4 Computational calculations.

### 4.4.1 Tris( $\beta$ -diketonato)manganese(III), Mn( $\beta$ -diketonato)<sub>3</sub>.

Density Functional Theory (DFT) calculations were carried out by the use of Amsterdam Density Functional 2009 (ADF) program<sup>13</sup> with OLYP or PW91 functional. Triple zeta polarized (TZP) basis set was used during the calculations. Initial calculations done on Mn(acac)<sub>3</sub> were performed with *D*<sub>3</sub> and *C*<sub>2</sub> symmetry constraint with a selection of spin states (*S* = 0/2, 2/2 and 4/2). Final calculations on [Mn( $\beta$ -diketonato)<sub>3</sub>]<sup>+</sup>, [Mn( $\beta$ -diketonato)<sub>3</sub>] and [Mn( $\beta$ -diketonato)<sub>3</sub>]<sup>-</sup> complexes were performed with *C*<sub>2</sub> (complexes with symmetrical  $\beta$ -diketonato

<sup>11</sup> H. Zhang, B. Li, E.V. Dikarev, *J Clust Sci* **2008** (19) 311-321.

<sup>12</sup> J.R. Bryant, J.E. Taves, J.M. Mayer, *Inorg. Chem.* **2002** (41) 2769-2776.

<sup>13</sup> G. Te Velde, F.M. Bickelhaupt, E.J. Baerends, C.F. Guerra, S.J.A. Van Gisbergen, J.G. Snijders, T. Ziegler, *J. Comput. Chem.* **2001** (22) 931-967.

ligands) and  $C_1$  (complexes with unsymmetrical  $\beta$ -diketonato ligands, arranged to have no symmetry operation at all) symmetry constraint. All the possible spin states of  $[\text{Mn}(\beta\text{-diketonato})_3]^+$ ,  $[\text{Mn}(\beta\text{-diketonato})_3]$  and  $[\text{Mn}(\beta\text{-diketonato})_3]^-$  complexes were calculated.

#### **4.4.2 Tris(acetylacetonato)metal(III), $\text{M}(\text{acac})_3$ (M = V, Cr, Fe and Co).**

Density Functional Theory (DFT) calculations were carried out by the use of Amsterdam Density Functional 2009 (ADF) program<sup>13</sup> with OLYP or PW91 functional. Triple zeta polarized (TZP) basis set was used during the calculations. Calculations done on  $\text{V}(\text{acac})_3$  were performed with  $D_3$  and  $C_2$  symmetry constraint and a selection of spin states ( $S = 0/2$  and  $2/2$ ). The rest of the  $\text{M}(\text{acac})_3$  complex series' (M = Cr, Fe and Co) calculations were carried out with  $D_3$  symmetry constraint and a selection of spin states (Cr:  $S = 1/2$  and  $3/2$ ; Fe:  $S = 1/2, 3/2$  and  $5/2$ ; Co:  $S = 1/2$  and  $3/2$ ).

# 5 Concluding remarks and future perspectives.

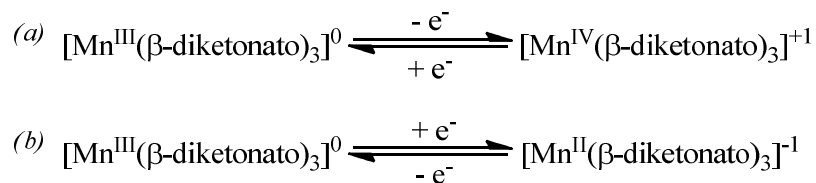
---

## 5.1 Concluding remarks.

### 5.1.1 Tris( $\beta$ -diketonato)manganese(III) / Mn( $\beta$ -diketonato)<sub>3</sub>.

Experimental and computational methods were used to study a series of Mn( $\beta$ -diketonato)<sub>3</sub> complexes ( $\beta$ -diketonato = acetylacetonate (acac) [1], benzoylacetonato (ba) [2], dibenzoylmethanato (dbm) [3], trifluoroacetylacetonato (tfaa) [4], thenoyltrifluoroacetonato (tfth) [5], trifluorofuroylacetonato (tffu) [6], trifluorobenzoylacetonato (tfba) [7], hexafluoroacetylacetonato (hfac) [8]). Four known and four novel Mn( $\beta$ -diketonato)<sub>3</sub> complexes were synthesized successfully. The complexes were characterized with mass spectroscopy, elemental analysis and by their melting points.

The electrochemical behaviour of the Mn( $\beta$ -diketonato)<sub>3</sub> complex series was studied by the use of cyclic voltammetry. Two redox reactions were observed for Mn( $\beta$ -diketonato)<sub>3</sub> complexes with  $\beta$ -diketonato = acac, ba and dbm:



The redox reaction (a) was found to be chemically reversible at a scan rate of 100 mV.s<sup>-1</sup>. The redox potentials shifted due to the different electronic densities at the manganese centre, which is attributed to the different R side groups of the  $\beta$ -diketonato ligands (RCOCHCOR'). With more electron withdrawing R and R' groups the redox potentials were found to shift to more positive potentials. Due to this shift and the solvent window, redox reaction (a) could not be observed for all the Mn( $\beta$ -diketonato)<sub>3</sub> complexes. Therefore, the study focused on redox reaction (b). The (b) redox reaction is neither chemically nor electrochemically reversible. The Mn( $\beta$ -diketonato)<sub>3</sub> reduction potentials of the Mn<sup>III</sup>/Mn<sup>II</sup> couple ( $E_{\text{pc}}$ ) were correlated to parameters related to the electron density around the manganese centre. The electronic parameters include the acid dissociation constant ( $\text{pK}_{\text{a}}$ ) of the uncoordinated  $\beta$ -diketone, total group electronegativities [ $\Sigma(\chi_{\text{R}}$

### Concluding remarks and future perspectives

+  $\chi_{R'}$ )] and the total Hammett sigma meta constants [ $\Sigma(\sigma_R + \sigma_{R'})$ ] of the  $\beta$ -diketonato ligands' R and R' groups. The linear equations ( $y = mx + c$ ) defining these relationships can be expressed as:

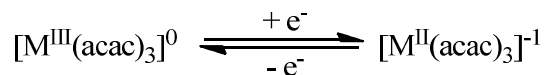
$$\begin{aligned} pK_a &= (-0.0025)E_{pc} + 6.85 & R^2 &= 0.86 \\ \chi_R + \chi_{R'} &= (-0.0027)E_{pc} + 11.66 & R^2 &= 0.93 \\ \chi_R + \chi_{R'} &= (-0.0014)E_{pc} + 15.69 & R^2 &= 0.77 \\ \chi_R + \chi_{R'} &= 18.06 \\ \sigma_R + \sigma_{R'} &= (0.0016)E_{pc} + 1.15 & R^2 &= 0.96 \end{aligned}$$

The above equations facilitate the prediction of the reduction potential of the  $Mn^{III}/Mn^{II}$  couple if the acid dissociation constant of the uncoordinated  $\beta$ -diketone, the electronegativities or Hammett sigma meta constants of  $Mn(\beta\text{-diketonato})_3$  complexes are known.

DFT studies, in agreement with experimental observations showed that  $Mn(acac)_3$  has a spin of 4/2 and a  $C_2$  symmetry. A more in-depth look into the symmetry of  $Mn(acac)_3$  and  $Mn(dbm)_3$  was conducted to explain the Jahn-Teller distortion of the crystal data that was obtained in this study as well as and previous studies. From previous experimental work the  $Mn(acac)_3$  complex was found to exhibit both positive and negative Jahn-Teller distortion. The computational study of this dissertation showed that the population of  $Mn(acac)_3$  with a negative Jahn-Teller distortion referenced to a positive distortion as 79 % : 21 % giving a natural explanation why both the Jahn-Teller distortions were observed in crystals. The population of  $Mn(dbm)_3$  with a negative Jahn-Teller distortion was calculated to be 91 % : 9 % relative to the positive Jahn-Teller distortion. Thus, the fact that  $Mn(dbm)_3$  mainly occurs with a negative Jahn-Teller distortion could be explained.

### 5.1.2 Tris(acetylacetonato)metal(III), $M(\text{acac})_3$ ( $M = \text{V}, \text{Cr}, \text{Fe}$ and $\text{Co}$ ).

The electrochemical behaviour of the  $M(\text{acac})_3$  complex series ( $M = \text{V}, \text{Cr}, \text{Mn}, \text{Fe}$  and  $\text{Co}$ ) were studied by the use of cyclic voltammetry. The redox reaction that was studied can be expressed as:



The redox reaction of  $\text{V}(\text{acac})_3$  at a scan rate of  $100 \text{ mV.s}^{-1}$  was found to be electrochemically reversible and not chemically reversible.  $\text{Cr}(\text{acac})_3$ ,  $\text{Mn}(\text{acac})_3$  and  $\text{Fe}(\text{acac})_3$  are not electrochemically or chemically reversible.  $\text{Co}(\text{acac})_3$  however does not reduce back to the  $\text{Co}^{\text{III}}(\text{acac})_3$  complex, this complex is therefore also not electrochemically or chemically reversible. The shift of the redox potentials could be assigned to the different electronic behaviours of the metal centres. The  $M(\text{acac})_3$  reduction potential of the  $M^{\text{III}}/M^{\text{II}}$  couple ( $E_{\text{pc}}$ ) was correlated to the electronegativities ( $\chi_{\text{Pauling}}$  and  $\chi_{\text{Mulliken}}$ ) of the metals which is related to the electrondensity around the metal centre. No correlation was found between the electronegativities of the metal and the reduction potential.

The  $\text{V}(\text{acac})_3$  complex is the only other complex in the  $M(\text{acac})_3$  series that has been found to show Jahn-Teller distortion. The Jahn-Teller distortion of  $\text{V}(\text{acac})_3$  was much less pronounced than that displayed by  $\text{Mn}(\text{acac})_3$ .

## 5.2 Future perspectives.

The study of the  $\text{Mn}(\beta\text{-diketonato})_3$  complex series can be expanded as follows:

- i. Anchor the  $\text{Mn}(\beta\text{-diketonato})_3$  complexes ( $\beta\text{-diketonato} = \text{acetylacetonate (acac)}$  [1], benzoylacetone (ba) [2], dibenzoylmethanato (dbm) [3], trifluoroacetylacetonato (tfaa) [4], thenoyltrifluoroacetone (tfth) [5], trifluorofuroylacetone (tffu) [6], trifluorobenzoylacetone (tfba) [7], hexafluoroacetylacetonato (hfac) [8]) on to silica (for potential heterogeneous catalysts).
- ii. Do a catalytic study on the  $\text{Mn}(\beta\text{-diketonato})_3$  complexes anchored on silica, to evaluate the catalytic activity of these complexes.
- iii. Conduct surface calculations on the heterogeneous catalyst series to determine a possible catalytic cycle.

<b>Concluding remarks and future perspectives</b>
---

The study of  $M(\text{acac})_3$  complex series studies can be expanded as follows:

- i. Synthesize a series of  $M(\text{acac})_3$  ( $M = \text{Ru}$  and  $\text{Os}$ ) to explore electrochemical trends of metals in the same group in the periodic table.
- ii. Calculate the electron affinity of the series  $M(\text{acac})_3$  ( $M = \text{Ru}$  and  $\text{Os}$ ) and compare with experimental data.



# Appendix.

## A. Crystal data.

**Table A.1:** Atomic coordinates ( $\times 10^4$ ) and equivalent isotropic displacement parameters ( $\text{\AA}^2 \times 10^3$ ) for  $\text{Mn}(\text{dbm})_3$ .

$U(\text{eq})$  is defined as one third of the trace of the orthogonalized  $U^{ij}$  tensor.

	x	y	z	U(eq)
C(1)	6441(1)	332(2)	5175(1)	16(1)
C(2)	6644(1)	-972(2)	4997(1)	19(1)
C(3)	7092(1)	-1904(2)	5369(1)	17(1)
C(4)	5866(1)	1151(2)	4771(1)	17(1)
C(5)	5630(1)	764(2)	4163(1)	24(1)
C(6)	5057(1)	1507(2)	3819(1)	28(1)
C(7)	4710(1)	2636(2)	4074(1)	25(1)
C(8)	4956(1)	3059(2)	4668(1)	26(1)
C(9)	5536(1)	2328(2)	5012(1)	23(1)
C(10)	7179(1)	-3335(2)	5148(1)	18(1)
C(11)	6959(1)	-3761(2)	4545(1)	30(1)
C(12)	7035(1)	-5116(2)	4378(1)	35(1)
C(13)	7317(1)	-6059(2)	4809(1)	27(1)
C(14)	7551(2)	-5649(2)	5404(1)	34(1)
C(15)	7485(1)	-4298(2)	5570(1)	29(1)
C(16)	9056(1)	971(2)	5968(1)	19(1)
C(17)	9379(1)	698(2)	6567(1)	23(1)
C(18)	8947(1)	116(2)	7037(1)	19(1)
C(19)	9571(1)	1415(2)	5459(1)	19(1)
C(20)	9215(1)	1842(2)	4892(1)	26(1)
C(21)	9682(1)	2247(2)	4407(1)	32(1)
C(22)	10514(1)	2229(2)	4485(1)	32(1)
C(23)	10874(1)	1798(2)	5043(1)	31(1)
C(24)	10408(1)	1391(2)	5528(1)	26(1)
C(25)	9326(1)	-150(2)	7667(1)	22(1)
C(26)	10152(1)	-332(2)	7771(1)	33(1)
C(27)	10476(1)	-543(2)	8371(1)	38(1)
C(28)	9986(1)	-561(2)	8870(1)	33(1)

## Appendix

C(29)	9164(1)	-404(2)	8775(1)	30(1)
C(30)	8830(1)	-204(2)	8176(1)	25(1)
C(31)	7152(1)	2411(2)	7332(1)	18(1)
C(32)	6694(1)	1440(2)	7648(1)	19(1)
C(33)	6444(1)	206(2)	7399(1)	16(1)
C(34)	7395(1)	3708(2)	7655(1)	18(1)
C(35)	7552(1)	4842(2)	7299(1)	24(1)
C(36)	7808(1)	6050(2)	7574(1)	28(1)
C(37)	7905(1)	6134(2)	8217(1)	28(1)
C(38)	7751(1)	5014(2)	8581(1)	32(1)
C(39)	7494(1)	3808(2)	8305(1)	27(1)
C(40)	5935(1)	-737(2)	7756(1)	17(1)
C(41)	6004(1)	-2129(2)	7659(1)	20(1)
C(42)	5524(1)	-3033(2)	7969(1)	24(1)
C(43)	4952(1)	-2553(2)	8365(1)	26(1)
C(44)	4878(1)	-1166(2)	8461(1)	27(1)
C(45)	5369(1)	-267(2)	8165(1)	22(1)
O(1)	6683(1)	925(1)	5688(1)	18(1)
O(2)	7419(1)	-1627(1)	5899(1)	19(1)
O(3)	8303(1)	869(1)	5811(1)	20(1)
O(4)	8200(1)	-229(1)	6973(1)	20(1)
O(5)	7375(1)	2271(1)	6780(1)	20(1)
O(6)	6610(1)	-255(1)	6856(1)	18(1)
Mn(1)	7444(1)	319(1)	6326(1)	16(1)

**Table A.2:** Bond lengths [ $\text{\AA}$ ] and angles [ $^\circ$ ] for  $\text{Mn}(\text{dbm})_3$ .

Bond	Bond length ( $\text{\AA}$ )	Bond angle	Angle ( $^\circ$ )
C(1)-O(1)	1.291(2)	O(1)-C(1)-C(2)	125.59(16)
C(1)-C(2)	1.386(3)	O(1)-C(1)-C(4)	114.45(16)
C(1)-C(4)	1.495(2)	C(2)-C(1)-C(4)	119.90(16)
C(2)-C(3)	1.405(3)	C(1)-C(2)-C(3)	125.38(16)
C(2)-H(2)	0.93	C(1)-C(2)-H(2)	117.3
C(3)-O(2)	1.265(2)	C(3)-C(2)-H(2)	117.3
C(3)-C(10)	1.495(3)	O(2)-C(3)-C(2)	124.17(17)
C(4)-C(9)	1.392(3)	O(2)-C(3)-C(10)	116.34(16)
C(4)-C(5)	1.394(2)	C(2)-C(3)-C(10)	119.45(16)
C(5)-C(6)	1.385(3)	C(9)-C(4)-C(5)	118.39(17)
C(5)-H(5)	0.93	C(9)-C(4)-C(1)	119.09(16)
C(6)-C(7)	1.378(3)	C(5)-C(4)-C(1)	122.50(17)
C(6)-H(6)	0.93	C(6)-C(5)-C(4)	120.58(19)
C(7)-C(8)	1.381(3)	C(6)-C(5)-H(5)	119.7
C(7)-H(7)	0.93	C(4)-C(5)-H(5)	119.7
C(8)-C(9)	1.387(3)	C(7)-C(6)-C(5)	120.32(18)
C(8)-H(8)	0.93	C(7)-C(6)-H(6)	119.8

# Appendix

C(9)-H(9)	0.93	C(5)-C(6)-H(6)	119.8
C(10)-C(15)	1.388(3)	C(6)-C(7)-C(8)	119.84(18)
C(10)-C(11)	1.391(3)	C(6)-C(7)-H(7)	120.1
C(11)-C(12)	1.388(3)	C(8)-C(7)-H(7)	120.1
C(11)-H(11)	0.93	C(7)-C(8)-C(9)	120.04(19)
C(12)-C(13)	1.376(3)	C(7)-C(8)-H(8)	120
C(12)-H(12)	0.93	C(9)-C(8)-H(8)	120
C(13)-C(14)	1.376(3)	C(8)-C(9)-C(4)	120.73(18)
C(13)-H(13)	0.93	C(8)-C(9)-H(9)	119.6
C(14)-C(15)	1.383(3)	C(4)-C(9)-H(9)	119.6
C(14)-H(14)	0.93	C(15)-C(10)-C(11)	118.05(18)
C(15)-H(15)	0.93	C(15)-C(10)-C(3)	118.35(16)
C(16)-O(3)	1.284(2)	C(11)-C(10)-C(3)	123.60(17)
C(16)-C(17)	1.395(3)	C(12)-C(11)-C(10)	120.45(19)
C(16)-C(19)	1.484(2)	C(12)-C(11)-H(11)	119.8
C(17)-C(18)	1.388(3)	C(10)-C(11)-H(11)	119.8
C(17)-H(17)	0.93	C(13)-C(12)-C(11)	120.46(19)
C(18)-O(4)	1.289(2)	C(13)-C(12)-H(12)	119.8
C(18)-C(25)	1.486(3)	C(11)-C(12)-H(12)	119.8
C(19)-C(24)	1.392(3)	C(14)-C(13)-C(12)	119.7(2)
C(19)-C(20)	1.392(3)	C(14)-C(13)-H(13)	120.1
C(20)-C(21)	1.386(3)	C(12)-C(13)-H(13)	120.1
C(20)-H(20)	0.93	C(13)-C(14)-C(15)	119.86(19)
C(21)-C(22)	1.386(3)	C(13)-C(14)-H(14)	120.1
C(21)-H(21)	0.93	C(15)-C(14)-H(14)	120.1
C(22)-C(23)	1.377(3)	C(14)-C(15)-C(10)	121.40(18)
C(22)-H(22)	0.93	C(14)-C(15)-H(15)	119.3
C(23)-C(24)	1.384(3)	C(10)-C(15)-H(15)	119.3
C(23)-H(23)	0.93	O(3)-C(16)-C(17)	123.64(16)
C(24)-H(24)	0.93	O(3)-C(16)-C(19)	114.89(16)
C(25)-C(26)	1.392(3)	C(17)-C(16)-C(19)	121.48(17)
C(25)-C(30)	1.397(3)	C(18)-C(17)-C(16)	123.87(18)
C(26)-C(27)	1.386(3)	C(18)-C(17)-H(17)	118.1
C(26)-H(26)	0.93	C(16)-C(17)-H(17)	118.1
C(27)-C(28)	1.375(3)	O(4)-C(18)-C(17)	124.18(17)
C(27)-H(27)	0.93	O(4)-C(18)-C(25)	114.43(16)
C(28)-C(29)	1.382(3)	C(17)-C(18)-C(25)	121.39(17)
C(28)-H(28)	0.93	C(24)-C(19)-C(20)	118.57(17)
C(29)-C(30)	1.387(3)	C(24)-C(19)-C(16)	121.82(17)
C(29)-H(29)	0.93	C(20)-C(19)-C(16)	119.60(17)

# Appendix

C(30)-H(30)	0.93	C(21)-C(20)-C(19)	120.8(2)
C(31)-O(5)	1.2632(19)	C(21)-C(20)-H(20)	119.6
C(31)-C(32)	1.415(3)	C(19)-C(20)-H(20)	119.6
C(31)-C(34)	1.499(3)	C(20)-C(21)-C(22)	119.8(2)
C(32)-C(33)	1.383(3)	C(20)-C(21)-H(21)	120.1
C(32)-H(32)	0.93	C(22)-C(21)-H(21)	120.1
C(33)-O(6)	1.290(2)	C(23)-C(22)-C(21)	119.91(19)
C(33)-C(40)	1.492(2)	C(23)-C(22)-H(22)	120
C(34)-C(35)	1.385(3)	C(21)-C(22)-H(22)	120
C(34)-C(39)	1.396(2)	C(22)-C(23)-C(24)	120.3(2)
C(35)-C(36)	1.385(3)	C(22)-C(23)-H(23)	119.8
C(35)-H(35)	0.93	C(24)-C(23)-H(23)	119.8
C(36)-C(37)	1.384(3)	C(23)-C(24)-C(19)	120.56(19)
C(36)-H(36)	0.93	C(23)-C(24)-H(24)	119.7
C(37)-C(38)	1.381(3)	C(19)-C(24)-H(24)	119.7
C(37)-H(37)	0.93	C(26)-C(25)-C(30)	119.02(18)
C(38)-C(39)	1.386(3)	C(26)-C(25)-C(18)	122.59(18)
C(38)-H(38)	0.93	C(30)-C(25)-C(18)	118.38(18)
C(39)-H(39)	0.93	C(27)-C(26)-C(25)	120.2(2)
C(40)-C(41)	1.391(3)	C(27)-C(26)-H(26)	119.9
C(40)-C(45)	1.395(2)	C(25)-C(26)-H(26)	119.9
C(41)-C(42)	1.386(3)	C(28)-C(27)-C(26)	120.3(2)
C(41)-H(41)	0.93	C(28)-C(27)-H(27)	119.8
C(42)-C(43)	1.388(3)	C(26)-C(27)-H(27)	119.8
C(42)-H(42)	0.93	C(27)-C(28)-C(29)	120.19(19)
C(43)-C(44)	1.387(3)	C(27)-C(28)-H(28)	119.9
C(43)-H(43)	0.93	C(29)-C(28)-H(28)	119.9
C(44)-C(45)	1.380(3)	C(28)-C(29)-C(30)	120.1(2)
C(44)-H(44)	0.93	C(28)-C(29)-H(29)	120
C(45)-H(45)	0.93	C(30)-C(29)-H(29)	120
O(1)-Mn(1)	1.9146(12)	C(29)-C(30)-C(25)	120.1(2)
O(2)-Mn(1)	2.1217(13)	C(29)-C(30)-H(30)	119.9
O(3)-Mn(1)	1.9244(12)	C(25)-C(30)-H(30)	119.9
O(4)-Mn(1)	1.9037(12)	O(5)-C(31)-C(32)	124.31(17)
O(5)-Mn(1)	2.1603(13)	O(5)-C(31)-C(34)	116.13(16)
O(6)-Mn(1)	1.9199(12)	C(32)-C(31)-C(34)	119.56(15)
		C(33)-C(32)-C(31)	124.53(16)
		C(33)-C(32)-H(32)	117.7
		C(31)-C(32)-H(32)	117.7
		O(6)-C(33)-C(32)	125.73(16)
		O(6)-C(33)-C(40)	113.24(16)
		C(32)-C(33)-C(40)	121.03(15)
		C(35)-C(34)-C(39)	118.45(18)
		C(35)-C(34)-C(31)	119.05(16)
		C(39)-C(34)-C(31)	122.47(17)

# Appendix

C(36)-C(35)-C(34)	121.33(18)
C(36)-C(35)-H(35)	119.3
C(34)-C(35)-H(35)	119.3
C(37)-C(36)-C(35)	119.60(19)
C(37)-C(36)-H(36)	120.2
C(35)-C(36)-H(36)	120.2
C(38)-C(37)-C(36)	119.93(19)
C(38)-C(37)-H(37)	120
C(36)-C(37)-H(37)	120
C(37)-C(38)-C(39)	120.30(19)
C(37)-C(38)-H(38)	119.8
C(39)-C(38)-H(38)	119.8
C(38)-C(39)-C(34)	120.38(19)
C(38)-C(39)-H(39)	119.8
C(34)-C(39)-H(39)	119.8
C(41)-C(40)-C(45)	118.88(17)
C(41)-C(40)-C(33)	118.93(16)
C(45)-C(40)-C(33)	122.13(17)
C(42)-C(41)-C(40)	120.51(18)
C(42)-C(41)-H(41)	119.7
C(40)-C(41)-H(41)	119.7
C(41)-C(42)-C(43)	120.11(19)
C(41)-C(42)-H(42)	119.9
C(43)-C(42)-H(42)	119.9
C(44)-C(43)-C(42)	119.60(18)
C(44)-C(43)-H(43)	120.2
C(42)-C(43)-H(43)	120.2
C(45)-C(44)-C(43)	120.34(18)
C(45)-C(44)-H(44)	119.8
C(43)-C(44)-H(44)	119.8
C(44)-C(45)-C(40)	120.51(19)
C(44)-C(45)-H(45)	119.7
C(40)-C(45)-H(45)	119.7
C(1)-O(1)-Mn(1)	129.47(12)
C(3)-O(2)-Mn(1)	125.48(12)
C(16)-O(3)-Mn(1)	127.77(11)
C(18)-O(4)-Mn(1)	126.97(12)
C(31)-O(5)-Mn(1)	122.89(12)
C(33)-O(6)-Mn(1)	128.42(12)
O(4)-Mn(1)-O(1)	178.17(6)
O(4)-Mn(1)-O(6)	87.50(5)
O(1)-Mn(1)-O(6)	92.40(5)
O(4)-Mn(1)-O(3)	90.91(5)
O(1)-Mn(1)-O(3)	89.20(5)
O(6)-Mn(1)-O(3)	178.38(6)

# Appendix

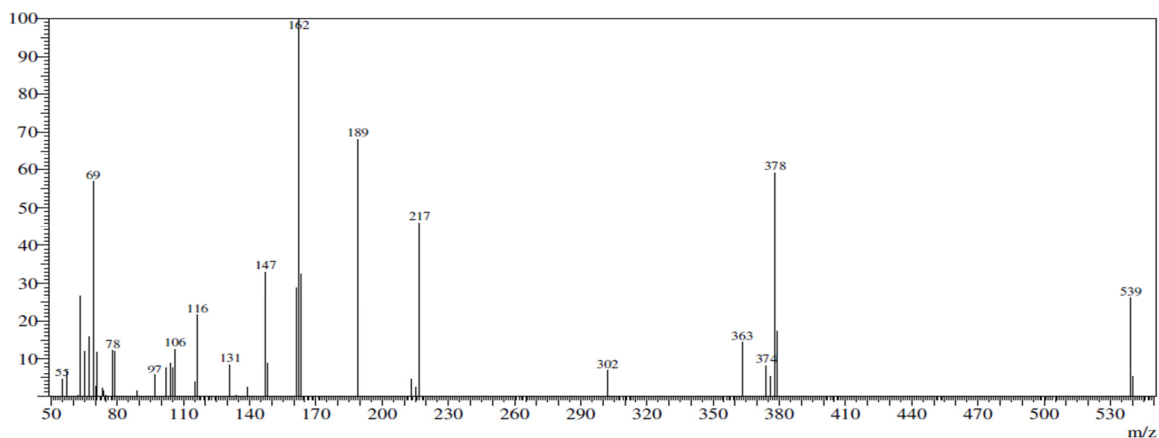
	O(4)-Mn(1)-O(2)	93.29(5)
	O(1)-Mn(1)-O(2)	88.54(5)
	O(6)-Mn(1)-O(2)	89.41(5)
	O(3)-Mn(1)-O(2)	90.40(5)
	O(4)-Mn(1)-O(5)	88.34(5)
	O(1)-Mn(1)-O(5)	89.82(5)
	O(6)-Mn(1)-O(5)	86.52(5)
	O(3)-Mn(1)-O(5)	93.72(5)
	O(2)-Mn(1)-O(5)	175.54(5)

**Table A.3:** Anisotropic displacement parameters ( $\text{\AA}^2 \times 10^3$ ) for  $\text{Mn}(\text{dbm})_3$ . The anisotropic displacement factor exponent takes the form:  $-2p^2 [h^2 a^{*2} U^{11} + \dots + 2h k a^* b^* U^{12}]$ .

	$U^{11}$	$U^{22}$	$U^{33}$	$U^{23}$	$U^{13}$	$U^{12}$
C(1)	13(1)	21(1)	14(1)	2(1)	3(1)	-3(1)
C(2)	24(1)	20(1)	14(1)	0(1)	-1(1)	0(1)
C(3)	15(1)	21(1)	15(1)	0(1)	4(1)	-4(1)
C(4)	15(1)	18(1)	19(1)	3(1)	2(1)	-4(1)
C(5)	30(1)	20(1)	23(1)	-1(1)	-5(1)	1(1)
C(6)	32(1)	27(1)	24(1)	2(1)	-9(1)	-1(1)
C(7)	16(1)	28(1)	30(1)	12(1)	0(1)	0(1)
C(8)	26(1)	26(1)	28(1)	3(1)	6(1)	6(1)
C(9)	26(1)	25(1)	18(1)	2(1)	3(1)	2(1)
C(10)	14(1)	21(1)	19(1)	1(1)	3(1)	-1(1)
C(11)	35(1)	27(1)	26(1)	-4(1)	-9(1)	13(1)
C(12)	40(1)	35(1)	30(1)	-14(1)	-15(1)	11(1)
C(13)	24(1)	21(1)	37(1)	-7(1)	0(1)	0(1)
C(14)	53(2)	20(1)	28(1)	4(1)	-3(1)	1(1)
C(15)	47(1)	23(1)	18(1)	-1(1)	-3(1)	-2(1)
C(16)	17(1)	15(1)	24(1)	-2(1)	4(1)	-1(1)
C(17)	16(1)	29(1)	25(1)	2(1)	-1(1)	-5(1)
C(18)	18(1)	17(1)	22(1)	-2(1)	-2(1)	0(1)
C(19)	19(1)	14(1)	25(1)	-1(1)	4(1)	-2(1)
C(20)	25(1)	24(1)	29(1)	4(1)	5(1)	4(1)
C(21)	40(1)	26(1)	31(1)	9(1)	9(1)	5(1)
C(22)	36(1)	21(1)	40(1)	5(1)	21(1)	-2(1)
C(23)	23(1)	26(1)	44(1)	-2(1)	14(1)	-4(1)
C(24)	20(1)	25(1)	32(1)	-2(1)	4(1)	-2(1)
C(25)	23(1)	20(1)	23(1)	2(1)	-6(1)	-4(1)
C(26)	24(1)	41(1)	33(1)	9(1)	-6(1)	-4(1)

# Appendix

C(27)	29(1)	43(2)	42(1)	11(1)	-18(1)	-7(1)
C(28)	45(1)	23(1)	30(1)	4(1)	-17(1)	-2(1)
C(29)	43(1)	23(1)	23(1)	1(1)	-5(1)	1(1)
C(30)	30(1)	21(1)	24(1)	1(1)	-4(1)	0(1)
C(31)	15(1)	20(1)	17(1)	0(1)	-1(1)	1(1)
C(32)	20(1)	23(1)	13(1)	1(1)	2(1)	0(1)
C(33)	12(1)	21(1)	16(1)	1(1)	-1(1)	1(1)
C(34)	14(1)	21(1)	20(1)	-1(1)	2(1)	-1(1)
C(35)	22(1)	25(1)	23(1)	1(1)	1(1)	-2(1)
C(36)	26(1)	20(1)	38(1)	2(1)	3(1)	-2(1)
C(37)	21(1)	24(1)	40(1)	-12(1)	1(1)	-3(1)
C(38)	34(1)	36(1)	24(1)	-8(1)	2(1)	-7(1)
C(39)	34(1)	27(1)	20(1)	-1(1)	2(1)	-10(1)
C(40)	17(1)	19(1)	14(1)	2(1)	-1(1)	-2(1)
C(41)	21(1)	23(1)	16(1)	-1(1)	-1(1)	1(1)
C(42)	33(1)	19(1)	20(1)	2(1)	-4(1)	-3(1)
C(43)	31(1)	26(1)	21(1)	4(1)	2(1)	-9(1)
C(44)	29(1)	31(1)	21(1)	2(1)	9(1)	-1(1)
C(45)	24(1)	21(1)	22(1)	0(1)	5(1)	-2(1)
O(1)	17(1)	22(1)	16(1)	-3(1)	-1(1)	2(1)
O(2)	18(1)	23(1)	15(1)	-1(1)	-1(1)	1(1)
O(3)	16(1)	26(1)	18(1)	1(1)	1(1)	-1(1)
O(4)	16(1)	25(1)	18(1)	1(1)	-2(1)	-3(1)
O(5)	22(1)	23(1)	14(1)	0(1)	3(1)	-3(1)
O(6)	16(1)	23(1)	16(1)	-3(1)	2(1)	-3(1)
Mn(1)	14(1)	21(1)	13(1)	-1(1)	1(1)	-1(1)

**B. Mass spectrometry (MS).**

**Figure B.1:** Gas chromatography-mass spectrometry (GC-MS) spectrum of  $\text{Mn}(\text{ba})_3$  [2], MS Calculated:  $M_r = 538.48$  g/mol, Found: 540.3 g/mol.

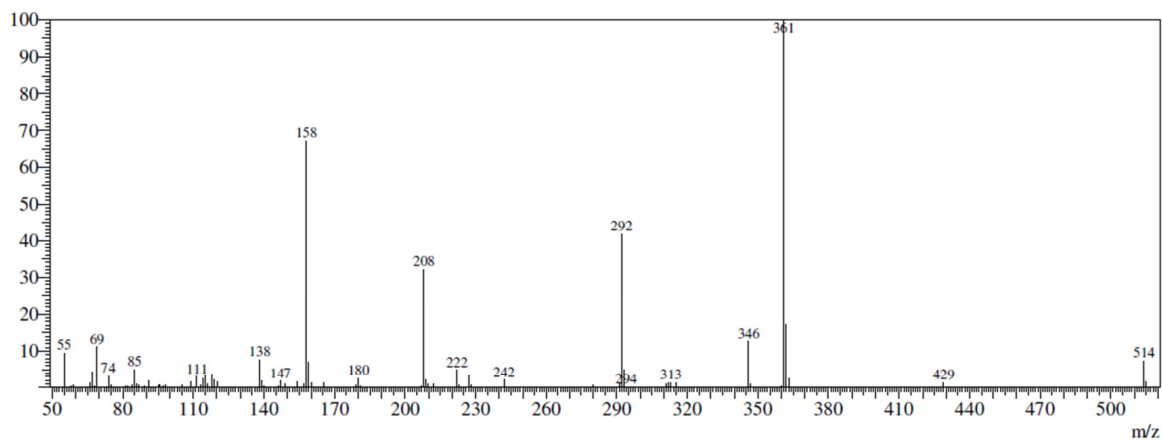


**Figure B.2:** Gas chromatography-mass spectrometry (GC-MS) spectrum of  $\text{Mn}(\text{tfaa})_3$  [4], MS Calculated:  $M_r = 514.18$  g/mol, Found: 515.1 g/mol.



## Appendix

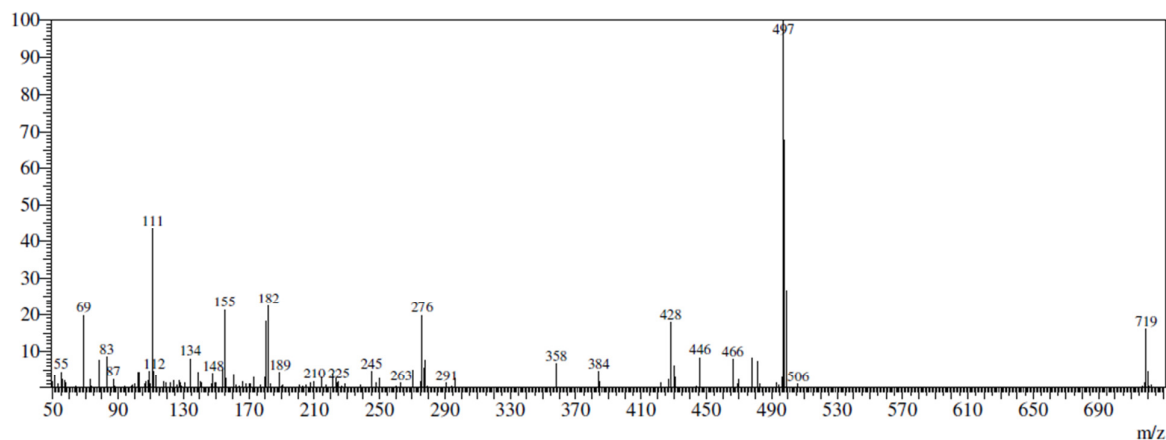


**Figure B.3:** Gas chromatography-mass spectrometry (GC-MS) spectrum of Mn(tfth)<sub>3</sub> [5], MS Calculated: Mr = 718.45 g/mol, Found: 722.10 g/mol.

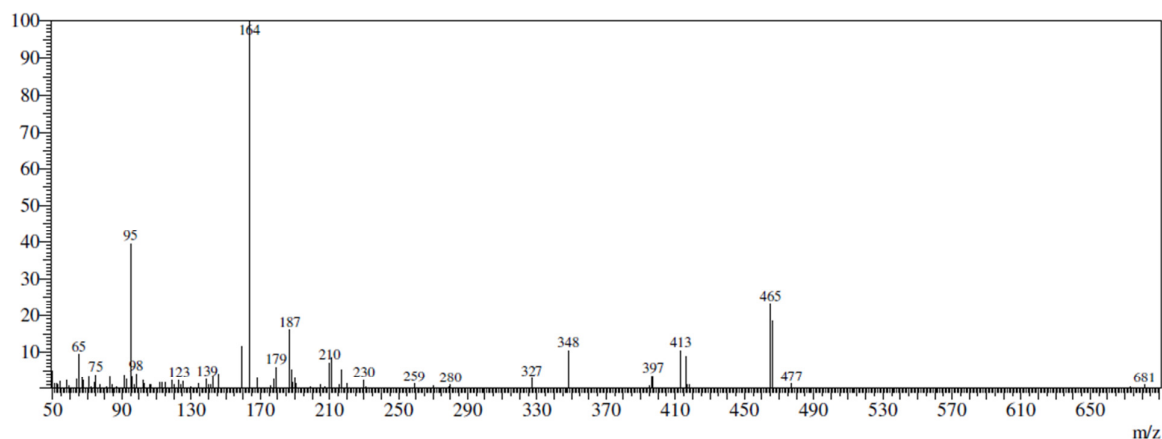


**Figure B.4:** Gas chromatography-mass spectrometry (GC-MS) spectrum of Mn(tffu)<sub>3</sub> [6], MS Calculated: Mr = 670.27 g/mol, Found: 681.20 g/mol.

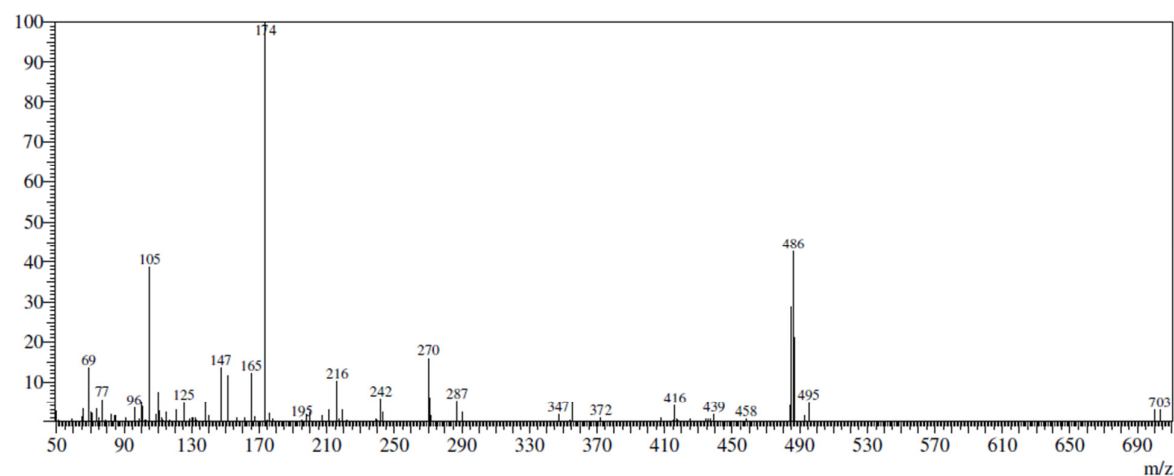


**Figure B.5:** Gas chromatography-mass spectrometry (GC-MS) spectrum of Mn(tfba)<sub>3</sub> [7], MS Calculated: Mr = 700.39 g/mol, Found: 703.25 g/mol.

## C. Cyclic Voltammetry data.

**Table C.1:** Electrochemical data of  $\text{Mn}(\text{ba})_3$  [2]. Solvent acetonitrile, supporting electrolyte tetrabutylammonium hexafluorophosphate, working electrode glassy carbon, concentration of 0.5 mM  $\text{Mn}(\text{ba})_3$  with potential vs  $\text{FcH}/\text{FcH}^+$ .

Scan Rate ( $\text{mV.s}^{-1}$ )	$\text{Mn}^{\text{III}} / \text{Mn}^{\text{II}}$							$\text{Mn}^{\text{III}} / \text{Mn}^{\text{IV}}$						
	$E_{\text{pa}}$ (mV)	$E_{\text{pc}}$ (mV)	$\Delta E_{\text{p}}$ (mV)	$\frac{E_{\text{pc}} - E_{\text{pa}}}{2}$ (mV)	$i_{\text{pa}}$ ( $\mu\text{A}$ )	$i_{\text{pc}}$ ( $\mu\text{A}$ )	$i_{\text{pa}}/i_{\text{pc}}$	$E_{\text{pa}}$ (mV)	$E_{\text{pc}}$ (mV)	$\Delta E_{\text{p}}$ (mV)	$\frac{E_{\text{pc}} - E_{\text{pa}}}{2}$ (mV)	$i_{\text{pa}}$ ( $\mu\text{A}$ )	$i_{\text{pc}}$ ( $\mu\text{A}$ )	$i_{\text{pc}}/i_{\text{pa}}$
50	-227	-609	382	-418	1.12	2.08	0.54	633	557	76	595	3.08	2.94	0.95
100	-226	-635	409	-431	1.38	2.38	0.58	633	553	80	593	4.15	4.10	0.99
150	-225	-642	417	-433	1.69	3.19	0.53	640	550	89	595	5.32	5.28	0.99
200	-223	-653	430	-438	1.93	3.42	0.56	640	550	90	595	6.19	6.08	0.98
250	-222	-654	432	-438	2.62	3.72	0.70	640	550	90	595	6.81	6.61	0.97
300	-218	-660	442	-439	2.76	4.25	0.65	645	549	95	597	7.16	6.63	0.93
500	-218	-678	460	-448	3.17	4.95	0.64	646	547	99	596	9.47	8.84	0.93

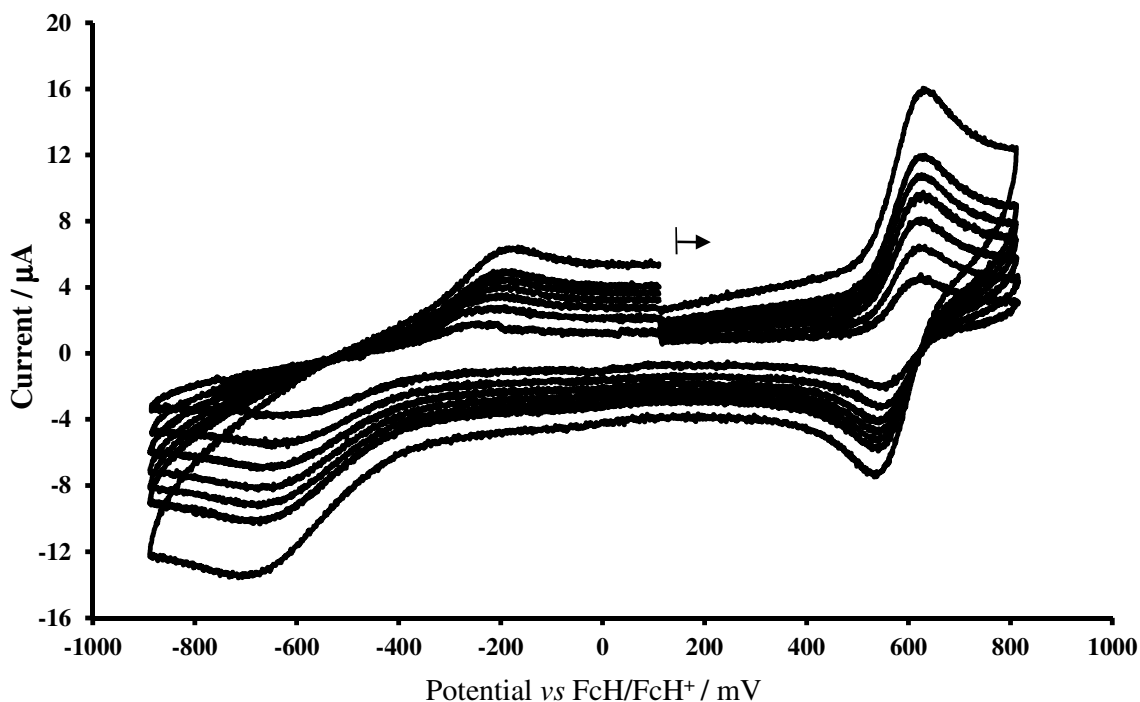


**Figure C.1:** Cyclic Voltammograms of  $\text{Mn}(\text{ba})_3$  [2] at scan rates 50, 100, 150, 200, 250, 300 and 500  $\text{mV.s}^{-1}$ . Scans initiated in the direction of the arrow. Solvent acetonitrile, supporting electrolyte tetrabutylammonium hexafluorophosphate, working electrode glassy carbon, concentration of 0.5 mM  $\text{Mn}(\text{ba})_3$  with potential vs  $\text{FcH}/\text{FcH}^+$ .

## Appendix

**Table C.2:** Electrochemical data of Mn(dbm)<sub>3</sub> [3]. Solvent acetonitrile, supporting electrolyte tetrabutylammonium hexafluorophosphate, working electrode glassy carbon, concentration of 0.5 mM Mn(dbm)<sub>3</sub> with potential vs FcH/FcH<sup>+</sup>.

Scan Rate (mV.s <sup>-1</sup> )	Mn <sup>III</sup> / Mn <sup>II</sup>							Mn <sup>III</sup> / Mn <sup>IV</sup>						
	E <sub>pa</sub> (mV)	E <sub>pc</sub> (mV)	ΔE <sub>p</sub> (mV)	$\frac{E_{pc} - E_{pa}}{2}$ (mV)	i <sub>pa</sub> (μA)	i <sub>pc</sub> (μA)	i <sub>pa</sub> /i <sub>pc</sub>	E <sub>pa</sub> (mV)	E <sub>pc</sub> (mV)	ΔE <sub>p</sub> (mV)	$\frac{E_{pc} - E_{pa}}{2}$ (mV)	i <sub>pa</sub> (μA)	i <sub>pc</sub> (μA)	i <sub>pc</sub> /i <sub>pa</sub>
50	-304	-397	-350	93	4.26	4.39	0.97	646	580	613	65	2.44	2.32	0.95
100	-302	-400	-351	99	5.94	6.18	0.96	647	580	613	67	4.13	4.00	0.97
150	-302	-400	-351	99	5.98	6.29	0.95	648	580	614	68	8.39	7.86	0.94
200	-297	-402	-350	105	7.68	8.57	0.90	652	579	615	73	11.63	9.82	0.84
250	-296	-406	-351	111	8.39	10.00	0.84	652	578	615	75	12.39	10.00	0.81
300	-294	-407	-350	113	9.15	11.27	0.81	652	576	614	76	14.37	12.11	0.84
500	-293	-413	-353	120	11.41	13.94	0.82	654	574	614	80	18.79	14.65	0.78

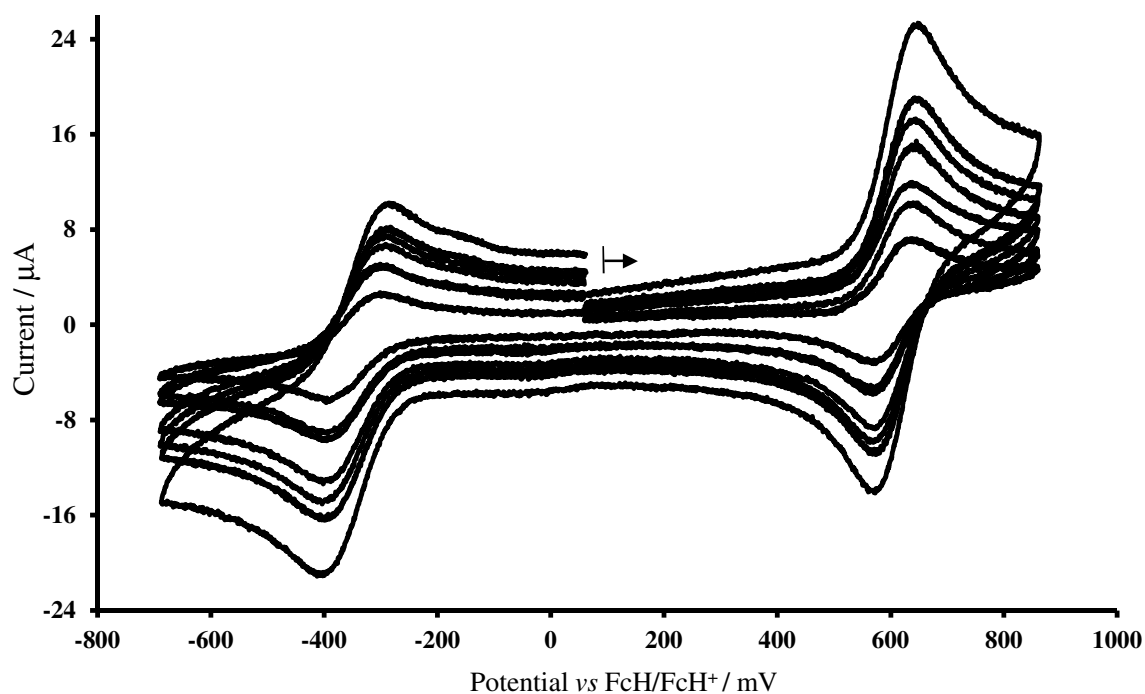


**Figure C.2:** Cyclic Voltammograms of Mn(dbm)<sub>3</sub> [3] at scan rates 50, 100, 150, 200, 250, 300 and 500 mV.s<sup>-1</sup>. Scans initiated in the direction of the arrow. Solvent acetonitrile, supporting electrolyte tetrabutylammonium hexafluorophosphate, working electrode glassy carbon, concentration of 0.5 mM Mn(dbm)<sub>3</sub> with potential vs FcH/FcH<sup>+</sup>.

## Appendix

**Table C.3:** Electrochemical data of  $\text{Mn}(\text{tfaa})_3$  [4]. Solvent acetonitrile, supporting electrolyte tetrabutylammonium hexafluorophosphate, working electrode glassy carbon, concentration of 0.5 mM  $\text{Mn}(\text{tfaa})_3$  with potential vs  $\text{FcH}/\text{FcH}^+$ .

Scan Rate ( $\text{mV.s}^{-1}$ )	$\text{Mn}^{\text{III}} / \text{Mn}^{\text{II}}$						
	$E_{\text{pa}}$ (mV)	$E_{\text{pc}}$ (mV)	$\Delta E_{\text{p}}$ (mV)	$\frac{E_{\text{pc}} - E_{\text{pa}}}{2}$ (mV)	$i_{\text{pa}}$ ( $\mu\text{A}$ )	$i_{\text{pc}}$ ( $\mu\text{A}$ )	$i_{\text{pa}}/i_{\text{pc}}$
50	491	-246	123	737	0.98	3.41	0.29
100	520	-256	132	775	2.35	4.59	0.51
150	543	-269	137	812	3.55	5.52	0.64
200	554	-280	137	834	4.71	6.35	0.74
250	564	-287	139	852	5.06	7.19	0.70
300	573	-292	140	865	5.46	7.22	0.76
500	595	-316	140	911	7.41	8.52	0.87

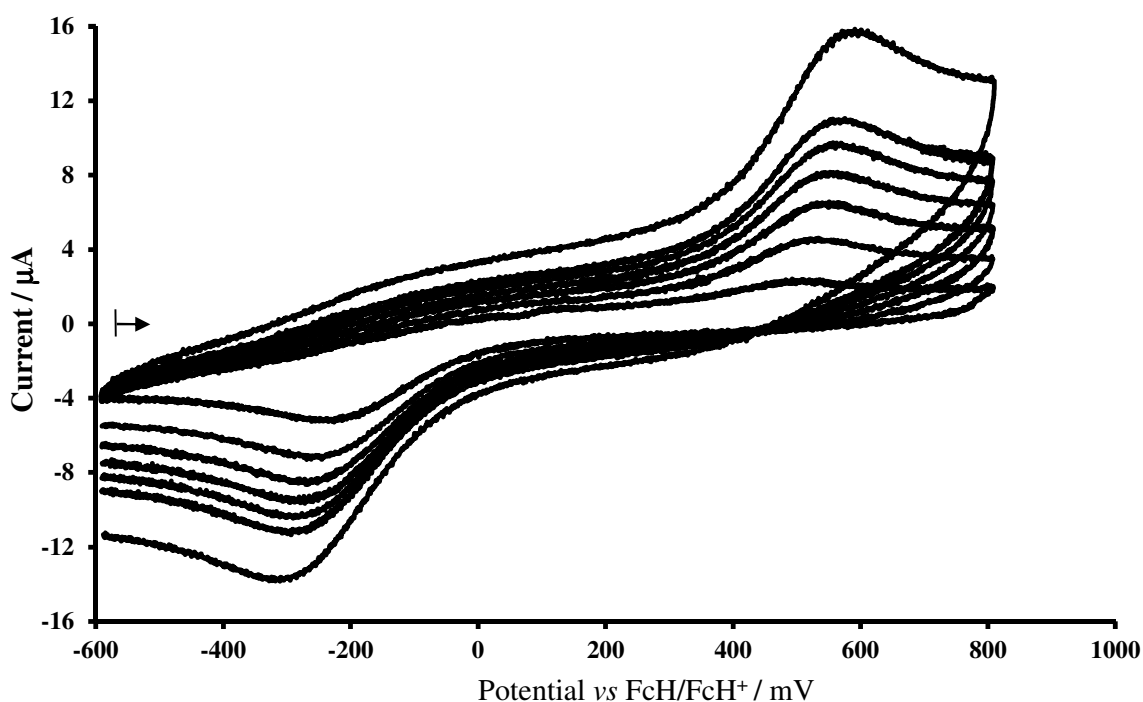


**Figure C.3:** Cyclic Voltammograms of  $\text{Mn}(\text{tfaa})_3$  [4] at scan rates 50, 100, 150, 200, 250, 300 and 500  $\text{mV.s}^{-1}$ . Scans initiated in the direction of the arrow. Solvent acetonitrile, supporting electrolyte tetrabutylammonium hexafluorophosphate, working electrode glassy carbon, concentration of 0.5 mM  $\text{Mn}(\text{tfaa})_3$  with potential vs  $\text{FcH}/\text{FcH}^+$ .

## Appendix

**Table C.4:** Electrochemical data of  $\text{Mn}(\text{tfth})_3$  [5]. Solvent acetonitrile, supporting electrolyte tetrabutylammonium hexafluorophosphate, working electrode glassy carbon, concentration of 0.5 mM  $\text{Mn}(\text{tfth})_3$  with potential vs  $\text{FcH}/\text{FcH}^+$ .

Scan Rate ( $\text{mV}\cdot\text{s}^{-1}$ )	$\text{Mn}^{\text{III}} / \text{Mn}^{\text{II}}$						
	$E_{\text{pa}}$ (mV)	$E_{\text{pc}}$ (mV)	$\Delta E_{\text{p}}$ (mV)	$\frac{E_{\text{pc}} - E_{\text{pa}}}{2}$ (mV)	$i_{\text{pa}}$ ( $\mu\text{A}$ )	$i_{\text{pc}}$ ( $\mu\text{A}$ )	$i_{\text{pa}}/i_{\text{pc}}$
50	287	158	222	129	2.78	2.88	0.96
100	296	149	223	147	3.51	3.62	0.97
150	303	140	222	164	4.64	4.80	0.97
200	308	129	219	179	4.93	5.19	0.95
250	311	115	213	196	5.07	5.23	0.97
300	314	106	210	208	5.12	5.25	0.98
500	329	90	209	239	6.96	7.23	0.96

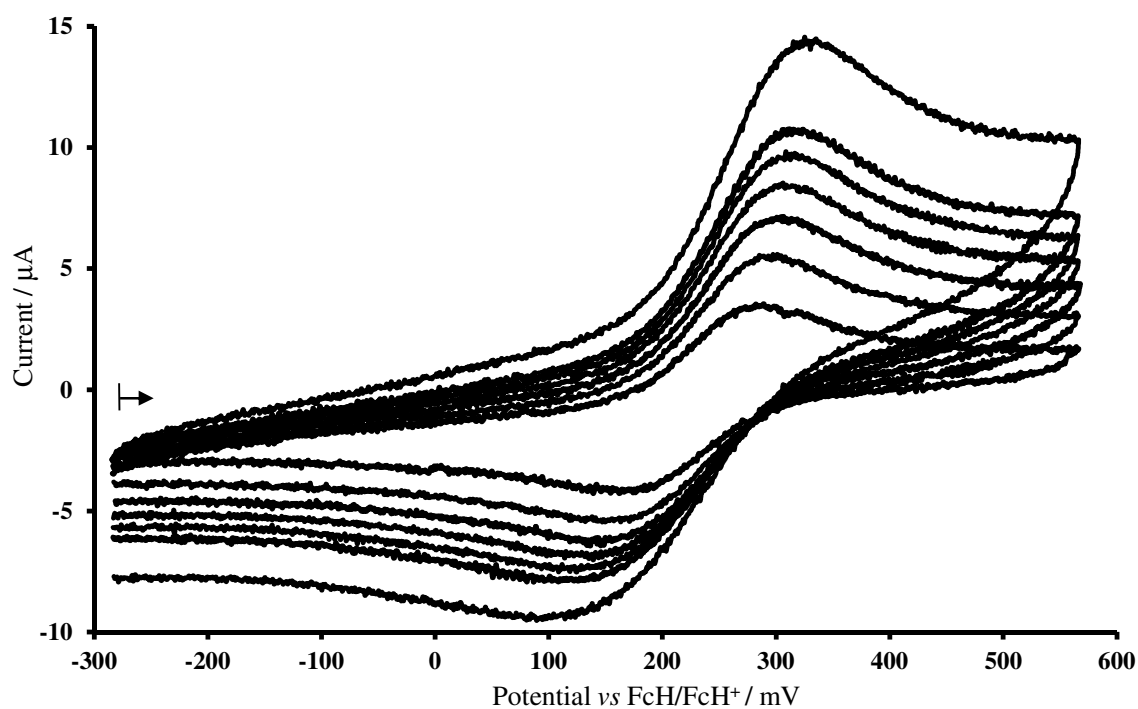


**Figure C.4:** Cyclic Voltammograms of  $\text{Mn}(\text{tfth})_3$  [5] at scan rates 50, 100, 150, 200, 250, 300 and 500  $\text{mV}\cdot\text{s}^{-1}$ . Scans initiated in the direction of the arrow. Solvent acetonitrile, supporting electrolyte tetrabutylammonium hexafluorophosphate, working electrode glassy carbon, concentration of 0.5 mM  $\text{Mn}(\text{tfth})_3$  with potential vs  $\text{FcH}/\text{FcH}^+$ .

## Appendix

**Table C.5:** Electrochemical data of  $\text{Mn}(\text{tffu})_3$  [6]. Solvent acetonitrile, supporting electrolyte tetrabutylammonium hexafluorophosphate, working electrode glassy carbon, concentration of 0.5 mM  $\text{Mn}(\text{tffu})_3$  with potential vs  $\text{FcH}/\text{FcH}^+$ .

Scan Rate ( $\text{mV.s}^{-1}$ )	$\text{Mn}^{\text{III}} / \text{Mn}^{\text{II}}$						
	$E_{\text{pa}}$ (mV)	$E_{\text{pc}}$ (mV)	$\Delta E_{\text{p}}$ (mV)	$\frac{E_{\text{pc}} - E_{\text{pa}}}{2}$ (mV)	$i_{\text{pa}}$ ( $\mu\text{A}$ )	$i_{\text{pc}}$ ( $\mu\text{A}$ )	$i_{\text{pa}}/i_{\text{pc}}$
50	296	179	237	117	3.78	3.95	0.96
100	309	162	236	147	4.73	4.82	0.98
150	316	149	233	167	5.62	5.78	0.97
200	324	139	231	185	6.30	6.43	0.98
250	324	124	224	200	6.31	6.52	0.97
300	331	113	222	217	7.60	7.75	0.98
500	344	88	216	255	8.99	9.05	0.99

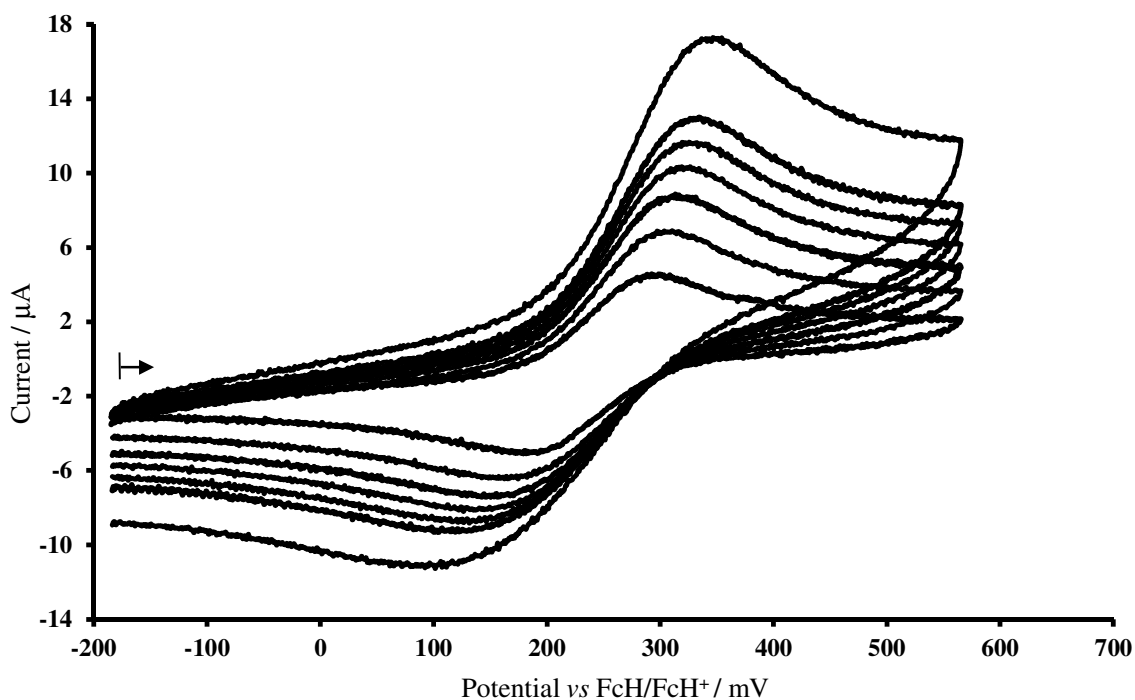


**Figure C.5:** Cyclic Voltammograms of  $\text{Mn}(\text{tffu})_3$  [6] at scan rates 50, 100, 150, 200, 250, 300 and 500  $\text{mV.s}^{-1}$ . Scans initiated in the direction of the arrow. Solvent acetonitrile, supporting electrolyte tetrabutylammonium hexafluorophosphate, working electrode glassy carbon, concentration of 0.5 mM  $\text{Mn}(\text{tffu})_3$  with potential vs  $\text{FcH}/\text{FcH}^+$ .

## Appendix

**Table C.6:** Electrochemical data of  $\text{Mn}(\text{tfba})_3$  [7]. Solvent acetonitrile, supporting electrolyte tetrabutylammonium hexafluorophosphate, working electrode glassy carbon, concentration of 0.5 mM  $\text{Mn}(\text{tfba})_3$  with potential vs  $\text{FcH}/\text{FcH}^+$ .

Scan Rate ( $\text{mV.s}^{-1}$ )	$\text{Mn}^{\text{III}} / \text{Mn}^{\text{II}}$						
	$E_{\text{pa}}$ (mV)	$E_{\text{pc}}$ (mV)	$\Delta E_{\text{p}}$ (mV)	$\frac{E_{\text{pc}} - E_{\text{pa}}}{2}$ (mV)	$i_{\text{pa}}$ ( $\mu\text{A}$ )	$i_{\text{pc}}$ ( $\mu\text{A}$ )	$i_{\text{pa}}/i_{\text{pc}}$
50	275	171	223	104	2.81	2.85	0.99
100	279	171	225	109	4.15	4.33	0.96
150	284	157	221	127	4.75	4.83	0.98
200	288	157	222	131	5.38	5.47	0.98
250	295	151	223	144	5.53	5.76	0.96
300	295	155	225	140	6.36	6.44	0.99
500	305	148	226	157	8.36	8.45	0.99

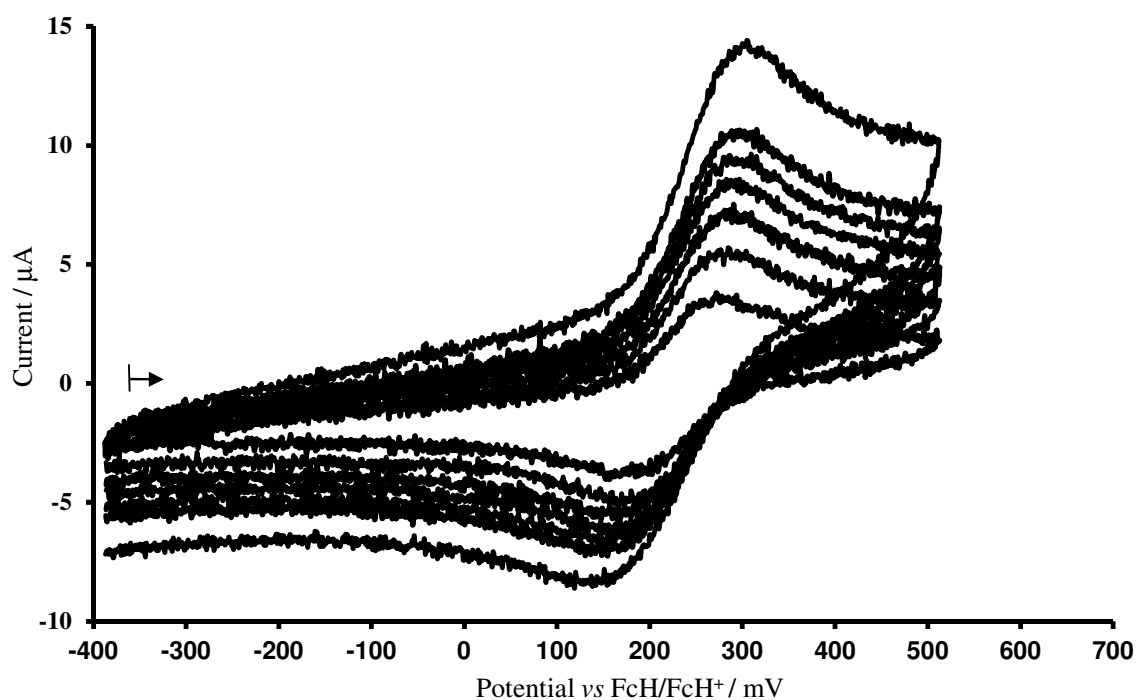


**Figure C.6:** Cyclic Voltammograms of  $\text{Mn}(\text{tfba})_3$  [7] at scan rates 50, 100, 150, 200, 250, 300 and 500  $\text{mV.s}^{-1}$ . Scans initiated in the direction of the arrow. Solvent acetonitrile, supporting electrolyte tetrabutylammonium hexafluorophosphate, working electrode glassy carbon, concentration of 0.5 mM  $\text{Mn}(\text{tfba})_3$  with potential vs  $\text{FcH}/\text{FcH}^+$ .

## Appendix

**Table C.7:** Electrochemical data of  $\text{Mn}(\text{thfac})_3$  [8]. Solvent acetonitrile, supporting electrolyte tetrabutylammonium hexafluorophosphate, working electrode glassy carbon with potential vs  $\text{FcH}/\text{FcH}^+$ .

Scan Rate ( $\text{mV}\cdot\text{s}^{-1}$ )	$\text{Mn}^{\text{III}} / \text{Mn}^{\text{II}}$						
	$E_{\text{pa}}$ (mV)	$E_{\text{pc}}$ (mV)	$\Delta E_{\text{p}}$ (mV)	$\frac{E_{\text{pc}} - E_{\text{pa}}}{2}$ (mV)	$i_{\text{pa}}$ ( $\mu\text{A}$ )	$i_{\text{pc}}$ ( $\mu\text{A}$ )	$i_{\text{pa}}/i_{\text{pc}}$
50	1128	1041	1085	88	4.39	8.77	0.50
100	1149	1041	1095	108	4.42	9.06	0.49
150	1141	1040	1091	101	5.85	9.12	0.64
200	1151	1039	1095	112	5.85	9.15	0.64
250	1162	1038	1100	124	7.02	9.18	0.76
300	1163	1034	1098	130	7.05	9.24	0.76
500	1176	1021	1099	154	8.51	9.65	0.88

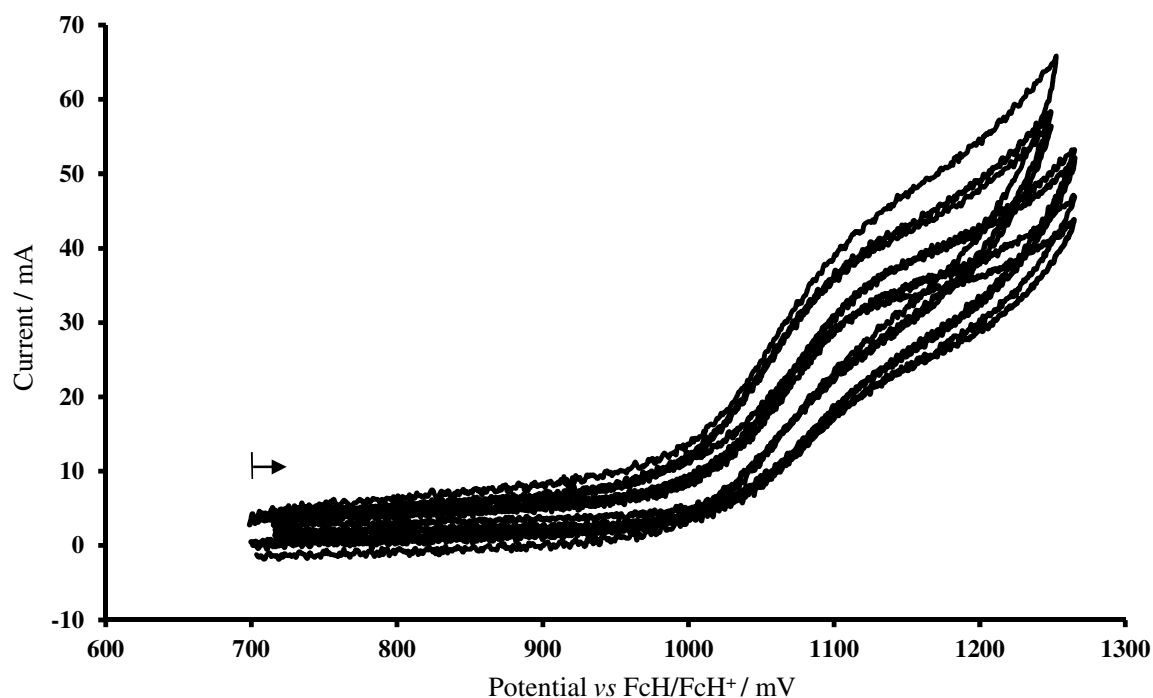


**Figure C.7:** Cyclic Voltammograms of  $\text{Mn}(\text{thfac})_3$  [8] at scan rates 50, 100, 150, 200, 250, 300 and 500  $\text{mV}\cdot\text{s}^{-1}$ . Scans initiated in the direction of the arrow. Solvent acetonitrile, supporting electrolyte tetrabutylammonium hexafluorophosphate, working electrode glassy carbon with potential vs  $\text{FcH}/\text{FcH}^+$ .



## D. Computational data.

Optimized Cartesian coordinates (Å)

All the compounds were optimized with ADF,OLYP/TZP

**Table D.1:** Optimized Cartesian coordinates of Mn(acac)<sub>3</sub> [1] S = 4/2 with C<sub>2</sub> symmetry.

	X	Y	Z
Mn	0.00000	0.00000	-0.05223
O	2.12578	0.71350	0.05556
O	0.52416	-1.32476	1.31352
O	-2.12578	-0.71350	0.05556
O	-0.52416	1.32476	1.31352
O	-0.42253	1.33027	-1.47477
O	0.42253	-1.33027	-1.47477
C	4.37899	0.93717	0.75915
C	3.01451	0.26741	0.83154
C	2.82925	-0.80216	1.75079
C	1.64317	-1.51530	1.92655
C	1.59293	-2.65312	2.92843
C	-4.37899	-0.93717	0.75915
C	-3.01451	-0.26741	0.83154
C	-2.82925	0.80216	1.75079
C	-1.64317	1.51530	1.92655
C	-1.59293	2.65312	2.92843
C	-0.75087	2.40916	-3.54125
C	-0.37058	1.17944	-2.74439
C	0.00000	0.00000	-3.40872
C	0.37058	-1.17944	-2.74439
C	0.75087	-2.40916	-3.54125
H	4.26627	1.99944	1.00170
H	4.75132	0.88020	-0.26918
H	5.11381	0.49194	1.43366
H	3.67726	-1.09793	2.36001
H	0.81918	-2.44557	3.67538
H	2.54946	-2.80411	3.43220
H	1.30561	-3.57633	2.41379
H	-4.75132	-0.88020	-0.26918
H	-5.11381	-0.49194	1.43366
H	-4.26627	-1.99944	1.00170
H	-3.67726	1.09793	2.36001
H	-1.30561	3.57633	2.41379
H	-0.81918	2.44557	3.67538
H	-2.54946	2.80411	3.43220
H	-1.76683	2.71460	-3.26974

## Appendix

H	-0.69879	2.24008	-4.61821
H	-0.08191	3.23285	-3.27037
H	0.00000	0.00000	-4.49303
H	0.08191	-3.23285	-3.27037
H	1.76683	-2.71460	-3.26974
H	0.69879	-2.24008	-4.61821

**Table D.2:** Optimized Cartesian coordinates of Mn(ba)<sub>3</sub> [2] S = 4/2 with no symmetry.

	X	Y	Z
Mn	0.095805	-0.06487	-0.07103
O	2.228567	0.617708	0.05737
O	0.615834	-1.41596	1.264184
O	-2.02422	-0.73843	0.028356
O	-0.40372	1.229412	1.324088
O	-0.30702	1.296038	-1.45695
O	0.52618	-1.35345	-1.52495
C	3.102376	0.214649	0.877683
C	2.890518	-0.8465	1.802608
C	1.712489	-1.5805	1.925972
C	1.642364	-2.72058	2.924052
C	-2.92059	-0.25669	0.776225
C	-2.72647	0.794806	1.710563
C	-1.51897	1.462391	1.934033
C	-0.57389	2.441037	-3.49508
C	-0.22975	1.179734	-2.73176
C	0.139102	0.021398	-3.42596
C	0.494442	-1.18636	-2.79595
H	3.716733	-1.15486	2.429596
H	0.861662	-2.5064	3.662054
H	2.590809	-2.8786	3.440888
H	1.353544	-3.64148	2.406565
H	-3.5944	1.132346	2.2616
H	-1.59276	2.750356	-3.23922
H	-0.49635	2.30864	-4.57568
H	0.096493	3.247485	-3.17953
H	0.192438	0.080472	-4.50432
H	5.039511	0.484738	2.869765
C	6.553613	1.586396	1.827688
C	4.447928	0.887575	0.825895
C	5.324457	0.933662	1.922807
C	4.836401	1.519883	-0.3665
H	4.155024	1.498063	-1.21149
C	6.070771	2.157991	-0.46753
H	7.212666	1.624062	2.692782
H	6.360041	2.630472	-1.40446
C	6.934991	2.194858	0.63004

## Appendix

H	7.896916	2.69851	0.554281
C	0.898404	-2.37479	-3.60917
C	1.729084	-3.34914	-3.02985
C	0.465775	-2.5609	-4.93365
H	2.058979	-3.21669	-2.00451
H	-0.20717	-1.84507	-5.3959
C	2.133992	-4.46297	-3.76175
C	0.860822	-3.68321	-5.65947
H	2.788455	-5.20061	-3.30193
H	0.505788	-3.81745	-6.67906
C	1.701966	-4.63513	-5.07896
H	2.014175	-5.5083	-5.64852
C	-4.30931	-0.86377	0.64349
H	-4.24975	-1.93718	0.852854
H	-4.64815	-0.75794	-0.39265
H	-5.04498	-0.40771	1.309855
C	-1.44501	2.574227	2.938391
C	-2.31386	2.653408	4.040199
C	-0.45962	3.565118	2.791457
H	-3.05937	1.881049	4.203923
H	0.227792	3.501943	1.953807
C	-2.21001	3.69868	4.956727
C	-0.36421	4.615745	3.701944
H	-2.88476	3.735324	5.809663
H	0.399433	5.378806	3.564587
C	-1.23889	4.688314	4.788418
H	-1.16019	5.505182	5.50334

**Table D.3:** Optimized Cartesian coordinates of  $\text{Mn}(\text{dbm})_3$  [3]  $S = 4/2$  with  $C_2$  symmetry.

	X	Y	Z
Mn	-2.64911	-0.28321	-0.71756
O	-0.46771	-0.73532	-0.56527
O	-2.87608	-1.87438	0.419705
O	-4.83115	0.090384	-0.59253
O	-2.50815	0.920885	0.827156
O	-2.31221	1.26279	-1.9065
O	-2.86127	-1.4051	-2.32895
C	0.072087	-1.72307	0.013624
C	-0.6537	-2.72323	0.716965
C	-2.04073	-2.74594	0.882013
C	-5.44128	0.688395	0.342332
C	-4.79103	1.382752	1.397425
C	-3.4095	1.492843	1.559286
C	-2.20758	1.302523	-3.18621
C	-2.38349	0.192151	-4.0287
C	-2.71127	-1.09251	-3.56778

## Appendix

H	-0.10482	-3.57012	1.099148
H	-5.40708	1.890068	2.123252
H	-2.19544	0.318197	-5.08302
H	1.882554	-3.09499	1.647978
C	3.739244	-2.6163	0.696426
C	1.570526	-1.82987	-0.08388
C	2.350916	-2.56974	0.820801
C	2.225505	-1.1329	-1.11285
H	1.628341	-0.54859	-1.80581
C	3.610957	-1.18921	-1.24593
H	4.326551	-3.18502	1.414631
H	4.097728	-0.65061	-2.05677
C	4.374708	-1.93095	-0.34107
H	5.45786	-1.97081	-0.44045
C	-2.89132	-2.22115	-4.53164
C	-2.72178	-3.54106	-4.0794
C	-3.24484	-2.01202	-5.87637
H	-2.45804	-3.71264	-3.04109
H	-3.4212	-1.00667	-6.24703
C	-2.8793	-4.61617	-4.95091
C	-3.41263	-3.08948	-6.7439
H	-2.7327	-5.63037	-4.58548
H	-3.69814	-2.90899	-7.7781
C	-3.22508	-4.39567	-6.28609
H	-3.3534	-5.23628	-6.96523
C	-2.85203	2.326832	2.673958
C	-3.54386	3.430623	3.202045
C	-1.58591	2.017288	3.198669
H	-4.50422	3.721945	2.786881
H	-1.03598	1.177741	2.785988
C	-2.99382	4.189541	4.234014
C	-1.04198	2.770542	4.237344
H	-3.54011	5.047563	4.620609
H	-0.06479	2.507759	4.637704
C	-1.74319	3.859125	4.760889
H	-1.31554	4.450913	5.568031
C	-1.15806	5.186046	-4.73014
C	-1.76791	4.25258	-5.5714
C	-0.90335	4.852035	-3.39797
H	-1.98508	4.509854	-6.60591
H	-0.43226	5.574386	-2.73473
C	-2.11011	2.991426	-5.08766
C	-1.25367	3.595476	-2.90981
H	-2.60578	2.291922	-5.75395
H	-1.06306	3.336814	-1.87316
C	-1.85301	2.641158	-3.75035
H	-0.8891	6.169769	-5.10999
C	-8.95916	0.441139	-1.05628

## Appendix

C	-9.75331	0.628543	0.078089
C	-7.57024	0.457077	-0.95009
H	-10.8386	0.61117	-0.00271
H	-6.94757	0.299771	-1.82555
C	-9.14504	0.831125	1.318603
C	-6.94487	0.679962	0.287757
H	-9.75462	0.960382	2.210713
C	-7.75448	0.861907	1.421765
H	-7.30452	0.998827	2.400684
H	-9.42487	0.279508	-2.02665
C	-4.02568	-4.20008	1.356051
C	-4.65973	-5.23893	2.034806
C	-2.68863	-3.86993	1.6353
H	-5.69294	-5.48438	1.797492
C	-3.97757	-5.9576	3.019127
C	-2.01567	-4.59496	2.633709
H	-4.47533	-6.76356	3.555017
H	-0.99606	-4.33577	2.903137
C	-2.6542	-5.627	3.319423
H	-2.11973	-6.16758	4.097995
H	-4.56033	-3.63328	0.600324

**Table D.4:** Optimized Cartesian coordinates of Mn(tfaa)<sub>3</sub> [4] S = 4/2 with no symmetry.

	X	Y	Z
Mn	0.181346	-0.08451	0.120863
O	2.076141	0.526246	0.14577
O	0.646779	-1.42836	1.519257
O	-1.69567	-0.69902	0.188035
O	-0.42289	1.419617	1.648191
O	-0.2045	1.242278	-1.28563
O	0.592152	-1.49881	-1.54559
C	3.017225	0.068635	0.870533
C	2.960783	-0.94459	1.817435
C	1.76553	-1.64189	2.095355
C	-2.71994	-0.26014	0.828626
C	-2.74168	0.83047	1.709858
C	-1.60141	1.579217	2.047614
C	-0.12083	1.186036	-2.56751
C	0.221706	0.057754	-3.32567
C	0.544324	-1.18727	-2.76066
H	3.859945	-1.21052	2.356449
H	-3.68752	1.094761	2.164078
H	0.239959	0.158557	-4.4028
C	-1.76324	2.763908	3.044139
F	-1.39617	3.927556	2.45572
F	-3.03555	2.928362	3.499451

## Appendix

F	-0.97161	2.58258	4.129041
C	0.892602	-2.36452	-3.71715
F	0.849638	-2.03119	-5.03581
F	2.138916	-2.82969	-3.46266
F	0.024924	-3.39034	-3.53642
C	4.367665	0.777214	0.593588
F	4.251891	2.110535	0.776552
F	5.367054	0.339836	1.402007
F	4.756254	0.561881	-0.68408
C	1.75486	-2.72412	3.147774
H	1.102065	-2.4113	3.970407
H	1.329213	-3.6385	2.723444
H	2.752334	-2.92861	3.539252
C	-3.98932	-1.04136	0.57087
H	-4.20265	-1.0445	-0.50299
H	-3.83593	-2.08314	0.872456
H	-4.84303	-0.63054	1.111896
C	-0.43022	2.49296	-3.26293
H	0.302637	3.245217	-2.95129
H	-0.40767	2.396072	-4.34942
H	-1.41515	2.85059	-2.94617

**Table D.5:** Optimized Cartesian coordinates of Mn(tfth)<sub>3</sub> [5] S = 4/2 with no symmetry.

	X	Y	Z
Mn	-0.7442	4.45694	-7.65192
O	0.25285	3.077054	-6.16639
O	0.935316	5.465281	-7.58091
O	-1.47031	5.892192	-9.17015
O	-0.13308	3.349719	-9.17592
O	-2.41771	3.423927	-7.63781
O	-1.51057	5.627475	-6.21902
C	1.426133	3.166617	-5.70795
C	2.343069	4.204267	-6.0781
C	2.026771	5.224612	-6.9449
C	-1.29126	5.755609	-10.4081
C	-0.70557	4.683218	-11.0874
C	-0.19304	3.536871	-10.4531
C	-3.50718	3.745835	-7.04708
C	-3.74538	4.801	-6.19137
C	-2.71916	5.700243	-5.79956
H	3.336109	4.206624	-5.65123
H	-0.66404	4.733013	-12.1663
H	-4.74352	4.927211	-5.79768
C	1.242672	0.350375	-11.8166
C	1.015237	0.868388	-13.0721
S	0.321766	2.431578	-13.0054

## Appendix

C	0.323697	2.424916	-11.2626
C	0.849705	1.234416	-10.7896
H	1.675202	-0.63034	-11.6461
H	1.2183	0.412407	-14.0335
H	0.93702	1.02573	-9.72967
C	1.09003	1.102925	-4.25301
C	1.860779	2.147232	-4.73483
S	3.446891	2.104098	-4.01376
C	3.060103	0.712933	-3.09596
C	1.768948	0.288531	-3.32281
H	0.066286	0.953583	-4.57631
H	3.802343	0.279308	-2.4367
H	1.332044	-0.57654	-2.83398
C	-2.71004	8.689587	-3.55079
C	-4.02297	8.384911	-3.26045
S	-4.55989	6.989544	-4.0889
C	-3.00918	6.77957	-4.85702
C	-2.13377	7.777335	-4.45618
H	-2.18895	9.54196	-3.12718
H	-4.70258	8.911726	-2.60149
H	-1.11632	7.832018	-4.82581
C	-4.65759	2.767263	-7.37814
F	-4.8877	2.730951	-8.70816
F	-4.34162	1.51315	-6.97492
F	-5.82581	3.104115	-6.7716
C	3.092435	6.304991	-7.24561
F	2.650438	7.528764	-6.86113
F	4.271296	6.087149	-6.60429
F	3.360851	6.361773	-8.56955
C	-1.81671	6.953495	-11.2482
F	-1.19903	8.100071	-10.8764
F	-1.62173	6.809762	-12.5885
F	-3.14786	7.121984	-11.0556

**Table D.6:** Optimized Cartesian coordinates of Mn(tfu)<sub>3</sub> [6] S = 4/2 with no symmetry.

	X	Y	Z
Mn	-0.88997	4.621025	-7.68543
O	-0.07869	3.172573	-6.19365
O	0.857507	5.532822	-7.53713
O	-1.62067	5.83338	-9.37829
O	-0.1996	3.40029	-9.04554
O	-2.63265	3.656678	-7.55786
O	-1.55358	5.925755	-6.3803
C	1.143437	3.029693	-5.90768
C	2.166135	3.983033	-6.22314
C	1.931568	5.124588	-6.96071

## Appendix

C	-1.31067	5.62745	-10.5811
C	-0.50817	4.606479	-11.1042
C	0.015255	3.571739	-10.3106
C	-3.59318	3.941678	-6.76712
C	-3.70464	5.003795	-5.88474
C	-2.6746	5.964732	-5.75285
H	3.169276	3.806123	-5.86186
H	-0.2892	4.599337	-12.1622
H	-4.60326	5.112321	-5.29524
C	2.276566	0.868627	-11.3852
C	2.004245	1.589693	-12.5161
O	1.157626	2.615492	-12.2467
C	0.877974	2.554351	-10.8997
C	1.548144	1.489975	-10.3386
H	2.924355	0.004442	-11.3191
H	2.323302	1.505523	-13.5457
H	1.515088	1.207791	-9.29631
C	0.733589	0.708752	-4.85135
C	1.502321	1.792853	-5.20955
O	2.812621	1.567054	-4.84457
C	2.849752	0.342794	-4.2601
C	1.605707	-0.22804	-4.23879
H	-0.32942	0.616426	-5.02394
H	3.821294	0.018853	-3.91328
H	1.356067	-1.19987	-3.83351
C	-2.66053	8.985779	-3.65725
C	-3.86077	8.37369	-3.4096
O	-3.98468	7.232236	-4.13101
C	-2.82637	7.104678	-4.86556
C	-1.98927	8.166592	-4.59826
H	-2.3121	9.909989	-3.2154
H	-4.69915	8.616452	-2.77127
H	-1.01486	8.320661	-5.04022
C	-4.74749	2.915527	-6.86304
F	-5.23131	2.852143	-8.12266
F	-4.30489	1.678994	-6.52563
F	-5.78831	3.207932	-6.04071
C	3.082559	6.137176	-7.16765
F	2.759661	7.334774	-6.61222
F	4.256104	5.742906	-6.60827
F	3.315762	6.348785	-8.48329
C	-1.94795	6.644119	-11.5695
F	-1.71558	7.916532	-11.1737
F	-1.48656	6.528798	-12.8447
F	-3.29322	6.466687	-11.6145



## Appendix

**Table D.7:** Optimized Cartesian coordinates of Mn(tfba)<sub>3</sub> [7] S = 4/2 with no symmetry.

	X	Y	Z
Mn	0.186784	-0.03408	-0.08286
O	2.290614	0.708532	0.079173
O	0.728986	-1.3781	1.243347
O	-1.91066	-0.73993	0.006184
O	-0.33824	1.255437	1.3107
O	-0.22491	1.292538	-1.49164
O	0.592473	-1.35352	-1.51275
C	3.192514	0.319763	0.870352
C	3.026792	-0.81007	1.737924
C	1.861433	-1.53831	1.830541
C	-2.7817	-0.26116	0.776509
C	-2.64039	0.760594	1.723509
C	-1.43997	1.455726	1.950349
C	-0.28017	1.069278	-2.74859
C	0.003287	-0.09606	-3.43713
C	0.443588	-1.27302	-2.78106
H	3.861929	-1.14627	2.331871
H	-3.51665	1.057235	2.278463
H	-0.14205	-0.10451	-4.50556
H	5.219991	0.352143	2.788019
C	6.603619	1.713323	1.890819
C	4.489704	1.06805	0.873849
C	5.420911	0.976763	1.923449
C	4.776101	1.921245	-0.2058
H	4.053994	2.001718	-1.0122
C	5.963212	2.64705	-0.24348
H	7.307191	1.639123	2.717069
H	6.173593	3.295312	-1.09159
C	6.881663	2.546157	0.805243
H	7.807993	3.116574	0.778559
C	0.749257	-2.50497	-3.55592
C	0.755654	-3.74494	-2.89123
C	1.038375	-2.47181	-4.93293
H	0.5353	-3.77689	-1.82914
H	1.073307	-1.52831	-5.46819
C	1.024285	-4.91836	-3.58955
C	1.320124	-3.64693	-5.62451
H	1.011588	-5.87143	-3.06576
H	1.552887	-3.6042	-6.68601
C	1.307906	-4.87389	-4.95699
H	1.520996	-5.79174	-5.50114
C	-1.38391	2.533967	2.98183
C	-2.27876	2.573238	4.066432
C	-0.39886	3.531984	2.883859
H	-3.02528	1.795302	4.191784

## Appendix

H	0.302048	3.503467	2.055802
C	-2.197	3.588023	5.016976
C	-0.32724	4.551648	3.829762
H	-2.89024	3.596237	5.855229
H	0.433677	5.322948	3.73277
C	-1.22523	4.584274	4.899277
H	-1.16555	5.378401	5.640864
C	-4.18556	-0.90865	0.602485
F	-4.67523	-0.64648	-0.63474
F	-4.11216	-2.25308	0.73948
F	-5.10941	-0.46456	1.500034
C	-0.72417	2.323899	-3.53863
F	0.150831	3.338731	-3.33895
F	-0.79175	2.108675	-4.87914
F	-1.94314	2.739364	-3.13347
C	1.82441	-2.77252	2.76316
F	0.838106	-2.65591	3.68141
F	1.587795	-3.90121	2.047074
F	2.985542	-2.96853	3.443111

**Table D.8:** Optimized Cartesian coordinates of  $\text{Mn}(\text{hfac})_3$  [8]  $S = 4/2$  with  $C_2$  symmetry.

	X	Y	Z
Mn	0.103757	-0.02905	-0.02026
O	2.219221	0.665702	0.08951
O	0.63266	-1.36502	1.319963
O	-2.01074	-0.72746	0.078798
O	-0.41705	1.262381	1.365754
O	-0.33565	1.311843	-1.42326
O	0.533634	-1.32387	-1.46918
C	3.089508	0.204918	0.859571
C	2.943255	-0.85888	1.779198
C	1.748171	-1.54588	1.920037
C	-2.87698	-0.2912	0.867481
C	-2.72566	0.742678	1.819788
C	-1.5296	1.42449	1.97666
C	-0.28834	1.16282	-2.68193
C	0.086548	0.023877	-3.39595
C	0.470894	-1.13617	-2.72196
H	3.787519	-1.15634	2.383961
H	-3.56678	1.020802	2.437944
H	0.079924	0.04049	-4.47582
C	-4.26868	-0.97882	0.735392
F	-4.79289	-0.72084	-0.48588
F	-4.14543	-2.31619	0.866268
F	-5.16363	-0.55463	1.662839
C	-0.71421	2.441431	-3.45296

## Appendix

F	0.087856	3.47221	-3.11981
F	-0.64751	2.278289	-4.79537
F	-1.9848	2.768061	-3.13784
C	1.667208	-2.72325	2.926946
F	0.717151	-2.4795	3.856519
F	1.343709	-3.86627	2.283641
F	2.83555	-2.93401	3.578671
C	-1.44278	2.568902	3.020441
F	-1.11777	3.731047	2.413302
F	-2.60872	2.761903	3.681914
F	-0.49091	2.292779	3.939094
C	0.889653	-2.3894	-3.53733
F	0.80092	-2.18676	-4.87307
F	2.166604	-2.71909	-3.25215
F	0.09758	-3.43344	-3.22248
C	4.479725	0.898338	0.743708
F	4.357035	2.228653	0.935196
F	5.384004	0.434281	1.642569
F	4.991851	0.695428	-0.49276

**Table D.9:** Optimized Cartesian coordinates of  $V(\text{acac})_3$   $S = 2/2$  with  $C_2$  symmetry.

	X	Y	Z
V	0.000000	0.000000	0.003233
O	2.030142	0.078548	0.035530
O	0.131708	-1.478958	1.334279
O	-2.030142	-0.078548	0.035530
O	-0.131708	1.478958	1.334279
O	-0.010260	1.387370	-1.500737
O	0.010260	-1.387370	-1.500737
C	4.304407	-0.147401	0.641829
C	2.846102	-0.518453	0.814998
C	2.473678	-1.481643	1.777072
C	1.158180	-1.919574	1.975276
C	0.857575	-3.000990	2.989947
C	-4.304407	0.147401	0.641829
C	-2.846102	0.518453	0.814998
C	-2.473678	1.481643	1.777072
C	-1.158180	1.919574	1.975276
C	-0.857575	3.000990	2.989947
C	-0.031749	2.525369	-3.570447
C	-0.013008	1.238827	-2.770116
C	0.000000	0.000000	-3.434762
C	0.013008	-1.238827	-2.770116
C	0.031749	-2.525369	-3.570447
H	4.424327	0.929895	0.800572
H	4.611135	-0.356174	-0.389001

## Appendix

H	4.960808	-0.686865	1.327876
H	3.258111	-1.941575	2.369347
H	0.129335	-2.625381	3.717219
H	1.751051	-3.340318	3.517985
H	0.393267	-3.853833	2.482352
H	-4.611135	0.356174	-0.389001
H	-4.960808	0.686865	1.327876
H	-4.424327	-0.929895	0.800572
H	-3.258111	1.941575	2.369347
H	-0.393267	3.853833	2.482352
H	-0.129335	2.625381	3.717219
H	-1.751051	3.340318	3.517985
H	-0.908079	3.117290	-3.284500
H	-0.051863	2.349470	-4.647998
H	0.853725	3.119610	-3.319145
H	0.000000	0.000000	-4.519656
H	-0.853725	-3.119610	-3.319145
H	0.908079	-3.117290	-3.284500
H	0.051863	-2.349470	-4.647998

**Table D.10:** Optimized Cartesian coordinates of  $\text{Cr}(\text{acac})_3$   $S = 3/2$  with  $D_3$  symmetry.

	X	Y	Z
Cr	0.000000	0.000000	0.000000
C	0.738577	2.680445	-1.027292
C	1.673335	2.898301	0.000000
C	1.952045	1.979849	1.027292
C	0.738577	-2.680445	1.027292
C	1.673335	-2.898301	0.000000
C	-2.690622	-0.700596	-1.027292
C	-3.346670	0.000000	0.000000
C	-2.690622	0.700596	1.027292
C	1.952045	-1.979849	-1.027292
O	0.014359	1.635349	-1.165199
O	1.409075	0.830110	1.165199
O	0.014359	-1.635349	1.165199
O	-1.423434	-0.805239	-1.165199
O	-1.423434	0.805239	1.165199
O	1.409075	-0.830110	-1.165199
H	-4.431474	0.000000	0.000000
H	2.215737	-3.837769	0.000000
H	2.215737	3.837769	0.000000
C	-3.505020	-1.410375	-2.089886
H	-4.580434	-1.312324	-1.929510
H	-3.248445	-1.000627	-3.072950
H	-3.236295	-2.472083	-2.103400
C	0.531090	-3.740624	2.089886

## Appendix

H	0.757654	-3.313550	3.072950
H	-0.522740	-4.038755	2.103400
H	1.153711	-4.622934	1.929510
C	2.973930	-2.330249	-2.089886
H	2.490791	-2.312923	-3.072950
H	3.759035	-1.566672	-2.103400
H	3.426723	-3.310610	-1.929510
C	-3.505020	1.410375	2.089886
H	-3.236295	2.472083	2.103400
H	-4.580434	1.312324	1.929510
H	-3.248445	1.000627	3.072950
C	2.973930	2.330249	2.089886
H	3.426723	3.310610	1.929510
H	2.490791	2.312923	3.072950
H	3.759035	1.566672	2.103400
C	0.531090	3.740624	-2.089886
H	-0.522740	4.038755	-2.103400
H	1.153711	4.622934	-1.929510
H	0.757654	3.313550	-3.072950

**Table D.11:** Optimized Cartesian coordinates of  $\text{Fe}(\text{acac})_3$   $S = 5/2$  with  $D_3$  symmetry.

	X	Y	Z
O	0.158213	-1.674714	-1.209421
O	1.371239	-0.974374	1.209421
O	0.158213	1.674714	1.209421
O	1.371239	0.974374	-1.209421
O	-1.529452	0.700341	-1.209421
O	-1.529452	-0.700341	1.209421
C	0.719333	-3.750222	-2.190981
C	0.861259	-2.730573	-1.076940
C	1.728341	-2.993575	0.000000
C	1.934116	-2.111159	1.076940
C	2.888121	-2.498072	2.190981
C	0.719333	3.750222	2.190981
C	0.861259	2.730573	1.076940
C	1.728341	2.993575	0.000000
C	1.934116	2.111159	-1.076940
C	2.888121	2.498072	-2.190981
C	-3.607454	1.252150	-2.190981
C	-2.795375	0.619414	-1.076940
C	-3.456682	0.000000	0.000000
C	-2.795375	-0.619414	1.076940
C	-3.607454	-1.252150	2.190981
H	1.012219	-3.287446	-3.139649
H	-0.333246	-4.037825	-2.284430
H	1.324363	-4.643793	-2.024727

## Appendix

H	2.270909	-3.933329	0.000000
H	3.663482	-1.730313	2.284430
H	3.359461	-3.468828	2.024727
H	2.340902	-2.520330	3.139649
H	-0.333246	4.037825	2.284430
H	1.324363	4.643793	2.024727
H	1.012219	3.287446	3.139649
H	2.270909	3.933329	0.000000
H	2.340902	2.520330	-3.139649
H	3.663482	1.730313	-2.284430
H	3.359461	3.468828	-2.024727
H	-3.330236	2.307512	-2.284430
H	-4.683824	1.174964	-2.024727
H	-3.353121	0.767116	-3.139649
H	-4.541817	0.000000	0.000000
H	-3.353121	-0.767116	3.139649
H	-3.330236	-2.307512	2.284430
H	-4.683824	-1.174964	2.024727
Fe	0.000000	0.000000	0.000000

**Table D.12:** Optimized Cartesian coordinates of  $\text{Co}(\text{acac})_3$   $S = 0/2$  with  $D_3$  symmetry.

	X	Y	Z
Co	0.000000	0.000000	0.000000
C	0.655026	2.574845	-1.011744
C	1.606491	2.782524	0.000000
C	1.902368	1.854692	1.011744
C	0.655026	-2.574845	1.011744
C	1.606491	-2.782524	0.000000
C	-2.557394	-0.720153	-1.011744
C	-3.212982	0.000000	0.000000
C	-2.557394	0.720153	1.011744
C	1.902368	-1.854692	-1.011744
O	-0.074969	1.537529	-1.161408
O	1.369024	0.703839	1.161408
O	-0.074969	-1.537529	1.161408
O	-1.294055	-0.833690	-1.161408
O	-1.294055	0.833690	1.161408
O	1.369024	-0.703839	-1.161408
H	-4.297662	0.000000	0.000000
H	2.148831	-3.721884	0.000000
H	2.148831	3.721884	0.000000
C	-3.373877	-1.452669	-2.059481
H	-4.447468	-1.352826	-1.889804
H	-3.128039	-1.057784	-3.050980

## Appendix

H	-3.104511	-2.513966	-2.055954
C	0.428890	-3.648198	2.059481
H	0.647952	-3.237853	3.050980
H	-0.624903	-3.945568	2.055954
H	1.052152	-4.528033	1.889804
C	2.944987	-2.195529	-2.059481
H	2.480087	-2.180069	-3.050980
H	3.729414	-1.431602	-2.055954
H	3.395316	-3.175207	-1.889804
C	-3.373877	1.452669	2.059481
H	-3.104511	2.513966	2.055954
H	-4.447468	1.352826	1.889804
H	-3.128039	1.057784	3.050980
C	2.944987	2.195529	2.059481
H	3.395316	3.175207	1.889804
H	2.480087	2.180069	3.050980
H	3.729414	1.431602	2.055954
C	0.428890	3.648198	-2.059481
H	-0.624903	3.945568	-2.055954
H	1.052152	4.528033	-1.889804
H	0.647952	3.237853	-3.050980

# Abstract.

---

A series of  $\text{Mn}^{\text{III}}(\beta\text{-diketonato})_3$  complexes ( $\beta\text{-diketonato}$  = acac, ba, dbm, tfaa, tfth, tffu, tfba and hfac) were synthesized and characterized with the aid of mass spectroscopy, elemental analysis, X-ray diffraction (crystallography) and melting point measurements. The electrochemical study (cyclic voltammetry) showed that for  $\text{Mn}^{\text{III}}(\beta\text{-diketonato})_3$  complexes with more electron withdrawing R and R' groups on the  $\beta\text{-diketonato}$  ligands ( $\text{RCOCHCOR}'$ ), the redox potential of the  $[\text{Mn}^{\text{III}}(\beta\text{-diketonato})_3] + \text{e}^- \rightleftharpoons [\text{Mn}^{\text{II}}(\beta\text{-diketonato})_3]$  redox reaction was found to shift to more positive potentials. The reduction potential of the  $\text{Mn}^{\text{III}}/\text{Mn}^{\text{II}}$  couple was correlated to electronic parameters (acid dissociation constant ( $\text{pK}_{\text{a}}$ ) of the uncoordinated  $\beta\text{-diketones}$  ( $\text{RCOCH}_2\text{COR}'$ ), the total group electronegativities  $[\Sigma(\chi_{\text{R}} + \chi_{\text{R}'})]$  and total Hammett sigma meta constant  $[\Sigma(\sigma_{\text{R}} + \sigma_{\text{R}'})]$  of the R and R' side groups of the  $\beta\text{-diketonato}$  ligands ( $\text{RCOCHCOR}'$ ) and the calculated electron affinity of  $\text{Mn}(\beta\text{-diketonato})_3$  complexes. DFT computational studies were done on the  $\text{Mn}(\text{acac})_3$  and  $\text{Mn}(\text{dbm})_3$  complexes to understand the Jahn-Teller distortion that  $\text{Mn}^{\text{III}}(\beta\text{-diketonato})_3$  complexes undergo.

Electrochemical (cyclic voltammetry) studies were done on  $\text{M}(\text{acac})_3$  complexes where  $\text{M} = \text{V}$ , Cr, Mn, Fe and Co. The reduction potential of the  $\text{M}^{\text{III}}/\text{M}^{\text{II}}$  couple was correlated to electronic parameters such as the metal electronegativity ( $\chi_{\text{Pauling}}$  and  $\chi_{\text{Mulliken}}$ ), calculated electron affinity and LUMO energy. DFT computational studies were done on the symmetry of  $\text{V}(\text{acac})_3$  to investigate the Jahn-Teller distortion of the  $\text{V}(\text{acac})_3$  complex. A DFT computational study was used to illustrate the  $d$ -orbital occupations of the  $\text{M}(\text{acac})_3$  complexes ( $\text{M} = \text{V}$ , Cr, Mn, Fe and Co).

**Keywords:** Manganese, tris(acetylacetonato)metal,  $\beta\text{-diketonato}$ , DFT, cyclic voltammetry.



# Opsomming.

---

'n Reeks van  $\text{Mn}^{\text{III}}(\beta\text{-diketonato})_3$  komplekse ( $\beta\text{-diketonato}$  = asas, ba, dbm, tfaa, tfth, tffu, tfba en hfac) is gesintetiseer en gekarakteriseer met behulp van massa spektroskopie, element analise, X-straal diffraksie (kristallografie) en smeltpunt metings. Die elektrochemiese studie met behulp van sikliese voltammetrie het gewys dat die  $\text{Mn}^{\text{III}}(\beta\text{-diketonato})_3$  komplekse met meer electrononttrekkende R en R' groepe van die  $\beta\text{-diketonato}$  ligand ( $\text{RCOCHCOR}'$ ), se reduksie potensiaal van die  $[\text{Mn}^{\text{III}}(\beta\text{-diketonato})_3] + e^- \rightleftharpoons [\text{Mn}^{\text{II}}(\beta\text{-diketonato})_3]$  redoks reaksie na meer positiewe potensiale verskuif het. Die  $\text{Mn}^{\text{III}}/\text{Mn}^{\text{II}}$  redoks koppel is chemies en elektrochemies onomkeerbaar. Die reduksie potensiaal van die  $\text{Mn}^{\text{III}}/\text{Mn}^{\text{II}}$  koppel was gekorreleer met elektroniese parameters (suurdissosiasie konstante ( $\text{pK}_a$ ) van die vrye  $\beta\text{-diketoon}$  ( $\text{RCOCH}_2\text{COR}'$ ), die totale groepelektronegatiwiteit en totale sigma meta Hammett konstante van die R en R' groepe van die  $\beta\text{-diketonato}$  ligande ( $\text{RCOCHCOR}'$ ) en die berekende elektronaantrekking van die  $\text{Mn}(\beta\text{-diketonato})_3$  komplekse. Kwantum-berekeningschemie studies was uitgevoer om die Jahn-Teller distorsie van  $\text{Mn}(\text{acac})_3$  en  $\text{Mn}(\text{dbm})_3$  beter te verstaan.

Elektrochemiese studies van die  $\text{M}(\text{acac})_3$  komplekse waar  $\text{M} = \text{V}, \text{Cr}, \text{Mn}, \text{Fe}$  en  $\text{Co}$  was uitgevoer met behulp van sikliese voltammetrie. Die reduksie potensiaal van die  $\text{M}^{\text{III}}/\text{M}^{\text{II}}$  koppel was gekorreleer met the metal se elektronegatiwiteit ( $\chi_{\text{Pauling}}$  en  $\chi_{\text{Mulliken}}$ ), berekende elektronaantrekking en the energie van die laagste ongevolde molekulêre orbitale. Kwantum-berekeningschemie studies was gedoen om die simmetrie van  $\text{V}(\text{acac})_3$  om die Jahn-Teller distorsie van die kompleks te ondersoek. Kwantum-berekeningschemie studies was uitgevoer om die  $d$ -orbitaal opvulling van die  $\text{M}(\text{acac})_3$  komplekse ( $\text{M} = \text{V}, \text{Cr}, \text{Mn}, \text{Fe}$  en  $\text{Co}$ ) te illustreer.

**Sleutelwoorde:** Mangaan, tris(asetielasetonato)metal(III),  $\beta\text{-diketonato}$ , kwantum-berekeningschemie, sikliese voltammetrie.